



Electromagnetic Form Factors of Hadrons in the Space-Like Region

Author:
Robert J. PERRY

Supervisors:
Prof. Anthony W. THOMAS
Ass. Prof. James ZANOTTI
Dr. Ayşe KIZILERSÜ
Ass. Prof. Ross YOUNG

*A thesis submitted in fulfilment of the requirements
for the degree of Doctor of Philosophy*

in the

School of Physical Sciences

September 2019

Declaration of Authorship

I certify that this work contains no material which has been accepted for the award of any other degree or diploma in my name, in any university or other tertiary institution and, to the best of my knowledge and belief, contains no material previously published or written by another person, except where due reference has been made in the text. In addition, I certify that no part of this work will, in the future, be used in a submission in my name, for any other degree or diploma in any university or other tertiary institution without the prior approval of the University of Adelaide and where applicable, any partner institution responsible for the joint-award of this degree.

I acknowledge that copyright of published works contained within this thesis resides with the copyright holder(s) of those works.

I also give permission for the digital version of my thesis to be made available on the web, via the University's digital research repository, the Library Search and also through web search engines, unless permission has been granted by the University to restrict access for a period of time.

I acknowledge the support I have received for my research through the provision of an Australian Government Research Training Program Scholarship.

Robert J. PERRY
September 2019

Abstract

Electromagnetic Form Factors of Hadrons in the Space-Like Region

by Robert J. PERRY

The theory of the strong force is unique amongst the known forces of nature in that the strength of its interactions grow with distance. It is postulated that this leads to the empirically observed colour confinement hypothesis. This hypothesis states that quarks and gluons, the fundamental degrees of freedom in the strong force form together into complex bound states called hadrons, rather than appearing as free particles. Thus the study of the strong force becomes the study of hadrons and their structure. One way we may study the structure of these composite bound states is through their electromagnetic interactions. In particular, information may be drawn about the structure of these hadrons from their elastic scattering data in the form of the hadron's *electromagnetic form factors*.

In this thesis, predictions are made of the nucleon and hyperon electromagnetic form factors by utilizing a non-perturbative quark model dressed by a pion cloud. Constraints from chiral symmetry arguments lead us to propose performing these chiral loop effects at the hadron level which leads to an improvement in a number of low energy observables related to the electromagnetic form factors.

The extraction of the pion form factor from pion electroproduction is also studied in detail. Constraints from gauge invariance are used to argue that the current model used to extract the pion form factor may be too simplistic. We study the model dependence in the context of a simple toy model, and find that the possible errors associated with this approximation could be as large as ten percent. We then proceed to perform a more in-depth calculation with a more sophisticated model, and show that the qualitative effects are the same. Together, these two studies imply that current measurements of the pion form factor are overestimated.

Acknowledgements

This work would not have been possible without the help and support of many people to whom I owe a great debt of gratitude. Firstly to my supervisor, Tony. Thank you for the knowledge and advice you have given me over the last five years. I will be forever grateful for the opportunities you have given me throughout my PhD. It has been an honour to work with you. To James, thank you for the discussions about physics and cricket, and for supporting my transition to lattice QCD. To Ross, who became an important sounding board for all things physics. Thank you for your endless patience, for entertaining my bold ideas, and then for explaining why they wouldn't work. Your intuitive insight into the problems I was confronting, and your willingness to offer solutions was always appreciated. To Ayse, thank you for your deep knowledge of perturbative and non-perturbative quantum field theory, and in particular for knowing the *correct* way to do d -dimensional algebra. Your support meant a lot when I was out of ideas. To Jason, Zach and Andre, my officemates since I began my honours, thanks for the many discussions and debates, both about physics and not. You have made the past five years fantastically enjoyable. Thanks also to all my other work friends, of whom there truly are too many to mention by name. There is a strong, supportive community amongst the collective CSSM and CoEPP students, and it is one of the things I will miss the most about leaving. For the shared lunch and coffee times, and for the after work drinks I thank you all. The support and advice you have all offered has been invaluable to the completion of this thesis. To Nick and Darcy, thanks for the many late night discussions and for ensuring I kept a level head throughout my PhD. You helped me keep my work in perspective when things were not working. To my mother, father and brother, thank you for your continuing love and support, and instilling in me a love of learning. Finally, to Kim who has been my constant strength and support since we met. Thank you for believing in me. With you next to me I know I can do anything. I love you.

Contents

Declaration of Authorship	iii
Abstract	v
Acknowledgements	vi
Contents	vii
1 Introduction	1
2 Quantum Chromodynamics	5
2.1 The Development of QCD	5
2.2 The Theory of QCD	8
2.2.1 Asymptotic Freedom	10
2.2.2 Colour Confinement	11
2.3 Chiral Effective Field Theory	14
2.3.1 The Accidental Chiral Symmetry of QCD	15
2.3.2 Conserved Charges	18
2.3.3 Realisations of a Symmetry	19
2.3.4 The Sigma Model	21
2.3.5 Effective Field Theories	26
2.3.5.1 Understanding Divergences	27
2.3.6 Constructing the Effective Lagrangian	29
2.3.6.1 Pseudo-Scalar Pion Nucleon Theory	30
2.3.6.2 Pseudo-Vector Pion Nucleon Theory	30
2.4 Conclusion	31
3 The Electromagnetic Structure of Hadrons	33
3.1 Baryon Electromagnetic Form Factors	33
3.2 The Pion's Electromagnetic Form Factor	37
3.3 Gauge Invariance and the Ward-Takahashi Identities	38
3.3.1 Classical Electromagnetic Gauge Invariance	38

3.3.2	Quantum Electrodynamics	40
3.3.3	The Ward-Takahashi Identity	43
3.3.3.1	Coupling Photon to External Line	44
3.3.3.2	Attaching Photon to Internal Loops	46
3.4	The Spin-Zero System	49
3.4.1	On-Shell Vertex	50
3.5	The Spin-Half System	51
3.5.1	The On-Shell Vertex	51
3.6	Conclusion	53
4	Chiral Corrections to Electromagnetic Form Factors in the Nambu–Jona-Lasinio Model	55
4.1	Baryon Electromagnetic Form Factors in the NJL Model	55
4.1.1	Quark Propagators and Dynamical Mass Generation	56
4.1.2	Mesons in the NJL Model	58
4.1.3	Calculating Electromagnetic Form Factors in the NJL Model	59
4.2	Constraints from Chiral Effective Field Theory	61
4.3	Implementations of Chiral Symmetry: A Comparison of Quark Level and Hadron Level Approaches	63
4.3.1	The Hadron Level Approach	64
4.3.2	The Quark Level Approach	64
4.3.3	Implementing Chiral Symmetry in Quark Models	65
4.4	Implementing the Chiral Corrections	66
4.4.1	Regularization and Renormalisation	68
4.4.2	Finite Range Regularisation	69
4.5	Nucleon Results	70
4.6	Chiral Corrections to Hyperon Form Factors	71
4.7	Hyperon Results	72
4.8	Conclusion	74
5	Investigating the Model Dependence of the Pion Electromagnetic Form Factor in a Scalar Field Theory	77
5.1	Exclusive Processes in Perturbative Quantum Chromodynamics	78
5.2	Measurements of the Pion Form Factor	80
5.2.1	The Pion’s Electromagnetic Form Factor at Intermediate Photon Virtuality	80
5.2.1.1	Preliminaries and Kinematics	81
5.2.1.2	A Model Independent Extraction: The Chew-Low Extraction Method	83
5.3	A Model Dependent Extraction: The VGL Model	85
5.3.1	Introduction to the Born Term Model	86
5.3.2	Incorporating Structure in the Born Term Model	90
5.3.3	Transforming the Born Term Model to the VGL Model	93
5.3.4	Using the VGL Model to Determine the Electromagnetic Form Factor of the Pion	94
5.3.5	Model Dependence of the Pion Form Factor	94

5.4	Scalar Pion Electroproduction Hadronic Matrix Element	95
5.4.1	VGL-like Model	96
5.4.2	Form Factors in the Toy Model	98
5.5	Extraction of the Pion Form Factor	99
5.6	Discussion of the Results	100
5.7	Conclusion	104
6	Investigating the Model Dependence of the Pion Electromagnetic Form Factor in Chiral Effective Field Theory	105
6.1	Fermionic Pion-Nucleon Theory	105
6.1.1	The Born Term Model	107
6.1.2	One-Loop Model	107
6.2	Algebraic Reduction and Numerical Calculation	109
6.2.1	Electromagnetic Form Factors in the Fermionic Model	110
6.3	Extraction of the Pion Form Factor	110
6.4	Discussion of Results	112
6.5	Conclusion	114
7	Summary and Outlook	117
A	Conventions and Useful Identities	119
A.1	The Group Structure of Isospin	119
A.2	The Group Structure of Colour	120
B	Pion Nucleon Feynman Rules	121
B.1	Pseudo-Scalar Pion Nucleon Effective Theory	121
B.2	Pseudo-Vector Pion Nucleon Effective Theory	123
C	Hadronic Charge Radii and Magnetic Moments	125
D	Derivation of the Pion Electroproduction Cross Section	127
D.1	Kinematic Variables and Reference Frames	127
D.1.1	Kinematic Variables	128
D.1.2	$p\gamma^*$ Centre of Momentum Frame	128
D.1.3	Cross Section Reduction	131
D.1.4	Evaluating $L_{\mu\nu}\mathcal{M}^{\mu\nu}$	135
D.1.5	Decomposing the Experimental Cross Section	135
E	Regularisation Prescriptions	137
E.1	Some Loop Integrals Diverge	137
E.2	The Wick Rotation	138
E.3	Proper Time Regularisation	139
E.4	Dimensional Regularization	141
E.4.1	Dimensional Analysis	142

E.4.2	Performing the Integration	144
E.4.3	Analytic Continuation	146
E.4.4	d -Dimensional Dirac Algebra	147
E.4.5	Trace Identities for d -Dimensional Dirac Algebra	147
E.4.6	Chiral Theories in Dimensional Regularization	149
F	Loop Diagrams for Scalar Pion Electroproduction	151
F.1	One Loop Diagrams	151
G	Loop Diagrams for Fermionic Pion Electroproduction	155
G.1	s -Channel Electromagnetic Vertex	155
G.2	s -Channel Self Energy	155
G.3	s -Channel Strong Vertex	156
G.4	t -Channel Electromagnetic Vertex	156
G.5	t -Channel Self Energy	156
G.6	t -Channel Strong Vertex	157
G.7	u -Channel Electromagnetic Vertex	157
G.8	Box Diagram	157
	Bibliography	159

It's a dangerous business, Frodo, going out your door. You step onto the road, and if you don't keep your feet, there's no knowing where you might be swept off to.

J.R.R. Tolkien
The Fellowship of the Ring
1954

Introduction

The Standard Model stands alone as the greatest achievement of modern theoretical particle physics. It is the culmination of over one hundred years of theoretical research, and describes our understanding of three of the four known fundamental forces in one unified framework. Of these three forces, the most complex is the *strong force*. The uninspired name is nothing if not descriptive. In fact, it is an empirical fact that the force is so strong that the fundamental objects which participate in strong interactions are confined, and thus only composite bound states may be observed. In the Standard Model, the strong force is described by a non-Abelian gauge field theory called *Quantum Chromodynamics* (QCD). The theory of QCD comprises fermionic *quarks*, which interact via exchange of bosonic *gluons*. The strength of the strong force interactions is partially determined by the coupling constant $\alpha_S = g^2/(4\pi)$ and is of the order one at low energy. This is to be contrasted with the coupling strength for quantum electrodynamics $\alpha = e^2/(4\pi) = 1/137$. The ‘traditional’ approach to analyzing interacting quantum field theories is perturbation theory. In order to utilize this approach, it is necessary to split the Hamiltonian H into two parts; H_0 and H_{int} , where H_0 is exactly solvable and H_{int} provides small corrections. In the case of quantum electrodynamics, the corrections are proportional to the coupling α . Due to the smallness of this coupling, the expansion in powers of α is well controlled, and the resulting predictions are impressively accurate. Indeed, the anomalous magnetic moment of the electron, first calculated by Schwinger in 1948 has now been calculated to order α^5 , agreeing within errors with the experimentally measured value to more than ten significant figures, making the magnetic moment of the electron the most accurately verified prediction in the history of physics. Application of a perturbative expansion in the coupling to QCD at low energies fails due to the largeness of the coupling strength. In this domain, other approaches must be pursued. In spite of these challenges (or perhaps because of them), much work has been done in making predictions in QCD. At this low energy scale, the only *ab-initio* way to perform calculations is via lattice QCD, where space-time is quantized on a four dimensional lattice, and numerical results are obtained with the aid of supercomputers. While it is undeniable that this method works, the results of a lattice calculation are often rather opaque in a way that analytic calculations almost never are.

While a perturbative expansion in the strong coupling is not a viable solution, it is not correct to say that perturbation theory is unsuitable for analysis of the strong force. The key is to recognize that while the fundamental degrees of freedom of the strong force are quarks and

gluons, the degrees of freedom relevant for studies of low energy QCD are composite baryons and mesons. By starting from a Lagrangian written in terms of these fields, it is possible to formulate a field theory which may be analysed with the conventional perturbative techniques. This approach is referred to as chiral effective field theory, and forms the basic tool of this thesis.

Since the low energy excitations of the strong force are composite bound states, it is of interest to understand their structure. Arguably the first measurement of hadron structure comes from Otto Stern, who measured the magnetic moment of the proton in 1933, and found it to be approximately three times the size of that predicted by the Dirac equation, which describes point-like fermions. Further evidence for the extended structure of the hadron appeared in elastic electron-proton scattering experiments of the the fifties. Again, these experiments demonstrated deviations in the cross sections from the behaviour expected from point-like hadrons. While quarks are believed to be confined inside hadrons, indirect evidence of their existence may be inferred from scattering data. For example, the quarks are electromagnetically charged particles, with the *up-type* quarks having charge $2/3$, and the *down-type* quarks having charge $-1/3$ in units of the electron charge. The quark's electromagnetic charge manifests itself at the level of hadrons as the net charge of the hadron. The electromagnetic charge of quarks thus gives us an indirect window into the dynamics of the strong force. In elastic scattering, the objects one may measure in this way are the hadron's electromagnetic form factors. These may be related to the charge distribution of the particular hadron, and thus the underlying quark distribution. As a result, the investigation of these electromagnetic form factors is of fundamental interest from both an experimental and theoretical perspective.

The electromagnetic form factors measured in elastic electron-hadron scattering are dependent on the invariant mass of the exchanged virtual photon, which we conventionally denote q^2 . In elastic electron-hadron scattering, the photon's virtuality is strictly less than zero. We refer to the electromagnetic form factors measured in this region as space-like form factors. This interaction is related to electron-positron annihilation to hadrons via a crossing relation where the photon virtuality is strictly greater than zero, and thus the measured form factors are known as the time-like form factors. There is much to be learnt about the structure of hadrons from both the space-like and time-like regions. However, in this thesis, we focus our attention on the space-like electromagnetic form factors.

We begin the thesis with a discussion the main concepts and underlying theory governing the strong force. In particular, we discuss the characteristic properties of QCD: *asymptotic freedom* and *colour confinement*. We then introduce chiral effective field theory which we shall utilize throughout the rest of the thesis. Finally, we discuss the formalism of electromagnetic form factors, and the constraints one can use from gauge invariance to constrain their form.

Having established the formalism and key concepts of the thesis, we make predictions for the electromagnetic form factors of the nucleon and sigma hyperons, where we incorporate corrections from chiral effective field theory. In particular, we demonstrate the importance of respecting the chiral symmetry when calculating the low energy behaviour of the electromagnetic form factors.

We then proceed to analyze current measurements of the pion's electromagnetic form factor. We examine in the context of a simple model, whether the current measurements of the pion form factor suffer from uncontrolled systematic errors. While the model examined is

not complex enough to make quantitative statements, we are able to conclude that it is likely that the current pion form factor is systematically overestimated. This stimulates the examination of this question within a more complex model. We again observe that the pion form factor extracted from the current approach employed in the experimental analysis leads to an overestimation of the underlying form factor.

Quantum Chromodynamics

The theory of the strong force is quantum chromodynamics (QCD). In this chapter we discuss the development of the theory from Yukawa’s proposal of a meson to bind protons and neutrons together in the atom, to the promotion of the colour quantum number to a gauge symmetry and subsequent derivation of the QCD Lagrangian. We then discuss characteristic features of QCD: asymptotic freedom and colour confinement and discuss the ways in which perturbative and non-perturbative methods allow for investigation of these effects. In particular, we explain the development of chiral effective field theory and its utility as a low energy effective description of the strong force.

2.1 The Development of QCD

The development of the study of the strong force arguably began with the realization that a nuclear force was required to bind protons and neutrons in the atom together. In particular, the protons in the nucleus experience a repulsive force due to the electromagnetic interaction, and thus another force is required to overcome this. Yukawa, in 1934, published a theoretical work postulating the existence of a new particle with a mass of about 100 MeV [1] to explain the binding of nucleons in the nucleus. By choosing a potential of the form

$$V(r) = -g^2 \frac{e^{-m_\pi r}}{r}, \quad (2.1)$$

Yukawa’s meson is constrained to only act over short distances, with the effective range of the interaction being proportional to the exchange of a massive boson. Importantly, as a result of the minus sign, this force is attractive. Thus the binding of nucleons in the nucleus could be understood as the result of the exchange of a massive boson, which came to be known as the pion. Initially the muon, having a mass of 105 MeV, was incorrectly identified as the meson of Yukawa’s theory. However the muon did not decay as was expected for a particle which could mediate the strong force. Yukawa’s pion was eventually discovered in 1947 leading to Yukawa receiving the Nobel Prize in Physics for 1949 for “his prediction of the existence of mesons on the basis of theoretical work on nuclear forces” [2]. As will be seen in much later work, Yukawa’s particle has become an integral component of the modern understanding of QCD via chiral symmetry arguments (see Refs. [3–5]).

TABLE 2.1: Pre-Eightfold Way classification of hadrons. Note that these examples all obey the Gell-Mann–Nishijima formula $Q = I_3 + \frac{1}{2}(B + S)$.

Hadron	Isospin (I_3)	Baryon No. (B)	Strangeness (S)	Charge (Q)
π^+	1	0	0	1
p	1/2	1	0	1
n	-1/2	1	0	0
Σ^-	-1	1	-1	-1

Although the success of Yukawa’s theory was undeniable, further development of the theory of the strong force was slow. This was in part due to the discovery of many hadronic resonances during the fifties and sixties, which were difficult to explain in terms of a theory of the nucleon and the pion. More generally though there were concerns about the consistency of quantum field theories, and in particular the divergences which appeared in loop calculations. These were exemplified in the prototypical example of a quantum field theory, Quantum Electrodynamics (QED). Originally discussed by Dirac in 1927 [6], it was only after the Second World War, when contributions from Kramers, Bethe [7], Schwinger [8–10], Feynman [11, 12], Tomonaga [13–17] and Dyson [18, 19] led to a coherent approach to perturbative calculations beyond tree-level though the theory of *renormalisation*. The success of this approach, gave a measure of confidence that quantum field theories may describe other forces of nature. For example, Yang and Mills, in 1955, approached the strong force by requiring local gauge invariance for the $SU(2)$ isospin group, in analogy with the local gauge invariance for the $U(1)$ gauge group in QED [20]. While the theory proposed by Yang and Mills failed to correctly describe the strong force, the term Yang-Mills theory is now taken to have a wider meaning as any gauge field theory based on the $SU(N)$ gauge group, of which the original theory proposed by Yang and Mills and the eventual theory of QCD are examples. Thus although the details were wrong, the theory due to Yang and Mills was a step in the right direction.

Attempts were made during the fifties and sixties to discover the reason behind the spectrum of hadronic particles. One particular relation noticed by Nishijima and Nakano [21] and later by Gell-Mann [22], relates the charge Q of the hadron to its isospin I_3 , baryon number B and strangeness S , and is known as the Gell-Mann–Nishijima formula:

$$Q = I_3 + \frac{1}{2}(B + S). \quad (2.2)$$

This pattern can be seen in Table 2.1. An early work of interest is that of Sakata, who in 1956 proposed a model in which the proton (p), neutron (n) and Lambda (Λ) baryons were elementary particles [23], from which other particles were composed. Although it turned out that Sakata was wrong to propose these particles as elementary, his approach motivated others including Gell-Mann who were able to provide a better explanation.

In 1961 and 1962 respectively, Ne’eman and Gell-Mann independently proposed a classification system for both the mesons and baryons [24, 25], based on the group structure of $SU(3)$. Gell-Mann, who coined the name ‘the Eightfold Way’, used the classification scheme to predict the existence of both a meson, the η [25], and a baryon, the Ω^- [26], which were later found in collider experiments (see for example [27]). Gell-Mann also noted, along with Zweig [28],

that the spectrum of particles could be understood, at least qualitatively by assuming that mesons and baryons were composite particles composed of two or three constituent particles, respectively, which Gell-Mann termed *quarks* [29]. Initially though, Gell-Mann was reluctant to consider the newly proposed quarks physical particles, since the quarks would require fractional electric charge. Further, in analogy with nuclear physics, where the proton and neutron are fairly weakly bound, one could imagine the nucleon's mass $m_N = 3m_q + E_{\text{binding}}$, where E_{binding} is small. Then the lightest quark would be stable and we would expect to observe that quark in particle detectors easily. But no bare quark was ever observed, and so Gell-Mann suggested that the quarks were purely formal mathematical objects; useful for bookkeeping, but nothing more.

It was a long time, relatively speaking, before quarks gained widespread acceptance as truly physical particles. Today, the non-observance of quarks is interpreted as evidence for the *colour confinement hypothesis*. As we shall see, theoretical evidence seems to suggest that this empirical fact occurs as a result of the dynamics of QCD. Nevertheless, a mathematical proof of confinement is still an unsolved problem. Quarks may be observed indirectly, however, by studying high energy hadronic processes.

In 1969, Bjorken, on the basis of infinite momentum dispersion relations, showed that the structure functions found in inelastic electron-proton scattering obeyed so-called 'Bjorken Scaling' [30]. One may parameterise inelastic scattering by two variables: the virtuality of the exchanged photon, $Q^2 = -q^2$ and $x = Q^2/(2q \cdot p)$, the so-called momentum fraction. As a result, one may define $W_1(Q^2, x)$ and $W_2(Q^2, x)$, the inelastic structure functions, the analogs of $F_1(Q^2)$ and $F_2(Q^2)$, the structure functions of elastic scattering. In the limit that Q^2 is large but x is kept fixed, Bjorken predicted that these structure functions would scale as

$$\lim_{Q^2 \rightarrow \infty, x \text{ fixed}} W_1(Q^2, x) \rightarrow g_1(x) \quad (2.3)$$

$$\lim_{Q^2 \rightarrow \infty, x \text{ fixed}} q \cdot p W_2(Q^2, x) \rightarrow g_2(x) \quad (2.4)$$

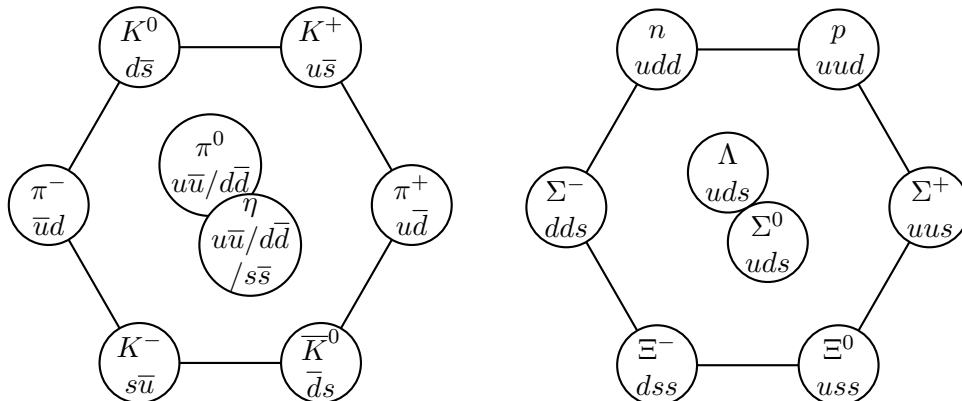


FIGURE 2.1: The baryon octet, showing the arrangement of spin-half baryons, as required by Nee'man and Gell-Mann's *Eightfold Way*.

where g_1 and g_2 are two functions dependent *only* on the momentum fraction x . In inelastic electron-proton scattering, the momenta of the exchanged virtual photon may be considered as the resolving power. Thus this scaling behaviour implied that the proton looked the same at all distance scales, in stark contrast to the elastic scattering data, which showed that the elastic structure of the proton was strongly dependent on the resolving power of the exchanged photon. Experiments performed at the Stanford Linear Accelerator (SLAC) in the late sixties and early seventies observed exactly this scaling behaviour [31]. Thus Bjorken's prediction of scaling was verified, but the underlying reason for this behaviour was unknown. The explanation came originally from Feynman, who had for a while been considering a model he termed the 'parton model'. In it, the proton was comprised of a number of massless point-like constituents. This hypothesis explained the scaling behaviour observed in the deep inelastic scattering experiments at SLAC, although it seemed at odds with the established understanding of the proton at lower energies. As a result of the apparent contradictions, Feynman's only paper on the subject from this era explicitly avoids mentioning partons at all [32]. Interestingly, some of the first explicit calculations in the 'parton model' appear to come from Bjorken [33]. In this paper, Bjorken showed that indeed the structure functions predicted in the parton model obeyed the scaling behaviour he had previously predicted on the basis of dispersion relations. Other theorists were quick to equate the partons of Feynman's model with the quarks Gell-Mann had introduced to classify the hadronic states. In a talk given by Gell-Mann, in association with Fritzsche titled 'Current Algebra: Quarks and What Else?' [34], Gell-Mann considered promoting the global colour symmetry to a local gauge symmetry, by analogy with the electromagnetic and weak forces. As it turned out, this was the correct way to proceed and led to the formulation of Quantum Chromodynamics or QCD, named after the colour gauge group on which the theory was based. We shall examine this theory of the strong force in the next section.

2.2 The Theory of QCD

In the Standard Model, the Strong Force is described by QCD, a non-abelian gauge field theory, based on promoting the global $SU(3)_c$ colour symmetry to a local one. The Lagrangian is given by

$$\mathcal{L}_{\text{QCD}}(x) = \sum_{f=u,d,c,s,t,b} \left[\bar{q}_c^f(x) (i\not{D}_{cd} + \delta_{cd}m^f) q_d^f(x) \right] - \frac{1}{4} \sum_{i=1}^8 G_i^{\mu\nu}(x) G_{i,\mu\nu}(x) + \mathcal{L}_{\text{GF}} + \mathcal{L}_{\text{FP}}, \quad (2.5)$$

where we have explicitly included the fermion flavour labels (latin superscripts) and the colour labels (latin subscripts). $q_c^f(x)$ are the colour $c = r, g, b$ quark fields with flavour f . The covariant derivative is given as

$$D_{cd}^\mu = \delta_{cd}\partial^\mu - igA_{cd}^\mu(x), \quad (2.6)$$

where the gauge fields $A_{cd}^\mu(x)$ are given as

$$A_{cd}^\mu(x) = \sum_{i=1}^8 A_i^\mu(x) t_{cd}^i, \quad (2.7)$$

where $A_i^\mu(x)$ are real valued fields and t^i are the generators of $SU(3)$ (in this case, $t^i = \lambda^i/2$, where λ^i written in the fundamental representation are the Gell-Mann matrices, given in Appendix A). The masses of the quarks are given by m^f , and $G_i^{\mu\nu}$ is the gluon field strength tensor:

$$G_i^{\mu\nu}(x) = \partial^\mu A_i^\nu(x) - \partial^\nu A_i^\mu(x) + gf_{ijk}A_j^\mu(x)A_k^\nu(x). \quad (2.8)$$

The third term is the result of the non-Abelian nature of the theory, and is believed to be a key feature which leads to confinement and asymptotic freedom—the characteristic properties of QCD [35]. The QCD Lagrangian is invariant under local $SU(3)$ field transformations of the form

$$q(x) \rightarrow q'(x) = \Omega(x)q(x), \quad (2.9)$$

$$A_\mu(x) \rightarrow A'_\mu(x) = \Omega(x)A_\mu(x)\Omega^\dagger(x) + \frac{i}{g}(\partial_\mu\Omega(x))\Omega^\dagger(x), \quad (2.10)$$

where $\Omega(x)$ is a general $SU(3)$ matrix given by

$$\Omega(x) = \exp\left(i\alpha_a(x)\frac{\lambda_a}{2}\right), \quad (2.11)$$

and λ_a are again the Gell-Mann matrices given explicitly in Appendix A.

Finally, \mathcal{L}_{GF} contains the gauge fixing terms, and \mathcal{L}_{FP} contains the contribution from the so-called Faddeev-Popov ghost fields $c(x)$, introduced to prevent the over counting of states;

$$\mathcal{L}_{GF} = -\frac{1}{2\xi} \sum_{i=1}^8 (\partial_\mu A_i^\mu(x)) (\partial_\mu A_i^\mu(x)), \quad (2.12)$$

$$\mathcal{L}_{FP} = \sum_{ij} \bar{c}^i(x) (-\partial_\mu D_{ij}^\mu) c^j(x). \quad (2.13)$$

In this thesis, we will primarily be concerned with models of QCD, rather than directly analyzing this Lagrangian, so we will say no more about these two terms.

While we have now written the QCD Lagrangian, it is not immediately clear how this theory reproduces the behaviour of the strong force observed in nature. In order to be consistent with the scaling behaviour of inelastic scattering originally observed at SLAC, the quarks

must behave as approximately free particles at short distances, while at large distances the quarks are not observed at all. Today these empirical facts are believed to be explained by asymptotic freedom and colour confinement respectively.

2.2.1 Asymptotic Freedom

One development in the theory of the strong force which we have not yet mentioned is the discovery by Gross and Wilczek [36], as well as independently by Politzer [37] of *Asymptotic Freedom*. The importance of this finding was recognized in 2004, with the three jointly receiving the Nobel Prize for physics [38]. In simple terms, Asymptotic Freedom expresses the property that a class of Yang-Mills theories (of which QCD is one example) are well defined in the ultraviolet. As we shall see, prior theories of nature contained a pathology which led many to conclude that quantum field theories were not self-consistent. Thus although we mention Asymptotic Freedom as one of the characteristic features of QCD, it has also been studied as a way to produce other theories which are self-consistent at all energy scales. This is the basic idea behind such beyond the standard model (BSM) theories such as *Technicolor* [39, 40]. Beyond ensuring the theory is well defined, the property of asymptotic freedom predicts that perturbation theory will become more accurate as the energy of the interaction increases.

The discussion of Asymptotic Freedom is based on analysis of the renormalisation group equations, which are beyond the scope of this thesis. Here we simply cite the main facts relevant to our discussion. For a more extended discussion of renormalisation group, see Refs. [41]. The prototypical quantum field theory is Quantum Electrodynamics. It is possible to define a renormalised effective charge which at one-loop order is given by

$$\alpha(Q^2; \mu^2) = \frac{\alpha}{1 - \alpha \left(\frac{1}{3\pi} \right) \ln \left(\frac{Q^2}{\mu^2} \right)} \quad (2.14)$$

where conventionally we choose the renormalisation scale $\mu \propto m_e^2$, the mass of the electron. This effective coupling is interpreted as due to the polarisation of the vacuum. The charge of the bare electron polarises virtual electron-positron pairs, leading to an observed charge which is momentum dependent. Importantly though, when we examine the effective coupling, we observe that for a finite value of Q^2 , the effective coupling becomes infinite. This behavior was first observed by Landau [42], and thus is known as the Landau Pole. The observation that the coupling was infinite at a finite momentum scale appeared to pose serious questions about the self consistency of Quantum Electrodynamics and Quantum Field Theories more generally. At the time there were no known theories which did not possess this same pathology.

It should be noted that the arguments provided by Landau are not watertight. Note that the derivation of the running coupling is based on a one-loop calculation, but this was used to make statements about the large coupling limit, exactly when one would expect the one-loop calculation to break down anyway. The renormalisation group provides a systematic way to study the behaviour of the coupling strength. In particular, that there exist three possibilities for the behaviour of the effective coupling strength; the coupling may diverge at a finite momentum value, as predicted by Landau, the coupling may not vary at all with momentum scale, or the coupling may run to small values at high momenta. It is theories of this third

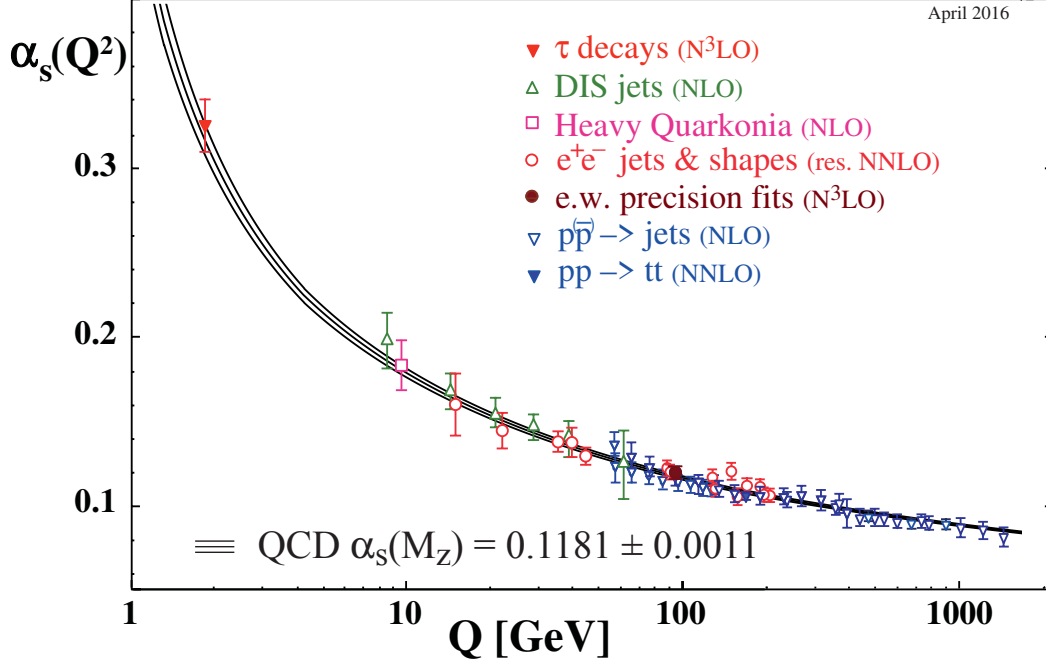


FIGURE 2.2: Running of the strong coupling. Note that unlike QED, the QCD coupling runs to zero at high energies without encountering a Landau Pole. Figure taken from PDG2018 [43].

kind which are referred to as asymptotically free. It is possible to show that for an $SU(N_c)$ gauge field theory with n_f quark flavours, the effective charge is given by [41]

$$\alpha_s(Q^2; \mu^2) = \frac{\alpha_s}{1 + \frac{\alpha_s}{4\pi} \left(\frac{11}{3} N_c - \frac{2}{3} n_f \right) \ln \left(\frac{Q^2}{\mu^2} \right)}. \quad (2.15)$$

The second term in the brackets has the same sign as for QED. In a sense, this is the ‘Abelian’ part of the theory. The first term is the result of the tree-level gluonic self interaction and in the case of QCD leads to asymptotic freedom. In QCD, $N_c = 3$ and $n_f = 6$, and thus the coefficient of the logarithm is positive in Eq. (2.15). This has dramatic ramifications for the running of the coupling, as the Landau pole we hypothesized in QED cannot appear here. As a result, QCD is well defined in the ultraviolet. This running of the coupling is an expression of asymptotic freedom; at high energies (or short distances) the interaction strength goes to zero and so the quarks behave approximately as free particles, as anticipated in Feynman’s parton model.

2.2.2 Colour Confinement

The running of the strong coupling $\alpha_s(Q^2; \mu^2)$ also implies that perturbation theory will become less accurate as the energy scale of the process is lowered. It should be noted that

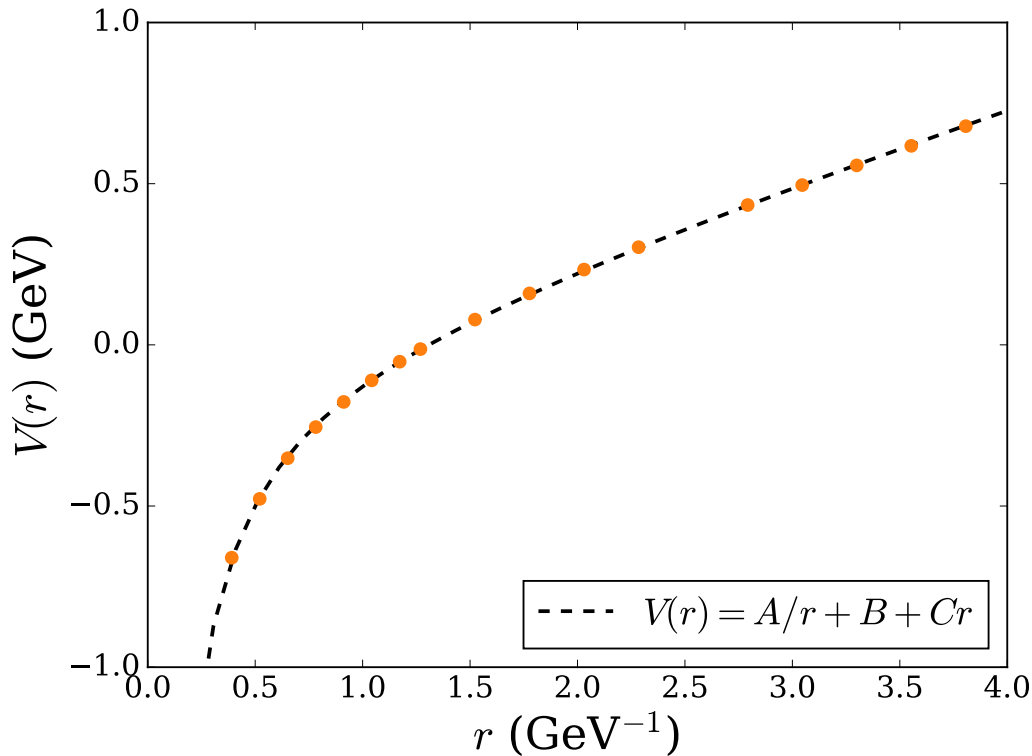


FIGURE 2.3: Static quark potential determined from a lattice QCD simulation in the ‘quenched’ approximation, where dynamical fermions are excluded. This data has been extrapolated to the continuum limit (roughly speaking corresponding to the lattice spacing $a \rightarrow 0$ limit). Note that the data is well described by the simple form $V(r) = A/r + B + Cr$. In particular, note that at large distances, the potential between two static quarks grows linearly. This linearly rising potential has been seen as evidence for confinement. Data taken from Ref. [46].

since the equation for the running coupling arises from a calculation in perturbation theory, it is only valid when perturbation theory is valid. Thus we cannot use this result to make conclusions about the infrared behaviour of the coupling. Models of QCD seem to suggest that this coupling saturates at a finite value [44, 45]. In any case, this large coupling invalidates perturbation theory at $\mathcal{O}(1 \text{ GeV})$.

In the low energy regime we must pursue different avenues of analysis if we are to gain some understanding of colour confinement. Lattice QCD and the Schwinger-Dyson equations for QCD both use the QCD path integral as the basis for their studies. In lattice QCD one numerically evaluates the path integral by discretization. This is done by introducing a smallest length a , called the *lattice spacing*, which acts as an ultraviolet regulator for the theory. In order to enable numerical evaluation, the physics is placed in a finite sized space-time box with length $L = na$. After doing this all terms in the theory are finite, and a numerical calculation of properties is possible. One important early result in this field is the calculation of the potential $V(r)$ between two static (infinitely heavy) quarks. It turns out that one may describe the potential with the general form

$$V(r) = \frac{A}{r} + B + Cr. \quad (2.16)$$

Thus at high energies (or short ranges), the potential appears to be approximately Coulombic. However, the long distance behavior of the force is completely different from QED. Instead of decreasing with separation distance, the potential instead rises linearly, resulting in a confining potential at large distances. These simulations are performed in the ‘quenched’ approximation, where the vacuum is prevented from containing quark anti-quark pairs. In a more realistic calculation, it is expected that as the separation of the quarks and thus the potential energy increases, the system reaches a point where it is more energetically favorable to produce an extra quark-antiquark pair than increasing the distance between the quarks. In this case, the result would be the production of two colourless mesons.

Another example of the emergent nature of QCD is the occurrence of dynamical mass generation. This is the process by which a bound state of three quarks with approximate mass $m_q \approx 5$ MeV produces a nucleon with a mass $m_N \approx 1$ GeV. Although the empirical fact is well accepted, the underlying mechanism was less clear. One advantage of a numerical simulation of the path integral of QCD is that the effects may be studied in a systematic way. In particular, recent work has shown that topological objects called center vortices are mainly responsible for the dynamical generation of mass [47, 48].

To reduce the whole field of Lattice QCD to a few paragraphs and a single figure is simplistic in the extreme. Today the field of Lattice QCD is a mature one, making contributions to hadronic spectroscopy, the QCD phase diagram and hadronic structure functions, to name a few. As a result of algorithmic improvements, as well as the increase in computational power, cutting edge lattice calculations are now contributing to precision calculations of Standard Model processes, including hadronic corrections to the anomalous magnetic moment of the muon [49, 50] and meson decay constants which allow CKM matrix elements to be further constrained [51]. Indeed, various studies have even been performed simulating the physics of gauge groups other than $SU(3)$ [52, 53].

While lattice QCD attempts a numerical simulation of the path integral, the Schwinger-Dyson equations attempt an analytical one. In principle, the Schwinger-Dyson equations constitute a complete formal solution to the quantum field theory. However, without simplification, their form is completely intractable; they comprise an infinite tower of coupled integral equations. Thus the approach pursued in the field has been to perform a number of simplifications, which reduce the infinite number of coupled integral equations to a small number, which are then solved. By building in the asymptotic behaviour of the approximated correlation functions and respecting the symmetries of the theory, modern Schwinger-Dyson approaches have been able to make impressive predictions about the hadronic spectrum [54] and structure functions [55, 56].

Importantly, the analytic nature of Schwinger-Dyson equations allows for more transparent studies of the origin of observed effects. In particular, we have already discussed the static quark potential calculated in lattice QCD as evidence of colour confinement. Schwinger-Dyson equations provide further evidence of this confinement, and also suggest a possible mechanism by which confinement occurs. An on-shell particle appears as a pole of the full propagator. Thus it has been suggested that colour confinement may manifest itself as the lack of a pole

in the full propagator of coloured objects. It is possible to show that the tree-level propagator for a gluon (valid in the large momentum range) is

$$G_{Fab}^{(0)\mu\nu}(q) = \frac{-i}{q^2 + i\epsilon} \left(g^{\mu\nu} - (1 - \xi) \frac{q^\mu q^\nu}{q^2} \right) \delta_{ab} \quad (2.17)$$

where ξ is the gauge fixing parameter, conventionally chosen to be $\xi = 1$ (Feynman gauge), and δ_{ab} acts in the colour gauge group space. If we were to use this propagator in the low energy regime (where perturbation theory breaks down), we would find a pole corresponding to the propagation of an on-shell gluon. However, solving the Schwinger-Dyson for the gluon propagator leads to the conclusion that the gluon's mass function varies in such a way that the perturbative pole is avoided.¹ Thus the colour confinement hypothesis may be interpreted as due to the lack of a single particle singularity in the two point correlation function, which arises from the non-perturbative dynamics of the theory.

As with lattice QCD, our discussion of the method of Schwinger-Dyson equations is necessarily limited. Along with lattice QCD, we shall use some results based on this non-perturbative technique but our primary avenue of investigation will employ chiral effective field theory. It is to this theoretical approach that we now turn.

2.3 Chiral Effective Field Theory

As we have seen, direct analysis of the QCD Lagrangian is possible if one chooses to use non-perturbative methods. These methods are technically challenging, and sometimes the physical mechanism underlying the final result remains opaque. In contrast to these approaches, which attempt to perform calculations on the underlying QCD Lagrangian, one can formulate a description - valid at low energies - in terms of the relevant degrees of freedom active in this energy range; that is, in terms of meson and baryon fields. This is the approach pursued in *chiral effective field theory*. In the following sections, we examine the approximate chiral symmetry of QCD, and describe how this symmetry may be used to build a low energy theory of QCD.

¹The astute reader may be confused on this point: generally speaking gauge bosons are required from acquiring a mass in order to be consistent with gauge invariance. This requirement is certainly respected for the gluon. In Feynman Gauge, the most general form of the gluon propagator is

$$G_{Fab}^{\mu\nu}(q) = \frac{-ig^{\mu\nu}}{[q^2 + i\epsilon][1 - \Pi(q^2)]} \delta_{ab} = \frac{-ig^{\mu\nu}}{q^2 - m_G^2(q^2) + i\epsilon} \delta_{ab}$$

where we have made the identification $m_G^2(q^2) = q^2 \Pi(q^2)$. This allows us to write the gluon propagator in a form which appears similar to that of a massive boson, but note that the mass parameter is a function of q^2 . In general, we must distinguish between the mass function $m_G^2(q^2)$, which in general is renormalisation scheme dependent, and thus not observable, and the pole mass, which would correspond to the propagation of an on-shell gluon. In the case of the gluon, Schwinger-Dyson studies show that the gluon mass function varies in such a way that the no low momentum pole appears in the propagator [57]. This behaviour is particular to strongly coupled theories.

2.3.1 The Accidental Chiral Symmetry of QCD

When attempting to make simplifications of a quantum field theory, symmetries are important to preserve. As we have previously discussed, QCD is a gauge field theory, based on a local $SU(3)$ gauge symmetry. Like all relativistic quantum field theories, it exhibits Poincaré symmetry and is also invariant under the combination of charge, parity and time reversal (C, P and T symmetry). There are also other symmetries which are approximately respected by the QCD Lagrangian. It turns out that it is possible to build a picture of low energy QCD by considering the approximate chiral symmetry of the Lagrangian. To see this, note that the current quark masses may be divided into two categories based on their mass; often referred to in the literature as the light and heavy quarks. This division is depicted in Table 2.2, below.

TABLE 2.2: Comparison of ‘light’ and ‘heavy;’ current quark masses in the QCD Lagrangian. Due to colour confinement, free quarks have not been observed. The quark mass parameters do not constitute observables and are renormalisation scheme dependent. These masses are the result of $\overline{\text{MS}}$ at $\mu = 2 \text{ GeV}$ [58].

Light Quarks	m_u	$0.0022_{-0.4}^{+0.6} \text{ GeV}$
	m_d	$0.0047_{-0.5}^{+0.4} \text{ GeV}$
	m_s	$0.096_{-4}^{+8} \text{ GeV}$
Heavy Quarks	m_c	$1.28 \pm 0.03 \text{ GeV}$
	m_b	$4.18_{-0.03}^{0.04} \text{ GeV}$
	m_t	$\sim 170 \text{ GeV}$

This hierarchy of masses suggests a simplification where we take the light quark masses to zero and the heavy quark masses to infinity so that they decouple from the theory. Recall the QCD Lagrangian we previously wrote:

$$\mathcal{L}_{\text{QCD}}(x) = \sum_{f=u,d,c,s,t,b} \left[\bar{q}_c^f(x) (i\not{D}_{cd} + \delta_{cd}m^f) q_d^f(x) \right] - \frac{1}{4} \sum_{i=1}^8 G_i^{\mu\nu}(x) G_{i,\mu\nu}(x) + \mathcal{L}_{\text{GF}} + \mathcal{L}_{\text{FP}}, \quad (2.18)$$

To emphasize the symmetry we are about to explore, we will suppress colour indices, and define a flavour triplet field ψ , given by

$$\psi(x) = \begin{bmatrix} q^u(x) \\ q^d(x) \\ q^s(x) \end{bmatrix}. \quad (2.19)$$

In the massless limit, where we have integrated out the heavy flavours, the Lagrangian becomes

$$\mathcal{L}_{QCD}^{(0)} = \bar{\psi}(x)i\mathcal{D}\psi(x) - \frac{1}{4} \sum_{i=1}^8 G_i^{\mu\nu}(x)G_{i,\mu\nu}(x). \quad (2.20)$$

In this approximation, the QCD Lagrangian possesses another symmetry: *chiral symmetry*. To see this, we define the usual chiral projection operators

$$P_R = \frac{1}{2}(1 + \gamma_5)\mathbb{I}^f, \quad (2.21)$$

$$P_L = \frac{1}{2}(1 - \gamma_5)\mathbb{I}^f. \quad (2.22)$$

These operators project out the left and right handed components of the quark fields. We have explicitly included the flavour space identity matrix \mathbb{I}^f to emphasize that we are projecting out the chirality of each field in the flavour triplet. We therefore define ψ_R and ψ_L by

$$\psi_R = P_R\psi = \frac{1}{2}(1 + \gamma_5)\psi = \begin{bmatrix} q_R^u(x) \\ q_R^d(x) \\ q_R^s(x) \end{bmatrix}, \quad (2.23)$$

$$\psi_L = P_L\psi = \frac{1}{2}(1 - \gamma_5)\psi = \begin{bmatrix} q_L^u(x) \\ q_L^d(x) \\ q_L^s(x) \end{bmatrix}, \quad (2.24)$$

where $\psi_L + \psi_R = \psi$. Using this definition, we may decompose the massless Lagrangian into its left and right chiral quark fields:

$$\mathcal{L}_{QCD}^{(0)} = (\psi_L + \psi_R)^\dagger \gamma_0 i\mathcal{D}(\psi_L + \psi_R) - \frac{1}{4} \sum_{i=1}^8 G_i^{\mu\nu}(x)G_{i,\mu\nu}(x). \quad (2.25)$$

Noting that the projection operator is Hermitian ($\gamma_5^\dagger = \gamma_5$), it is possible to see that the cross terms vanish, and we are left with

$$\mathcal{L}_{QCD}^{(0)} = \bar{\psi}_L i\mathcal{D}\psi_L + \bar{\psi}_R i\mathcal{D}\psi_R - \frac{1}{4} \sum_{i=1}^8 G_i^{\mu\nu}(x)G_{i,\mu\nu}(x). \quad (2.26)$$

Thus in the massless limit of QCD, the left handed and right handed fields decouple. Note that it is possible to show that the addition of a mass term spoils this symmetry. Now consider two unitary matrices U_L and U_R . We are free to perform transformations on the quark fields individually:

$$\begin{bmatrix} q_L^u \\ q_L^d \\ q_L^s \end{bmatrix} \rightarrow \begin{bmatrix} q_L^{u'} \\ q_L^{d'} \\ q_L^{s'} \end{bmatrix} = U_L \begin{bmatrix} q_L^u \\ q_L^d \\ q_L^s \end{bmatrix}, \quad (2.27)$$

and similarly

$$\begin{bmatrix} q_R^u \\ q_R^d \\ q_R^s \end{bmatrix} \rightarrow \begin{bmatrix} q_R^{u'} \\ q_R^{d'} \\ q_R^{s'} \end{bmatrix} = U_R \begin{bmatrix} q_R^u \\ q_R^d \\ q_R^s \end{bmatrix}. \quad (2.28)$$

Thus, the massless *classical* QCD Lagrangian possesses a global $U(3)_L \times U(3)_R$ symmetry. Note here that we emphasize the classical nature of our theory: we are yet to promote the fields to operators and impose commutation relations. Naively, one would expect these symmetries to persist in the quantum mechanical theory, but as we shall see *this is not the case*.

We can write a general unitary matrix as

$$U = \exp\left(i \sum_{i=1}^9 \alpha_i \frac{\lambda_i}{2}\right) \quad (2.29)$$

where $\lambda_1, \dots, \lambda_8$ are the usual Gell-Mann identities and $\lambda_9 = 2\mathbb{I}^f$, where we emphasize again that we are performing these transformations in flavour space. Noether's theorem implies that for every continuous symmetry of the system, there exists a corresponding quantity whose value is conserved in time. We write the conserved current as

$$J^\mu = \frac{\partial \mathcal{L}}{\partial(\partial_\mu \psi)} \delta \psi \quad (2.30)$$

where $\delta \psi$ is the infinitesimal variation in the field, and $\partial_\mu J^\mu = 0$. We find

$$J_{L,i}^\mu = \bar{\psi}_L \gamma^\mu \frac{\lambda_i}{2} \psi_L, \quad i = 1, \dots, 8, \quad (2.31)$$

$$J_{R,i}^\mu = \bar{\psi}_R \gamma^\mu \frac{\lambda_i}{2} \psi_R, \quad i = 1, \dots, 8, \quad (2.32)$$

$$J_L^\mu = \bar{\psi}_L \gamma^\mu \mathbb{I}^f \psi_L, \quad (2.33)$$

$$J_R^\mu = \bar{\psi}_R \gamma^\mu \mathbb{I}^f \psi_R. \quad (2.34)$$

There are thus 18 conserved currents in the *classical* theory. It is convenient to consider the linear combinations of these currents:

$$J_{V,i}^\mu = J_{L,i}^\mu + J_{R,i}^\mu = \bar{\psi}\gamma^\mu \frac{\lambda_i}{2}\psi, \quad i = 1, \dots, 8, \quad (2.35)$$

$$J_{A,i}^\mu = J_{L,i}^\mu - J_{R,i}^\mu = \bar{\psi}\gamma_5\gamma^\mu \frac{\lambda_i}{2}\psi, \quad i = 1, \dots, 8, \quad (2.36)$$

$$J_V^\mu = J_L^\mu + J_R^\mu = \bar{\psi}\gamma^\mu \mathbb{1}^f \psi, \quad (2.37)$$

$$J_A^\mu = J_L^\mu - J_R^\mu = \bar{\psi}\gamma_5\gamma^\mu \mathbb{1}^f \psi, \quad (2.38)$$

which transform under the parity operator as vector and axial-vector current densities, respectively, and we therefore label them accordingly. As it turns out, the singlet axial current is only conserved in the classical theory; in the process of quantizing the theory, extra terms appear which spoil the symmetry. The lack of conservation of a current which is conserved in the classical theory is referred to as an anomaly. Rather than vanishing, one may show that the divergence of the current is

$$\partial_\mu J_A^\mu = \frac{3g^2}{2(4\pi)^2} \epsilon_{\mu\nu\alpha\beta} \sum_{i=1}^8 G_i^{\mu\nu} G_i^{\alpha\beta}, \quad (2.39)$$

where $G_a^{\mu\nu}$ is the gluonic field strength tensor. Thus, after quantization the massless QCD Lagrangian is invariant under $SU(3)_V \times SU(3)_A \times U(1)_V$.

2.3.2 Conserved Charges

From each of the conserved currents defined above, we may define a corresponding charge operator Q . In general, one may find determine the charge operator for a particular conserved current $\partial_\mu j^\mu(x) = 0$ via

$$Q = \int d^3x j^0(x). \quad (2.40)$$

Importantly, the charge operator is a constant of motion:

$$\begin{aligned} \frac{d}{dt}Q &= \int d^3x \partial_0 j^0(x) \\ &= \int d^3x \nabla \cdot \mathbf{j}(x) = 0, \end{aligned} \quad (2.41)$$

where we have assumed that the current is suitably well behaved at infinity. It is possible to show that this implies that the charge operator commutes with the Hamiltonian:

$$[H, Q] = 0. \quad (2.42)$$

We may construct conserved charges for the vector J_V^μ and the chiral $J_{V,i}^\mu, J_{A,i}^\mu$ currents. For example, consider the vector current $J_{V,i}^\mu$. The corresponding charges are

$$Q_{V,i} = \int d^3x j_{V,i}^0(x). \quad (2.43)$$

The axial vector charges are

$$Q_{A,i} = \int d^3x j_{A,i}^0(x). \quad (2.44)$$

Consider the eigenstate of the QCD Hamiltonian $|N^+\rangle$, the positive parity nucleon:

$$H |N^+\rangle = E_N |N^+\rangle. \quad (2.45)$$

The action of the axial charge operator $Q_{A,i}$ is to transform a positive parity state into a negative parity state. That is

$$Q_{A,i} |N^+\rangle = |N^-\rangle. \quad (2.46)$$

Noting that the Hamiltonian commutes with this charge operator, we have that

$$\begin{aligned} H |N^-\rangle &= H Q_{A,i} |N^+\rangle \\ &= Q_{A,i} H |N^+\rangle \\ &= E_N |N^-\rangle. \end{aligned} \quad (2.47)$$

In other words, we expect there to exist a degenerate mass parity partner of the nucleon. This is not observed in nature, with the the lowest mass excitation of the nucleon with the correct quantum numbers being over 500 MeV heavier! Thus while the axial vector current is a symmetry of the Hamiltonian, the spectrum does not exhibit this symmetry.

2.3.3 Realisations of a Symmetry

To understand the apparent contradiction between the symmetries of the Hamiltonian, and the observed symmetries described at the end of the last section, we must make a distinction between a *Lagrangian symmetry*, and a *vacuum symmetry* [59]. As we shall see, symmetry of the Lagrangian does not necessarily imply invariance of the vacuum. It is this fact which we will employ to explain the lack of parity doublets we discussed in the last section. A Lagrangian symmetry implies that

$$[H, Q] = 0, \quad (2.48)$$

and thus Q corresponds to a conserved current j^μ . A vacuum symmetry implies that the vacuum is invariant under unitary transformations of the conserved charge:

$$\exp(i\alpha Q) |0\rangle = |0\rangle. \quad (2.49)$$

This implies that the conserved charge Q annihilates the vacuum:

$$Q |0\rangle = 0. \quad (2.50)$$

Coleman's Theorem [60–62] states that if a charge Q annihilates the vacuum, then it is a constant of motion. That is

$$Q |0\rangle = 0 \implies [H, Q] = 0. \quad (2.51)$$

In other words, if one observes a symmetry in the spectrum, this symmetry must be present in the Lagrangian. This is known as the Wigner-Weyl realisation of the Lagrangian symmetry. Note that this implication is one way. The converse of this is Goldstone's theorem. Consider the case where we have a symmetry of our Lagrangian and thus

$$[H, Q] = 0, \quad (2.52)$$

that is, Q is a constant of motion associated with a conserved current j^μ . Then there are two possibilities. Either

$$Q |0\rangle = 0, \quad (2.53)$$

in which case we have again the Wigner-Weyl realisation of the symmetry, and so the Lagrangian symmetry is expressed in the spectrum, or we have

$$Q |0\rangle \neq 0. \quad (2.54)$$

The case that the charge does not annihilate the vacuum is covered by Goldstone's Theorem. In this case, the Lagrangian symmetry of the system does not manifest itself as a symmetry of the spectrum. Instead, the non-annihilation of the vacuum implies the emergence of massless bosons; so-called Nambu-Goldstone bosons. In particular, for each charge which does not annihilate the vacuum, there exists a corresponding massless excitation.

Recall that we began this discussion by noting that while the axial vector current is conserved ($\partial_\mu j_{A,i}^\mu = 0$), the spectrum does not exhibit parity doublets. Thus we must conclude that the axial vector charge *does not* annihilate the vacuum,

$$Q_{A,i} |0\rangle \neq 0 \quad (2.55)$$

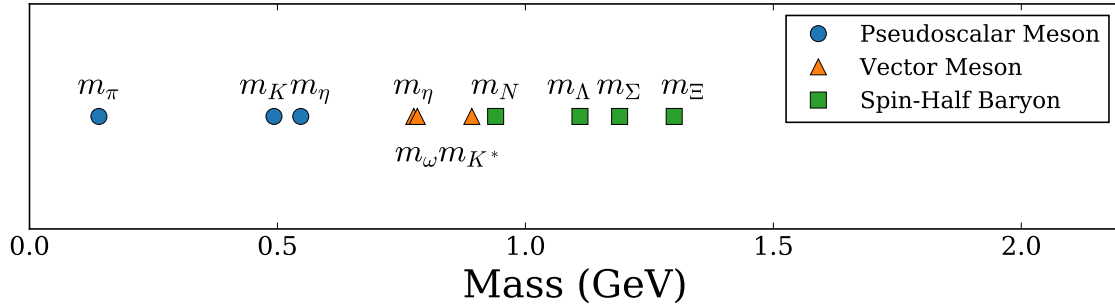


FIGURE 2.4: Mass hierarchy of hadronic states. Note that the pion is extremely light, when compared to the other members of the pseudoscalar octet, and to the other hadronic states. In the modern understanding, the pion is a pseudo Nambu-Goldstone boson, the result of a dynamical chiral symmetry breaking event. In the limit of massless quarks, the pion is expected to become a true massless Nambu-Goldstone boson.

and the Goldstone realization of the symmetry occurs. In $SU(3)_V \times SU(3)_A$ chiral symmetry, there are eight charges which we expect do not annihilate the vacuum, and thus we anticipate eight Nambu-Goldstone bosons. If the chiral symmetry was an exact symmetry of the QCD Lagrangian, then we would expect massless hadrons to appear in the spectrum. However, recall that the quark mass term

$$\mathcal{L}_{\text{mass}} = m\bar{q}q \quad (2.56)$$

mixes left and right handed fields and thus spoils the exact chiral symmetry. We say that chiral symmetry is *explicitly broken* by the quark masses. Thus instead of true Nambu-Goldstone bosons, we anticipate the appearance of unnaturally light hadronic states. In either case, the assumption that the conserved axial vector charge does not annihilate the vacuum requires that the generated Nambu-Goldstone bosons share the conserved current's quantum numbers. In $SU(2)_V \times SU(2)_A$ chiral symmetry, the bosons correspond to the pion triplet, while in $SU(3)_V \times SU(3)_A$ chiral symmetry, the bosons correspond to the entire pseudoscalar octet. Note from Fig. 2.4 that these states are indeed the lightest hadronic states observed.

While ‘proofs’ of Goldstone’s theorem may be found in a number of places, many of these fail to rigorously prove the theorem [63]. Goldstone’s theorem has been proved [64, 65], but the arguments are rather involved, and beyond the scope of this discussion. In lieu of a proof, we shall provide a simple example, the Sigma Model, originally proposed by Gell-Mann and Lévy [66] as a model which incorporates the constraints of $SU(2)_L \times SU(2)_R$ chiral symmetry, and exhibits the spontaneously broken symmetry and emergence of massless excitations, in agreement with Goldstone’s Theorem.

2.3.4 The Sigma Model

Let us review the theoretical arguments which brought us to this point. We began from the QCD Lagrangian and derived the conserved currents. We then noted that the axial vector charges $Q_{A,i}$ did not correspond to a symmetry of the spectrum and concluded that the

symmetry occurred in the Goldstone realisation. Historically though, the Sigma Model was introduced prior to the discovery of the QCD Lagrangian. From this perspective, it is not clear why one would wish to write down a Lagrangian consistent with a symmetry not observed in nature. The answer is the so-called Partially Conserved Axial Current (PCAC) hypothesis, which requires that the divergence of the axial current $j_{A,i}^\mu(x)$ is ‘small’. To place this in more concrete terms, we write the π -to-vacuum matrix element:

$$\langle \pi_j(q) | j_{A,i}^\mu(x) | 0 \rangle = -i \delta_{ij} f_\pi q^\mu e^{iq \cdot x} \quad (2.57)$$

where $\langle \pi_j(q) |$ is a physical pion state, and f_π is the pion decay constant. Taking the divergence of this matrix element, we have that

$$\langle \pi_j(q) | \partial_\mu j_{A,i}^\mu(x) | 0 \rangle = \delta_{ij} f_\pi q^2 e^{iq \cdot x} = \delta_{ij} f_\pi m_\pi^2 e^{iq \cdot x} \quad (2.58)$$

where for an on-shell pion, $q^2 = m_\pi^2$. Thus the divergence of this matrix element is non-zero. But noting the pion’s characteristically light mass, Nambu proposed that one assume the operator relation to be approximately conserved:

$$\partial_\mu j_{A,i}^\mu(x) \approx 0 \quad (2.59)$$

Based on the approximation that the axial current is approximately conserved, it is possible to formulate so-called ‘soft-pion theorems’, which give good agreement with data. Thus the PCAC hypothesis is the reason for the requirement that the axial current should be a conserved current of any low energy theory of QCD. Armed with this knowledge, we proceed to analyse the Sigma model. We wish to write a model for low energy QCD. Consider the free nucleon Lagrangian:

$$\mathcal{L} = \bar{\Psi}_N (i \not{\partial} - m_N) \Psi_N, \quad (2.60)$$

where

$$\Psi = \begin{bmatrix} \psi_p \\ \psi_n \end{bmatrix}. \quad (2.61)$$

We want our final Lagrangian to be invariant under $SU(2)_V \times SU(2)_A$. Clearly the Lagrangian is invariant under $SU(2)_V$ transformations:

$$\Psi_N \rightarrow \Psi'_N = \exp\left(i\theta_i \frac{\tau_i}{2}\right) \Psi_N, \quad (2.62)$$

$$\bar{\Psi}_N \rightarrow \bar{\Psi}'_N = \bar{\Psi}_N \exp\left(i\theta_i \frac{\tau_i}{2}\right). \quad (2.63)$$

But as with the QCD Lagrangian, the nucleon mass term spoils invariance under the $SU(2)_A$ transformation

$$\Psi_N \rightarrow \Psi'_N = \exp\left(i\gamma_5\theta_i\frac{\tau_i}{2}\right)\Psi_N, \quad (2.64)$$

$$\bar{\Psi}_N \rightarrow \bar{\Psi}'_N = \bar{\Psi}_N \exp\left(i\gamma_5\theta_i\frac{\tau_i}{2}\right). \quad (2.65)$$

As with electromagnetic gauge invariance, the non-interacting Lagrangian is not consistent with the desired symmetry. We must introduce new fields to compensate for this non-conservation. In particular, we introduce the isospin singlet field σ and the pseudoscalar isospin triplet $\boldsymbol{\pi} = (\pi_1, \pi_2, \pi_3)$ and replace the chiral symmetry spoiling mass term $m_N\bar{\Psi}_N\Psi_N$ with $g\bar{\Psi}_N(\sigma + i\gamma_5\boldsymbol{\tau} \cdot \boldsymbol{\pi})\Psi_N$, where we require that this combination should transform as

$$(\sigma + i\gamma_5\boldsymbol{\tau} \cdot \boldsymbol{\pi}) \rightarrow (\sigma' + i\gamma_5\boldsymbol{\tau} \cdot \boldsymbol{\pi}') = \exp\left(-i\gamma_5\theta_i\frac{\tau_i}{2}\right)(\sigma + i\gamma_5\boldsymbol{\tau} \cdot \boldsymbol{\pi})\exp\left(-i\gamma_5\theta_i\frac{\tau_i}{2}\right). \quad (2.66)$$

While we have suggestively named our new fields σ and $\boldsymbol{\pi}$, we shall refrain from referring to them as the sigma and pion for now. It is possible to show that the most general renormalisable Lagrangian of the nucleon σ and $\boldsymbol{\pi}$ is

$$\mathcal{L} = \bar{\Psi}_N i\not{\partial}\Psi_N + g\bar{\Psi}_N(\sigma + i\gamma_5\boldsymbol{\tau} \cdot \boldsymbol{\pi})\Psi_N + \frac{1}{2}(\partial_\mu\sigma)^2 + \frac{1}{2}(\partial_\mu\boldsymbol{\pi})^2 - \frac{\lambda^2}{4}\left((\sigma^2 + \boldsymbol{\pi}^2) - v^2\right)^2, \quad (2.67)$$

where λ^2 and v are undetermined constants. As we have stressed, by construction this Lagrangian is invariant under $SU(2)_V \times SU(2)_A$ transformations. Thus we have the corresponding currents

$$j_{V,i}^\mu = \Psi_N\gamma^\mu\frac{\tau_i}{2}\Psi_N + \epsilon_{ijk}\pi_j\partial^\mu\pi_k, \quad (2.68)$$

$$j_{A,i}^\mu = \Psi_N\gamma^\mu\gamma_5\frac{\tau_i}{2}\Psi_N - \pi_i\partial^\mu\sigma + \sigma\partial^\mu\pi_i, \quad (2.69)$$

which are conserved:

$$\partial_\mu j_{V,i}^\mu = 0, \quad (2.70)$$

$$\partial_\mu j_{A,i}^\mu = 0. \quad (2.71)$$

Let us examine the last term in our model more closely. We may extract the potential by noting that $\mathcal{V} = -\mathcal{L}_{\text{int}}$

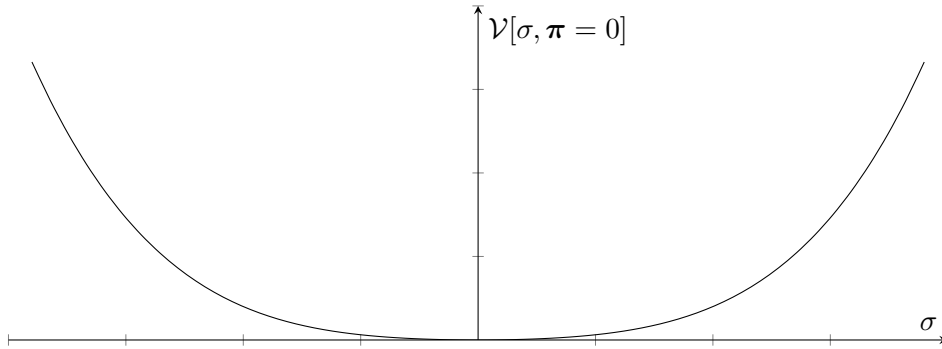


FIGURE 2.5: Wigner-Weyl realisation of symmetry in the sigma model. For simplicity, we choose the slice $\pi = 0$. The minimum of the potential exists at $\sigma_0 = 0$

$$\begin{aligned} \mathcal{V}[\sigma, \pi] &= \frac{\lambda^2}{4} \left((\sigma^2 + \pi^2) - v^2 \right)^2 \\ &= \frac{\lambda^2}{4} (\sigma^2 + \pi^2)^2 - \frac{\lambda^2 v^2}{2} (\sigma^2 + \pi^2) + \frac{\lambda^2 v^4}{4}. \end{aligned} \quad (2.72)$$

In order to ensure that the system is stable, we require that $\lambda^2 > 0$. Note however that there is no constraint on the sign of v^2 . Thus there are two possibilities. First consider $v^2 \leq 0$. In this case, the second term gives a mass term for the σ and π fields, and the potential in this case has its minimum at $\sigma_0 = \pi_0 = 0$ (see Fig. 2.5). In this case, both the sigma and pion have the same degenerate mass

$$m^2 = m_\sigma^2 = m_\pi^2 = \frac{\lambda^2 v^2}{2}, \quad (2.73)$$

while the nucleon remains massless. In this case, the π and σ are degenerate parity partners. This is exactly the Wigner-Weyl realisation of symmetry we have discussed. In other words, the symmetry of the Lagrangian manifests as a symmetry of the spectrum. As we have explained, this is not the realisation we observe in nature, so let us examine the case that $v^2 > 0$. Then we note that the potential no longer has a minimum at $\sigma = \pi = 0$. Rather, the potential now exhibits the so-called ‘Mexican hat’ potential, and the point $\sigma = \pi = 0$ corresponds to a local maximum (see Fig. 2.6). In this case, this point is no longer stable. Instead, the minimum of the potential occurs at

$$(\sigma^2 + \pi^2) - v^2 = 0. \quad (2.74)$$

This equation defines a surface in our abstract coordinates, and thus constitutes an infinite number of ground states. A sensible perturbation may be obtained around the vacuum state $\sigma_0 = v$, the vacuum expectation value. Thus we perform the change of variables

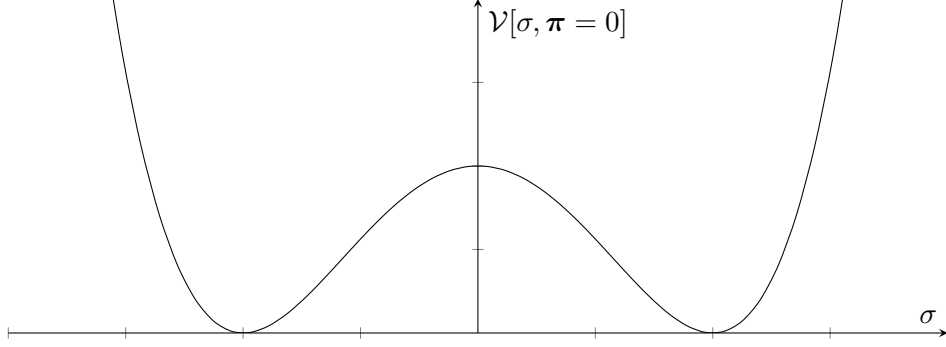


FIGURE 2.6: Goldstone realisation of symmetry in the sigma model. For simplicity, we choose the slice $\pi = 0$. Note that a minimum of the potential no longer exists at $\sigma = 0$.

$$\sigma \rightarrow \sigma_0 + \sigma. \quad (2.75)$$

Performing this substitution in the original Lagrangian, we find

$$\begin{aligned} \mathcal{L} = & \bar{\Psi}_N(i\not{\partial} + gv)\Psi_N + g\bar{\Psi}_N(\sigma + i\gamma_5\boldsymbol{\tau} \cdot \boldsymbol{\pi})\Psi_N + \frac{1}{2}(\partial_\mu\sigma)^2 - \frac{1}{2}(2\lambda^2v^2)\sigma^2 + \frac{1}{2}(\partial_\mu\boldsymbol{\pi})^2 \\ & - \frac{\lambda^2}{4}(\sigma^2 + \boldsymbol{\pi}^2)^2 - v\lambda^2\sigma(\sigma^2 + \boldsymbol{\pi}^2). \end{aligned} \quad (2.76)$$

We see that this process has produced a nucleon mass term

$$m_N = -g\sigma_0, \quad (2.77)$$

and also a mass for the σ field

$$m_\sigma^2 = 2\lambda^2\sigma_0^2, \quad (2.78)$$

but has left the triplet $\boldsymbol{\pi}$ field massless! That is

$$m_\pi^2 = 0. \quad (2.79)$$

This is the prediction of Goldstone's Theorem. We may now drop the pretense, and identify the isospin triplet field $\boldsymbol{\pi}$ as the pion field, since the field transforms as a pseudoscalar, and by deliberate construction, the theory possesses chiral symmetry and a massless pion. To describe this process as symmetry breaking is quite misleading. We emphasize again that the chiral symmetry which was explicit in the initial Lagrangian still exists as a conserved current:

$$\partial_\mu j_{V,i}^\mu = 0, \quad (2.80)$$

$$\partial_\mu j_{A,i}^\mu = 0, \quad (2.81)$$

but now this Lagrangian symmetry does not appear as a symmetry of our predicted spectrum. A better description would be that the symmetry has been *hidden*.

Note that thus far, we have spoken about massless pions. Recall that chiral symmetry is also explicitly broken by the small but non-zero quark mass terms. Thus we expect the pion to be a Pseudo-Goldstone Boson, rather than an exactly massless boson. In order to make contact with reality, we add an explicit symmetry breaking term $\mathcal{L}_{\text{SB}} = c\sigma$. This leads to non-conservation of the axial vector current, as required by PCAC.

Much more may be said about the Sigma Model, but for our purposes, this will suffice. Let us recall the main facts which led us here. We began by noting that while the massless QCD Lagrangian is invariant under $SU(3)_V \times SU(3)_A$, the spectrum is only invariant under $SU(3)_V$. We discussed the Wigner-Weyl and Goldstone realisations of a Lagrangian symmetry, and produce exactly the symmetry pattern we desired. We also noted that as a consequence of the Goldstone realisation, massless excitations, called Nambu-Goldstone bosons would appear in our spectrum. We then considered the Sigma Model as an explicit example of symmetry breaking, and the emergence of Nambu-Goldstone bosons, which after adding an explicit symmetry breaking term we were able to identify as the characteristically light pions.

2.3.5 Effective Field Theories

The Sigma Model is an example of a class of theories generally referred to as *effective field theories*. Effective field theories are integral to our understanding of nature. In particular, they allow us to neglect physics which occurs at energy scales Λ far higher than the energy scale of the experiment energy scale p (in other words, when $p/\Lambda \ll 1$), and thus focus on the physics relevant to the situation. This premise is rather intuitive and even perhaps self evident on reflection. It is the basis upon which the dynamics of non-relativistic objects may be predicted using Newtonian mechanics alone, without recourse to General Relativity. The same logic applies to quantum mechanical systems. Recall in the calculation of the energy levels of the Hydrogen atom that the Hamiltonian in the center of momentum frame is given by

$$H = \frac{\mathbf{p}^2}{2\mu} - \frac{\alpha}{r}, \quad (2.82)$$

where μ is the reduced mass of the electron. The predicted energy levels

$$E_n = -\frac{1}{2} \frac{\mu\alpha^2}{n^2} = \frac{-13.6 \text{ eV}}{n^2}, \quad (2.83)$$

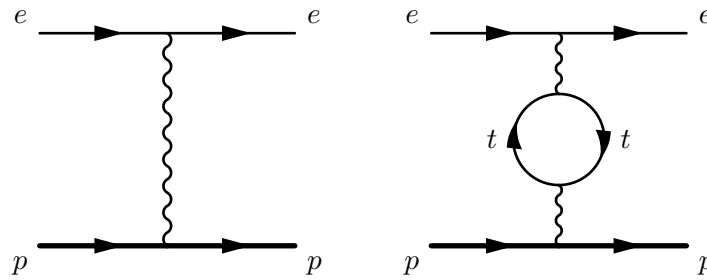


FIGURE 2.7: Diagrams which contribute to proton-electron bound state.

agree remarkably well with the experimental data. Note that a ‘more complete’ model of this process would describe the proton as a complicated QCD bound state where hadronic corrections to the electromagnetic interactions would also be calculated (see Fig. 2.7). Why then does our relatively simple quantum mechanical model of the hydrogen atom lead to such good predictions? We may understand this by considering the relative momentum scales in the problem. The natural energy scale for the exchanged photon is of the order of the electron mass, whereas the contribution from the hadronic vacuum polarisation diagram leads to a correction of the order

$$\delta E_{\bar{q}q} \propto \frac{m_e^2}{m_q^2} \lesssim 0.01. \quad (2.84)$$

In other words, this correction from quarks is very small, and ‘explains’ why our original predictions which neglected these effects gave such accurate results. The same argument can be used to explain why a description of the proton (with a mass of approximately 1 GeV) as a structureless object is valid. In other words, an effective field theoretic approach emphasizes the *physically relevant* degrees of freedom.

2.3.5.1 Understanding Divergences

Previously, we discussed the Sigma Model, as an example of a field theory which exhibits chiral symmetry breaking. One of the constraints which we used in writing down our Lagrangian was the requirement of *renormalisability*. While certainly important, a modern understanding of renormalisation leads us to the conclusion that the constraint of renormalisability on a quantum field theory has reduced importance. This section will motivate the form of the Lagrangian for chiral effective field theory.

As we have previously mentioned, the divergences one usually encounters when calculating loop corrections to amplitudes in quantum field theories were for a long time a source of confusion and concern. Even after the formal renormalisation procedure was developed much confusion existed about the procedure’s consistency. Notable amongst the doubters was Feynman, who was awarded the Nobel prize in part for his work in developing renormalisation and the cancellation of these divergences [11, 12]. In these calculations, the divergences are ‘tamed’ by modifying the loop integral to introduce a cutoff Λ at high momenta. In renormalisable theories, after the process of renormalisation is performed, resulting observables are independent of the cutoff, and one is free to ‘take Λ to infinity’. As we shall explain, the

modern interpretation due to Wilson [41] reinterprets the cutoff Λ as a physically meaningful energy scale at which the theory is expected to break down, rather than a mathematical trick used to ‘hide’ the divergences of the theory. To begin, we note that we conventionally define the action for a general field theory as

$$S = \int d^4x \mathcal{L} \quad (2.85)$$

where the important point is that we require the integration over all space. Taken literally, the above relation asserts that the field theory is well defined at all distances. There are reasons to believe that this is overconfident. Consider a description of QCD in terms of baryons and mesons. We expect that this theory can only be correct up to some energy scale where the internal effects of quarks and gluons can no longer be neglected. Let this energy scale be Λ . In the case of chiral effective field theory, it is not hard to imagine that the distance scale $1/\Lambda$ should be related to the size of the hadrons described in the theory. For distances much larger than this distance, we expect that an effective description should be valid, while for distances approaching our characteristic distance scale $1/\Lambda$, the probability of interactions between quarks and gluons in the hadrons becomes non-negligible and our description breaks down. Clearly, we should ‘cut off’ the theory at this energy scale. Importantly, we note that in the case of chiral effective field theory, the cutoff is *physically motivated*. While we have presented this argument for chiral effective field theory, Wilson [41] proposes that we understand this as a general requirement for field theories. In order to make this statement concrete, we modify our definition of the action to indicate that we should only integrate over the distance scales where we believe the theory to be well defined. We write

$$S \rightarrow S_\Lambda = \int_{1/\Lambda} d^4x \mathcal{L}, \quad (2.86)$$

where we again emphasize that in general, the cutoff Λ should be related to some physical restriction on the theory. This redefinition of our action has important consequences for the matrix elements we calculate and our understanding of renormalisation. The full implications of this redefinition of the action are beyond the scope of this discussion, but some important facts can be stated which will help to explain the development of chiral effective field theory discussed in the next section.

We first note that the modification to include a cutoff in the theory has the effect of rendering all matrix elements finite. Even within renormalisable field theories, infinities appeared, which were absorbed into the definitions of couplings and masses in the process of renormalisation. While this process led to predictions which were in agreement with experimental data, practitioners were concerned that the infinite corrections implied that the theory was not internally consistent. With Wilson’s modification, these divergences are now large but finite, and their mathematical manipulations are better behaved.

The finite cutoff Λ has further benefits. Wilson showed that if one considered the most general Lagrangian consistent with the symmetries (including the infinite number of non-renormalisable interactions):

$$\mathcal{L} = \sum_{i=0}^{\infty} g_i \mathcal{L}_{\text{int}}^i, \quad (2.87)$$

and considered a calculation at a momentum scale p far lower than the theory's cutoff Λ ($p \ll \Lambda$), that non-renormalisable interactions were proportional to positive powers of (p/Λ) , and were thus suppressed, leaving only renormalisable interactions. In other words, Wilson's analysis *explains* the requirement of renormalisable interactions [41]. As long as the momentum scale is sufficiently low when compared to the cutoff scale of the theory, only renormalisable interactions will be present in the low energy effective field theory. Historically, the renormalisation procedure was completed by 'taking $\Lambda \rightarrow \infty$ ', at the end of the calculation. Since in a renormalisable theory all observables are independent of the cutoff Λ , this has no effect on the predictions. In the Wilsonian understanding of renormalisation, we understand that the lack of dependence on Λ in physical quantities is a manifestation of the intuitive argument presented at the beginning of the section on effective field theories; namely that low energy processes (of energy scale $p \ll \Lambda$) are independent on the physics which occurs at a much higher energy scale Λ . In chiral effective field theory it turns out that the energy scales we wish to evaluate processes at are close to the cutoff scale Λ . As a result, we obtain contributions from so-called non-renormalisable interactions.

2.3.6 Constructing the Effective Lagrangian

We begin this section by quoting a postulate due to Weinberg [67]:

Quantum Field Theory has no content besides unitarity, analyticity, cluster decomposition and symmetries.

In general, there will be an infinite number of terms which satisfy these requirements, with most of these being traditionally regarded as non-renormalisable and thus 'bad'. As we have argued in the last section, in the context of effective field theories, these terms may be handled consistently, and after renormalisation, the theory will enable finite predictions. Following the theorem of Weinberg, we write

$$\mathcal{L} = \sum_{i=0}^{\infty} g_i \mathcal{L}_{\text{int}}^i, \quad (2.88)$$

where each term in this sum is consistent with the symmetries of the theory. Obviously, in order to make predictions, we must only retain a finite number of terms. In chiral effective field theory, we are interested in describing the *low energy* behavior of QCD. Thus we choose to arrange our interactions in terms of powers of momenta, or equivalently in position space, in powers of the derivative ∂_μ . In the following section, we construct the $SU(2)_L \times SU(2)_R$ chiral Lagrangian.

2.3.6.1 Pseudo-Scalar Pion Nucleon Theory

In this thesis, we shall mention two different pion-nucleon Lagrangians motivated by chiral symmetry. These two Lagrangians are known as the pseudo-scalar (PS) and pseudo-vector (PV) interactions, due to the form of the pion-nucleon coupling. As we shall explain, these two representations of the theory are equivalent, and lead to the same predictions for matrix elements. However the pseudo-scalar Lagrangian is unwieldy to use, as it requires a delicate cancellation of contributions from the pion and sigma fields to obtain the correct predictions.

We recall the Sigma Model we discussed previously:

$$\begin{aligned} \mathcal{L} = & \bar{\Psi}_N(i\not{\partial} + m_N)\Psi_N - g_{\pi N}\bar{\Psi}_N(\sigma + i\gamma_5\boldsymbol{\tau} \cdot \boldsymbol{\pi})\Psi_N + \frac{1}{2}(\partial_\mu\sigma)^2 - \frac{1}{2}m_\sigma^2\sigma^2 + \frac{1}{2}(\partial_\mu\boldsymbol{\pi})^2 \\ & - \frac{\lambda^2}{4}(\sigma^2 + \boldsymbol{\pi}^2)^2 - v\lambda^2\sigma(\sigma^2 + \boldsymbol{\pi}^2), \end{aligned} \quad (2.89)$$

where we have made the identifications $m_N = g_{\pi N}v$ and $m_\sigma^2 = 2\lambda^2v^2$. We introduce a mass term for the pion which explicitly breaks the chiral symmetry

$$\mathcal{L}_{\text{SB}} = -\frac{1}{2}m_\pi^2\boldsymbol{\pi}^2. \quad (2.90)$$

Thus to lowest order in the derivatives of the pion field, the Lagrangian is

$$\begin{aligned} \mathcal{L} = & \bar{\Psi}_N(i\not{\partial} + m_N)\Psi_N - g_{\pi N}\bar{\Psi}_N(\sigma + i\gamma_5\boldsymbol{\tau} \cdot \boldsymbol{\pi})\Psi_N + \frac{1}{2}(\partial_\mu\sigma)^2 - \frac{1}{2}m_\sigma^2\sigma^2 \\ & + \frac{1}{2}(\partial_\mu\boldsymbol{\pi})^2 - \frac{1}{2}m_\pi^2\boldsymbol{\pi}^2 - \frac{\lambda^2}{4}(\sigma^2 + \boldsymbol{\pi}^2)^2 - v\lambda^2\sigma(\sigma^2 + \boldsymbol{\pi}^2). \end{aligned} \quad (2.91)$$

Due to the difficulty with identifying the sigma meson, it was conventional to drop the sigma field, although this breaks the chiral symmetry. Nevertheless, this is the Lagrangian we refer to when we discuss the pseudo-scalar interaction:

$$\mathcal{L}_{\text{PS}} = \bar{\Psi}_N(i\not{\partial} + m_N)\Psi_N - g_{\pi N}\bar{\Psi}_Ni\gamma_5\boldsymbol{\tau} \cdot \boldsymbol{\pi}\Psi_N + \frac{1}{2}(\partial_\mu\boldsymbol{\pi})^2 - \frac{1}{2}m_\pi^2\boldsymbol{\pi}^2. \quad (2.92)$$

2.3.6.2 Pseudo-Vector Pion Nucleon Theory

Prior to neglecting the sigma field, the Sigma Model is chirally symmetric. However, it is unwieldy to deal with and modern implementations of chiral symmetry use a different Lagrangian. A result initially due to Haag [68] states that if two fields are non-linearly related the S-matrix elements and thus the physical predictions are equivalent. Thus we are free to perform non-linear transformations on our fields. Following Ref. [69], it is possible to perform

a non-linear transformation on the nucleon, pion and sigma fields which leaves the Lagrangian invariant under chiral $SU(2)_V \times SU(2)_A$, which leads to

$$\begin{aligned} \mathcal{L}_{\text{PV}} = & \bar{\Psi}_N(i\not{\partial} + m_N)\Psi_N + \frac{g_A}{2f_\pi}\Psi_N\gamma^\mu\gamma_5\boldsymbol{\tau}\cdot\partial_\mu\boldsymbol{\pi}\Psi_N - \frac{1}{2f_\pi^2}\Psi_N\gamma^\mu\boldsymbol{\tau}\cdot(\boldsymbol{\pi}\times\partial_\mu\boldsymbol{\pi})\Psi_N + \frac{1}{2}(\partial_\mu\boldsymbol{\pi})^2 \\ & - \frac{1}{2}m_\pi^2\boldsymbol{\pi}^2, \end{aligned} \tag{2.93}$$

where we have also used the Goldberger-Treiman relation

$$\frac{g_A}{f_\pi} = \frac{g_{\pi N}}{m_N}. \tag{2.94}$$

Note that we have removed reference to the sigma field. This is because after we perform the change of variables, the sigma field becomes irrelevant to the chiral symmetry, and it is possible to remove it without spoiling this symmetry. This is in contrast with the pseudo-scalar Lagrangian, where retention of the sigma field was necessary to preserve the chiral symmetry of the Lagrangian.

2.4 Conclusion

This concludes our discussion of quantum chromodynamics. We began by recalling the historical developments which culminated in the writing of the QCD Lagrangian. We then discussed the general properties of the Lagrangian formulation. In particular we saw how the non-Abelian nature of the theory led to differences in the gluonic field strength tensor when compared with the Abelian field strength tensor of Quantum Electrodynamics. This discussion of the differences between QCD and other field theories motivated a discussion of the characteristic features of QCD: asymptotic freedom and confinement. We emphasized that due to asymptotic freedom, QCD was a member of a class of physical theories which were well defined in the ultraviolet. This enabled us to make perturbative calculations at high energy, but invalidated this approach at low energy. We explained that in this energy regime, there is much evidence that QCD is confining, and we presented some of this evidence including the static quark potential calculated from lattice QCD. This explains the non-observation of quarks at low energy. Instead, low energy QCD is the study of hadrons; the composite bound states which appear due to the dynamics of QCD. This motivated the development of a low energy effective description in terms of these low energy excitations. We concluded by writing both the pseudoscalar and pseudovector forms of chiral effective field theory. These will be used in the following chapters.

The Electromagnetic Structure of Hadrons

How do we learn about more about the strong force? As we have seen, the strong force acts over short distances to ‘hide’ the fundamental degrees of freedom - the quarks and gluons - in colourless hadrons. This process is non-perturbative and, even today, is not well understood. Thus the objects we have at our disposal are the composite bound states of QCD. Note that while these particles are colour singlets, the quarks in QCD are also charged under the $U(1)$ of electromagnetism, and thus the bound states may also be electrically charged. Since QED is well understood and in particular perturbative, the use of electromagnetic probes gives us a way to precisely and cleanly study the structure of hadrons.

These electromagnetic interactions may be divided into two categories based on the final state of the hadron. The more complicated of these processes is so-called deep inelastic scattering where the final state of the hadron is not detected. As we have discussed, the deep inelastic structure functions carry a wealth of information about the dynamics of QCD. In comparison with deep inelastic scattering, elastic scattering requires that the initial and final hadron are the same. Some of the most well studied processes in this field are $ep \rightarrow ep$ and $e\pi \rightarrow e\pi$. In this chapter, we will discuss the structure functions available to us through these processes, and the current measurements of physical observables associated with these structure functions. We will then examine the form factors from a more theoretical perspective and show how the measured form factors arise from quantum field theory.

3.1 Baryon Electromagnetic Form Factors

Historically, the first hints of hadron structure go back to Otto Stern, who measured the magnetic moment of the proton in 1933 [70, 71]. While the Dirac equation predicts a magnetic moment of

$$\mu_N = \frac{e}{2m_p}, \tag{3.1}$$

where m_p is the proton mass, Stern and colleagues observed a much larger magnetic moment. Precise measurements today cite the magnetic moment as [43]

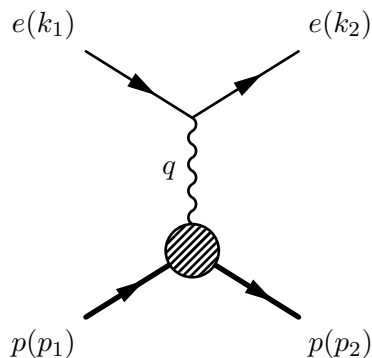


FIGURE 3.1: Elastic electron-proton scattering in the one-photon-exchange approximation. The momentum of the exchanged virtual photon is q .

$$\mu_p = 2.7928473446 \pm 0.0000000008 \mu_N. \quad (3.2)$$

In other words, it is almost three times as large! Further evidence for the internal structure was observed in elastic electron-proton scattering experiments in 1953 [72–74], where it was shown that in order to model the experimental data, a *form factor* which described the extended charge density was required. It is this particular approach which we will focus on in this thesis. Since the electron does not participate in strong interactions, this process leads to a clean measurement of the strong force dynamics. The lowest order QED contribution to this process is termed the *one-photon-exchange approximation* and the corresponding diagram is shown in Fig. 3.1. At this level of approximation (good to about one percent), electron-proton scattering may be understood to be mediated by a single virtual photon with four-momentum q . Momentum conservation requires that $q = p_2 - p_1 = k_1 - k_2$. Note that it is simple to show that in this process the photon is always space-like ($q^2 < 0$). Modern discussions of these form factors often define the invariant Q^2 , which is related to the photon virtuality q^2 via

$$Q^2 = -q^2, \quad (3.3)$$

so that space-like data will correspond to positive Q^2 . We shall also follow this convention. Although this study used only one form factor, in principle there exist two independent form factors for the proton. This is related to the two spin states of the proton. A particular parameterisation of these two structure functions is

$$\langle N(p_2) | J^\mu(q) | N(p_1) \rangle = \bar{u}(p_2) \left[\gamma^\mu F_1(Q^2) + \frac{i\sigma^{\mu\nu} q_\nu}{2m_N} F_2(Q^2) \right] u(p_1), \quad (3.4)$$

where the two form factors $F_1(Q^2)$ and $F_2(Q^2)$ are sometimes known as the Dirac and Pauli form factors respectively. This leads to a cross section of the form [75]

$$\frac{d\sigma}{d\Omega} = \left(\frac{d\sigma}{d\Omega} \right)_{\text{Mott}} \left(F_1^2(Q^2) + \frac{Q^2}{(2m_N)^2} \left[F_2^2(Q^2) + 2(F_1(Q^2) + F_2(Q^2))^2 \tan^2 \frac{\theta}{2} \right] \right), \quad (3.5)$$

where the Mott differential cross section is the predicted cross section for the scattering of a relativistic electron on spinless point-like particles. An elementary Dirac particle has

$$F_1(Q^2) = 1, \quad (3.6)$$

$$F_2(Q^2) = 0. \quad (3.7)$$

Often, the Sachs form factors are used. These are a re-parameterisation of the Dirac and Pauli form factors and are related by

$$G_E(Q^2) = F_1(Q^2) - \frac{Q^2}{4m_N^2} F_2(Q^2), \quad (3.8)$$

$$G_M(Q^2) = F_1(Q^2) + F_2(Q^2), \quad (3.9)$$

which allow for a simple extraction of G_E and G_M using the so-called Rosenbluth method. G_E and G_M are also known as the electric and magnetic form factors, since in the non-relativistic limit, they may be related to the Fourier transform of the electric and magnetic charge distributions. Note that modern experiments utilize a different technique, which utilizes polarization observables since it has been found that this method allows for a more sensitive extraction of the ratio of G_E/G_M [94]. Apart from the electromagnetic form factors themselves, there are several observables of interest which may be extracted from form factor data. We have already mentioned the magnetic moment, μ_B , of a baryon B . This may be extracted from the magnetic form factor evaluated at $Q^2 = 0$. More specifically, the ratio of the baryon's magnetic moment to the nuclear magneton, μ_N (defined above) is given by

$$\frac{\mu_B}{\mu_N} = G_M^B(0). \quad (3.10)$$

For completeness the proton and neutron magnetic moments are [43]:

$$\mu_p = 2.7928473446 \pm 0.0000000008 \mu_N, \quad (3.11)$$

$$\mu_n = -1.9130427 \pm 0.0000005 \mu_N. \quad (3.12)$$

The electric charge radius may also be extracted from form factor data. In particular, the square of the charge radius for a charged baryon is given by

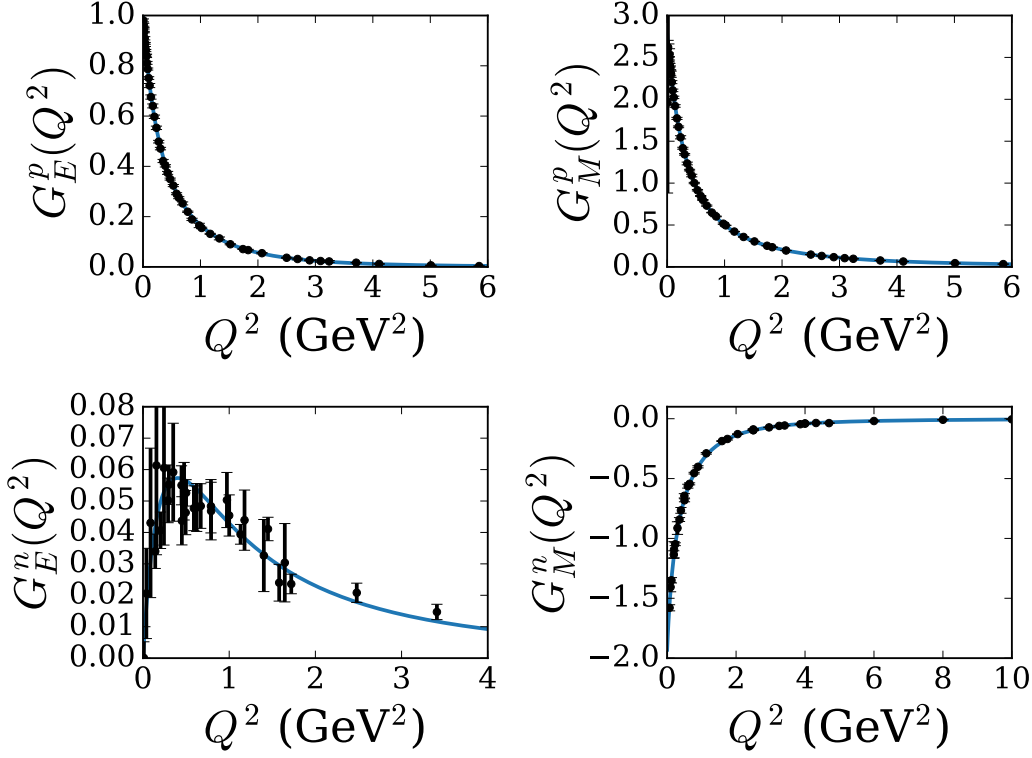


FIGURE 3.2: Electromagnetic form factors of the nucleon in the time-like region. Experimental data for the electric and magnetic form factors taken from the global analysis of Ref. [76]. Data for the electric form factor of the neutron is compiled from Refs. [77–85], while the magnetic form factor data is compiled from Refs. [86–92]. A simple empirical parameterization of the experimental data from Ref. [93] is also shown to guide the eye.

$$\langle r_i^2 \rangle_B = -\frac{6}{G_i^B(0)} \left. \frac{dG_i^B(Q^2)}{dQ^2} \right|_{Q^2=0}, \quad (3.13)$$

where $i = E, M$. The electric charge radius for neutral particles may be found by replacing the factor $G_i^B(0)$ with unity. The electric charge radii for the proton and neutron are (note that we have taken the square root):

$$\langle r_E^2 \rangle_p^{1/2} = 0.84087 \pm 0.00039 \text{ fm}, \quad (3.14)$$

$$\langle r_E^2 \rangle_p^{1/2} = 0.8751 \pm 0.0061 \text{ fm}, \quad (3.15)$$

$$\langle r_E^2 \rangle_n^{1/2} = 0.864 \pm 0.009 \text{ fm}. \quad (3.16)$$

These results are taken from Ref. [43]. Note that we have included two values for the proton charge radius. The first comes from spectroscopic measurements of muonic hydrogen, while

the second comes from low energy electron-proton elastic scattering. At the time of writing, these two measurements disagree by over 7σ [43].

3.2 The Pion's Electromagnetic Form Factor

The pion is a spin zero meson. Thus unlike the nucleon, the pion only has one electromagnetic form factor. In analogy with the above discussion for the nucleon, the electromagnetic structure of the pion may be probed by performing electron-pion elastic scattering. This is shown in Fig. 3.3. Again, we label the momentum of the virtual photon q . The pion form factor is defined as

$$\langle \pi(k_2) | J^\mu(q) | \pi(k_1) \rangle = (k_1 + k_2)^\mu F_\pi(Q^2), \quad (3.17)$$

where k_1 and k_2 are the initial and final four-momentum vectors of the pion, respectively. The electric charge radius of the pion is defined by

$$\langle r_E^2 \rangle_\pi = -6 \frac{dF_\pi(Q^2)}{dQ^2}. \quad (3.18)$$

Experimentally, this is measured to be [95]:

$$\langle r_E^2 \rangle_\pi^{1/2} = 0.672 \pm 0.008 \text{ fm}. \quad (3.19)$$

So far our discussion has focused on the experimental observables we may obtain from studying the electromagnetic form factors. Having now appreciated the importance of the measurement of these structure functions, we now consider these functions from a theoretical perspective. In particular, we show how these form factors emerge from quantum field theory by considering the gauge symmetry of the electromagnetic interaction.

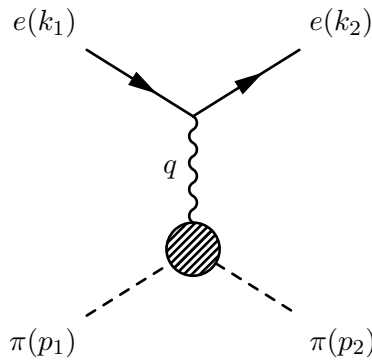


FIGURE 3.3: Elastic electron-pion scattering in the one-photon-exchange approximation. The momentum of the exchanged virtual photon is q .

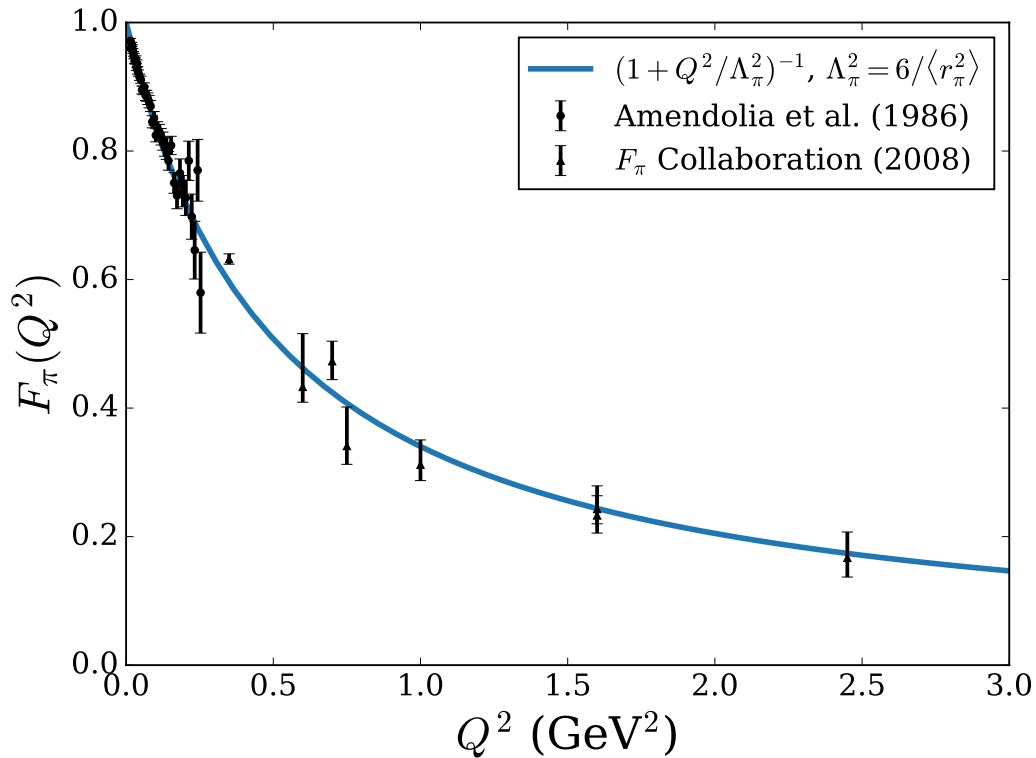


FIGURE 3.4: Electromagnetic form factor for the pion in the space-like region. Experimental data has been taken from Refs. [96, 97] and a simple monopole fit has been included to guide the eye.

3.3 Gauge Invariance and the Ward-Takahashi Identities

While our earlier discussion of the electromagnetic form factors was based on the experimental observables, we now take a theoretical point of view, and derive the most general form of the matrix element for electromagnetic interactions with hadrons. By applying certain limits, we see how this matrix element reduces to the forms discussed in the previous sections. Of the symmetries used, the gauge symmetry of Quantum Electrodynamics is particularly important, and we pause our discussion of electromagnetic form factors to explore this concept in more detail.

3.3.1 Classical Electromagnetic Gauge Invariance

We begin our discussion of electromagnetic gauge invariance with classical electromagnetism. There, we define the four-vector A^μ as

$$A^\mu = (V, \mathbf{A}), \quad (3.20)$$

where V is the scalar potential and \mathbf{A} is the vector potential. This decision is motivated by a desire to produce a covariant formulation of electromagnetism. One defines the field strength tensor $F_{\mu\nu}$ as

$$F_{\mu\nu} = \partial_\mu A_\nu - \partial_\nu A_\mu. \quad (3.21)$$

This enables us to write the Lagrangian density for electromagnetism as

$$\mathcal{L} = -\frac{1}{4}F_{\mu\nu}F^{\mu\nu}. \quad (3.22)$$

Applying the Euler-Lagrange equations yields the classical equations of motion for the photon.

$$\partial_\mu F^{\mu\nu} = \partial^2 A^\nu - \partial_\mu \partial^\nu A^\mu = 0. \quad (3.23)$$

The issue of gauge invariance arises because there are transformations of the A^μ field which leave the equations of motion unchanged; performing the field redefinition $A^\mu \rightarrow A'^\mu = A^\mu + \partial^\mu \chi$ leads to the same Lagrangian and thus the same equations of motion. This will lead to an overcounting of physically distinct states. Physically, we may understand this complication by noting that electromagnetic waves have two possible polarization states but the Lagrangian currently has four independent degrees of freedom. Thus we have two redundant degrees of freedom, and we must apply two constraints to fully define the field equations. We call these conditions gauge fixing conditions. The first of these conditions is

$$\partial_\mu A^\mu = 0. \quad (3.24)$$

This reduces the number of independent degrees of freedom of the A^μ field from four to three. In the classical theory of electromagnetism, this condition is known as the Lorenz Condition; in the quantized theory, it corresponds to Feynman gauge. In any case, with this condition, the equation of motion for the electromagnetic field becomes

$$\partial^2 A^\nu = 0. \quad (3.25)$$

Note that the aforementioned gauge freedom has been removed. Since we are still dealing with the classical field, we may immediately solve this differential equation to yield the plane wave solutions for A^μ :

$$A^\mu = N \epsilon^\mu e^{-ik \cdot x}, \quad (3.26)$$

where ϵ^μ is the so-called polarization tensor. As a result of the equation of motion, we have the constraint that $k^2 = 0$. Physically, this is a result of the photon being massless. The gauge fixing condition leads to the further constraint on the polarization tensor that

$$k \cdot \epsilon = 0. \quad (3.27)$$

There is still one residual gauge degree of freedom. Consider the transformation $A^\mu \rightarrow A'^\mu = A^\mu + \partial^\mu \phi$, where we require that additionally, ϕ is a solution to the massless Klein-Gordon Equation:

$$\partial^2 \phi = 0. \quad (3.28)$$

With this extra constraint, the gauge fixed equation of motion still exhibits gauge freedom. This symmetry in A^μ corresponds to the property that ϵ'^μ is also a valid polarization tensor provided it is related to ϵ^μ via

$$\epsilon'^\mu = \epsilon^\mu + \beta k^\mu, \quad (3.29)$$

since

$$k \cdot \epsilon' = k \cdot \epsilon + \beta k^2 = 0, \quad (3.30)$$

where the *physical* photon is massless. We can further gauge fix by choosing β such that the time component of the polarization vector vanishes. Thus we take

$$\beta = -\frac{\epsilon^0}{k^0}. \quad (3.31)$$

As a result of this choice, we have the two constraints

$$\epsilon^0 = 0, \quad (3.32)$$

$$\mathbf{k} \cdot \boldsymbol{\epsilon} = 0. \quad (3.33)$$

Thus our two constraints reduce the four polarization states to two, as anticipated. Having now studied the classical theory, we move to the quantum theory, where there arise some extra difficulties from the quantization of the theory. Although we will discuss briefly these complications, and their solution, we mention QED mainly to examine the Ward-Takahashi Identities which are applicable to QCD, and our study of hadronic form factors.

3.3.2 Quantum Electrodynamics

The prototypical quantum field theory is Quantum Electrodynamics. Importantly, from a modern standpoint, the electromagnetic interactions may be understood as a result of the gauge principle. The Lagrangian density is given as

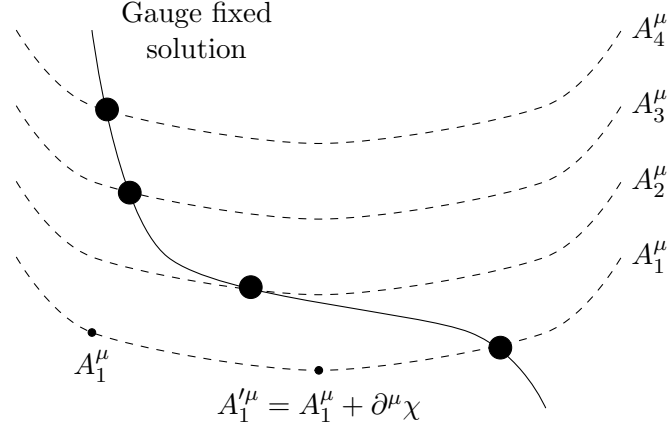


FIGURE 3.5: In calculating physical processes, we would like to count each physically distinct state only once. However, before gauge fixing there exist an infinite number of valid configurations for $A^\mu, A'^\mu, A''^\mu, \dots$ related by the gauge transformation $A^\mu \rightarrow A'^\mu = A^\mu + \partial^\mu \chi$ which correspond to the same physical state. These ‘lines of constant physics’ are depicted as dashed lines. The gauge transformation propagates us along this line. Each of the physically distinct states is denoted with a subscript. By gauge fixing, we pick out a subspace, which chooses from each line of constant physics, exactly one configuration. Thus the gauge fixed solution may be depicted as a curve which intercepts each gauge orbit exactly once.

$$\mathcal{L}_{\text{QED}} = \bar{\psi}(i\not{\partial} - m)\psi - \frac{1}{4}F_{\mu\nu}F^{\mu\nu} + \bar{\psi}A\psi. \quad (3.34)$$

This Lagrangian possesses the same gauge symmetries as the classical theory, and it can be shown that these gauge symmetries lead to difficulties when the photon propagator is calculated. The problem with these gauge symmetries is most easily understood in the path integral formalism but the full development of this idea is beyond the scope of this discussion. Note however that in the path integral formalism heuristically we ‘sum over all possible field configurations’. In this summation, we include an infinite number of states related by a gauge transformation which correspond to the same physical state. Thus clearly we must gauge fix to prevent the over counting of physical states (see Fig. 3.5). Since we now interpret $A^\mu(x)$ as an operator, we cannot implement the Lorenz condition $\partial_\mu A^\mu = 0$. Instead, it is possible to show that one may implement the gauge fixing condition by modifying the Lagrangian to incorporate the term

$$\mathcal{L}_{\text{GF}} = -\frac{1}{2\xi}(\partial_\mu A^\mu)^2. \quad (3.35)$$

The (formal) equation of motion is now

$$\partial_\mu F^{\mu\nu} = \partial^2 A^\nu - \left(1 - \frac{1}{\xi}\right)\partial_\mu \partial^\nu A^\mu = 0. \quad (3.36)$$

For $\xi = 1$, we obtain the equivalent of the Lorenz gauge fixing condition. Thus the gauge fixed QED Lagrangian is

$$\mathcal{L}_{\text{QED}} = \bar{\psi}(i\not{\partial} - m)\psi - \frac{1}{4}F_{\mu\nu}F^{\mu\nu} + \bar{\psi}\not{A}\psi - \frac{1}{2\xi}(\partial_\mu A^\mu)^2. \quad (3.37)$$

As with the classical theory, even after gauge fixing, this theory still exhibits residual gauge symmetry. The Lagrangian is invariant under the simultaneous gauge transformations

$$\psi \rightarrow \psi' = e^{i\chi(x)}\psi, \quad (3.38)$$

$$A^\mu \rightarrow A'^\mu = A^\mu + \partial^\mu\chi(x), \quad (3.39)$$

provided $\partial^2\chi(x) = 0$. As with the classical theory, we further restrict the polarization vector for physical photons by requiring that $\epsilon^0 = 0$. Thus the polarization vector is the same as the classical case.

$$\epsilon^0 = 0, \quad (3.40)$$

$$\mathbf{k} \cdot \boldsymbol{\epsilon} = 0. \quad (3.41)$$

From Noether's Theorem, we expect this symmetry to produce a conserved current $j^\mu(x)$. As we have seen in the previous chapter, classical symmetries do not necessarily survive the quantization procedure. In the case of the gauge symmetry, this is not the case, although quantization does modify the form of this conserved current. In particular, for physical external photons, the conserved current is exactly as in the classical theory. However, for matrix elements with virtual photons which are off their mass shell, there are modifications to the classical result. One may understand why this must be so by considering the second gauge invariance of the classical theory. Recall that the residual degree of freedom arose because we were able to define a new polarization tensor ϵ'^μ via

$$\epsilon'^\mu = \epsilon^\mu + \beta k^\mu, \quad (3.42)$$

since the physical photon was massless, and thus satisfied a massless dispersion relation $k^2 = 0$. In quantum field theory, photons which are off their mass shell will not have $k^2 = 0$, and thus in this case, there is no additional symmetry. In the quantum field theory, the conservation of this current is expressed in momentum space by the so-called *Ward-Takahashi Identities*, which we shall now derive explicitly.

While this discussion is based on electrodynamics, we note that Nishijima has shown that even in the absence of the explicit form of the Lagrangian, the gauge symmetry will lead to a conserved current, and corresponding Ward-Takahashi Identities [98]. Thus although our discussion of gauge invariance and current conservation has focused on QED, the general principles are also applicable to the electromagnetic interactions in QCD.

3.3.3 The Ward-Takahashi Identity

We begin our discussion of the Ward-Takahashi Identity by first determining the result from the classical theory. It is possible to show that Noether's Theorem implies that the current

$$j_{\text{clas.}}^\mu(x) = \bar{q}(x)\gamma^\mu q(x) \quad (3.43)$$

is conserved. The Ward-Takahashi Identities are usually written in momentum space. We may convert this relation to momentum space by using the Fourier transform:

$$\begin{aligned} \partial_\mu j_{\text{clas.}}^\mu(x) = 0 &= \partial_\mu \int \frac{d^4k}{(2\pi)^4} e^{-ik \cdot x} \Gamma_{\text{clas.}}^\mu(k) \\ &= \int \frac{d^4k}{(2\pi)^4} e^{-ik \cdot x} (-ik_\mu) \Gamma_{\text{clas.}}^\mu(k), \end{aligned} \quad (3.44)$$

where we have defined the Fourier transform of the conserved current $j_{\text{clas.}}^\mu(x)$ as $\Gamma_{\text{clas.}}^\mu(k)$. Thus in our classical theory, we have

$$-ik_\mu \Gamma_{\text{clas.}}^\mu(k) = 0. \quad (3.45)$$

In this section, we shall derive the quantum mechanical version of this relation. As we have alluded to, the virtual particles modify the classical result, resulting in

$$-ik_\mu \Gamma^\mu(k; p_1, p'_1) = S_F^{-1}(p'_1) - S_F^{-1}(p_1). \quad (3.46)$$

We will see that in the limit that all the particles go on-shell, we recover the classical result. This more general result is also known as one of the Ward-Takahashi Identities. These identities are true order-by-order, and so it suffices to prove them for a diagram of arbitrary order. This proof is partially diagrammatic, so for completeness, we recall the Feynman Rules for QED. We write the fermionic propagator as:

$$\begin{array}{c} \longrightarrow \\ p \end{array} = S_F(p) = \frac{i(\not{p} + m)}{p^2 - m^2}, \quad (3.47)$$

the photon (in Feynman gauge) as:

$$\begin{array}{c} \mu \\ \text{~~~~~} \\ k \end{array} \nu = \frac{-ig^{\mu\nu}}{k^2}, \quad (3.48)$$

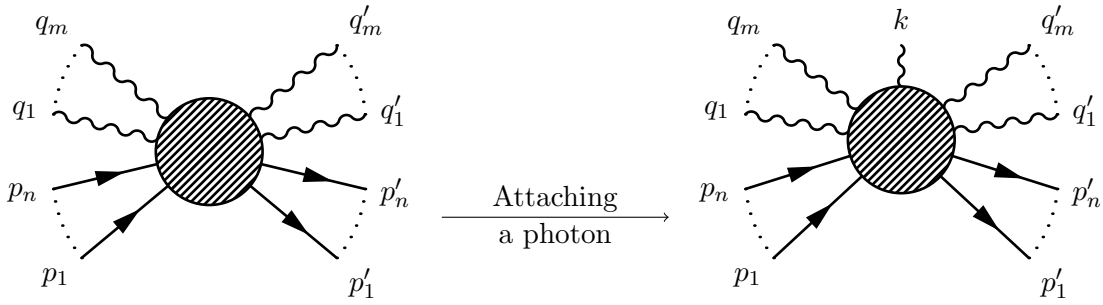


FIGURE 3.6: An electromagnetic process involving n fermions and m photons. Initial states have ingoing momentum, and final states have outgoing momentum, so that conservation of momentum gives $\sum p_i + \sum q_j = \sum p'_i + \sum q'_j$.

and the interaction as

$$\begin{array}{c} \text{wavy line} \\ | \\ \text{--->--->} \end{array} = -ie\gamma^\mu. \tag{3.49}$$

Consider a diagram which contributes at order $\mathcal{O}(\alpha^n)$ to the process involving n fermions and m photons, where the momenta of the individual particles is shown in Fig. 3.6. We may calculate the related process where there are $m + 1$ photons by attaching this photon in all possible ways to all diagrams which contribute to the amplitude containing m photons. We denote one contribution to this amplitude as $\delta\mathcal{M}_0$. From the Feynman Rules it is trivial to see that the photon may only couple to the fermion field (there is no tree level photon self interaction). In any diagram, fermion lines are either external legs, which pass through the diagram, or internal loops. Thus when attaching a photon to the graph $\delta\mathcal{M}_0$ one may only attach it to an external fermion line, or to an internal fermion loop. In order to attach a photon in all possible ways, both cases must be considered.

3.3.3.1 Coupling Photon to External Line

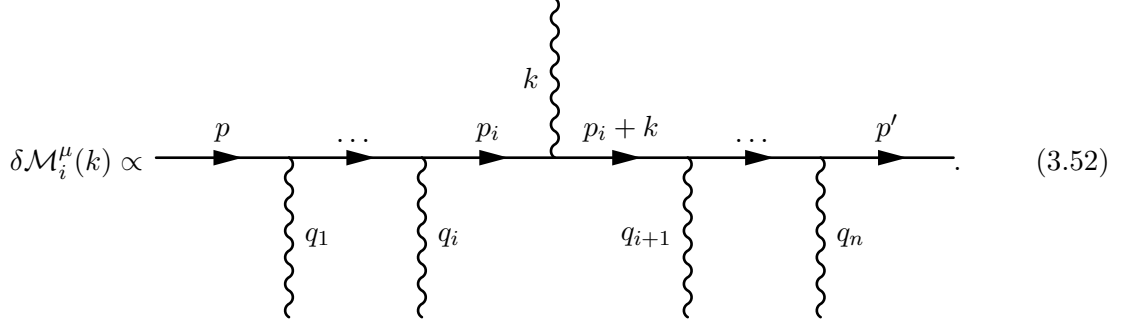
Consider first the case where the photon connects to an external line. Prior to the insertion, the relevant part of the graph $\delta\mathcal{M}_0$ will be given by

$$\delta\mathcal{M}_0 \propto \begin{array}{c} \text{--->--->} \\ | \quad | \quad | \quad | \\ \text{wavy} \quad \text{wavy} \quad \text{wavy} \quad \text{wavy} \\ q_1 \quad q_2 \quad q_{n-1} \quad q_n \end{array} \tag{3.50}$$

Using the Feynman Rules, it is possible to write this part of the diagram as

$$\delta\mathcal{M}_0 \propto S_F(p')(-ie\gamma^{\nu_n})S_F(p_{n-1})(-ie\gamma^{\nu_{n-1}})\dots(-ie\gamma^{\nu_1})S_F(p). \quad (3.51)$$

Consider attaching the photon after the i^{th} internal photon exchange. This new diagram will contribute to $\mathcal{M}^\mu(k)$.



$$\delta\mathcal{M}_i^\mu(k) \propto \text{---} \xrightarrow{p} \text{---} \xrightarrow{\dots} \xrightarrow{p_i} \text{---} \xrightarrow{p_i+k} \text{---} \xrightarrow{\dots} \xrightarrow{p'} \text{---}. \quad (3.52)$$

As before, one may write the amplitude for this diagram as

$$\begin{aligned} \delta\mathcal{M}_i^\mu \propto S_F(p'+k)(-ie\gamma^{\nu_n})S_F(p_{n-1}+k)(-ie\gamma^{\nu_{n-1}})\dots S_F(p_i+k) \\ \times (-ie\gamma^\mu)S_F(p_i)\dots(-ie\gamma^{\nu_1})S_F(p). \end{aligned} \quad (3.53)$$

Consider contracting this amplitude with k_μ . We can write

$$\begin{aligned} S_F(p_i+k)(-ie\cancel{k})S_F(p_i) &= eS_F(p_i+k)[-i(\cancel{k} + \not{p}_i - m) + i(\not{p}_i - m)]S_F(p_i) \\ &= eS_F(p_i+k)[S_F^{-1}(k+p_i) - S_F^{-1}(p_i)]S_F(p_i) \\ &= e[S_F(p_i) - S_F(p_i+k)]. \end{aligned} \quad (3.54)$$

Inserting this in the above expression leads to

$$\begin{aligned} k_\mu \delta\mathcal{M}_i^\mu \propto S_F(p'+k)(-ie\gamma^{\nu_n})S_F(p_{n-1}+k)(-ie\gamma^{\nu_{n-1}})\dots \\ \times e[S_F(p_i) - S_F(p_i+k)]\dots(-ie\gamma^{\nu_1})S_F(p). \end{aligned} \quad (3.55)$$

Consider now inserting the photon one place further to the left. This will lead to

$$\begin{aligned} k_\mu \delta\mathcal{M}_{i-1}^\mu \propto S_F(p'+k)(-ie\gamma^{\nu_n})S_F(p_{n-1}+k)(-ie\gamma^{\nu_{n-1}})\dots \\ \times e[S_F(p_{i-1}) - S_F(p_{i-1}+k)]\dots(-ie\gamma^{\nu_1})S_F(p). \end{aligned} \quad (3.56)$$

Adding these two expressions (since in general one wishes to sum over i), leads to cancellation between the second term of (3.55) and the first term of (3.56). It is easy to see that this pattern will continue between adjacent sites, and so after summing up all possible insertions, the external ends of this sum will be the only surviving terms. That is

$$\sum_{\text{insertions}} k_\mu \delta \mathcal{M}_i^\mu \propto e \left[S_F(p')(-ie\gamma^{\nu_n})S_F(p_{n-1})(-ie\gamma^{\nu_{n-1}}) \dots (-ie\gamma^{\nu_1})S_F(p) \right. \\ \left. - S_F(p'+k)(-ie\gamma^{\nu_n})S_F(p_{n-1}+k)(-ie\gamma^{\nu_{n-1}}) \dots (-ie\gamma^{\nu_1})S_F(p+k) \right]. \quad (3.57)$$

Pictorially one may write this relation as

$$\sum_{\text{insertions}} k_\mu \delta \mathcal{M}_i^\mu \propto e \left[\begin{array}{c} \xrightarrow{p} \xrightarrow{p'} \\ \begin{array}{c} \text{wavy } q_1 \\ \vdots \\ \text{wavy } q_n \end{array} \end{array} - \begin{array}{c} \xrightarrow{p+k} \xrightarrow{p'+k} \\ \begin{array}{c} \text{wavy } q_1 \\ \vdots \\ \text{wavy } q_n \end{array} \end{array} \right]. \quad (3.58)$$

Note that so far, we have only considered coupling photons to external fermion lines. We must now consider the coupling of photons to internal loops.

3.3.3.2 Attaching Photon to Internal Loops

Consider a general fermion loop, again with n photon insertions. Since this will also contribute to \mathcal{M}_0 , one has

$$\delta \mathcal{M}_0 \propto \begin{array}{c} q_1 \\ \begin{array}{c} \text{wavy } q_1 \\ \text{wavy } q_2 \\ \vdots \\ \text{wavy } q_i \\ \text{wavy } q_{i+1} \\ \text{wavy } q_n \end{array} \end{array} \quad (3.59)$$

As before, it is simple to write down the contribution to the amplitude from this fermion loop. One finds

$$\delta \mathcal{M}_0 \propto \int \frac{d^4 p_1}{(2\pi)^4} (-1) \text{Tr} \left[S_F(p_n)(-ie\gamma^{\nu_n}) \dots (-ie\gamma^{\nu_2})S_F(p_1)(-ie\gamma^{\nu_1}) \right]. \quad (3.60)$$

Consider attaching a photon between the i^{th} and $(i+1)^{\text{th}}$ photon insertions. This will lead to a rather similar situation to the above case of an external fermion line. One may represent this as

$$\delta\mathcal{M}^\mu(k) \propto \text{Diagram} \quad (3.61)$$

and so

$$\delta\mathcal{M}^\mu(k) \propto \int \frac{d^4 p_1}{(2\pi)^4} (-1) \text{Tr} \left[S_F(p_n + k)(-ie\gamma^{\nu_n}) \dots S_F(p_{i+1} + k)(-ie\gamma^\mu) S_F(p_i) \dots \right. \\ \left. \times (-ie\gamma^{\nu_2}) S_F(p_1)(-ie\gamma^{\nu_1}) \right]. \quad (3.62)$$

Contracting against k_μ again leads to

$$k_\mu \delta\mathcal{M}^\mu \propto \int \frac{d^4 p_1}{(2\pi)^4} (-1) \text{Tr} \left[S_F(p_n + k)(-ie\gamma^{\nu_n}) \dots e[S_F(p_i) - S_F(p_i + k)] \dots \right. \\ \left. \dots (-ie\gamma^{\nu_2}) S_F(p_1)(-ie\gamma^{\nu_1}) \right]. \quad (3.63)$$

In exactly the same way as for the external fermion line, summing over all possible photon insertions leads to cancellation between adjacent terms, and only the initial and final terms survive.

$$\sum_{\text{insertions}} k_\mu \delta\mathcal{M}^\mu \propto \int \frac{d^4 p_1}{(2\pi)^4} (-1) \text{Tr} \left[S_F(p_n)(-ie\gamma^{\nu_n}) \dots (-ie\gamma^{\nu_2}) S_F(p_1)(-ie\gamma^{\nu_1}) \right] \\ - \int \frac{d^4 p_1}{(2\pi)^4} (-1) \text{Tr} \left[S_F(p_n + k)(-ie\gamma^{\nu_n}) \dots (-ie\gamma^{\nu_2}) S_F(p_1 + k)(-ie\gamma^{\nu_1}) \right]. \quad (3.64)$$

Note however that since p_1 is a dummy variable which is integrated over, we may shift the integration variable $p_1 \rightarrow p_1 + k$ and so these two terms cancel as well. Thus diagrams in which a photon couples to an internal loop sum to zero:

$$\sum_{\text{insertions}} k_\mu \delta \mathcal{M}^\mu = 0. \quad (3.65)$$

As a result, the only contributions to the object $k_\mu \mathcal{M}^\mu$ originate from coupling a photon to an external fermion line. For each external line, we obtain a contribution of the form (3.57), and so summing over all contributing diagrams leads to the final Ward-Takahashi Identity

$$k_\mu \mathcal{M}^\mu(k; p_1, \dots, p_n, p'_1, \dots, p'_n) = e \sum_{i=1}^n \left[\mathcal{M}_0(p_1, \dots, p_n, p'_1, \dots, (p'_i - k), \dots, p'_n) - \mathcal{M}_0(p_1, \dots, (p_i + k), \dots, p_n, p'_1, \dots, p'_n) \right], \quad (3.66)$$

where we recall that the initial matrix element is

$$\mathcal{M}_0(p_1, \dots, p_n, p'_1, \dots, p'_n) = \text{Diagram} \quad (3.67)$$

and the matrix element which contains an extra photon is

$$\mathcal{M}^\mu(k; p_1, \dots, p_n, p'_1, \dots, p'_n) = \text{Diagram} \quad (3.68)$$

The most well known of these Ward-Takahashi Identities relates the fermion propagator with the electromagnetic vertex. Using the relation we have proved, we have

$$k_\mu \mathcal{M}^\mu(k; p_1, p'_1) = e[\mathcal{M}_0(p_1) - \mathcal{M}_0(p'_1)]. \quad (3.69)$$

The quantities on the right hand side are simply the fully dressed fermion propagators evaluated at p_1 and p'_1 , respectively. The full three point amplitude is a product of the fully dressed fermion propagators times the amputated scattering diagram. In this case, this is just the vertex function $\Gamma^\mu(k; p_1, p'_1)$. Thus we have

$$S_F(p'_1)[-iek_\mu \Gamma^\mu(k; p_1, p'_1)]S_F(p_1) = e[S_F(p_1) - S_F(p'_1)]. \quad (3.70)$$

A simple manipulation of this expression leads to the well known result:

$$-ik_\mu \Gamma^\mu(k; p_1, p'_1) = S_F^{-1}(p'_1) - S_F^{-1}(p_1). \quad (3.71)$$

It is this relation which we will use to constrain the form of the electromagnetic interactions. Note that in the limit that the initial and final fermions are physical, this relation reduces to

$$k_\mu \Gamma^\mu(k; p_1, p'_1) = 0. \quad (3.72)$$

Thus ensuring that for physical matrix elements the current is conserved, as we would expect from the classical theory. Having now discussed in detail the Ward-Takahashi Identity, we are now in a position to understand the theoretical basis for the electromagnetic form factors of hadrons we described at the beginning of the chapter. We begin this analysis with the spin-zero system.

3.4 The Spin-Zero System

In order to constrain the most general form of the electromagnetic vertex, we note that the electromagnetic field $A_\mu(x)$ transforms as a vector under Lorentz boosts. To form a Lorentz scalar suitable for an interaction term in the Lagrangian, we conclude that we must contract $A_\mu(x)$ with a current which also transforms as a vector. That is,

$$\mathcal{L}_{\text{int}} = J^\mu(x)A_\mu(x), \quad (3.73)$$

where the current $J^\mu(x)$ is a product of fields. We define the most general form of the electromagnetic vertex Γ^μ which we require to transform as a vector under Lorentz transformations. We can further decompose this function by considering its momentum dependence. We denote the spin-zero hadron's initial momentum by k_1 and its final momentum k_2 . Conservation of momentum requires that the photon have momentum $q = k_2 - k_1$. In general, the vertex function will be dependent on all three of these variables and so

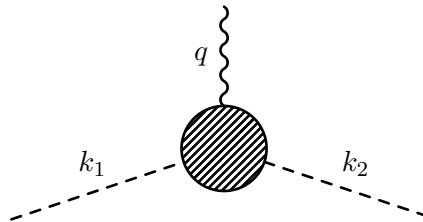


FIGURE 3.7: Electromagnetic vertex for spin-zero hadron. We denote the initial hadron momentum as k_1 , the final hadron momentum as k_2 and the photon momentum as q . The flow of momentum is fixed by the condition $k_2 = k_1 + q$

$$\Gamma^\mu = \Gamma^\mu(k_1, k_2; q). \quad (3.74)$$

Pictorially, we represent the dressed vertex as shown in Fig. 3.7. Since the vertex function transforms as a vector, so must all the terms which comprise it. Only the external four-momenta of the particles have the correct transformation properties. We note that since the three momenta are constrained by momentum conservation ($k_2 = k_1 + q$), there are only two degrees of freedom. Thus we only need two vectors to span the space. A particular choice gives

$$\Gamma^\mu(k_1, k_2; q) = f_1(k_1^2, k_2^2; q^2)(k_1 + k_2)^\mu + f_2(k_1^2, k_2^2; q^2)(k_1 - k_2)^\mu, \quad (3.75)$$

where f_1 and f_2 must be Lorentz invariant scalar functions.

3.4.1 On-Shell Vertex

Finally, we may use the Ward-Takahashi identity to further constrain the form factors. We note that the relevant Ward-Takahashi identity is

$$-iq_\mu \Gamma^\mu(k_1, k_2; q) = D_F^{-1}(k_2) - D_F^{-1}(k_1), \quad (3.76)$$

where D_F is the most general form of the corresponding Feynman propagator for a spin-zero field:

$$D_F(k_1) = \frac{i}{k_1^2 - m^2 - \Sigma(k_1^2)}. \quad (3.77)$$

We define $\Sigma(k_1^2)$ as the self-energy, which may be obtained as the sum of one-particle-irreducible (1PI) graphs. Note that in the limit where $k_1^2 = k_2^2 = m^2$, the Ward Takahashi Identity reduces to

$$q_\mu \Gamma^\mu(k_1, k_2; q) = 0. \quad (3.78)$$

Thus in this limit, the Ward Takahashi provides a further constraint on the form of the electromagnetic form factors for the spin-zero system. We note that

$$q \cdot (k_1 + k_2) = k_2^2 - k_1^2 = 0 \quad (3.79)$$

in the on-shell limit. Thus the Ward-Takahashi identity reduces to

$$q_\mu \Gamma^\mu(k_1, k_2; q) = 0 = f_2(m^2, m^2; q^2)q^2. \quad (3.80)$$

Since we have no further constraints, this relation must be true at arbitrary photon momentum. Thus we must conclude that

$$\Gamma^\mu(k_1, k_2; q) = f_1(m^2, m^2; q^2)(k_1 + k_2)^\mu. \quad (3.81)$$

Comparing this with our earlier discussion of the pion form factor, we may make the identification

$$F_\pi(q^2) = f_1(m^2, m^2; q^2). \quad (3.82)$$

3.5 The Spin-Half System

We now move to the electromagnetic vertex function for the spin-half system, and repeat the arguments we used for the spin-zero system. Free spin-half particles of mass m obey the Dirac Equation

$$(i\gamma^\mu \partial_\mu - m)\psi(x) = 0. \quad (3.83)$$

Thus we note that the gamma matrix γ^μ is required to correctly describe spin-half particles and so we must add γ^μ to our list of available four-vectors. We may write

$$\Gamma^\mu(p_1, p_2; q) = A(p_1^2, p_2^2; q^2)\gamma^\mu + B(p_1^2, p_2^2; q^2)p_1^\mu + C(p_1^2, p_2^2; q^2)q^\mu. \quad (3.84)$$

Note however, the functions A , B and C may have extra gamma matrix structure of the form \not{p}_1 and \not{q} . We may explicitly write the most general form of the electromagnetic vertex as

$$\begin{aligned} \Gamma^\mu(p_1, p_2; q) = & \gamma^\mu f_1(p_1^2, p_2^2; q^2) + p_1^\mu f_2(p_1^2, p_2^2; q^2) + q^\mu f_3(p_1^2, p_2^2; q^2) \\ & + \gamma^\mu \not{p}_1 f_4(p_1^2, p_2^2; q^2) + p_1^\mu \not{p}_1 f_5(p_1^2, p_2^2; q^2) + q^\mu \not{p}_1 f_6(p_1^2, p_2^2; q^2) \\ & + \not{q} \gamma^\mu f_7(p_1^2, p_2^2; q^2) + \not{q} p_1^\mu f_8(p_1^2, p_2^2; q^2) + \not{q} q^\mu f_9(p_1^2, p_2^2; q^2) \\ & + \not{q} \gamma^\mu \not{p}_1 f_{10}(p_1^2, p_2^2; q^2) + \not{q} p_1^\mu \not{p}_1 f_{11}(p_1^2, p_2^2; q^2) + \not{q} q^\mu \not{p}_1 f_{12}(p_1^2, p_2^2; q^2), \end{aligned} \quad (3.85)$$

where f_1, \dots, f_{12} are Lorentz invariant scalar functions of p_1^2 , p_2^2 and q^2 . We may relate these form factors to the Dirac and Pauli form factors discussed previously by considering the on-shell limit.

3.5.1 The On-Shell Vertex

While this is the simplest form for extracting form factors from loop calculations, as before, there is a more physical decomposition. We again consider the case that the spin-half system is on-shell. Then this vertex will sit between Dirac spinors:

$$\bar{u}(p_2)\Gamma^\mu(p_1, p_2; q)u(p_1). \quad (3.86)$$

The Dirac Equation allows us to use the relations $\not{p}u(p) = mu(p)$ and $\bar{u}(p)\not{p} = \bar{u}(p)m$. Thus the on-shell case amounts to the replacements $\not{p}_1, \not{p}_2 \rightarrow m$. Doing this leads to

$$\begin{aligned} \Gamma^\mu(p_1, p_2; q)|_{\not{p}_1=\not{p}_2=m} &= (f_1 + mf_4 + 2mf_7 + 2m^2f_{10})\gamma^\mu \\ &+ (f_2 + mf_5 - 2f_7 - 2mf_{10})p_1^\mu \\ &+ (f_3 + mf_6)q^\mu, \end{aligned} \quad (3.87)$$

where we have used the fact that $\bar{u}(p_2)\not{q}u(p_1) = 0$. It is possible to transform this representation to

$$\Gamma^\mu(p_1, p_2; q)|_{\not{p}_1=\not{p}_2=m} = g_1\gamma^\mu + g_2(p_1 + p_2)^\mu + g_3(p_1 - p_2)^\mu, \quad (3.88)$$

where one may relate the two representations as

$$g_1 = f_1 + mf_4 + 2mf_7 + 2m^2f_{10} \quad (3.89)$$

$$g_2 = \frac{1}{2}(f_2 + mf_5 - 2f_7 - 2mf_{10}) \quad (3.90)$$

$$g_3 = \frac{1}{2}(f_2 - 2f_3 + mf_5 - 2mf_6 - 2f_7 - 2mf_{10}). \quad (3.91)$$

The Ward Takahashi Identity in this limit requires that

$$q_\mu\Gamma^\mu(p_1, p_2; q)|_{\not{p}_1=\not{p}_2=m} = 0 = g_3(m^2, m^2; q^2)q^2, \quad (3.92)$$

and so we must have that $g_3(m^2, m^2; q^2) = 0$. Thus the on-shell vertex function reduces to a sum of two Lorentz invariant scalar functions g_1 and g_2 . Note that we may use the Gordon Identity

$$\bar{u}(p_2)(p_1 + p_2)^\mu u(p_1) = \bar{u}(p_2)(2m\gamma^\mu)u(p_1) - \bar{u}(p_2)(2m)\frac{i\sigma^{\mu\nu}q_\nu}{2m}u(p_1), \quad (3.93)$$

to rewrite this vertex as

$$\Gamma^\mu(p_1, p_2; q)|_{\not{p}_1=\not{p}_2=m} = \gamma^\mu F_1(q^2) + \frac{i\sigma^{\mu\nu}q_\nu}{2m}F_2(q^2), \quad (3.94)$$

where F_1 and F_2 are the well known Dirac and Pauli form factors. It is straightforward to show that

$$F_1(q^2) = g_1(m^2, m^2, q^2) + (2m)g_2(m^2, m^2, q^2) \quad (3.95)$$

$$F_2(q^2) = -(2m)g_2(m^2, m^2, q^2). \quad (3.96)$$

3.6 Conclusion

This completes our development of the formalism surrounding the electromagnetic form factors. We began by discussing the experimental data for the nucleon and pion electromagnetic form factors. We explained how the low energy data enabled measurements of the charge radius and the magnetic moments of the nucleon. We then paused our discussion of electromagnetic form factors to develop our understanding of gauge invariance, and the Ward Takahashi Identity. With this result, we showed how one could relate the experimental form factors to the most general form of the electromagnetic vertex.

Chiral Corrections to Electromagnetic Form Factors in the Nambu–Jona-Lasinio Model

As discussed extensively in the previous chapters, the theory of the strong force is resistant to direct analysis of its Lagrangian in the low energy regime due to the strong coupling strength and non-Abelian dynamics. One solution to this difficulty is to utilize simplified models of QCD. The following chapter considers this approach to calculate electromagnetic form factors for the nucleon and a number of hyperons using the Nambu–Jona-Lasinio (NJL) Model, a relativistic quark model. In particular, this work focuses on the implementation of the pionic contributions motivated by chiral symmetry arguments. These effects may be incorporated at one of two scales; at the *quark level* or at the *hadron level*. The exact meaning of these two terms will be defined later in this chapter.

From our previous discussion of chiral effective field theory, we know that one may build up a systematic picture of the low energy behaviour of hadronic systems as a power series in m_π . In particular, the non-analytic terms in chiral effective field theory constitute model independent predictions, which are also respected in QCD. These constraints on the amplitude may be used to guide the building of models of QCD. In the following chapter, these constraints are used to inform the implementation of pion loop effects on the nucleon and strangeness -1 hyperons.

As a result of ensuring the correct leading non-analytic behaviour of the hadronic observables, a particular parameter set is determined which yields a good description of low energy nucleon properties, and also leads to an improvement for the Σ^- magnetic moment when compared to a previous calculation by others where the chiral corrections were implemented at the quark level. This demonstrates in a practical way the importance of correctly implementing these chiral corrections. The results of this chapter are published in Refs. [99, 100].

4.1 Baryon Electromagnetic Form Factors in the NJL Model

Although the main point of this work is the implementation of chiral symmetry, we begin this chapter with a summary of the calculation of electromagnetic form factors in the NJL

Model [101, 102]. Previously, theoretical studies of these form factors were based on quark models, ranging from constituent quark models [103, 104] to the MIT bag model [105], with more recent studies employing the Schwinger-Dyson based approaches [106] utilising the Nambu–Jona-Lasinio (NJL) model [107, 108]. The calculation reported on here is based on earlier work in Refs. [109, 110], where the electromagnetic form factors of the nucleon and sigma hyperons are calculated. Here, we review the calculation of the electromagnetic form factors in the NJL Model. The Lagrangian density for the $SU(3)_F$ flavour NJL Model, in its Fierz symmetric form is given as [110]:

$$\mathcal{L} = \bar{\psi}(i\cancel{\partial} - \hat{m})\psi + \frac{1}{2}G_\pi[(\bar{\psi}\lambda_i\psi)^2 - (\bar{\psi}\gamma_5\lambda_i\psi)^2] - \frac{1}{2}G_\rho[(\bar{\psi}\gamma^\mu\lambda_i\psi)^2 + (\bar{\psi}\gamma^\mu\gamma_5\lambda_i\psi)^2], \quad (4.1)$$

where $\hat{m} = \text{diag}(m_u, m_d, m_s)$ and λ_i are the eight generators of $SU(3)$ in the Gell-Mann representation (see Appendix A), plus $\lambda_0 = \sqrt{2/3}\mathbb{1}$.

In the NJL Model, interactions are described by effective four-point fermion contact interactions which are non-renormalisable. Thus the model is only fully in the context of a particular regularisation prescription to render the resulting interactions finite. The NJL Model used as the basis for this work uses the proper-time regularisation prescription [111] (see Appendix E for details), with an ultraviolet cutoff Λ_{UV} . One of the drawbacks in the NJL Model is that the model lacks the property of colour confinement; coloured quark states are free to propagate, rather than being confined in hadrons. It is possible to repair this pathology by introducing an infrared cutoff Λ_{IR} , which (if suitably chosen) removes the singularities due to the propagation of colored states. In the following explanation of the calculation of electromagnetic form factors in the NJL model, all momentum integrals should be understood to be regularised using this prescription.

4.1.1 Quark Propagators and Dynamical Mass Generation

In the NJL Model, hadrons are described as bound states of quarks. Thus we begin our discussion of the calculation with an examination of the quark propagator in the NJL Model. The free-field quark propagator $S_F^{(0)}(p)$ is given as usual by

$$S_F^{(0)}(p) = \frac{i}{\cancel{p} - m_{f,0}}, \quad (4.2)$$

where f is the quark flavour. Note that in this work, we shall take the isospin symmetric limit $m_{u,0} = m_{d,0}$. In a non-perturbative calculation, we require the dressed version of this propagator, rather than the bare propagator. We may relate the two via

$$S_F(p) = \frac{i}{\cancel{p} - m_f^{(0)} - \Sigma(p)}, \quad (4.3)$$

where $\Sigma(p)$ is the sum of all one-particle-irreducible (1PI) diagrams. In order to proceed, the self energy, $\Sigma(p)$ must be determined. In order to make the equation more tractable, the so-called Hartree-Fock approximation is used [109, 112, 113]. One can understand this

approximation in the following way. Consider perturbatively expanding the propagator diagrammatically:

$$S_F(p) = \text{---} \text{---} \text{---} \text{---} \text{---} = \text{---} \text{---} \text{---} + \text{---} \text{---} \text{---} \text{---} \text{---} + \text{---} \text{---} \text{---} \text{---} \text{---} + \dots + \text{---} \text{---} \text{---} \text{---} \text{---} + \dots, \quad (4.4)$$

where lines with a blob denote the full propagator, and solid lines denote the bare propagator. In the Hartree-Fock approximation, we *assume* that it is sufficient to only consider a subclass of diagrams; the so-called bubble diagrams. In other words, the self energy is given as

$$-i\Sigma(p) = \text{---} \text{---} \text{---} \text{---} \text{---} + \text{---} \text{---} \text{---} \text{---} \text{---} + \dots. \quad (4.5)$$

This is known as the *Random Phase Approximation*. Thus one may understand the Hartree-Fock approximation as a resummation of a certain subclass of diagrams. One obtains:

$$S_F(p) = \text{---} \text{---} \text{---} \text{---} \text{---} = \text{---} \text{---} \text{---} \text{---} \text{---} + \text{---} \text{---} \text{---} \text{---} \text{---}, \quad (4.6)$$

where we note that the propagator which now appears in the loop is the dressed propagator, consistent with the approximation of the self energy we have just discussed. We may explicitly write the above diagrammatic relation as

$$S_F^{-1}(p) = S_F^{(0)-1}(p) - \sum_{\Omega} K_{\Omega} \int \frac{d^4k}{(2\pi)^4} \text{Tr}[\bar{\Omega} S_F(k)]. \quad (4.7)$$

Note that since the dressed propagator appears on both sides of the equation, this must be solved self-consistently. It is possible to show, that for sufficiently strong coupling $G_{\pi} > G_{\text{critical}}$ a dynamically generated quark mass appears. As a result, we may write the dressed quark propagator as

$$S_F(p) = \frac{i}{\not{p} - m_f}, \quad (4.8)$$

where m_f is now the dressed quark mass, and is related to the bare quark mass via

$$m_f = m_f^{(0)} + 12G_\pi \int \frac{d^4k}{(2\pi)^4} \text{Tr}_D[S_F(k)]. \quad (4.9)$$

We see that the act of resumming the bubble diagrams has led to a constituent quark with dressed mass m_f , which will survive even in the chiral limit ($m_f^{(0)} \rightarrow 0$). Thus the NJL Model exhibits dynamical chiral symmetry breaking, and dynamical mass generation, two features which we understand to occur in QCD.

4.1.2 Mesons in the NJL Model

In the NJL Model, the hadron is modeled as a quark-diquark bound state. In order to describe the diquark (a quark-quark bound state), it will be useful to understand the calculation of mesons (quark-antiquark bound states) in the NJL Model. The starting point for a non-perturbative description of a bound state is the Bethe-Salpeter Equation:

$$T(q) = K + \int \frac{d^4k}{(2\pi)^4} K S_F(k+q) T(q) S_F(k). \quad (4.10)$$

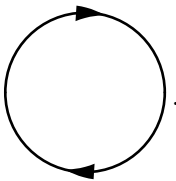
It is possible to show that the solution to the Bethe-Salpeter Equation in the $\bar{q}q$ channel with the quantum numbers of the pion has the form

$$T_{\alpha\beta,\gamma\delta}^\pi(q) = (\gamma_5 \tau_i)_{\alpha\beta} t_\pi(q) (\gamma_5 \tau_i)_{\gamma\delta}, \quad (4.11)$$

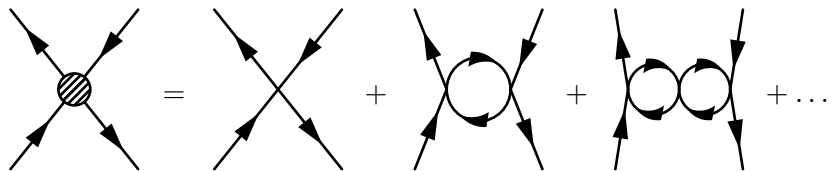
where $t_\pi(q)$ takes the form

$$t_\pi(q) = \frac{-2iG_\pi}{1 + 2G_\pi \Pi_{PP}(q^2)}, \quad (4.12)$$

and Π_{PP} is the single bubble diagram:

$$\Pi_{PP}(q^2) = \text{Diagram} \quad (4.13)$$


The form of $t_\pi(q^2)$ originates from resumming the infinite series of bubble diagrams in a geometric series, as is done for the self energy:

$$\text{Diagram} = \text{Diagram} + \text{Diagram} + \text{Diagram} + \dots \quad (4.14)$$


Near the pion pole, the T -matrix solution behaves as a pion pole would. Expanding around $q^2 = m_\pi^2$, and equating it with the pole form gives

$$T_{\alpha\beta,\gamma,\delta}^\pi(q) = (\gamma_5\tau_i)_{\alpha\beta} \frac{-2iG_\pi}{1 + 2G_\pi\Pi_{PP}(m_\pi^2) + 2G_\pi\frac{\partial}{\partial q^2}\Pi(q^2)\Big|_{q^2=m_\pi^2}} (\gamma_5\tau_i)_{\gamma\delta} = \frac{\Gamma_i(q)\bar{\Gamma}_i(q)}{q^2 - m_\pi^2}, \quad (4.15)$$

where $\Gamma_i(q)$ is the Bethe-Salpeter vertex function, which describes the hadronisation of the two constituent quarks into a bound state (in this case, the pion). Comparing the two expressions gives

$$1 + 2G_\pi\Pi_{PP}(m_\pi^2) = 0, \quad (4.16)$$

With these identities, it is possible to conclude that the Bethe-Salpeter vertex function $\Gamma_i(q)$ in this approximation is constant, and is given by

$$\Gamma_i(q) = \sqrt{Z_\pi}\gamma_5\tau_i, \quad (4.17)$$

where

$$Z_\pi^{-1} = -\frac{\partial}{\partial q^2}\Pi_{PP}(q^2)\Big|_{q^2=m_\pi^2}. \quad (4.18)$$

This concludes our discussion of mesons in the NJL Model. This procedure, of calculating the T -matrix using the Bethe-Salpeter Equation and then performing the pole approximation to simplify this expression is repeated for the calculation of diquark bound states, except for a number of small differences. Thus we move directly to a description of the calculation of Baryon electromagnetic form factors in the NJL Model.

4.1.3 Calculating Electromagnetic Form Factors in the NJL Model

Recall that baryons in this framework are described as quark-diquark bound states. One may write the baryon electromagnetic vertex as the sum of diagrams where the photon couples to the quark, and diagrams where the photon couples to the diquark:

$$\Gamma_H^{\text{NJL},\mu}(q; p, p') = \text{diagram 1} + \text{diagram 2}. \quad (4.19)$$

Thus, in order to calculate baryon electromagnetic form factors one must understand how the photon couples to the quark and diquark structures. To begin with, the quark photon vertex $\Gamma_{\gamma q}^\mu(q; p, p')$ is determined by solving the inhomogeneous Bethe-Salpeter Equation:

$$\Gamma_{\gamma q}^\mu(q; p, p') = \gamma^\mu \left(\frac{1}{6} + \frac{\tau_3}{2} \right) + i \sum_{\Omega} K_{\Omega} \Omega \int \frac{d^4 k}{(2\pi)^4} \text{Tr} [\bar{\Omega} S_F(k+q) \Gamma_{\gamma q}^\mu(q; p, p') S_F(k)]. \quad (4.20)$$

From this, the diquark vertex function $\Gamma_{\gamma qq}^\mu(q; p, p')$ is calculated as the sum of two Feynman Diagrams:

$$\Gamma_{\gamma qq}^\mu(q; p, p') = \text{Diagram 1} + \text{Diagram 2}. \quad (4.21)$$

With both the quark and diquark vertex functions in hand, the baryon electromagnetic form factors may be calculated.

Effects of the virtual pion cloud are included in the calculation of baryon electromagnetic form factors in two places. Firstly, the incorporation of pions leads to an extra contribution to the mass of the full quark propagator, and secondly the virtual pion cloud also modifies the calculated quark form factors, as shown in Fig. 4.1. It is important to note that these effects are implemented at the quark level. The implications of this approach will be discussed later in this chapter.

This concludes the discussion of the NJL Model component of this calculation. We began by examining the NJL Model Lagrangian, and noted that since the model is non-renormalisable, a regularisation prescription is required to fully define the model. We then discussed the quark propagator, and showed that resumming a subclass of diagrams led naturally to the dynamical generation of mass, and thus dynamical chiral symmetry breaking. We explained that mesons are described as quark-antiquark bound states in the NJL Model. We summarised how the baryon electromagnetic form factors are built up from quark and diquark electromagnetic vertices, and finally, explained how pion loops are incorporated at the quark level. It is these chiral loop effects which we now turn to. In particular, we shall show why the implementation of chiral loops just described is inconsistent with chiral perturbation theory, and then improve the model calculation by correctly implementing the chiral loop effects.

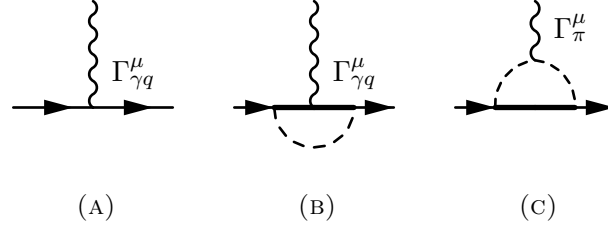


FIGURE 4.1: Pion loop corrections to the quark-photon vertex. The strength of the quark-pion vertex is given by the Bethe-Salpeter vertex function $\Gamma_i(q) = \sqrt{Z_\pi} \gamma_5 \tau_i$, and the pion-photon coupling $\Gamma_\pi(q; k, k')$ is approximated by its on-shell form $\Gamma_\pi(q; k, k') = (k + k')^\mu F_\pi(q^2)$, where the pion form factor $F_\pi(q^2)$ is also calculated in the NJL Model.

4.2 Constraints from Chiral Effective Field Theory

Let us now directly investigate the constraints on the hadronic observable from chiral effective field theory. In particular, we wish to examine the modification of the *free* nucleon mass due to the presence of the pion cloud. Recall that these effects will occur due to self energy corrections, which lead to a dressed mass of the form

$$m_N = m_N^{(0)} + \Sigma(\not{p} = m_N). \quad (4.22)$$

In particular, we seek terms which are non-analytic in the quark mass parameter, since these terms are model independent, relying only on the symmetries built into the effective field theory. We may write the chiral expansion of the nucleon mass m_N as

$$m_N = \{a_0 + a_2 m_\pi^2 + a_4 m_\pi^4 + \dots\} + \{\chi_{\pi N} I_{\pi N}(m_\pi) + \chi_{\pi \Delta} I_{\pi \Delta}(m_\pi) + \dots\}. \quad (4.23)$$

Recall that the pion mass is related to the quark mass via $m_\pi \propto \sqrt{m_q}$. In other words, odd powers of the pion mass will lead to terms non-analytic in m_q . Thus we have separated this expansion as

$$m_N = \{\text{terms analytic in } m_q\} + \{\text{chiral loop corrections}\}. \quad (4.24)$$

The lowest order chiral loop correction is the single pion contribution to the nucleon self energy. This diagram is shown below in Fig. 4.2. Using the Feynman Rules discussed in Appendix B, we may write the amplitude for this process as

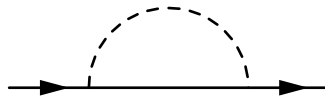


FIGURE 4.2: Virtual one-pion contribution to nucleon mass.

$$-i\Sigma(\not{p}) = \int \frac{d^4k}{(2\pi)^4} \frac{g_A}{2f_\pi} \gamma_5 \not{k} S_F^N(p-k) \frac{g_A}{2f_\pi} \gamma_5 \not{k} S_F^\pi(k) + \text{neutral pion contribution}, \quad (4.25)$$

where we have not written the explicit expression for the neutral pion. The only difference between the diagrams is the size of the coupling, which is a factor of 2 smaller. One thus finds for the sum of the two diagrams

$$-i\Sigma(\not{p}) = \frac{3g_A^2}{4f_\pi^2} \int \frac{d^4k}{(2\pi)^4} \gamma_5 \not{k} \frac{(\not{p} - \not{k} + m_N)}{(p-k)^2 - m_N^2} \gamma_5 \not{k} \frac{1}{k^2 - m_\pi^2}. \quad (4.26)$$

It is possible to show (see Ref. [114]), that the Leading Non-Analytic term due to this expression is

$$\Sigma(m_N) \stackrel{\text{LNA}}{=} \chi_{\pi N} m_\pi^3 = -\frac{3g_A^2}{32\pi f_\pi^2} m_\pi^3. \quad (4.27)$$

The chiral expansion takes the form

$$m_N = c_0 + c_2 m_\pi^2 + \chi_{\pi N} m_\pi^3 + c_4 m_\pi^4 + \dots, \quad (4.28)$$

and thus the leading non-analytic term appears at $\mathcal{O}(m_\pi^3)$. As has been previously stressed, this term constitutes a model independent constraint which must be respected if the theory is to be consistent with chiral symmetry and its pattern of breaking. Similar leading non-analytic terms appear in the calculation of baryon magnetic moments [115]. Following the same arguments as above, we may write the chiral expansion for the magnetic moment as

$$\mu_B = \{d_0 + d_2 m_\pi^2 + d_4 m_\pi^4 + \dots\} + \{\chi_{\pi N} I_{\pi N}(m_\pi) + \chi_{\pi \Delta} I_{\pi \Delta}(m_\pi) + \dots\}. \quad (4.29)$$

In the case of the magnetic moment, it is possible to show that the Leading Non-Analytic term is [115]

$$\mu_B^{\text{LNA}} = \chi_{\pi N} m_\pi = \frac{m_N}{8\pi f_\pi^2} \beta_{\pi B} m_\pi, \quad (4.30)$$

where $\beta_{\pi B}$ are the pion-baryon couplings. In other words, unlike the nucleon mass, the leading non-analytic term appears at $\mathcal{O}(m_\pi)$:

$$\mu_B = \mu_B^0 + \chi_{\pi N} m_\pi + \dots \quad (4.31)$$

Although the LNA term does not necessarily dominate the physics of hadronic properties, in the case of the magnetic moment, it is of practical importance, because this term appears

at first order in the Taylor series, and has been found to be numerically large [115]. Recall that the magnetic moment may be extracted from the vertical intercept of the magnetic form factor $G_M(0)$. Thus the low energy behaviour of the magnetic form factor will be particularly sensitive to the implementation of chiral symmetry.

4.3 Implementations of Chiral Symmetry: A Comparison of Quark Level and Hadron Level Approaches

While the importance of chiral symmetry, especially for low energy hadron properties, was first recognised more than fifty years ago in the context of soft pion theorems [116], its modern realisation as we have seen - is based upon the chiral symmetry of QCD itself. While chiral effective field theory demonstrates the importance in including the pion as an explicit degree of freedom in calculations of hadronic properties, there have been a number of different approaches to the implementation of the chiral loop corrections in the literature which broadly speaking may be divided into two categories; *quark level* calculations and *hadron level* calculations.

A simple quantum mechanical argument will help to elucidate the way the pion effects must be incorporated. The so-called time-energy uncertainty relation is

$$\Delta E \Delta t \geq 1/2, \quad (4.32)$$

where ΔE is the uncertainty in the energy of the state, and Δt is the lifetime of the state. Let us consider the ‘best case’ scenario where $\Delta E \Delta t = 1/2$. A simple rearrangement gives

$$\Delta t = \frac{1}{2\Delta E}. \quad (4.33)$$

Consider the transition $A \rightarrow B\pi$. The initial energy is $E_i = \sqrt{m_A^2 + \mathbf{p}^2}$, and the final energy is $E_f = \sqrt{m_B^2 + (\mathbf{p} - \mathbf{k})^2} + \sqrt{m_\pi^2 + \mathbf{k}^2}$, where we integrate over all \mathbf{k} . We have

$$\Delta E = E_f - E_i = \sqrt{m_B^2 + (\mathbf{p} - \mathbf{k})^2} + \sqrt{m_\pi^2 + \mathbf{k}^2} - \sqrt{m_A^2 + \mathbf{p}^2}. \quad (4.34)$$

We may place a lower bound on the uncertainty in the states by considering the nucleon rest frame. Then we can show that

$$\Delta E \geq \delta m + m_\pi, \quad (4.35)$$

where $\delta m = m_B - m_A$. In the chiral limit ($m_\pi \rightarrow 0$), the lifetime of the virtual state is limited by the mass difference

$$\Delta t \leq \frac{1}{2\delta m}. \quad (4.36)$$

In the case that the source mass does not change, for example in the process $N \rightarrow N\pi$ the lifetime of the state is unbounded ($\Delta t \leq \infty$). This result has important implications for a calculation of the electric charge radius. Let us examine the implications for hadron level and quark level approaches.

4.3.1 The Hadron Level Approach

Firstly, consider a *hadron level approach*. As we have seen, when the source mass does not change, the virtual pion may travel infinitely far from the source. Thus for the process $p \rightarrow n\pi^+$, shown in Fig. 4.3a, the charge of the proton may be carried by the pion an infinite distance from the source. In other words, the contribution to the proton charge radius from this diagram will become infinite in the chiral limit. Compare this with the contribution from the process $p \rightarrow \Delta^0\pi^+$, shown in Fig. 4.3b. In the chiral limit, the Delta-nucleon mass difference is $\delta m = m_\Delta - m_N$. Due to the non-zero mass difference between the nucleon and delta baryons, the range of the virtual pion is therefore limited to the range $1/\delta m$.

4.3.2 The Quark Level Approach

In a *quark level approach*, first introduced by Georgi and Manohar [117], the pion loops are evaluated on individual quarks rather than the hadron as a whole. This approach, while simple, unfortunately yields the wrong infrared behaviour. To see this, consider the contribution to the charge radius from the process $u \rightarrow d\pi^+$. Since the u and d are mass degenerate, the pion may travel an infinite distance from the source. Imagine placing this quark inside a proton. Then for the process $p \rightarrow n\pi^+$ this contribution will indeed match that predicted from the hadron level approach. Note however that the range of the pion in the process $p \rightarrow \Delta^0\pi^+$ in this quark level approach will also be infinite, rather than being limited to the mass difference δm . In other words, the prediction of the contribution to the charge radius from the $\Delta\pi$ state will be incorrect. The reason for this is that although the Δ^0 has the same valence quark content, it is in a different spin state ($\frac{3}{2}$ versus $\frac{1}{2}$). However, in a quark level approach, the individual quark *does not know which of the baryon spin states it is part of*. As a result, the long distance behaviour for the pion cloud for these two processes is not respected. In such a quark level implementation, there is no way of keeping track of these differences. Thus in order to ensure the correct chiral behaviour of certain observables, we *must perform the chiral loop corrections at the hadron level*.

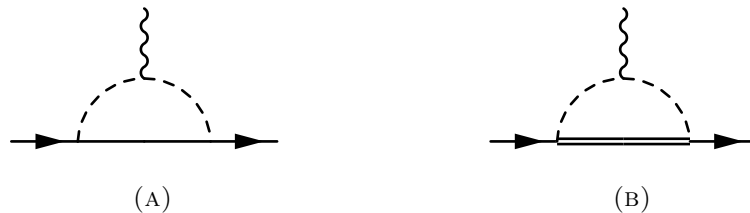


FIGURE 4.3: Contributions to proton charge radius from the process $p \rightarrow n\pi^+$ (4.3a) and $p \rightarrow \Delta^0\pi^+$ (4.3b). Since the mass difference between the proton and neutron is zero, in the chiral limit, this off-shell pion may carry the charge an infinite distance from the source, and thus the contribution to the charge radius from this process is infinite.

4.3.3 Implementing Chiral Symmetry in Quark Models

It must be noted that it is possible to incorporate these chiral loop effects in a quark model and also respect the constraints of chiral symmetry. The key step is to project the quark space Hamiltonian onto the space of colourless baryons. This process has been performed (for example) in the Cloudy Bag Model [3]. In that formalism, the nucleon self energy due to the pion loop may be calculated as [3]

$$\Sigma(m_N) = -\frac{3}{\pi} \frac{f_{\pi N}^2}{(4\pi)m_\pi^2} \int_0^\infty dk \frac{k^4 u^2(k)}{k^2 + m_\pi^2}, \quad (4.37)$$

where $u(k)$ arises naturally as the result of the confined quarks, and may be interpreted as a hadronic form factor, which describes the finite size of the baryon. Using the Goldberger-Treiman relation and further relating the pseudovector and pseudoscalar couplings as is done in Ref. [118] using

$$\frac{f_{\pi N}}{m_\pi} = \frac{g_A}{2f_\pi}, \quad (4.38)$$

the self energy may be brought to the form

$$\Sigma(m_N) = -\frac{3g_A^2}{32\pi f_\pi^2} \frac{2}{\pi} \int_0^\infty dk \frac{k^4 u^2(k)}{k^2 + m_\pi^2}, \quad (4.39)$$

which is in exact agreement with a calculation of this quantity in Heavy Baryon Effective Field Theory [119], except that in the effective field theory, there is no ultraviolet regulator, and the theory is formally divergent. The form factor $u(k)$ which ensures convergence is one of the benefits of starting from a microscopic picture of the hadron. Since we are only interested in the infrared behaviour of the integral, we are free to choose an ultraviolet regulator. Here, we use a simple dipole regulator, rather than the regulator obtained consistently from the Cloudy Bag Model. That is, we take

$$u(k) = \left(1 + \frac{k^2}{\Lambda^2}\right)^{-2}. \quad (4.40)$$

Doing this leads to an integrated self energy of the form:

$$\Sigma(m_N, \Lambda) = -\frac{3g_A^2}{32\pi f_\pi^2} \frac{1}{16} \frac{\Lambda^5 (m_\pi^2 + 4m_\pi \Lambda + \Lambda^2)}{(m_\pi + \Lambda)^4}, \quad (4.41)$$

from which a chiral expansion yields the leading non-analytic term:

$$\chi_{\pi N} m_\pi^3 = -\frac{3g_A^2}{32\pi f_\pi^2} m_\pi^3, \quad (4.42)$$

which is indeed in agreement with the leading non-analytic behaviour calculated in chiral effective field theory. In other words, projecting the quark Hamiltonian onto the space of colourless hadrons leads to a chiral effective field theory where the convergence of the theory is naturally ensured by the existence of the form factor $u(k)$ which is the result of the finite size of the hadron. Thus we may perform chiral loop corrections on quark model results by first calculating the quark model observables, and then performing the chiral loop corrections in a chiral effective field theory, where the convergence of the model is ensured by the inclusion of a form factor which describes the finite size of the baryon.

4.4 Implementing the Chiral Corrections

For this work we choose to use the pseudoscalar pion nucleon coupling¹ (see Appendix B for details). The interaction term in the Lagrangian is

$$\mathcal{L}_{\pi N} = -g_{\pi N} \bar{\psi}_N i\gamma_5 \tau \cdot \pi \psi_N . \quad (4.43)$$

Introducing the electromagnetic interaction, (see Appendix B), leads to an electromagnetic coupling to the hadrons. As a result, one obtains three diagrams at first loop order. These three diagrams are shown below in Fig. 4.4. Taking guidance from the methodology of the Cloudy Bag Model, we shall replace the electromagnetic vertex due to the point-like nucleon $\Gamma_N^{(0)\mu}(q; p, p') = \gamma^\mu$, with the dressed quark model vertex $\Gamma_N^{\text{NJL},\mu}(q; p, p')$, which in general should take its most general form (see Chapter 3 for more details). For this study, we choose to approximate both the nucleon and pion electromagnetic vertices by their on-shell versions. That is, we choose

$$\Gamma_N^{\text{NJL},\mu}(q; p, p') = \gamma^\mu F_1^{\text{NJL}}(q^2) + \frac{i\sigma^{\mu\nu} q_\nu}{2m_N} F_2^{\text{NJL}}(q^2) , \quad (4.44)$$

$$\Gamma_\pi^{\text{NJL},\mu}(q; k, k') = (k + k')^\mu F_\pi^{\text{NJL}}(q^2) . \quad (4.45)$$

This simplification is consistent with the Ward-Takahashi identity:

$$\bar{u}(p') \left[q_\mu \Gamma_H^\mu(q; p, p') \right] u(p) = 0 , \quad (4.46)$$

¹ The choice of pseudoscalar coupling follows the choice of Miller in the light-cone cloudy bag model [120, 121]. It also matches the choice made for the quark-pion coupling in the NJL Model with which we compare. However, it is known that using the pseudoscalar pion-nucleon coupling and neglecting the sigma field - as we do here - leads to different predictions for the leading non-analytic behaviour [122], which are inconsistent with chiral symmetry. The pseudovector form of the pion nucleon coupling, described in Appendix B ensures the correct chiral behaviour. It would have been preferable to choose a pseudovector pion-nucleon coupling in both cases.

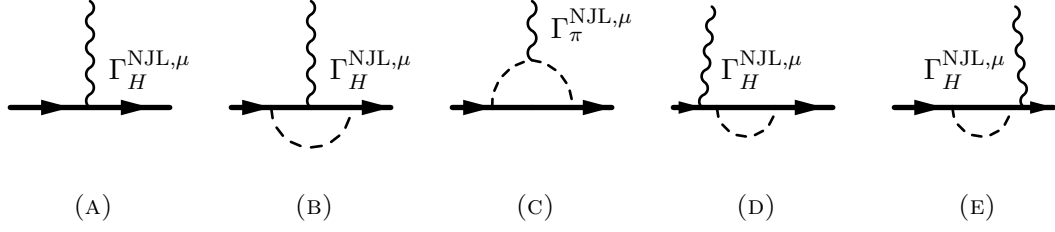


FIGURE 4.4: Diagrams which contribute to the calculation of electromagnetic form factors. Note that contributions from Δ intermediate states are not considered in this calculation. Note that diagrams 4.4d and 4.4e do not modify the vertex function, but will be essential in renormalising this amplitude, so we include them here.

and thus respects current conservation². This calculation was carried out by Miller in Refs. [120, 121], and we simply repeat the results here. The first diagram (Fig. 4.4a) is the quark model result, while the chiral corrections to these form factors are provided by the diagrams shown in Figs. 4.4b and 4.4c. The electromagnetic vertex obtained from this amplitude is

$$\Gamma_H^\mu(q; p, p') = \Gamma_H^{a,\mu}(q; p, p') + \Gamma_H^{b,\mu}(q; p, p') + \Gamma_H^{c,\mu}(q; p, p'), \quad (4.47)$$

from which one may extract the contributions to $F_{1,H}$ and $F_{2,H}$ as [121]:

$$F_{i,H}(q^2) = Z_H [F_{i,H}^a(q^2) + F_{i,H}^b(q^2) + F_{i,H}^c(q^2)], \quad (4.48)$$

where $i = 1, 2$, H is the hadron in question, a , b and c refer to diagrams 4.4a, 4.4b and 4.4c, respectively, and Z_H is hadron wave function renormalisation constant which ensures that the charge of the proton is unity. More will be said about Z_H in Sec. 4.4.1. The (unrenormalised) contributions from diagram 4.4b to the Dirac and Pauli form factors are

$$F_{1,H}^b(Q^2) = \frac{g_{\pi N}^{(0)2}}{(4\pi)} \int_0^1 dx x \int \frac{d^2L}{(2\pi)^2} \frac{\mathcal{F}_1(Q^2)(\mathbf{L}^2 + x^2 m_N^2 - \frac{1}{4}x^2 Q^2) - \mathcal{F}_2(Q^2)(\frac{x^2 Q^2}{2})}{D(\mathbf{L}_+^2, x)D(\mathbf{L}_-^2, x)}, \quad (4.49)$$

$$F_{2,H}^b(Q^2) = -\frac{g_{\pi N}^{(0)2}}{(4\pi)} \int_0^1 dx x \int \frac{d^2L}{(2\pi)^2} \frac{\mathcal{F}_1(Q^2)(2x^2 m_N^2) + \mathcal{F}_2(Q^2)(\mathbf{L}^2 + x^2 m_N^2 - \frac{1}{4}x^2 Q^2)}{D(\mathbf{L}_+^2, x)D(\mathbf{L}_-^2, x)}. \quad (4.50)$$

In the course of renormalisation, we will replace the unrenormalised coupling $g_{\pi N}^{(0)}$ with its renormalised version $g_{\pi N}$ (see Sec. 4.4.1). \mathcal{F}_1 and \mathcal{F}_2 are combinations of the quark model

²While it is true that the approximation preserves current conservation in the case where the initial and final nucleon legs are on their respective mass shells, it should be noted that this approximation does not lead to a vertex which respects the Ward Takahashi Identity for the case where either or both of the legs are off their mass shells. Further discussion on this point may be found in Chapter 3

form factors and are given as

$$\mathcal{F}_i = \begin{cases} 2F_{i,n}^a + F_{i,p}^a, & \text{for the proton} \\ 2F_{i,p}^a + F_{i,n}^a, & \text{for the neutron} \end{cases}, \quad (4.51)$$

The factors of two in the above expression arise from the different isospin couplings for the charged and neutral pions. The denominator $D(\mathbf{l}_\perp, x)$ may be written explicitly as

$$D(\mathbf{l}_\perp, x) = \mathbf{l}_\perp^2 + x^2 m_N^2 + (1-x)m_\pi^2, \quad (4.52)$$

where $\mathbf{L}_\pm = \mathbf{L}_\perp \pm \frac{1}{2}x\mathbf{q}_\perp$. Similarly, one may write the contributions from diagram (c) as

$$F_{1,H}^c = \frac{g_{\pi N}^{(0)2}}{(4\pi)} I_\tau F_\pi^{\text{NJL}}(Q^2) \int_0^1 dx x \int \frac{d^2 K}{(2\pi)^2} \frac{\mathbf{K}^2 + x^2 m_N^2 - \frac{1}{4}(1-x)^2 Q^2}{D(\mathbf{K}_+, x)D(\mathbf{K}_-, x)}, \quad (4.53)$$

$$F_{1,H}^c = \frac{g_{\pi N}^{(0)2}}{(4\pi)} I_\tau (2m_N^2) F_\pi^{\text{NJL}}(Q^2) \int_0^1 dx x^2 (1-x) \int \frac{d^2 K}{(2\pi)^2} \frac{1}{D(\mathbf{K}_+, x)D_N(\mathbf{K}_-, x)}. \quad (4.54)$$

The denominator $D(\mathbf{l}_\perp, x)$ is the same as before, but here, $\mathbf{K}_\pm = \mathbf{K}_\perp \pm \frac{1}{2}(1-x)\mathbf{q}_\perp$. Finally, the pion-nucleon isospin coefficient I_τ is given as

$$I_\tau = \begin{cases} 2, & \text{for the proton} \\ -2, & \text{for the neutron} \end{cases}. \quad (4.55)$$

The minus sign for the neutron arises from the fact that the positively charged pion cloud in the proton becomes a negatively charged pion cloud in the neutron, and thus the coupling of the photon to the charged pion changes sign.

Diagrams 4.4d and 4.4e are self energy contributions which contribute to the wave function renormalisation, and also to the modification of the hadron mass, as has been previously explained. These diagrams have also been previously calculated, and the result may be stated as [123]

$$\Sigma(\not{p} = m_N) = \frac{g_{NN\pi}^{(0)2}}{(4\pi)^2} \frac{I_\tau}{4m_N} \int_0^\infty dt \frac{t}{(t+m_\pi^2)} \left(\frac{t}{m_N^2} - \sqrt{\frac{t^2}{m_N^4} + \frac{4t}{m_N^2}} \right). \quad (4.56)$$

The self energy is logarithmically divergent, and requires a regularisation prescription to be explicitly evaluated. In this work, we use a form factor regularisation prescription, the details of which we shall now explain.

4.4.1 Regularization and Renormalisation

As with any loop calculation in a quantum field theory, the free field parameters (masses, couplings and the overall normalizations) are modified. In order to ensure that these parameters coincide with their physical values, we must renormalise the amplitude. Here we summarize the procedure used in this work. Before renormalising, we must first regularise the above integrals. As we have emphasized previously, this ultra-violet regulator leaves the infra-red behaviour of the integral unchanged, and thus preserves the non-analytic behaviour. Motivated

by our discussion of the Cloudy Bag Model, we will use a momentum dependent form factor to regulate the high energy behaviour of the integral. In this work, we choose to use a t -dependent form factor (with Λ the regulator mass parameter), given as

$$F(\mathbf{l}_\perp, x) = \exp \left[-\frac{D(\mathbf{l}_\perp^2, x)}{(1-x)\Lambda^2} \right]. \quad (4.57)$$

where, as before, the factor $D(\mathbf{l}_\perp^2, x)$ is given by

$$D(\mathbf{l}_\perp, x) = \mathbf{l}_\perp^2 + x^2 m_N^2 + (1-x)m_\pi^2. \quad (4.58)$$

This particular choice corresponds to the preferred form of regulator in a recent study [124] of the origin of the $\bar{d} - \bar{u}$ asymmetry in the proton arising from chiral effects [125, 126]. After regularising the integrals, we next must renormalise the calculation. We have two constraints on the form of the nucleon propagator which we will use to fix the values of the wave function renormalisation constant Z_H and the nucleon mass $m_N^{(0)}$. We find that to ensure the same behaviour near the pole, we must require that

$$m_N = m_N^{(0)} + \Sigma(m_N), \quad (4.59)$$

$$Z_H^{-1} = 1 - \left. \frac{d}{d\phi} \Sigma(\phi) \right|_{\phi=m_N}. \quad (4.60)$$

These two conditions allow us to relate the bare mass $m_N^{(0)}$ to its physical value, and the bare coupling $g_{\pi N}^0$ to its physical value. Since we have regularised the loop integrals, the self energy becomes dependent on the cutoff Λ :

$$m_N = m_N^{(0)}(\Lambda) + \Sigma(m_N, \Lambda), \quad (4.61)$$

$$Z_H^{-1}(\Lambda) = 1 - \left. \frac{d}{d\phi} \Sigma(\phi, \Lambda) \right|_{\phi=m_N}. \quad (4.62)$$

We perform the renormalisation of the amplitude by taking

$$Z_H(\Lambda) g_{\pi N}^{(0)2}(\Lambda) = g_{\pi N}^2, \quad (4.63)$$

where the renormalised coupling takes its physical value: $g_{\pi N}^2/(4\pi) = 13.5$.

4.4.2 Finite Range Regularisation

For this work, we choose to use a Finite Range Regularisation, which is discussed in Ref. [127]. The essential difference between the ‘conventional’ approach to regularisation and the approach employed in Finite Range Regularisation is that the choice of cutoff parameter Λ remains finite.

As we have explained, the Non-Analytic behaviour of the integral is preserved, with the only downside being that our model will contain an additional parameter, the regulator mass Λ . All that remains is to determine the explicit value of this regulator. Numerous studies within the cloudy bag model [128], Dyson-Schwinger equations [129] and lattice motivated studies of the $\Delta - N$ mass difference as a function of quark mass [130], suggest that the self-energy contribution from the process $N \rightarrow N\pi$ is of the order 100-150 MeV. As an illustration, we choose the regulator mass to fix this self-energy at 130 MeV (so $\Lambda = 0.72$ GeV).

This concludes our discussion of the chiral corrections to the bare NJL Model result. We began by describing the Lagrangian used to perform the chiral corrections, before explicitly describing the contributions to the amplitude. We further discussed the regularisation prescription and renormalisation conditions, and in particular, noted that we used the Finite Range Regularisation Prescription, where the characteristic property of the prescription is that rather than taking the cutoff mass to infinity, it is kept finite, and instead fit to data. With the model fully defined, we proceed to determine the numerical results for the baryon electromagnetic form factors.

4.5 Nucleon Results

The bare NJL Model used in this study was calculated using the parameters in Table 4.1. This set was obtained by fitting the predicted baryon masses for the nucleon and Ξ to their experimental values. The resulting octet masses are shown in Table 4.2, Although the predicted values of the Λ and Σ masses differ slightly from the experimental values, as a result of an underestimate of the spin-spin interaction in the NJL model, the hierarchy of states is correct, that is, $m_N < m_\Lambda < m_\Sigma < m_\Xi$.

This choice of parameters leads to a relatively good agreement between the predicted nucleon electromagnetic form factors and the empirical parameterization of Ref. [93], shown in Fig. 4.5. In particular, it is certainly of comparable quality to the previous NJL calculation, where the pion corrections were calculated at the quark level (coloured blue in plots).

We may examine the effects of the pion loops in a more concrete way by considering the predicted charge radius and in particular the magnetic moments, since this observable is particularly sensitive to the implementation of chiral symmetry. These observables are explicitly shown in Fig. 4.6, and numerical values are given in Appendix C. While a comparison of the two calculations suggests that the quark level approach appears to lead to slightly better values, it seems that the nucleon is rather insensitive to the implementation of chiral symmetry.

TABLE 4.1: Chosen NJL model parameters, where all masses and regularization parameters are given in units of GeV, and the Lagrangian couplings in units of GeV^{-2} .

Λ_{IR}	Λ_{UV}	m_l	m_s	G_π	G_ρ	G_s	G_a
0.24	0.67	0.35	0.52	14.53	8.12	4.11	3.14

TABLE 4.2: Calculated baryon octet masses, compared with the experimental values (all in units of GeV).

	m_N	m_Λ	m_Σ	m_Ξ
NJL- Σ	0.940	1.176	1.217	1.318
Experiment	0.940	1.116	1.193	1.318

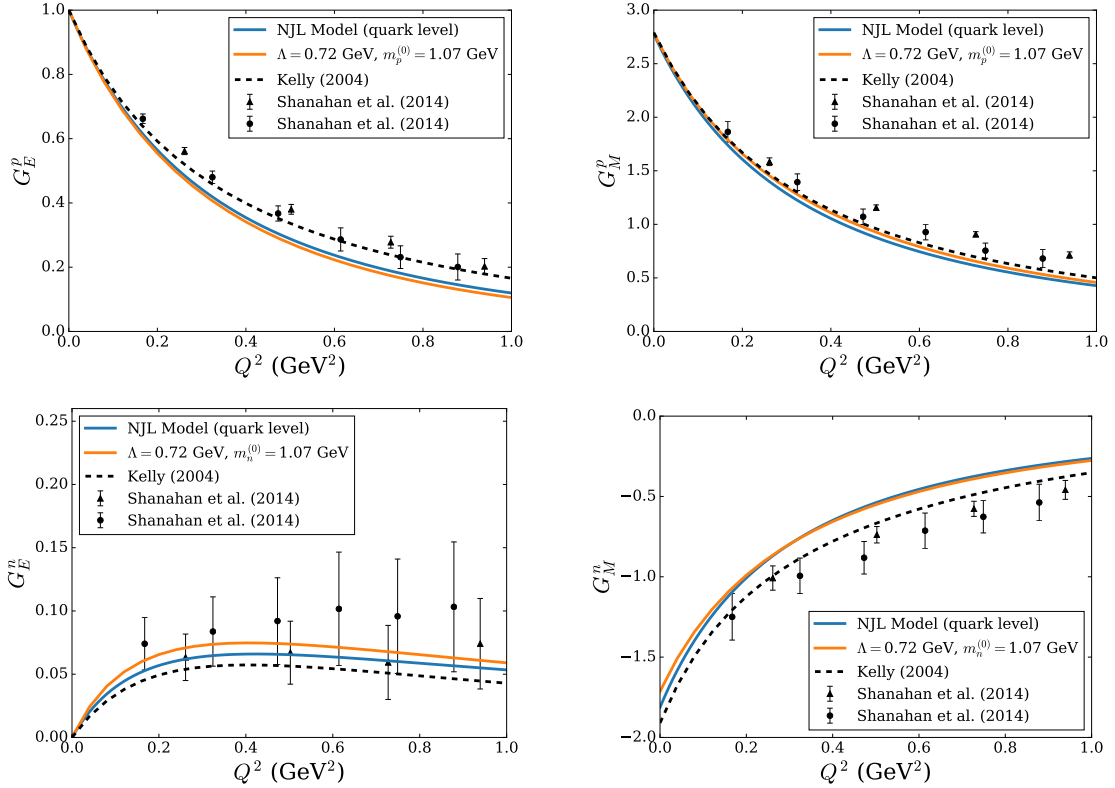


FIGURE 4.5: Predicted electromagnetic form factors for the nucleon calculated using the NJL Model, with chiral loop corrections calculated either at the quark level (blue line) or at the hadron level (orange line). The dashed line is taken from an empirical parameterisation of experimental data from Ref. [93] and data points are lattice data taken from Refs. [131, 132].

4.6 Chiral Corrections to Hyperon Form Factors

As explained earlier, we examine not only the chiral corrections to nucleon form factors but also to the Σ hyperons. The motivation for this lies in the work of Carrillo-Serrano *et al.* [110], which extended the earlier calculation of the nucleon electromagnetic form factors [109] to the baryon octet. Following the work of de Swart [133], under the assumption of $SU(3)_F$ flavour symmetry, we have various relationships between the couplings of the baryons. The couplings relevant to this work are

$$g_{\Lambda\Sigma\pi} = \frac{2}{\sqrt{3}}(1 - \alpha)g_{NN\pi}, \quad (4.64)$$

$$g_{\Sigma\Sigma\pi} = 2\alpha g_{NN\pi}, \quad (4.65)$$

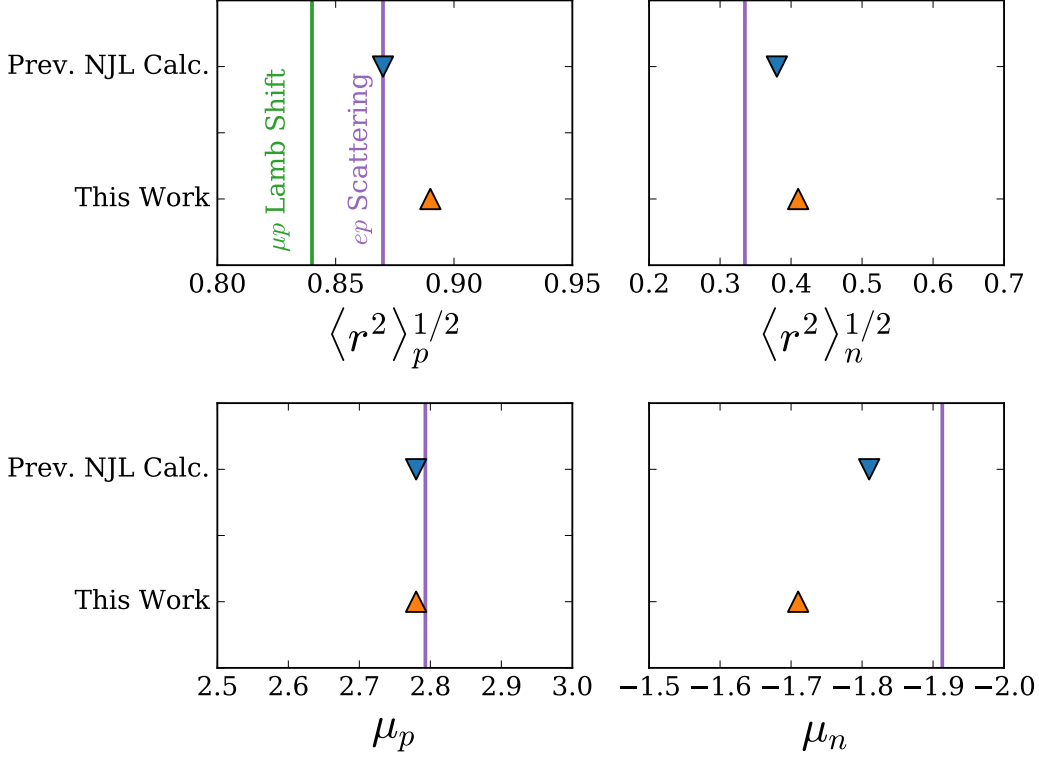


FIGURE 4.6: Comparison of predicted nucleon charge radii and magnetic moments with experimental results taken from Ref [43].

where we set $\alpha = 2/5$. We may calculate chiral corrections to hyperon electromagnetic form factors by making the following substitutions to equations (4.49) - (4.53):

$$m_N \rightarrow m_H, \quad (4.66)$$

$$F_i = 4 \left[\frac{(1-\alpha)^2}{3} F_{i,a}^\Lambda + \alpha^2 F_{i,a}^{\Sigma^0} + \alpha^2 F_{i,a}^{\Sigma^-} \right], \quad (4.67)$$

$$I_\tau = 4 \left[\frac{(1-\alpha)^2}{3} + \alpha^2 \right]. \quad (4.68)$$

Note that we take the Σ^0 and Λ to be mass degenerate in the calculation of loop diagrams. With these simple modifications, we may immediately incorporate pion loop effects on the quark model form factor calculation for the charged sigma hyperons.

4.7 Hyperon Results

The predicted form factors for the charged sigma hyperons are shown below in Fig. 4.7. Due to their shorter lifetimes, the form factors of the hyperons are experimentally undetermined, although some data exists for the charge radii and magnetic moments. Instead of experimental data, we compare our predicted form factors to form factors calculated in Lattice QCD in Refs. [131, 132]. From the comparison with this lattice data, it appears that the implementation

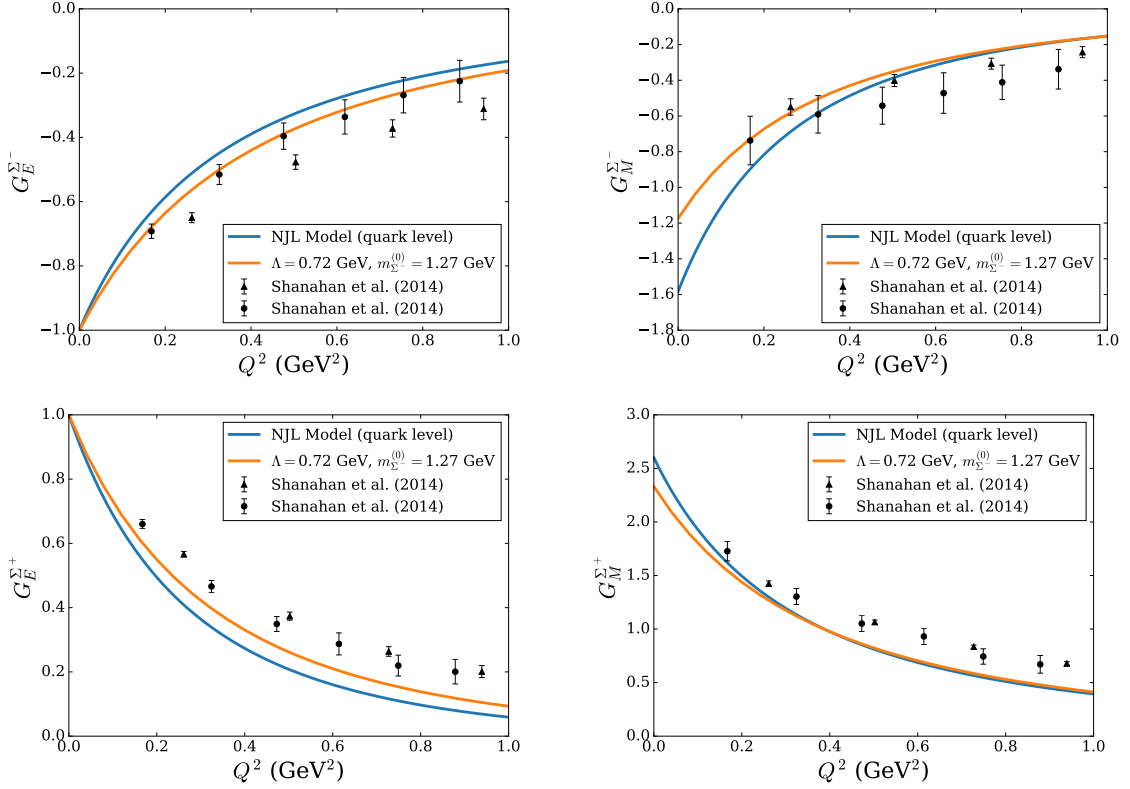


FIGURE 4.7: (Colour online) Electromagnetic form factors for the Σ^- and Σ^+ . Points with error bars correspond to lattice results from [131, 132]. Note that the previous NJL calculation of the Σ^- magnetic moment gives a value of $-1.58 \mu_N$, while the method employed in this work yields a value of $-1.17 \mu_N$. The experimental value is quoted as $-1.16 \mu_N$.

of chiral symmetry at the hadron level leads to a superior prediction of the form factors up to 1 GeV^2 .

Comparing the predicted and experimental magnetic moments in Fig. 4.6, we see that the proton magnetic moment agrees with the experimental value, while the predicted neutron magnetic moment is slightly worse than the previous NJL Model prediction. The Σ^+ magnetic moment shows a comparable level of agreement with experiment as the previous NJL model. However, it is for the Σ^- magnetic moment that one finds a remarkable difference when the chiral corrections are implemented correctly. Whereas evaluating the loops on individual quarks leads to $\mu_{\Sigma^-} = -1.58$, far larger than the empirical value ($\mu_{\Sigma^-}^{\text{Exp}} = -1.160 \pm 0.025$ [43]), when implemented correctly at the hadronic level one finds $\mu_{\Sigma^-} = -1.17$, which is in good agreement with experiment.

The reason for the overestimate in the Σ^- case is that the pion cloud on a d -quark dramatically increases its magnetic moment. The relative increase for a u -quark is also significant and all three quarks give a negative correction to the Σ^- as the valence u -quark has spin down. Thus the present calculation produces an overall description of the nucleon and Σ^- charge radii of a similar quality to those generated in the earlier, parton level model. For the Σ^+ we stress that the lattice QCD result for the charge radius still suffers some systematic uncertainties, as discussed in the original work [131, 132].

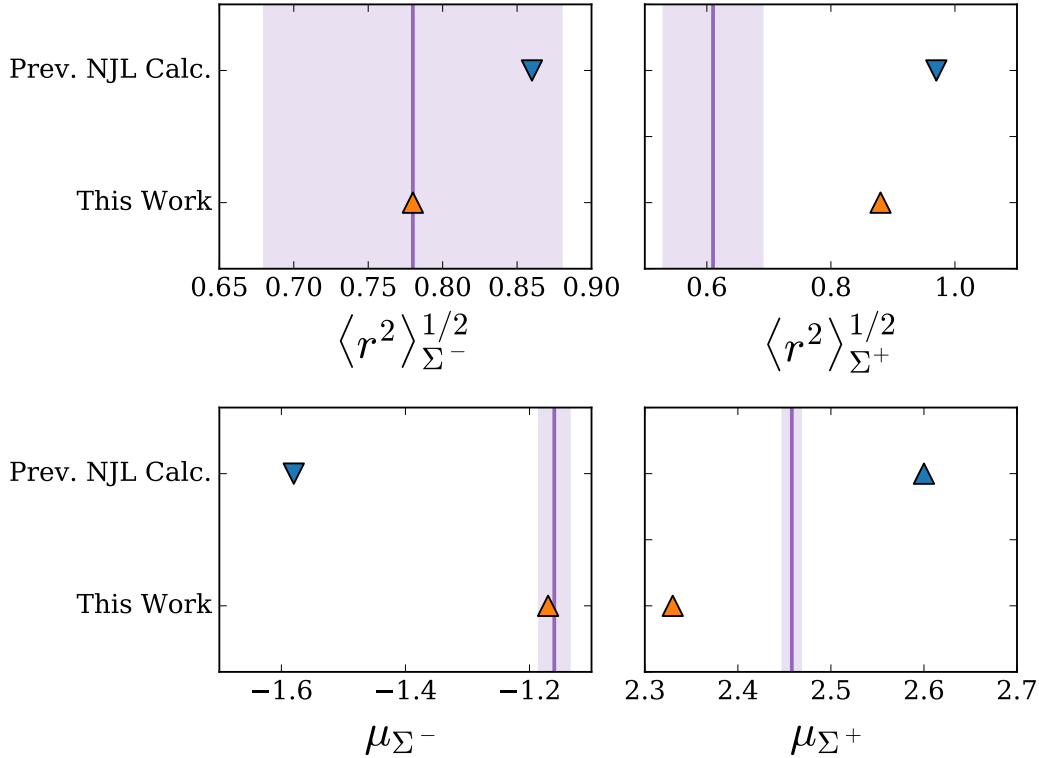


FIGURE 4.8: Comparison of predicted hyperon charge radii and magnetic moments with experimental results taken from Ref. [43].

4.8 Conclusion

In this chapter, we began by explaining how baryon electromagnetic form factors are calculated in the NJL Model, before discussing the constraints on hadronic amplitudes from the approximate chiral symmetry using the formalism of chiral effective field theory. We explained that the leading non-analytic behaviour of observables was an important check of the model's implementation of chiral symmetry, and explained why the previous calculation's implementation of the pion field was not consistent with chiral symmetry. To examine the empirical importance of this fact, we investigated the electromagnetic form factors of the nucleons and Sigma hyperons. The NJL model was used to evaluate the form factors of the underlying quark structure, while the pion loop corrections were evaluated at the baryon level using chiral effective field theory. The results were compared with experimental data where available, or with the results of a recent lattice QCD simulation if no experimental value existed.

For the proton and neutron, there was little practical difference between the results of implementing the chiral corrections at the hadron or parton level. On the other hand, for the magnetic form factor of the Σ^- , there was an improvement when the pion corrections were evaluated correctly. In particular, the Σ^- magnetic moment was reduced by roughly 30% compared with an evaluation at the individual quark level, with the new result now in agreement with experiment.

In summary, while it is convenient to evaluate pion loop corrections on individual quarks, independent of the hadronic environment, the results reported here illustrate very clearly that such an approach can deliver (at least for the hyperons studied) inaccurate results. Worse, there seems to be no obvious way to predict ahead of time whether or not the calculated values may be expected to be reliable. Hence, it is clear that a theoretically consistent, reliable result may only be obtained by performing the chiral corrections at the hadron level.

Investigating the Model Dependence of the Pion Electromagnetic Form Factor in a Scalar Field Theory

We have seen from our study of nucleon and hyperon electromagnetic form factors that pionic contributions play an important role, especially in the low energy regime. It should be clear from this study, as well as the previous discussion of chiral effective field theory more generally (see Chap. 2), that the pion is integral for understanding the low energy behaviour of QCD. While the treatment of the pion in chiral effective field theory as a fundamental field is certainly valid when the momentum scales small enough to neglect the internal structure, this description fails around $4\pi f_\pi$. Owing to asymptotic freedom arising from the running of the strong coupling $\alpha_S(Q^2; \mu^2)$, QCD becomes perturbative at large energies. In this high energy regime, a different picture of the pion emerges as a bound state of two valence quarks, mediated by gluon exchange. Based on this simple picture, predictions may be made about the pion's high energy properties, including its electromagnetic form factor. As a result of these predictions, a number of experimental searches have been conducted in an attempt to observe this expected behaviour, but these have so far been unsuccessful. The latest of these searches was conducted in 2008 at the Jefferson Laboratory, where measurements of the pion form factor were extracted from pion electroproduction data [97, 134]. The measured values for the pion form factor obtained from the 2008 analysis are model dependent, and require the use of the Vanderhaeghen, Guidal and Laget (VGL) Regge Model for their extraction. As we shall see, the extracted values of the pion form factor are yet to show any signs of deviation from the Vector Meson Dominance monopole prediction. As with any model dependent analysis, questions may be raised about the validity and applicability of the chosen model. By understanding the fundamental constraint of gauge invariance leads to the conclusion that the implementation of gauge invariance in the VGL Model is unnatural.

Using a simple model of pion electroproduction, we simulate the electroproduction cross section, and attempt to extract the pion form factor using a VGL-like Model, mirroring the approximation currently used by the F_π collaboration. We conclude that the reconstructed model form factor is a reasonable representation of the true model form factor for the kinematics chosen, although we note that the extracted form factor is larger than the true form factor. This suggests that current extracted values of the pion form factor may be overestimated. We

begin this chapter with a discussion of the pion form factor at high energies. The results of this chapter are published in Ref. [135].

5.1 Exclusive Processes in Perturbative Quantum Chromodynamics

The pion is an excellent testing ground for theoretical predictions since its relatively simple valence structure readily lends itself to analysis. In 1979 Farrar and Jackson used the light cone Bethe-Salpeter equation to make a prediction about the asymptotic form of the pion's electromagnetic form factor [136]. For (space-like) momenta Q^2 greater than some large mass scale μ^2 , they showed that

$$Q^2 F_\pi(Q^2) \rightarrow 16\pi f_\pi^2 \alpha_s(Q^2; \mu^2), \quad (5.1)$$

where $f_\pi \approx 0.132$ GeV is the pion decay constant, and $\alpha_s(Q^2; \mu^2)$ is the renormalised strong coupling constant, which to one-loop order is given by

$$\alpha_s(Q^2; \mu^2) = \frac{\alpha_S}{1 + \frac{\alpha_S}{4\pi} \left(\frac{11}{3} N_c - \frac{2}{3} n_f \right) \ln \left(\frac{Q^2}{\mu^2} \right)}. \quad (5.2)$$

A generalization of this result was given by Lepage and Brodsky, who used a different approach to show that the pion form factor is given by [137, 138]:

$$Q^2 F_\pi(Q^2) = 16\pi f_\pi^2 \alpha_s(Q^2; \mu^2) \omega^2(\mu^2) + \mathcal{O}(\alpha_s^2(\mu^2)). \quad (5.3)$$

The factor $\omega(\mu^2)$ is given by

$$\omega(\mu^2) = \frac{1}{3} \int_0^1 dx \frac{1}{x} \phi_\pi(x, \mu^2), \quad (5.4)$$

where $\phi_\pi(x, \mu^2)$ is known as the pion's light cone distribution amplitude, and is interpreted as the probability amplitude of converting a pion into a $q\bar{q}$ pair where one of the partons has longitudinal momentum fraction x and the other has longitudinal momentum fraction $(1-x)$. This is shown in Fig. 5.1. In light-cone gauge, ϕ is related to the so-called hadronic wave function, ψ , which is the positive energy projection of the Bethe-Salpeter wave function evaluated at light-front time $z^+ = z^0 + z^3 = 0$ [138].

Each quark may carry a fraction of momentum between zero and one, and so the light cone distribution amplitude is defined on $x \in [0, 1]$. It is possible to write a decomposition of ϕ in terms of a complete, orthonormal set of basis functions on $[0, 1]$. One common choice is to use the Gegenbauer polynomials, $C_j^{3/2}(2x-1)$. This leads to the following expression for the distribution amplitude

$$\phi_\pi(x; \mu^2) = 6x(1-x) \left[1 + \sum_{j=2,4,\dots}^{\infty} a_j^{3/2}(\mu^2) C_j^{3/2}(2x-1) \right], \quad (5.5)$$

where it is important to note that the coefficients $a_j^{3/2}(\mu^2)$ are dependent on the renormalization mass scale μ^2 . In the limit that μ^2 is asymptotically large, these coefficients vanish logarithmically, leading to the so-called asymptotic form of the pion's light cone distribution amplitude which is given as

$$\phi_\pi(x; \infty) = 6x(1-x). \quad (5.6)$$

If one uses the asymptotic form of the light cone distribution amplitude in the definition of $\omega(\mu^2)$, it is possible to show that this term reduces to unity, and thus one obtains the original prediction of Farrar and Jackson as a limiting case of Lepage and Brodsky's result. While the use of the asymptotic form of the pion light cone amplitude leads to a simpler form of the expression, it is not clear that the currently reachable energy scales are consistent with this mass scale. In other words, it is not clear that $\mu^2 \approx Q^2 \approx \infty$. As we shall see, it appears that the current experimental scale is not consistent with this asymptotic renormalisation scale. Current measurements of the pion form factor disagree with predictions using the asymptotic form of the pion light cone distribution amplitude by about a factor of four.

While it may not be possible to observe the asymptotic behavior of the pion form factor predicted by Farrar and Jackson, modern analyses which use inputs from Schwinger-Dyson studies suggest that it may still be possible to verify the relation proposed by Lepage and Brodsky by choosing the renormalisation mass scale μ^2 to better reflect the scales present in current day experiments. For example, the authors of Ref. [139] use a Schwinger-Dyson based approach to calculate the pion's light cone distribution amplitude at $\mu^2 = 4 \text{ GeV}^2$ as

$$\phi_\pi(x; \mu^2 = 4 \text{ GeV}^2) = \frac{\Gamma(2(p+1))}{\Gamma(p+1)^2} x^p (1-x)^p, \quad (5.7)$$

where $p = 0.3$. The comparison between these two predictions is shown in Fig. 5.2. Using a more suitable mass scale leads to an improved prediction even with the inclusion of the non-asymptotic form of the pion light cone distribution amplitude, but a disparity still exists between theory and experimental data.

The highest energy data for the pion's electromagnetic form factor comes from pion electroproduction measurements, and compared with lower energy data has larger errors. One source of uncertainty in the current high energy measurements of the pion form factor arises due to the model dependence of the extraction process. This model uncertainty is particularly important here if it leads to a systematically larger extracted value than the 'true' form factor. In other words, unnatural simplifications used in the extraction model could contribute to the observed discrepancy between the theory and the data. It is this hypothesis which we attempt to examine in this chapter. Before moving to a discussion of the particular model used in the current extraction of the pion electromagnetic form factor, we must first understand the reason a model dependent analysis is employed. To this end, we begin by explaining the

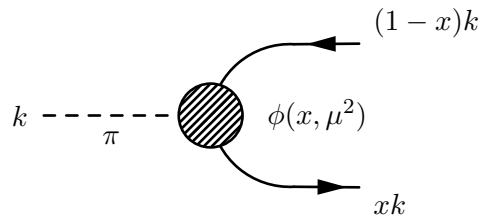


FIGURE 5.1: The pion's light cone distribution amplitude gives the probability amplitude of converting a pion into a $q\bar{q}$ pair, where one of the quarks carries longitudinal momentum fraction x . Momentum conservation requires that the second quark must have longitudinal momentum fraction $1 - x$ so that the two fractions sum to one.

measurement of the pion form factor, and in particular, the reason pion electroproduction is used.

5.2 Measurements of the Pion Form Factor

In principle, the pion's electromagnetic form factor may be measured by elastic $e\pi$ scattering. In the one photon exchange approximation, this process results in a cross section proportional to the square of the pion electromagnetic form factor, and is given by [96]:

$$\frac{d\sigma}{dq^2} = \frac{k}{q^4} \left(1 - \frac{q^2}{q_{\max}^2}\right) |F_\pi(q^2)|^2, \quad (5.8)$$

where q_{\max}^2 is the maximum four-momentum which may be exchanged between the electron and the pion. In the center of mass frame, this corresponds to backwards scattering. With a 300 GeV pion beam, q_{\max}^2 reaches a value of $q_{\max}^2 = 0.288 \text{ GeV}^2$. Thus measurements of the pion form factor directly through elastic scattering are virtuality-limited due to the difficulties in creating high energy pion beams. Nevertheless, measurements of this process have been performed at Fermilab [140, 141], and at CERN SPS [96, 142], and enable an accurate measurement of the pion charge radius which we remind the reader, may be extracted from the slope of the form factor at $Q^2 = 0$. Results from the CERN SPS experiment are shown in Fig. 5.2. The highest energy measurement in this dataset is $Q^2 = 0.25 \text{ GeV}^2$, clearly far below the scales at which QCD is expected to be perturbative, and thus below the scale at which the Lepage-Brodsky prediction becomes applicable. If this prediction is to be tested, another method must be used to extract the pion form factor. One such method is via an analysis of the related process *pion electroproduction*. This is the process which we shall now focus on.

5.2.1 The Pion's Electromagnetic Form Factor at Intermediate Photon Virtuality

As we have seen, kinematic limitations of pion beams and unfavorable momentum transfer at intermediate energies [143] mean that a direct measurement of the pion form factor using elastic $e\pi^+$ scattering becomes prohibitively difficult, and thus will not allow us to study the Lepage-Brodsky result. The current approach is to extract the pion form factor from

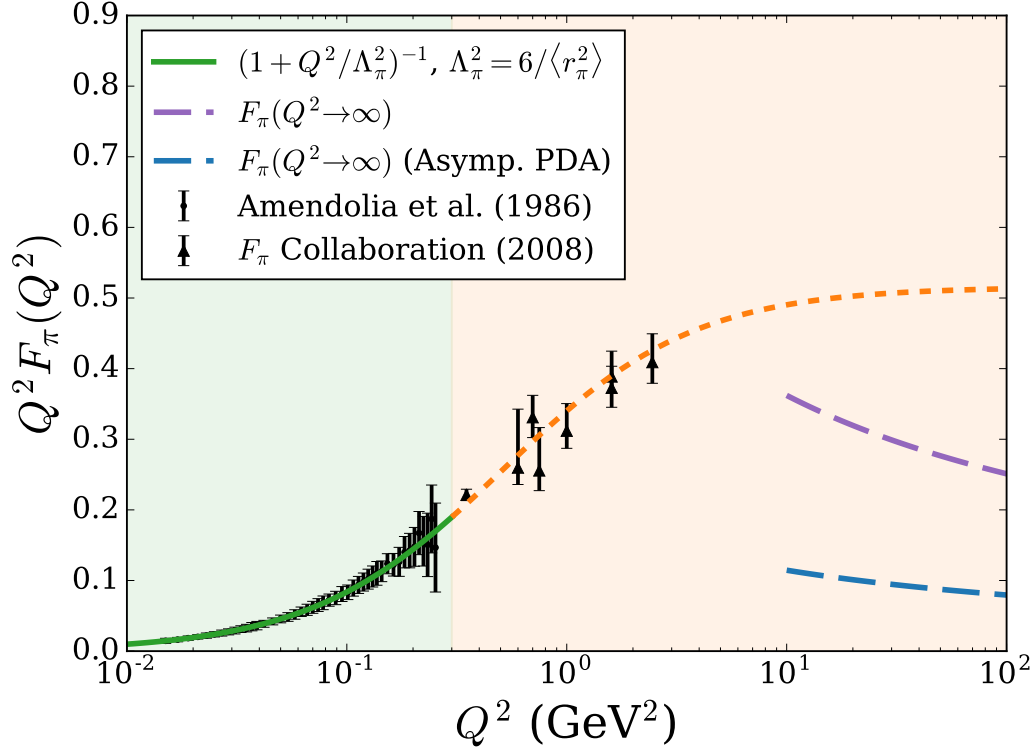


FIGURE 5.2: The pion electromagnetic form factor F_π scaled by photon virtuality Q^2 . Low energy data (below 0.3 GeV^2) is obtained from elastic $e\pi$ scattering. To probe the intermediate energy regime, pion electroproduction has been used. Superimposed on top of the data is a monopole parameterisation of the data based on vector meson dominance (VMD) arguments. Predictions using Farrar and Jackson's asymptotic prediction and Lepage and Brodsky's generalised relation are shown. Currently there is no agreement between the perturbative prediction and experimental data.

electroproduction of pions on the proton. The physical nucleon may be thought of as the result of dressing a bare nucleon with a pion cloud. With this in mind, it is clear that the measurement of the pion form factor from $ep \rightarrow en\pi^+$ is at least possible in principle. However, complications abound over the direct measurement of the form factor at low momentum transfer. As we shall discuss, the kinematics of pion electroproduction do not allow for a direct measurement of the pion's electromagnetic form factor; an extrapolation to unphysical kinematics must be performed. Secondly, unlike $e\pi$ elastic scattering, there are processes which contribute to the measured cross section which do not contribute to the pion form factor. Thus the dependence of the pion form factor on the cross section is more complicated.

5.2.1.1 Preliminaries and Kinematics

For a coincidence experiment in which the scattered electron and pion are detected, and the initial electron and proton four-momenta are known, it is possible to fully reconstruct the kinematics of the system. Importantly, the measured unpolarized differential cross section

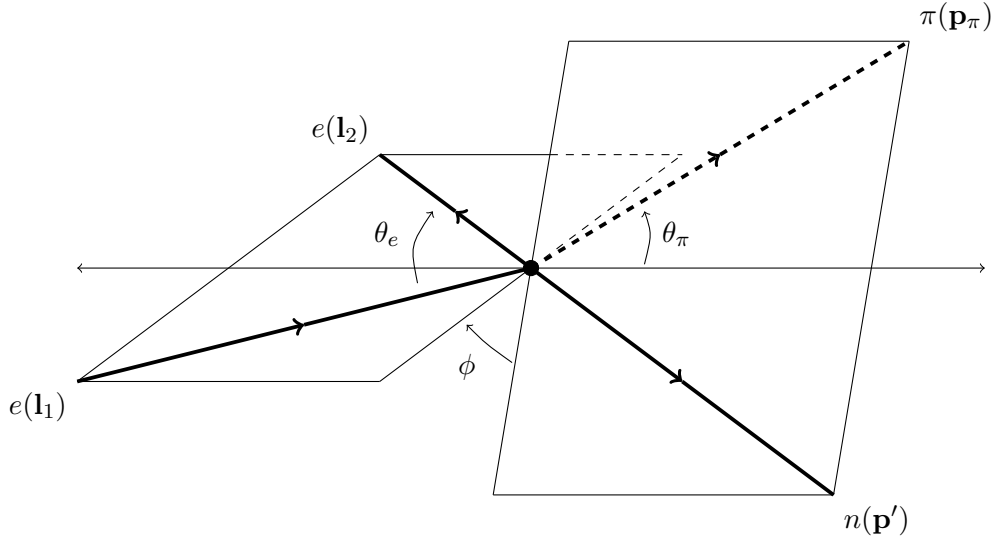


FIGURE 5.3: Pion Electroproduction in the lab frame. Electrons from the CEBAF accelerator are scattered off a liquid hydrogen target. The recoiling electron and produced charged pion are measured. Although the neutron is not measured, its momentum may be inferred by ensuring conservation of momentum.

may be separated according to the polarization states of the virtual photon into transverse (T), longitudinal (L) polarizations as well as two interference terms (LT and TT) [134]

$$(2\pi) \frac{d^2\sigma}{dt d\phi} = \frac{d\sigma_T}{dt} + \epsilon \frac{d\sigma_L}{dt} + \sqrt{2\epsilon(\epsilon+1)} \frac{d\sigma_{LT}}{dt} \cos\phi + \epsilon \frac{d\sigma_{TT}}{dt} \cos 2\phi, \quad (5.9)$$

where ϵ is a measure of the virtual photon polarization, and is related to experimental quantities via $\epsilon = (1 + \frac{2|\mathbf{q}|^2}{Q^2} \tan^2 \frac{\theta_e}{2})^{-1}$, \mathbf{q} is the three-momentum of the virtual photon, ϕ is the angle between the lepton scattering plane and the hadron decay plane and θ_e is the angle between the initial and final electron three-momenta, all measured in the lab frame. The experimental setup is shown diagrammatically in Fig. 5.3

We label the initial proton momentum p , the final proton momentum p' , the virtual photon momentum q , and the pion momentum p_π . This is shown in Fig. 5.4. It will be useful to define the Mandelstam variables

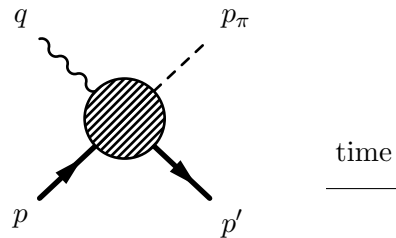


FIGURE 5.4: Hadronic component on pion electro-production in the one-photon exchange approximation (o.p.e.a.). Overall conservation of momentum gives $p + q = p' + p_\pi$. This sets the direction of the external momenta.

$$p_s = p + q = p' + p_\pi, \quad (5.10)$$

$$p_t = p - p' = p_\pi - q, \quad (5.11)$$

$$p_u = p - p_\pi = p' - q, \quad (5.12)$$

where total momentum conservation requires that $p + q = p' + p_\pi$. This sets the directions of the four momenta, which flow into diagrams. Experimentally, the cross section was described in terms of three scalar variables; Q^2 , W and t . These are given explicitly as

$$Q^2 = -q^2, \quad (5.13)$$

$$W^2 = s = (p + q)^2, \quad (5.14)$$

$$t = (p_\pi - q)^2. \quad (5.15)$$

More details about the kinematic variables and their relation to the cross section are given in Appendix D.

Having discussed the conventions for kinematical variables, we next discuss possible approaches to the extraction of the pion form factor. In the next suggestion, we examine the Chew-Low Method, which in principle allows for a model independent extraction of the pion form factor. However, as we shall see, the model is not able to suitably constrain the form factor. We conclude that a model dependent approach is required, and describe the approach used to extract the pion form factor with the aid of a hadronic model.

5.2.1.2 A Model Independent Extraction: The Chew-Low Extraction Method

Originally proposed as a possible method to measure the pion form factor by Frazer in 1959 [144], the Chew-Low extraction method uses a kinematic extrapolation to the pion pole, where it is possible to show that the cross section is proportional to the pion form factor. At the pion pole the only term which can contribute is due to an on-shell pion. It is well known that the t channel diagram dominates the longitudinal differential cross section $d\sigma_L/dt$ [145], so it suffices to only study this structure function. Actor *et al.* provide an expression for the longitudinal differential cross section at the pion pole as:

$$\frac{d\sigma_L}{dt} = \frac{\alpha}{2N} \left[g_{\pi N}^2 \frac{-tQ^2}{(t - m_\pi)^2} F_\pi^2(Q^2) \right], \quad (5.16)$$

where $g_{\pi N}$ is the pion-nucleon form factor and α is the fine structure constant. This result comes from only considering the t -channel diagram. Away from the pion pole, this result is not gauge invariant, but since it will be used to extrapolate to the pion pole, this property is irrelevant. The normalisation N is given by

$$N = (W^2 - m_N^2) \sqrt{(W^2 - m_N^2)^2 + Q^4 + 2Q^2(W^2 - m_N^2)}. \quad (5.17)$$

Rearranging this expression to solve for the pion form factor F_π gives:

$$\frac{t}{m_\pi^2} F_\pi^2(Q^2) = -\frac{1}{m_\pi^2} \frac{2N}{\alpha} \frac{(t - m_\pi^2)^2}{g_{\pi N}^2} \frac{1}{Q^2} \frac{d\sigma_L}{dt}. \quad (5.18)$$

Note that we have divided both sides by a factor of the mass squared, so that at $t = m_\pi^2$, the left hand side is exactly the pion form factor. We define the right hand side $F^2(t)$:

$$F^2(t) = -\frac{1}{m_\pi^2} \frac{2N}{\alpha} \frac{(t - m_\pi^2)^2}{g_{\pi N}^2} \frac{1}{Q^2} \frac{d\sigma_L}{dt}, \quad (5.19)$$

so that we have

$$F^2(t) = \frac{t}{m_\pi^2} F_\pi^2(Q^2). \quad (5.20)$$

In electroproduction, t is kinematically constrained to be less than zero (see Fig. 5.5). Thus in order to measure the pion form factor from electroproduction, we must perform an extrapolation of $F^2(t)$ in t from the last experimental point to the pion pole, where we know this quantity is equal to the pion form factor squared. Note that the t dependence is not fixed between the experimental results, and at the pion pole. The linear dependence in the above relations is the result of the chosen model. We expect the deviations from the linear dependence to be small, and as a result, consider the difference in extracted form factor using linear, quadratic and cubic extrapolations. Unfortunately, even with the most accurate data, it was found that quadratic and higher order polynomials fits provided indistinguishable descriptions of the data in the physical region, but resulted in an extrapolated value for the pion form factor which differed by as much as 15% from the ‘true’ value [97]. For an example of this, see Fig. 5.6. Today, the accepted consensus is that, even with current precision of the measurements of the differential cross section, the Chew-Low extrapolation technique is too imprecise to produce a realistic pion form factor. Indeed, the members of the Jefferson Lab F_π Collaboration stated that the Chew-Low Extraction method ‘... cannot be used to reliably determine the pion form factor from a realistic σ_L data set’ [97].

The key failing of the Chew-Low extrapolation method is that the behaviour of the amplitude away from the pion pole is not determined, and must be parameterised as a polynomial in t . While this leads to a model independent approach, the extrapolation distance is too large for the Chew-Low approach to be feasible. In the context of a particular model however, this t dependence is entirely determined, and, as we shall see, allows the extraction of the pion form factor in a model dependent approach.

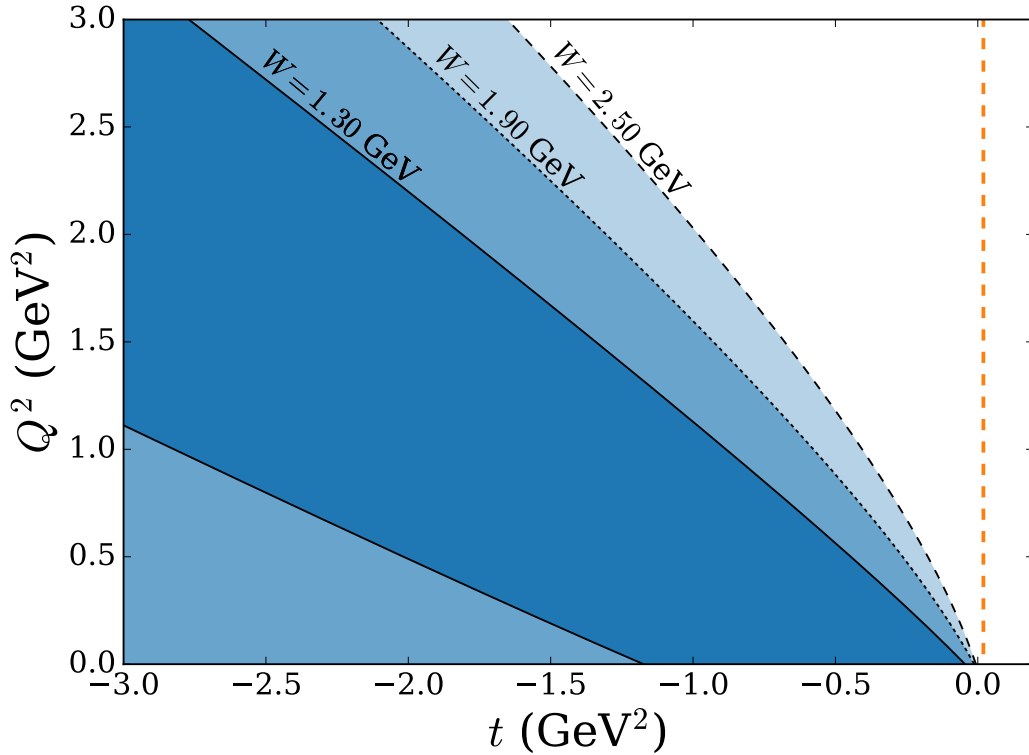


FIGURE 5.5: In pion electroproduction, t is constrained to be less than zero. The exact kinematic range of t may be determined for fixed Q^2 and W . Kinematic ranges for a number of different choices of W are stacked on top of each other. Note that as W increases, the allowed kinematic range in t becomes larger, and in particular, this allows one to reach smaller absolute values of t . Also displayed on the plot is the line $t = m_\pi^2$. In a Chew-Low extrapolation, the distance between the smallest absolute value of t and $t = m_\pi^2$ is the *extrapolation distance*.

5.3 A Model Dependent Extraction: The VGL Model

In 2008, the F_π Collaboration released results for the pion form factor measured from pion electroproduction [97, 134]. In order to perform the extraction, they found as we have shown that a model independent analysis failed to sufficiently constrain the pion form factor and they were forced to use a model dependent analysis. In this analysis, an effective field theoretic model called the Vanderhaeghen Guidal and Laget (VGL) Model was used to extract the pion form factor by fitting the differential cross section data. While the use of a model is necessary in the case of pion electroproduction, care must be taken to ensure that assumptions and simplifications made in the development of the model do not drastically effect the extracted values of the pion form factor and lead to undetermined systematic errors. Unfortunately, there is no simple way of ensuring that the simplifications made lead to negligible systematic errors. However, it is possible to identify possible sources of error by examining theoretical constraints on the amplitude. In particular, we shall examine the implementation of the gauge symmetry of QED and argue that this implementation may lead to a model which overextracts the pion form factor. We shall begin our discussion of the VGL Model by examining the Born Term Model upon which it is based.

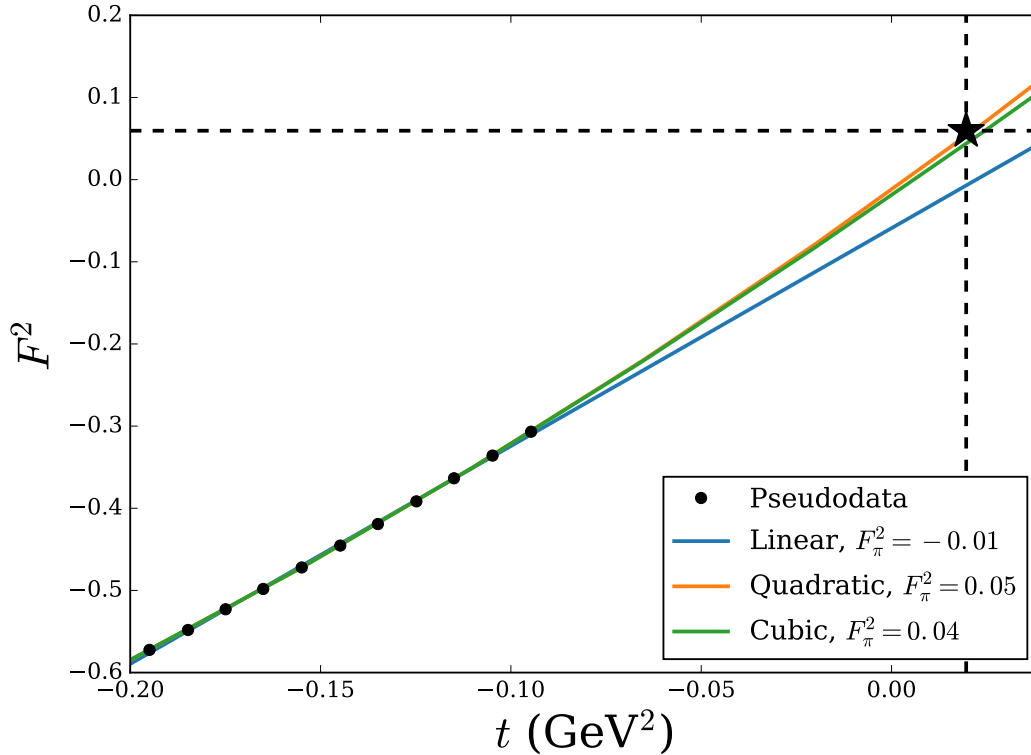


FIGURE 5.6: Attempting to perform the Chew-Low extrapolation method on simulated high precision pion electroproduction cross section data for the kinematic point $Q^2 = 1.59 \text{ GeV}^2$, $W = 2.21 \text{ GeV}$. Pseudodata is generated using the Vanderhaeghen Guidal and Laget Model, and is represented here with black circles. It is known that the pion form factor F_π may be extracted from this plot by extrapolating to the pion mass $t = m_\pi^2$, although it is unknown what the functional form of this extrapolation is. To examine the viability of this approach linear, quadratic and cubic fits were performed on the data. While each fit agreed reasonably well in the physical region, differences were observed in the extrapolated pion form factor. This plot has been adapted from Ref. [97].

5.3.1 Introduction to the Born Term Model

Before understanding how to incorporate electromagnetic form factors, it is useful to understand the Born Term Model from which the VGL model is derived. Let us begin our discussion by isolating the part of the electroproduction amplitude which we wish to calculate. We will work to $\mathcal{O}(\alpha_{\text{QED}})$, where $\alpha_{\text{QED}} = e^2/(4\pi) \approx 1/137$. This is called the one photon exchange approximation, and leads to diagrams of the form shown in Fig. 5.7. The tree level pion electroproduction amplitude may be written as

$$\begin{aligned}
 i\mathcal{M} &= \bar{u}(k')(ie)\gamma^\mu u(k) \frac{(-ig_{\mu\nu})}{q^2} e\mathcal{M}^\nu \\
 &= l_\mu \mathcal{M}^\mu,
 \end{aligned}
 \tag{5.21}$$

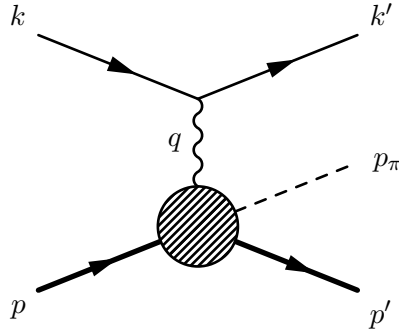


FIGURE 5.7: In the One Photon Exchange Approximation, the electromagnetic and hadronic parts of the matrix element may be factorised. This factorisation allows us to focus on the part of the amplitude which is unknown.

where

$$l_\mu = \frac{e^2}{q^2} \bar{u}(k') \gamma^\mu u(k) \quad (5.22)$$

is the leptonic component of the matrix element and \mathcal{M}^μ is the hadronic matrix element. Recall that the differential cross section $d\sigma$ is proportional to the matrix element squared. Thus

$$\begin{aligned} d\sigma &\propto \sum_{\text{spins}} |i\mathcal{M}|^2 \\ &\propto \frac{2e^4}{q^4} L_{\mu\nu} M^{\mu\nu}, \end{aligned} \quad (5.23)$$

where we define

$$L_{\mu\nu} = \frac{1}{4} \sum_{\text{spins}} l_\mu l_\nu^\dagger \quad (5.24)$$

$$M^{\mu\nu} = \frac{1}{2} \sum_{\text{spins}} \mathcal{M}^\mu \mathcal{M}^{\nu\dagger}. \quad (5.25)$$

The physics of QED is well understood, and may be analysed using perturbative techniques. A standard calculation leads to¹:

$$L_{\mu\nu} = k_\mu k'_\nu + k'_\mu k_\nu + \frac{1}{2} g_{\mu\nu} q^2. \quad (5.26)$$

¹See for example, Ref. [41], pp. 131-135.

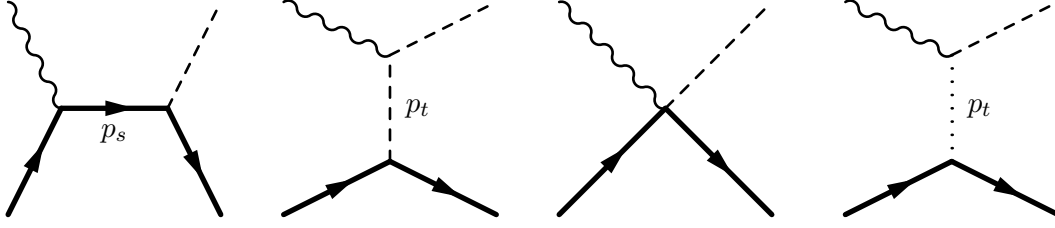


FIGURE 5.8: Tree level diagrams which contribute to the Born Term Model. The contact term is also known as the Kroll-Ruderman term and is the result of using a pseudovector pion-nucleon coupling. The final diagram is due to the exchange of a rho meson, which we exclude from our discussion.

This ‘factorisation’ of the amplitude is extremely useful, as it allows us to focus on the hadronic matrix element. It is the evaluation of this hadronic matrix element to which we now turn. The starting point for an effective field theoretic description of pion electroproduction is a chiral effective field theory of pions and nucleons with a pseudo-vector pion-nucleon interaction of the form

$$\mathcal{L}_{\pi N} = \frac{g_A}{2f_\pi} \bar{\Psi}_N \gamma^\mu \gamma_5 \boldsymbol{\tau} \cdot \partial_\mu \boldsymbol{\pi} \Psi_N - \frac{1}{(2f_\pi)^2} \bar{\Psi}_N \gamma^\mu \boldsymbol{\tau} \cdot (\boldsymbol{\pi} \times \partial_\mu) \Psi_N, \quad (5.27)$$

where $f_\pi = 0.093$ GeV is the pion decay constant, and $g_A = 1.267$ is the nucleon axial vector charge. $\Psi_N = (\psi_p, \psi_n)$ is the nucleon doublet, and $\boldsymbol{\pi} = (\pi^+, \pi^-, \pi^0)$ is the pion triplet. Electromagnetic interactions are introduced to ensure invariance under $U(1)$ gauge transformations (see Appendix B for details). This leads to electromagnetic interactions of the form

$$\begin{aligned} \mathcal{L}_{\gamma\pi N} = & -\bar{\Psi}_N \gamma^\mu \hat{Q} \Psi_N A_\mu + i(\partial^\mu \boldsymbol{\pi}) \cdot (\hat{Q} \boldsymbol{\pi}) A_\mu + \frac{ig_A}{2f_\pi} \bar{\Psi}_N \gamma^\mu \gamma_5 \boldsymbol{\tau} \cdot \hat{Q} \boldsymbol{\pi} \Psi_N A_\mu \\ & - \frac{i}{(2f_\pi)^2} \bar{\Psi}_N \gamma^\mu \boldsymbol{\tau} \cdot (\boldsymbol{\pi} \times \hat{Q} \boldsymbol{\pi}) \Psi_N A_\mu. \end{aligned} \quad (5.28)$$

This approach treats the pion and nucleon fields as *elementary*. That is to say, that the particles have no structure. As we have explained, this description of hadronic particles as elementary fields is good when the characteristic momentum scale of the problem is considerably less than the size of the hadrons involved. The resulting tree level diagrams which contribute to the process $p(p) + \gamma(q) \rightarrow n(p') + \pi^+(p_\pi)$ are shown in Fig. 5.8. Ignoring the rho meson, we have three contributions to the Born Term Model. They are:

$$i\mathcal{M}_s^\mu = \frac{g_A}{\sqrt{2}f_\pi} \bar{u}_N(p') \gamma_5 \not{p}_\pi S_F(p_s) (-ie\gamma^\mu) u_N(p), \quad (5.29)$$

$$i\mathcal{M}_t^\mu = \frac{g_A}{\sqrt{2}f_\pi} \bar{u}_N(p') \gamma_5 \not{p}_t u_N(p) D_F(p_t) (-ie)(p_t + p_\pi)^\mu, \quad (5.30)$$

$$i\mathcal{M}_{\text{K.R.}}^\mu = -\frac{g_A e}{\sqrt{2}f_\pi} \bar{u}_N(p') \gamma_5 \gamma^\mu u_N(p). \quad (5.31)$$

Note that in Fig. 5.8 we also have a t -channel diagram due to the exchange of a ρ meson. While this diagram is also included in the VGL Model, its inclusion here adds nothing to the discussion of gauge invariance, and so we ignore it. Thus the Born Term Model hadronic matrix element is

$$i\mathcal{M}_{\text{BTM}}^\mu = \frac{g_A}{\sqrt{2}f_\pi} \bar{u}_N(p') \gamma_5 \left[\not{p}_\pi S_F(p_s) (-ie\gamma^\mu) + \not{p}_t D_F(p_t) (-ie)(p_t + p_\pi)^\mu - \gamma^\mu \right] u_N(p). \quad (5.32)$$

Note that one may show that this amplitude satisfies the Ward-Takahashi Identity which in this case amounts to $q_\mu \mathcal{M}^\mu = 0$. Contracting q_μ into the hadronic amplitude gives

$$iq_\mu \mathcal{M}^\mu = \frac{g_A e}{\sqrt{2}f_\pi} \bar{u}_N(p') \gamma_5 \left[\not{p}_\pi \frac{(\not{p}_s + m_N)}{s - m_N^2} \not{q} + \not{p}_t \frac{q \cdot (p_t + p_\pi)}{t - m_\pi^2} - \not{q} \right] u_N(p). \quad (5.33)$$

Using the relations for the Mandelstam Variables described in previously, we have

$$\not{q} = \not{p}_s - \not{p}, \quad (5.34)$$

$$q = -p_t + p_\pi. \quad (5.35)$$

Noting that the Dirac equation gives $\not{p}u_N(p) = m_N u(p)$, we have

$$iq_\mu \mathcal{M}^\mu = \frac{g_A e}{\sqrt{2}f_\pi} \bar{u}_N(p') \gamma_5 \left[\not{p}_\pi \frac{(\not{p}_s + m_N)(\not{p}_s - m_N)}{s - m_N^2} - \not{p}_t \frac{(p_t - p_\pi) \cdot (p_t + p_\pi)}{t - m_\pi^2} - \not{q} \right] u_N(p). \quad (5.36)$$

Expanding the brackets allows us to cancel the denominators and the expression reduces to

$$iq_\mu \mathcal{M}^\mu = \frac{g_A e}{\sqrt{2}f_\pi} \bar{u}_N(p') \gamma_5 \left[\not{p}_\pi - \not{p}_\pi + \not{q} - \not{q} \right] u_N(p) = 0, \quad (5.37)$$

where we have used $p_t = p_\pi - q$. Thus the hadronic current is conserved. Note that this is true even at $q^2 \neq 0$, as it must be. Importantly though, tracing the origins of the terms back,

it is possible to see that a precise cancellation occurs between the t , s and Kroll-Ruderman terms. While the simplicity of this model is extremely attractive, the simple Born Term Model is unsuitable to describe pion electroproduction data. Away from the photoproduction point $q^2 = 0$, this model overpredicts the cross section. This is because the model does not incorporate the extended structure of the pion and nucleon.

While the Born Term Model is unsuitable to describe pion electroproduction, its simplicity is attractive. In the next section, we discuss a modification of the Born Term Model proposed by Vanderhaeghen Guidal and Laget, which attempts to include the structure of the hadrons and thus improve the description of electroproduction data. As we shall see, constraints from gauge invariance restrict the way structure may be incorporated within the Born Term Model, and ultimately lead to a factorization which we will argue is unnatural.

5.3.2 Incorporating Structure in the Born Term Model

From our discussion of electromagnetic form factors from Chap. 3, we know that the most general form of the electromagnetic vertex for the nucleon contains twelve independent form factors. In the limit that the two nucleon legs are on their mass-shells, this reduces to three form factors. Requiring that this vertex satisfies the Ward-Takahashi Identity provides a further constraint which reduces the degrees of freedom from three to two. We thus arrive at

$$\Gamma_N^\mu(p_1, p_2; q) = \gamma^\mu F_1(q^2) + \frac{i\sigma^{\mu\nu} q_\nu}{2m_N} F_2(q^2). \quad (5.38)$$

A similar argument for the pion (which has spin-zero) leads to

$$\Gamma_\pi^\mu(k_1, k_2; q) = (k_1 + k_2)^\mu F_\pi(q^2). \quad (5.39)$$

In the context of pion electroproduction, it is tempting to use the on-shell forms of these vertex functions, in place of the vertices one obtains from perturbation theory. That is, making the replacements

$$\gamma^\mu \rightarrow \gamma^\mu F_1(q^2) + \frac{i\sigma^{\mu\nu} q_\nu}{2m_N} F_2(q^2), \quad (5.40)$$

$$(p_t + p_\pi)^\mu \rightarrow (p_t + p_\pi)^\mu F_\pi(q^2), \quad (5.41)$$

in the Born Term Model matrix elements. Since the pion electroproduction measurements are made at small $|t|$, it may be argued that the approximation of the on-shell pion electromagnetic vertex is acceptable. Further, since measurements are made at $W = 1.95$ GeV and $W = 2.2$ GeV, $s \geq 3.8$ GeV², although the on-shell nucleon vertex function may be a poor approximation for the s -channel diagram, these contributions will be suppressed by a factor

$$\frac{1}{s^2 - m_N^2} \approx 0.3, \quad (5.42)$$

so these contributions may be small. As it turns out, while these arguments may suggest that a simple modification of the Born Term Model could lead to a model which incorporates electromagnetic structure, fundamental constraints on the amplitude from gauge invariance invalidate this approach. Let us examine this argument now. Consider the minimal case where electromagnetic structure is incorporated. The minimal Born Term Model in which structure has been incorporated at the electromagnetic vertices is given below.

$$i\mathcal{M}_{\text{struc.}}^\mu = \frac{g_A e}{\sqrt{2}f_\pi} \bar{u}_N(p') \left[\gamma_5 \not{p}_\pi \frac{(\not{p}_s + m_N)}{s - m_N^2} \gamma^\mu F_1^p(q^2) + \gamma_5 \not{p}_\pi \frac{(\not{p}_s + m_N)}{s - m_N^2} \frac{i\sigma^{\mu\nu} q_\nu}{2m_N} F_2(q^2) \right. \\ \left. + \gamma_5 \not{p}_t \frac{(p_t + p_\pi)^\mu}{t - m_\pi^2} F_\pi(q^2) - \gamma_5 \gamma^\mu g(q^2) \right] u_N(p). \quad (5.43)$$

We have ignored the contribution from the neutron, which would in principle enter as a u -channel diagram. The neutron electric form factor is rather small and, as we shall see, the Pauli form factors are irrelevant to our discussion of gauge invariance. To keep the discussion as general as possible, we have chosen to incorporate a form factor $g(q^2)$ on the Kroll-Ruderman contact interaction. One may recover the structureless result by setting $g = 1$. We now consider the constraint on the amplitude due to the Ward Takahashi Identity. Since external hadronic legs are on their respective mass shells, the relation reduces to

$$q_\mu \mathcal{M}_{\text{struc.}}^\mu = 0. \quad (5.44)$$

Contracting this ‘generalized amplitude’ with q_μ gives

$$iq_\mu \mathcal{M}_{\text{struc.}}^\mu = \frac{g_A e}{\sqrt{2}f_\pi} \bar{u}_N(p') \left[\gamma_5 \not{p}_\pi \frac{(\not{p}_s + m_N)}{s - m_N^2} \not{q} F_1^p(q^2) + \gamma_5 \not{p}_t \frac{q \cdot (p_t + p_\pi)}{t - m_\pi^2} F_\pi(q^2) - \gamma_5 \not{q} g(q^2) \right] u_N(p). \quad (5.45)$$

Note that as advertised, the terms proportional to the Pauli Form Factor vanish, since $q_\mu \sigma^{\mu\nu} q_\nu = 0$. Except for the different functions of q^2 which multiply each of the diagrams, this matrix element is identical for the Born Term Model. Thus we may use the above results here to immediately find

$$iq_\mu \mathcal{M}_{\text{struc.}}^\mu = \frac{g_A e}{\sqrt{2}f_\pi} \bar{u}_N(p') \gamma_5 \left[\not{p}_\pi F_1(q^2) + (-\not{p}_\pi + \not{q}) F_\pi(q^2) - \not{q} g(q^2) \right] u_N(p). \quad (5.46)$$

If this amplitude is to be consistent with the Ward-Takahashi Identity, we must have that

$$F_1(q^2) = F_\pi(q^2), \quad (5.47)$$

$$F_\pi(q^2) = g(q^2). \quad (5.48)$$

Applying these constraints, one arrives at

$$\mathcal{M}_{\text{struc.}}^\mu = F_\pi(q^2)\mathcal{M}_{\text{BTM}}^\mu. \quad (5.49)$$

In other words, the only way to modify the Born Term Model and retain gauge invariance is by multiplying the amplitude by an overall factor. Given that as we have argued, only the t -channel diagram should know anything about the pion form factor, this factorization appears to be a rather unnatural implementation of gauge invariance.

We may understand the above constraint on the amplitude by considering the requirements of gauge invariance. Recall that as consequence of gauge invariance, the propagator and the vertex function are related via the Ward-Takahashi Identity:

$$-iq_\mu\Gamma^\mu(p, p'; q) = S_F^{-1}(p') - S_F^{-1}(p), \quad (5.50)$$

where $S_F(p)$ is the dressed propagator and Γ^μ is the corresponding dressed vertex function. The Born Term Model is defined by calculating the cross section at tree level, and thus amounts to the approximations

$$\Gamma^\mu(p, p'; q) = \gamma^\mu, \quad (5.51)$$

$$S_F(p) = \frac{i}{\not{p} - m_N}. \quad (5.52)$$

Since the Ward-Takahashi identity is true order-by-order, it is possible to see that the vertex and propagator are consistent with gauge invariance. The left hand side of the Ward Takahashi Identity is

$$-iq_\mu\Gamma^\mu(p, p'; q) = -i\not{q}, \quad (5.53)$$

while the right hand side is

$$S_F^{-1}(p') - S_F^{-1}(p) = -i(\not{p}' - m_N - \not{p} + m_N) = -i\not{q}, \quad (5.54)$$

where we have noted that $q = p' - p$, and so the Born Term Model electromagnetic vertex and propagator are certainly consistent. Note that a modification of the vertex function to

$$\Gamma^\mu(p, p'; q) = \gamma^\mu F_1(q^2) + \frac{i\sigma^{\mu\nu}q_\nu}{2m_N} F_2(q^2), \quad (5.55)$$

without a corresponding change in the propagator will lead to contradictions. This is the essential reason one cannot modify the vertex function and retain the same propagator in a gauge invariant way.

5.3.3 Transforming the Born Term Model to the VGL Model

Originally developed by Vanderhaeghen Guidal and Laget as a model of pion photoproduction [146], it was quickly realized that the generalization to electroproduction was straightforward, leading to the so-called VGL Model [147]. The VGL Model is based on the Born Term Model we have discussed, and implements hadronic structure in consistently with gauge invariance by utilizing the ‘factorization’ we discussed in the previous section. However, when applied to electroproduction data, it was found that the model still overpredicted the measured cross section.

In order to improve agreement over the Born Terms alone, the pion propagator in the VGL approach is *Reggeized*, which amounts to replacing the pion propagator $D_\pi(t)$ with the Regge version $D_\pi^R(t)$, given by

$$D_\pi^R(s, t) = i \frac{(s/s_0)^{\alpha_\pi(t)}}{\sin(\pi\alpha_\pi(t))} \frac{\pi\alpha'}{\Gamma(1 + \alpha(t))}, \quad (5.56)$$

where $s_0 = 1 \text{ GeV}^2$ sets the mass scale of the trajectory, $s = W^2$ and the so-called Regge Trajectory is $\alpha_\pi(t) = \alpha'_\pi(t - m_\pi^2)$, and $\alpha'_\pi = 0.7 \text{ GeV}^{-2}$. A Taylor series around $t = m_\pi^2$ gives

$$D_\pi^R(s, t) \underset{t \rightarrow m_\pi^2}{=} \frac{i}{t - m_\pi^2} + \text{finite parts}. \quad (5.57)$$

Given our previous discussion of gauge invariance, the astute reader may be wondering about the damage done to gauge invariance by replacing the propagator for the t -channel only. Indeed their concern would be well founded. The solution proposed by Vanderhaeghen Guidal and Laget is to also perform the same transformation on the other diagrams. To understand this, consider defining a function $g(s, t)$ given by

$$g(s, t) = \frac{D_\pi^R(s, t)}{D_\pi(t)}. \quad (5.58)$$

Then the VGL prescription for Reggeizing the amplitude in a gauge invariant way is to take the structured Born Term Model, and multiply it by this overall function. Thus

$$\mathcal{M}_{\text{VGL}}^\mu = g(s, t) \mathcal{M}_{\text{struc.}}^\mu = [g(s, t) F_\pi(q^2)] \mathcal{M}_{\text{BTM}}^\mu. \quad (5.59)$$

Written this way, it is clear that the incorporation of structure, as well as the Reggeization of the trajectory both utilize the same approach to preserve the gauge invariance of the amplitude. Thus the Reggeization of this amplitude must be viewed with the same caution as the introduction of gauge invariance. Of course, any hadronic model will contain a number of simplifications. In order to truly determine the effects of particular approximations on the considered model, comparisons must be made with experimental data. In the next section,

we describe this process for the VGL Model, and thus discuss how the pion form factor is extracted from pion electroproduction.

5.3.4 Using the VGL Model to Determine the Electromagnetic Form Factor of the Pion

We can now summarize the procedure used by the F_π Collaboration to fit the VGL Model to experimental data. The functional form of the pion form factor is taken to be the monopole form:

$$F_\pi(Q^2) = \frac{1}{1 + Q^2/\Lambda_\pi^2}, \quad (5.60)$$

and the transition form factor for the ρ is assumed to have the same functional form:

$$F_{\gamma\rho\pi}(Q^2) = \frac{1}{1 + Q^2/\Lambda_\rho^2}, \quad (5.61)$$

where Λ_π^2 and Λ_ρ^2 are the only free parameters in the model. As mentioned previously, the longitudinal cross section is insensitive to the rho meson, so effectively only Λ_π^2 must be fit to obtain the longitudinal cross section.

For some points it sufficed to fit the differential cross section measured fixed Q^2 and W values for small $|t|$ values by varying the value of Λ_π^2 value. In this case, the extracted pion form factor corresponds to the best fit value of Λ_π^2 . However, for a number of kinematic points, this procedure was not sufficient to extract the pion form factor well. An example of this is shown in the first plot of Fig. 5.9. Here, the VGL Model fails to completely describe the t -dependence of the data. In this case each data point was fitted to the corresponding measured differential cross section point individually. Thus for each data point, there is a corresponding extracted Λ_π^2 . This is shown in the second plot of Fig. 5.9. Note that in general, data points measured at smaller values of t tend to result in larger values of Λ_π^2 , and thus larger values of $F_\pi(Q^2)$. It has been suggested that this is due to interfering backgrounds not included in the VGL model [97]. In practice, an extrapolation of Λ_π^2 to the minimum experimentally allowed t value for the chosen Q^2 and W values is performed and it is this value of Λ_π^2 which is taken to correspond to the best estimate of $F_\pi(Q^2)$. These values are shown in Fig. 5.2.

While the agreement between the VGL Model and data is quite good, as we have shown, there is room to improve the implementation of gauge invariance. We aim to understand whether it is worth improving the implementation of gauge invariance, by studying whether the current approach can successfully extract the form factor in a toy model. It is this question we now attempt to answer.

5.3.5 Model Dependence of the Pion Form Factor

As with any model dependent extraction, it is possible to highlight possible failings of the model. In the previous sections, this is what we have endeavoured to do. Of course, one may argue that the only measure of the model's validity is its ability to describe the experimental cross section data and indeed, in this case, the VGL Model appears to be rather successful. We take a more cautious outlook. As we have shown, the model's incorporation of the pion

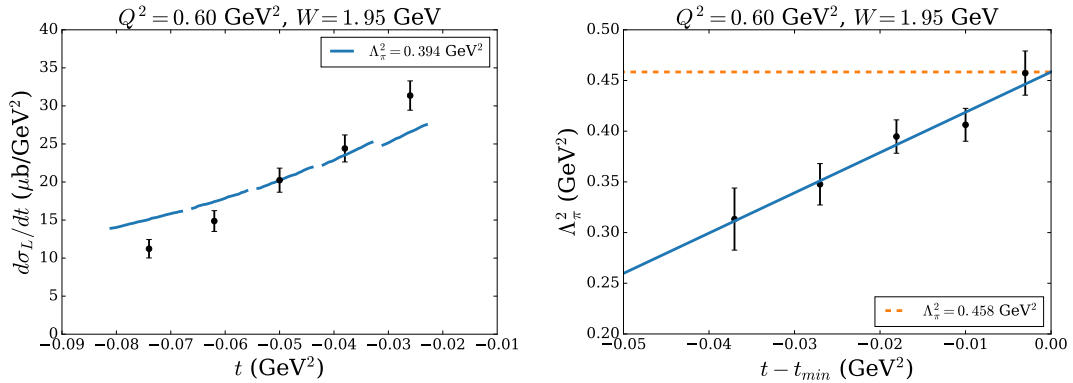


FIGURE 5.9: Plots adapted from the F_π Collaboration’s extraction of the pion form factor (Ref. [97], Fig. 2, Fig. 5). The left plot shows the fitted longitudinal cross section, compared to experimental data. Note that the theory curve for the longitudinal cross section is plotted for a single value of Λ_π^2 to demonstrate the general agreement of the VGL Model with data. As explained, when performing the extraction, the model is fit to each data point independently. The right plot shows the corresponding extracted values of Λ_π^2 . The best fit value for Λ_π^2 for this set of kinematics is $\Lambda_\pi^2 = 0.458 \pm 0.031_{-0.068}^{+0.255} \text{ GeV}^2$ [97].

form factor is constrained by the requirement of gauge invariance. This leads to an unnatural ‘factorisation’ of the pion form factor from the matrix element.

While the consistency of this approach has been checked at low photon virtuality where pion form factor may also be measured directly using elastic electron pion scattering, this consistency check only ensures that the model dependence is small at *low photon virtuality*; it says nothing about systematic model dependence as Q^2 increases. This point is particularly important, since as we have seen, one main motivation for measuring the pion form factor to higher Q^2 is the attempt to observe the transition to perturbative behaviour, predicted by Brodsky and Lepage in Ref. [137]. While modern predictions have brought the theory and current experimental data closer, the current consensus is that higher energy data is required to observe the transition to perturbative QCD. However, as we shall show, this interpretation may be too pessimistic: by studying the extraction of the pion form factor in a simple model of pion electroproduction, where it is possible to explicitly calculate the form factors, a direct comparison of the calculated and extracted form factors allows us to make more concrete statements about the model dependence of the currently extracted pion form factor.

5.4 Scalar Pion Electroproduction Hadronic Matrix Element

We have now seen how the VGL Model preserves gauge invariance. In order to determine the consequences for the extracted pion form factor, we will examine how well the approach works in a simple toy model where we can calculate the form factor and cross section exactly. Our criteria for a suitable model are twofold; it must be gauge invariant and the nucleon and pion must have different (calculable) form factors.

A suitable model for this is Miller’s simple model of the nucleon’s electromagnetic form factors, described in Ref. [148]. In this simple model, we consider a quantum field theory describing the interaction of a scalar ‘nucleon’ and scalar ‘pion’. To be clear, we define a scalar ‘nucleon’

doublet Ψ_N

$$\Psi_N = \begin{bmatrix} \psi_p \\ \psi_n \end{bmatrix}, \quad (5.62)$$

and a scalar ‘pion’ triplet $\boldsymbol{\pi}$

$$\boldsymbol{\pi} = \begin{bmatrix} \pi^+ \\ \pi^- \\ \pi^0 \end{bmatrix}, \quad (5.63)$$

where $\pi^+ = (\pi_1 - i\pi_2)/\sqrt{2}$ and $\pi^- = (\pi_1 + i\pi_2)/\sqrt{2}$. We may write the Lagrangian as

$$\mathcal{L} = \frac{1}{2}(\partial_\mu \Psi_N)^2 - \frac{1}{2}m_N^2 \Psi_N^2 + \frac{1}{2}(\partial_\mu \boldsymbol{\pi})^2 - \frac{1}{2}m_\pi^2 \boldsymbol{\pi}^2 - g_{\pi N} \Psi_N^\dagger \boldsymbol{\tau} \cdot \boldsymbol{\pi} \Psi_N, \quad (5.64)$$

where $\boldsymbol{\tau}$ is the isospin vector. Gauging the Lagrangian leads to electromagnetic interactions between the charged particles in the theory. We are interested in (scalar) $\gamma^* + p \rightarrow \pi^+ + n$. In order to preserve gauge invariance, we calculate one-loop corrections to the tree level cross section. Since gauge invariance is preserved order-by-order in perturbation theory, the resulting theory will certainly be gauge invariant. At one loop, we have 13 diagrams we must evaluate, plus 6 counter terms. We show these diagrams in Fig. 5.10.

Explicit expressions for these diagrams are given in Appendix F. Since we are calculating this model at one loop order, divergences appear which we must absorb into the definitions of our couplings and masses. We use the on-shell renormalisation scheme:

$$\Sigma(p^2) \Big|_{p^2=m^2} = 0, \quad (5.65)$$

$$\frac{d}{dp^2} \Sigma(p^2) \Big|_{p^2=m^2} = 0, \quad (5.66)$$

$$\lim_{q \rightarrow 0} (-ie) \Gamma^\mu(p, p') = (-ie) 2p^\mu. \quad (5.67)$$

Amaldi, Fubini and Furlan in Ref. [149] provide the details of the relationship between the hadronic matrix element and the differential cross section, decomposed in terms of the longitudinal, transverse and interference terms. We include some of this discussion of Appendix D. We use the Mathematica package FEYNCALC [150, 151] to determine our final expression for these structure functions, and then perform the loop integrals using QCDDLOOP [152].

5.4.1 VGL-like Model

The VGL-like model arising from scalar pion electroproduction is simply the sum of the s- and t-channel tree level diagrams already calculated above. These are

$$i\mathcal{M}^{(0a)\mu} = (-i\sqrt{2}g_{\pi N}) D_F^N(p_s) (-ie)(p + p_s)^\mu, \quad (5.68)$$

$$i\mathcal{M}^{(0b)\mu} = (-i\sqrt{2}g_{\pi N}) D_F^\pi(p_t) (-ie)(p_t + p_\pi)^\mu, \quad (5.69)$$

where $p_s = p + q$, and $p_t = p_\pi - q$. The resulting Born Term Model is thus

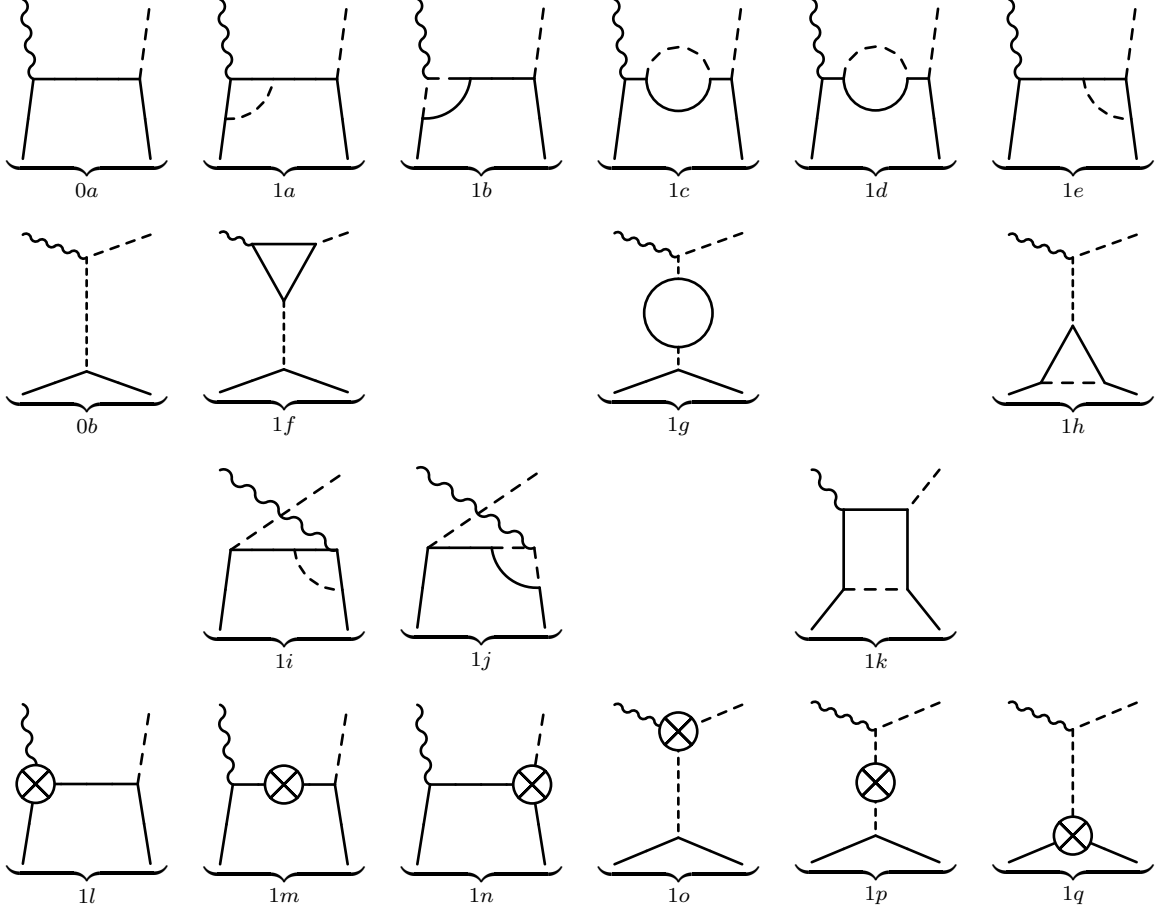


FIGURE 5.10: Diagrams included in the calculation of the $\gamma^* + p \rightarrow \pi n$ amplitude. Note that diagrams 1c and 1d correspond to exchange of π^+ and π^0 , respectively. Since the neutron is a neutral field in this theory, the photon does not couple to it at tree level. The neutron's form factor is generated purely by loop corrections.

$$i\mathcal{M}_{\text{BTM}}^\mu = i\mathcal{M}^{(0a)\mu} + i\mathcal{M}^{(0b)\mu}. \quad (5.70)$$

We can show that this model satisfies the Ward Takahashi Identity $q_\mu \mathcal{M}^\mu = 0$. Using the relations

$$q \cdot (p + p_s) = p_s^2 - m_N^2 = -iD_F^{N-1}(p_s), \quad (5.71)$$

$$q \cdot (p_t + p_\pi) = -(p_t^2 - m_\pi^2) = iD_F^{\pi-1}(p_t), \quad (5.72)$$

we have

$$q_\mu \mathcal{M}^{(0)\mu} = (-i\sqrt{2}g_{\pi N})(-ie) \left[D_F^N(p_s)q \cdot (p + p_s) + D_F^\pi(p_t)q \cdot (p_t + p_\pi) \right] = 0. \quad (5.73)$$

Importantly, the gauge invariance in this model also requires a cancellation between the s- and t-channel terms, as occurs in the VGL Model. Thus if one wishes to modify this matrix element to incorporate the structure of the pion, the same constraints apply. We define the *VGL-like Model* as

$$i\mathcal{M}_{\text{VGL-like}}^\mu = i\mathcal{M}_{\text{BTM}}^\mu F_\pi(q^2). \quad (5.74)$$

Before proceeding to extract the pion form factor from our model of pion electroproduction, we must first calculate the ‘true’ pion form factor in this model. With this in hand, it will then be able to make a direct comparison between the ‘true’ form factor and the extracted pion form factor.

5.4.2 Form Factors in the Toy Model

By considering only the diagrams which contribute to the nucleon and pion electromagnetic vertices, we may directly calculate the form factors predicted by this model. Because our model is perturbative in nature, the corrections to the form factors generated by the inclusion of the loop diagrams are quite small and since we are requiring the one-loop diagrams to contribute *all* the Q^2 behavior, this is problematic. In order to rectify this, we have chosen to change the coupling which controls the strength of the loop corrections, as well as the masses of the particles propagating in the loops. In other words, we take $m_N \rightarrow m'_N$, $m_\pi \rightarrow m'_\pi$ and $g_{\pi N} \rightarrow g'_{\pi N}$ in the loop integrals only. One may understand this as modeling the scalar pion and nucleon as bound states of two different particles with masses m'_N and m'_π . If we were to correctly incorporate spin, this model could be understood as a quark-diquark picture of the nucleon.

Our chosen parameters are given in Table 5.1. We select these parameters to ensure a reasonable separation between F_p and F_π and also so that F_π falls off slower than F_p , as occurs in nature. Since we wish to describe the pion form factor with a monopole form factor, it is important to check that this is a good approximation. We find that the model form factor is well described for a monopole mass parameter of $\Lambda_\pi^2 = 5.56 \text{ GeV}^2$. This fit is shown in Fig. 5.11.

With the free parameters in our model chosen, we may proceed to calculate the cross section and attempt to extract the model pion form factor.

TABLE 5.1: Tree level and loop parameters used in this study. All parameters are in units of GeV.

$g_{\pi N}$	m_N	m_π	$g'_{\pi N}$	m'_N	m'_π
1.4	0.94	0.14	20	0.7	0.71

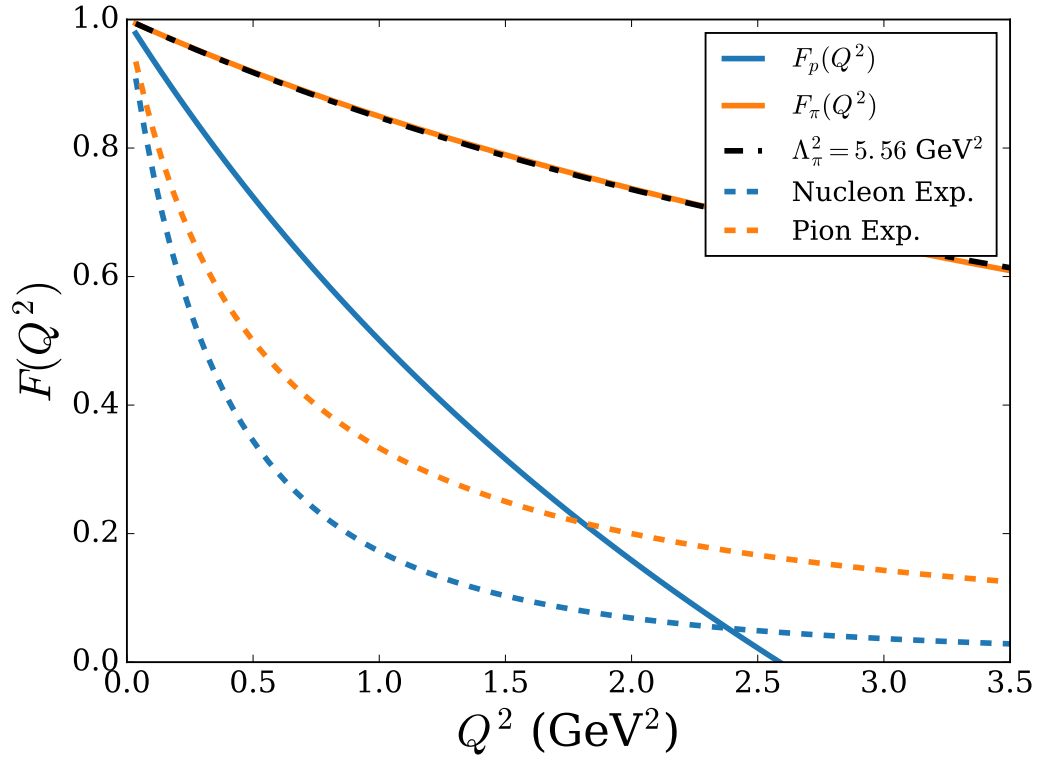


FIGURE 5.11: Comparison of predicted electromagnetic form factors with parameterizations of the pion and nucleon form factors from data. In principal, there is also a neutron form factor, but due to the chosen mass parameters ($m'_N \approx m'_\pi$), the neutron form factor is approximately zero (see Appendix F for details). We show the fitted monopole form factor. The agreement between the true pion form factor and a monopole form is excellent.

5.5 Extraction of the Pion Form Factor

The F_π Collaboration reports the pion electromagnetic form factor for eight kinematic points, so in our first analysis, we attempt to extract those same points. We follow a simplified version of their analysis outlined above in Sec. 5.3.4. We outline the steps of the analysis here:

1. We calculate the loop corrected cross section, with the form factors described in previous section. This cross section is called *pseudodata* in the following step.
2. We generate pseudodata for a range of t values for fixed Q^2 and W (dashed green line in Fig. 5.13). As with the F_π Collaboration, we choose the range of t to start near the minimum allowed value for the chosen kinematics. Specifically, the cross section is calculated between the minimum and maximum values of t measured (see Ref. [134] for explicit values).
3. We define our model to be the tree level matrix element, and incorporate the pion form factor as a multiplicative factor to the amplitude. This mirrors the approach in the

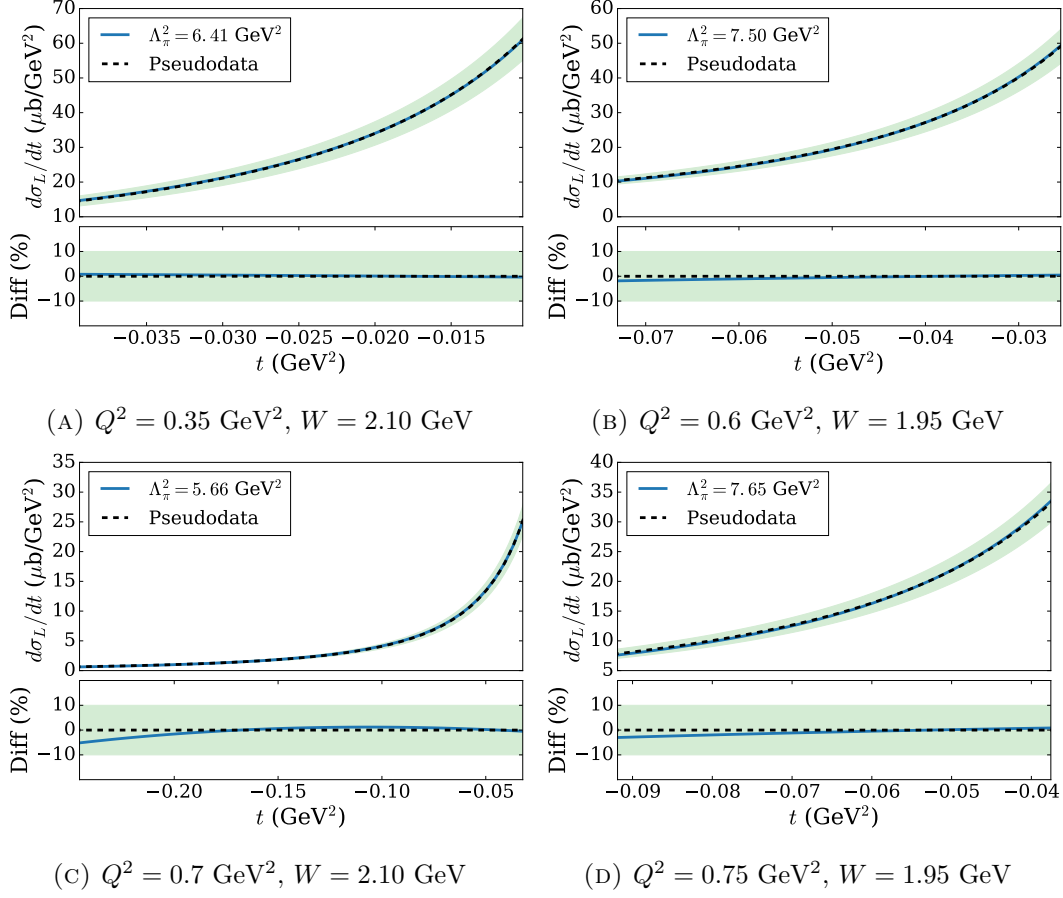


FIGURE 5.12: Fitting simplified model of cross section to model cross section for low Q^2 data. Both the pseudodata (dashed green) and simplified model (blue) sit over one another. The extracted Λ_π^2 is related to the extracted pion form factor via $F_\pi(Q^2) = (1 + Q^2/\Lambda_\pi^2)^{-1}$.

VGL Model. Thus our model matrix element is

$$i\mathcal{M}^\mu = i\mathcal{M}_{\text{BTM}}^\mu F_\pi(Q^2). \quad (5.75)$$

4. We fit our model to the pseudodata to obtain a best fit for the parameter Λ_π^2 . This value of Λ_π^2 corresponds to the extracted pion form factor (solid blue line in Fig. 5.13).
5. We plot the resulting extracted pion form factors (see Figs. 5.14, 5.15).

5.6 Discussion of the Results

Examining the fitted model cross sections shown in Figs. 5.12, 5.13, we can see that the level of agreement of the fitted model cross section when compared with pseudodata decreases slightly as we go to larger Q^2 . We note however, that with the exception of the $(Q^2, W) = (1.6, 1.95)$ and $(2.45, 2.22)$ kinematics, the disagreement between the model and pseudodata is less than ten percent (see Fig. 5.15). Given that the current experimental uncertainties are of this order,

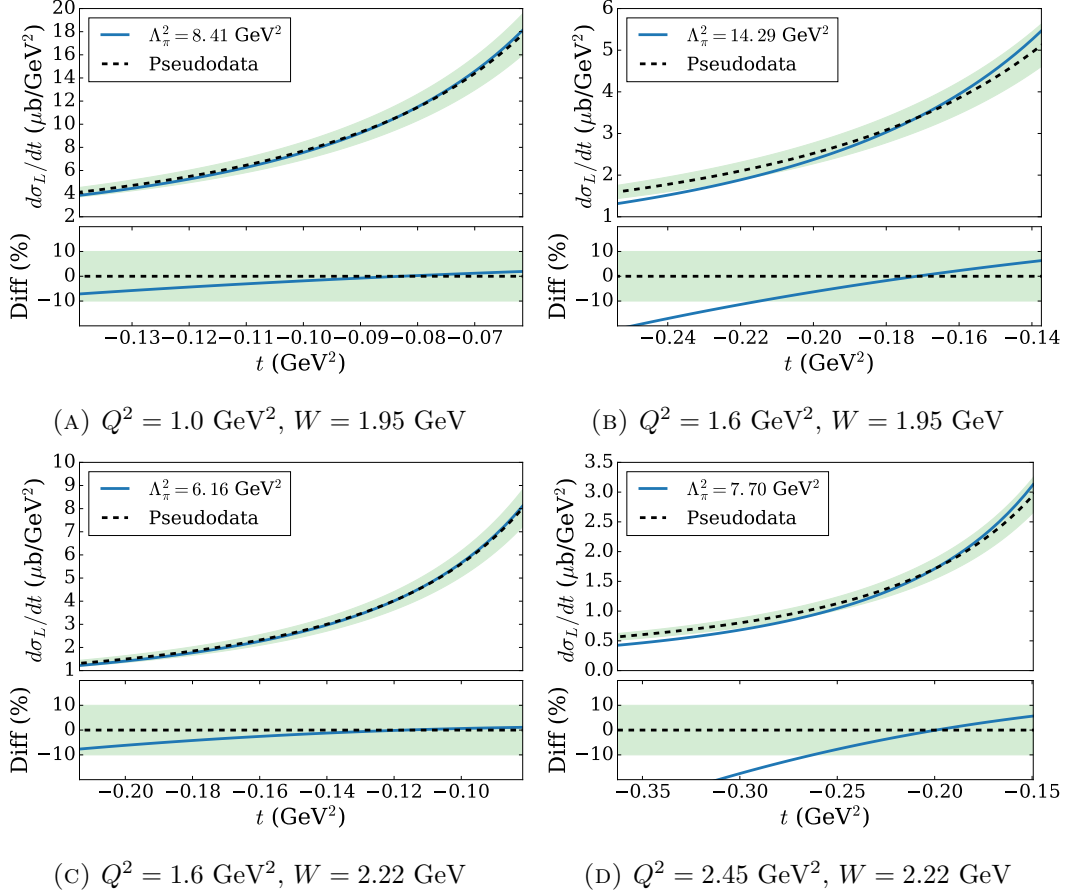


FIGURE 5.13: Fitting simplified model of cross section to model cross section for high Q^2 data. Both the pseudodata (dashed green) and simplified model (blue) sit over one another. The extracted Λ_π^2 is related to the extracted pion form factor via $F_\pi(Q^2) = (1 + Q^2/\Lambda_\pi^2)^{-1}$.

we conclude that the VGL model implementation of gauge invariance should model the cross section reasonably well over the kinematic range examined. This conclusion is borne out by the experimental data in Ref [97].

At low momentum transfer, we find that our extracted form factor is in good agreement with the true form factor in the toy model, although in general we find a better agreement for data points extracted at larger W . As the momentum transfer increases, the extracted form factor tends to become a slightly worse representation of the true form factor. In particular, we note from Fig. 5.16, that the extracted form factor appears to trend away from the true form factor. As noted in Ref. [134], the smallest kinematically allowed absolute value of t , denoted $|t_{\min}|$ may be reduced by measuring at larger W , or at smaller Q^2 . This is important, as this reduces the distance that one has to extrapolate to in order to reach the pion pole. In other words, for smaller absolute value of t , the pion photon interaction which occurs in the t -channel looks more like the pion electromagnetic form factor measured in elastic $e^- + \pi^+$ scattering.

To verify our explanation, we extracted the model form factor at $W = 1.95 \text{ GeV}$ and $W = 2.2 \text{ GeV}$, for a range of Q^2 between 0 and 3 GeV^2 , using the method outline above. The

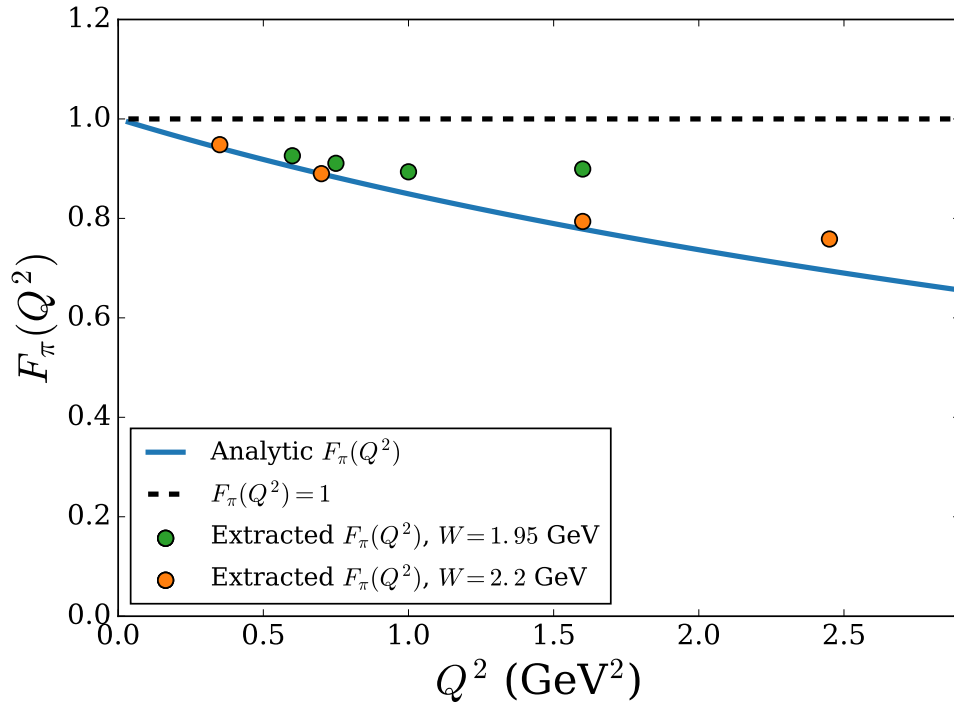


FIGURE 5.14: Extracted F_π in our Toy Model, compared with true model form factor.

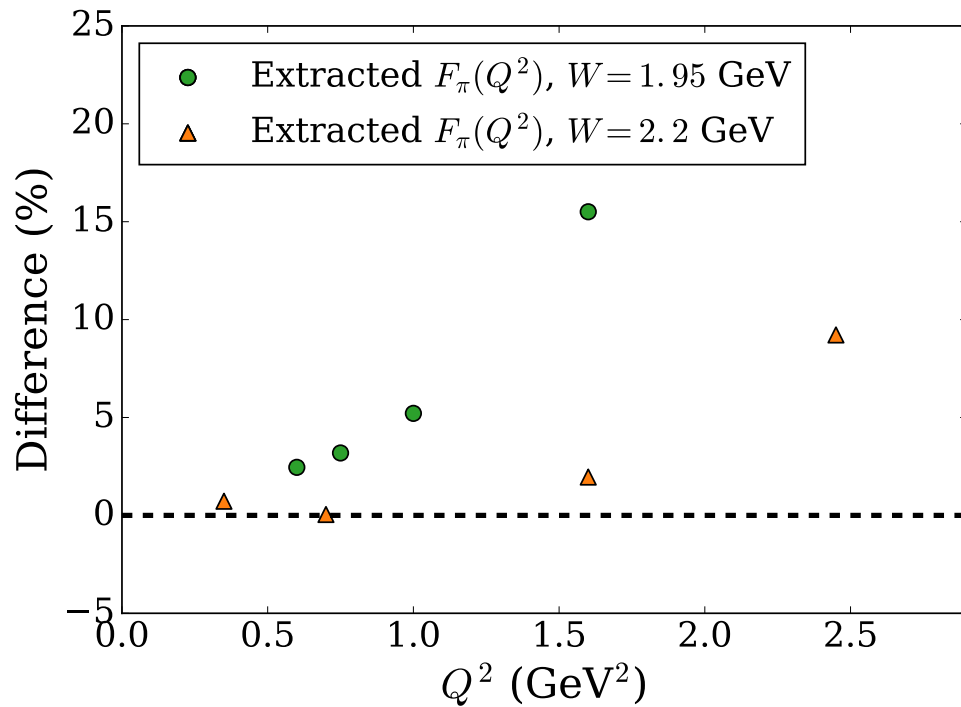


FIGURE 5.15: Percentage difference between our extracted form factor and the true model form factor. Note that a positive difference corresponds to an overestimation of F_π . Thus for the kinematic points surveyed, the extracted form factor is overestimated.

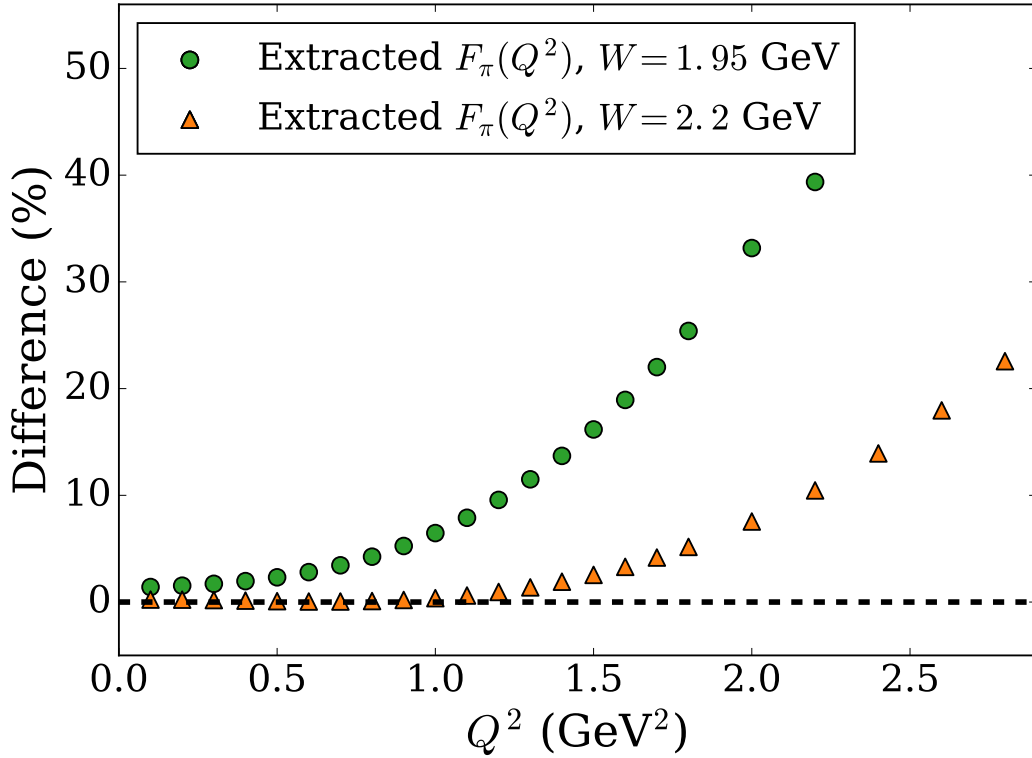


FIGURE 5.16: Extracting the pion form factor near the minimum kinematically allowed t value. Note that the agreement between the true form factor and the extracted form factor worsens sooner for the $W = 1.95$ GeV data, because $|t_{\min}|$ is larger. Thus the pion photon interaction looks less like the on-shell pion electromagnetic form factor.

experimental data approximately spans the first five percent of the allowed t range. We therefore attempt to fit our model cross section to the pseudodata over the first five percent of the allowed t kinematic range for the chosen Q^2 and W .

The results of this process are shown in Fig 5.16. As predicted, the agreement between the extracted form factor and the model form factor are good for a larger range of Q^2 when the $W = 2.2$ GeV data is used. This data clearly shows the way the model form factor is being systematically overestimated for increasing Q^2 .

It is interesting to speculate about the way this result could carry over to the extraction of the real pion form factor from real data. Indeed, if the relation between the extracted and true pion form factor remained quantitatively the same, this would suggest (experimental uncertainties notwithstanding) that the extracted pion form factor values are currently overestimated. This effect - if observed - would imply that the ‘true’ pion form factor was smaller, bringing the extracted pion form factor a little closer to the asymptotic limit predicted by perturbative QCD.

5.7 Conclusion

We began by discussing the theoretical drawbacks with the implementation of gauge invariance in the VGL Model. In particular, we discussed the unnatural factorization of the pion form factor from the matrix element. We proposed a simple toy model which was used to generate pseudodata for pion electro-production. We followed the F_π Collaboration's approach to extract the toy model's pion form factor. The extracted pion form factor was compared to the true form factor, and it was found that our extracted form factor was in all cases *larger* than the true form factor. If this result were to hold in the extraction of the experimental pion form factor, it would suggest that the extracted pion form factor is currently overestimated.

Investigating the Model Dependence of the Pion Electromagnetic Form Factor in Chiral Effective Field Theory

In the previous chapter, we observed in the context of a simple toy model that the pion form factor extracted from pion electroproduction may be overestimated. In that analysis, the spin of the nucleon involved was neglected. Thus in order to ensure the validity of results determined in that study, we seek to perform the calculation in a theory which correctly implements the nucleon's spin. For this work, we choose a pseudoscalar pion-nucleon interaction, and perform a similar analysis to the previous chapter. We show that inclusion of the spin degrees of freedom leads to qualitatively similar conclusions.

6.1 Fermionic Pion-Nucleon Theory

We now consider a more physical model of the pion-nucleon interaction, where the spin of the nucleon is correctly implemented, and the pion and nucleon interact via a pseudoscalar interaction motivated by chiral symmetry (see Chap. 2 and Appendix B). We recall the essential details here. We define a nucleon doublet Ψ_N

$$\Psi_N = \begin{bmatrix} \psi_p \\ \psi_n \end{bmatrix}, \quad (6.1)$$

and a pion triplet $\boldsymbol{\pi}$

$$\boldsymbol{\pi} = \begin{bmatrix} \pi_+ \\ \pi_- \\ \pi_0 \end{bmatrix}, \quad (6.2)$$

we may write the effective Lagrangian as

$$\mathcal{L} = \bar{\Psi}_N (i\not{\partial} + m_N) \Psi_N + \frac{1}{2} (\partial_\mu \boldsymbol{\pi})^2 - \frac{1}{2} m_N^2 \boldsymbol{\pi}^2 - g_{\pi N} \bar{\Psi}_N i\gamma_5 \boldsymbol{\tau} \cdot \boldsymbol{\pi} \Psi_N. \quad (6.3)$$



FIGURE 6.1: Lowest order nucleon mass splitting contribution. While this diagram would be present in the case of the proton, it is absent for the neutron, which has no tree level electromagnetic coupling. In our mixed coupling expansion, we only expand to leading order in the electromagnetic coupling, so this diagram is not present.

After incorporating the electromagnetic interaction via the principle of minimal substitution, we obtain

$$\begin{aligned} \mathcal{L} = & \bar{\Psi}_N(i\not{\partial} + m_N)\Psi_N + \frac{1}{2}(\partial_\mu\boldsymbol{\pi})^2 - \frac{1}{2}m_\pi^2\boldsymbol{\pi}^2 - \frac{1}{4}F^{\mu\nu}F_{\mu\nu} - g_{\pi N}\bar{\Psi}_Ni\gamma_5\boldsymbol{\tau}\cdot\boldsymbol{\pi}\Psi_N \\ & - e\bar{\Psi}_N\hat{Q}\gamma^\mu\Psi_NA_\mu + ie(\partial^\mu\boldsymbol{\pi})\cdot(\hat{Q}\boldsymbol{\pi})A_\mu, \end{aligned} \quad (6.4)$$

where \hat{Q} is the charge operator which gives the electric charge of the particle it acts on. Since we wish to calculate this amplitude to one loop order, we must perform renormalisation. With this in mind, we interpret the above expression for the Lagrangian as the unrenormalised Lagrangian. To denote this we add noughts to our fields and couplings to make it clear that we are talking about unrenormalised quantities. We will use renormalised perturbation theory. Thus the first step is to perform a field redefinition $\Phi_0 \rightarrow \sqrt{Z_\Phi}\Phi$ to allow for wave function renormalisations.

Note that while QCD possesses an approximate global $SU(2)$ isospin symmetry, the electromagnetic interaction breaks this approximate symmetry. As a result, the wave function and charge counter terms are no longer degenerate between the proton and neutron. In general, the mass renormalisation will also differ between the proton and neutron. Note however, that we are performing a mixed expansion in the electromagnetic and strong couplings. We are only expanding to lowest order in the electromagnetic coupling, and thus this diagram is not present (see Fig. 6.1). We define the renormalised masses and charges as

$$Z_p m_{N0} = m_N + \delta_{m_N}, \quad (6.5)$$

$$Z_\pi m_{\pi0}^2 = m_\pi^2 + \delta_{m_\pi^2}, \quad (6.6)$$

$$g_{\pi N0} Z_p \sqrt{Z_\pi} = g_{\pi N} Z_{g_{\pi N}}, \quad (6.7)$$

$$g_{\pi N0} Z_n \sqrt{Z_\pi} = g_{\pi N} Z_{g_{\pi N}}, \quad (6.8)$$

$$e_0 Z_p \sqrt{Z_A} = e Z_{e_p}, \quad (6.9)$$

$$e_0 Z_\pi \sqrt{Z_A} = e Z_{e_\pi}, \quad (6.10)$$

where we write the multiplicative renormalisation terms as

$$Z_p = 1 + \delta_p, \quad (6.11)$$

$$Z_n = 1 + \delta_n, \quad (6.12)$$

$$Z_\pi = 1 + \delta_\pi, \quad (6.13)$$

$$Z_A = 1 + \delta_A, \quad (6.14)$$

$$Z_{g_{\pi N}} = 1 + \delta_{g_{\pi N}}, \quad (6.15)$$

$$Z_{e_p} = 1 + \delta_{e_p}, \quad (6.16)$$

$$Z_{e_\pi} = 1 + \delta_{e_\pi}. \quad (6.17)$$

We note that a counter term only appears when there is a corresponding elementary vertex in the Lagrangian. Since there is no electromagnetic interaction for the neutron, no charge counter term appears. At one loop, the neutron obtains a non-trivial form factor. It is a consequence of the Ward-Takahashi identity that the charge of the neutron is neutral to all orders in perturbation theory. The cancellation of the two loop diagrams which comprise the neutron form factor in the limit $q^2 \rightarrow 0$ is one cross-check of the validity of the calculation. This result may be seen in Fig. 6.3.

6.1.1 The Born Term Model

It is possible to derive the Feynman Rules for the Lagrangian discussed. These are summarized in Appendix B. At tree level, there are two diagrams we must calculate. The s -channel diagram is

$$i\mathcal{M}^{(0a)\mu} = \bar{u}(p')(\sqrt{2}g_{\pi N})\gamma_5 S_F^{(0)}(p_s)(-ie)\gamma^\mu u(p), \quad (6.18)$$

where $p_s = p + q$. The tree level t -channel diagram is

$$i\mathcal{M}^{(0b)\mu} = \bar{u}(p')(\sqrt{2}g_{\pi N})\gamma_5 u(p)D_F^{(0)}(p_t)(-ie)(p_t + p_\pi)^\mu u(p), \quad (6.19)$$

where $p_t = p_\pi - q$, and the propagators $S_F^{(0)}(p_s)$ and $D_F^{(0)}(p_t)$ take their perturbative forms given in Appendix B. These two diagrams define the Born Term Model:

$$i\mathcal{M}_{\text{BTM}}^\mu = i\mathcal{M}^{(0a)\mu} + i\mathcal{M}^{(0b)\mu}. \quad (6.20)$$

It is a simple exercise to show that this model satisfies gauge invariance, as it must.

6.1.2 One-Loop Model

We may decompose the general structure of the matrix element based on the pole structure. Either the diagram is the result of a single particle exchange, or it is not. We write these contributions separately as

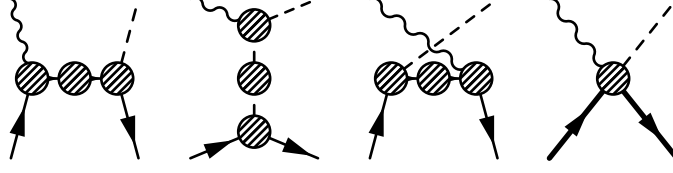


FIGURE 6.2: Decomposing the amplitude based on the singularity structure of the diagrams. Single particle exchange may arise through the s - t - or u -channel diagrams. We collect all contributions which cannot be described as the result of single particle exchange in a single ‘generalized contact term’.

$$i\mathcal{M}^\mu = \sum i\mathcal{M}_s^\mu + \sum i\mathcal{M}_t^\mu + \sum i\mathcal{M}_u^\mu + \sum i\mathcal{M}^{\text{contact}}. \quad (6.21)$$

This is shown diagrammatically in Fig. 6.2. In our model, the explicit terms are given as

$$i\mathcal{M}_s^\mu = \bar{u}(p')(\sqrt{2}g_{\pi N})\Gamma_5(p_s, p_\pi, p')S_F(p_s)(-ie)\Gamma_p^\mu(p, q, p_s)u(p), \quad (6.22)$$

$$i\mathcal{M}_t^\mu = \bar{u}(p')(\sqrt{2}g_{\pi N})\Gamma_5(p, p_t, p')u(p)D_F(p_t)(-ie)\Gamma_\pi^\mu(p_t, q, p_\pi)u(p), \quad (6.23)$$

$$i\mathcal{M}_u^\mu = \bar{u}(p')(-ie)\Gamma_n^\mu(p_u, q, p')S_F(p_u)(\sqrt{2}g_{\pi N})\Gamma_5(p, p_\pi, p_u)u(p), \quad (6.24)$$

where now

$$S_F(p) = \frac{i}{\not{p} - m_N - \Sigma(\not{p})}, \quad (6.25)$$

and

$$D_F(p) = \frac{i}{p^2 - m_\pi^2 - \Sigma(p^2)}, \quad (6.26)$$

where $\Sigma(\not{p}_s)$ and $\Sigma(t)$ are the particles respective self energies. In each case, we approximate the structure functions with their approximation at one loop order. For example, the electromagnetic vertex is

$$\Gamma_p^\mu(p, q, p_s) = \gamma^\mu + \delta\Gamma_p^\mu(p, q, p_s) + \mathcal{O}(g_{\pi N}^4). \quad (6.27)$$

Further details on the specific loop contributions are given in Appendix G.

6.2 Algebraic Reduction and Numerical Calculation

Going beyond tree level requires the calculation of eleven loop diagrams. These are shown in Appendix G. We utilize the Passarino-Veltman reduction to reduce the general one-loop integrals to a basis in terms of four scalar loop functions [153]. In our conventions, they are given as

$$A_0(m_1^2) = \int \frac{d^4k}{(2\pi)^2} \frac{1}{[k^2 - m_1^2]}, \quad (6.28)$$

$$B_0(q_1^2; m_1^2, m_2^2) = \int \frac{d^4k}{(2\pi)^4} \frac{1}{[k^2 - m_1^2]} \frac{1}{[(k + q_1)^2 - m_2^2]}, \quad (6.29)$$

$$C_0(q_1^2, q_2^2, (q_1 + q_2)^2; m_1^2, m_2^2, m_3^2) = \int \frac{d^4k}{(2\pi)^4} \frac{1}{[k^2 - m_1^2]} \frac{1}{[(k + q_1)^2 - m_2^2]} \frac{1}{[(k + q_2)^2 - m_3^2]}, \quad (6.30)$$

$$\begin{aligned} D_0(q_1^2, q_2^2, q_3^2, q_4^2, (q_1 + q_2)^2, (q_2 + q_3)^2, m_1^2, m_2^2, m_3^2, m_4^2) \\ = \int \frac{d^4k}{(2\pi)^4} \frac{1}{[k^2 - m_1^2]} \frac{1}{[(k + q_1)^2 - m_2^2]} \frac{1}{[(k + q_2)^2 - m_3^2]} \frac{1}{[(k + q_3)^2 - m_4^2]}. \end{aligned} \quad (6.31)$$

Further details about this procedure may be found in Ref. [153]. In practice, we utilize the Mathematica package FEYN CALC [150, 151] to implement this method. Importantly, the increased complexity of these diagrams leads to large expressions which in turn makes the algebraic manipulation of these equations timely. To address this, the calculation is split into a number of steps. For completeness, we summarize these here. We begin by decomposing the matrix element for pion electroproduction into its most general form where we explicitly factorize the Dirac structure.

$$\begin{aligned} i\mathcal{M}^\mu = & A_1(s, t, u)\gamma^\mu\gamma_5 + A_2(s, t, u)p^\mu\gamma_5 + A_3(s, t, u)p'^\mu\gamma_5 + A_4(s, t, u)q^\mu\gamma_5 \\ & + A_5(s, t, u)\not{q}\gamma^\mu\gamma_5 + A_6(s, t, u)\not{p}p^\mu\gamma_5 + A_7(s, t, u)\not{p}p'^\mu\gamma_5 + A_8(s, t, u)\not{q}q^\mu\gamma_5. \end{aligned} \quad (6.32)$$

Using this general matrix element, we calculate the L , T , TT and LT structure functions. Details about this may be found in Appendix D. Next, we calculate the pion electroproduction matrix element for our specific model. Using FEYN CALC, we extract the contributions to each of the eight scalar functions A_i from the matrix element. By separating the calculation into several steps, we ensure that the equations produced are suitable for numerical evaluation. We use the implementation of the scalar loop integrals provided by QCDLOOP [152].

TABLE 6.1: Renormalised coupling constants and masses in our chiral effective field theory

$g_{\pi N}^2/(4\pi)$	m_N (GeV)	m_π (GeV)
14.3	0.94	0.14

6.2.1 Electromagnetic Form Factors in the Fermionic Model

We use the parameters given in Table. 6.1 for the numerical evaluation. As with our previous calculation in the scalar field theory, we begin our analysis of this model by examining the predicted electromagnetic form factors. These are shown in Fig. 6.3. For comparison, we include the empirical parameterisation of experimental data due to Ref. [93]. A summary of the predicted electric charge radii and magnetic moments are given in Table 6.2. We can see from these observables, and from the general shape of the form factors that our model can only yield a crude description of the physical nucleon form factors. This is acceptable for our present purposes where we explore the effects of ensuring gauge invariance with different form factors. Clearly a quantitative extraction of the pion form factor from data would require a more sophisticated model.

We also calculate the pion's electromagnetic form factor. The resulting form factor is shown in Fig. 6.3. As with the predicted nucleon form factors, the overall prediction of the pion form factor is rather poor. Since our primary interest in this study is to examine the self consistency of the extraction process, the poor representation of the physical form factors is acceptable.

6.3 Extraction of the Pion Form Factor

We seek to understand whether the VGL Model's implementation of gauge invariance allows one to successfully extract the pion form factor. To be clear, we define the VGL matrix element as

$$i\mathcal{M}_{\text{VGL}}^\mu = F_\pi(Q^2)i\mathcal{M}_{\text{BTM}}^\mu, \quad (6.33)$$

where $i\mathcal{M}_{\text{BTM}}^\mu$ is the sum of the two tree-level diagrams described above. We emphasize that we do not Reggeize the amplitude as is done in the original VGL Model.

TABLE 6.2: Comparison of the predicted magnetic moments to experimental results for the proton and neutron. Experimental results are taken from Refs. [93, 154]. Magnetic moments are in units of nuclear magnetons ($\mu_N = e/2m_N$).

	$\langle r^2 \rangle^{\frac{1}{2}}$ (fm)		μ (μ_N)	
	p	n	p	n
This Work	0.56	0.56	1.50	-3.7
Exp.	0.84	0.335	2.793	-1.913

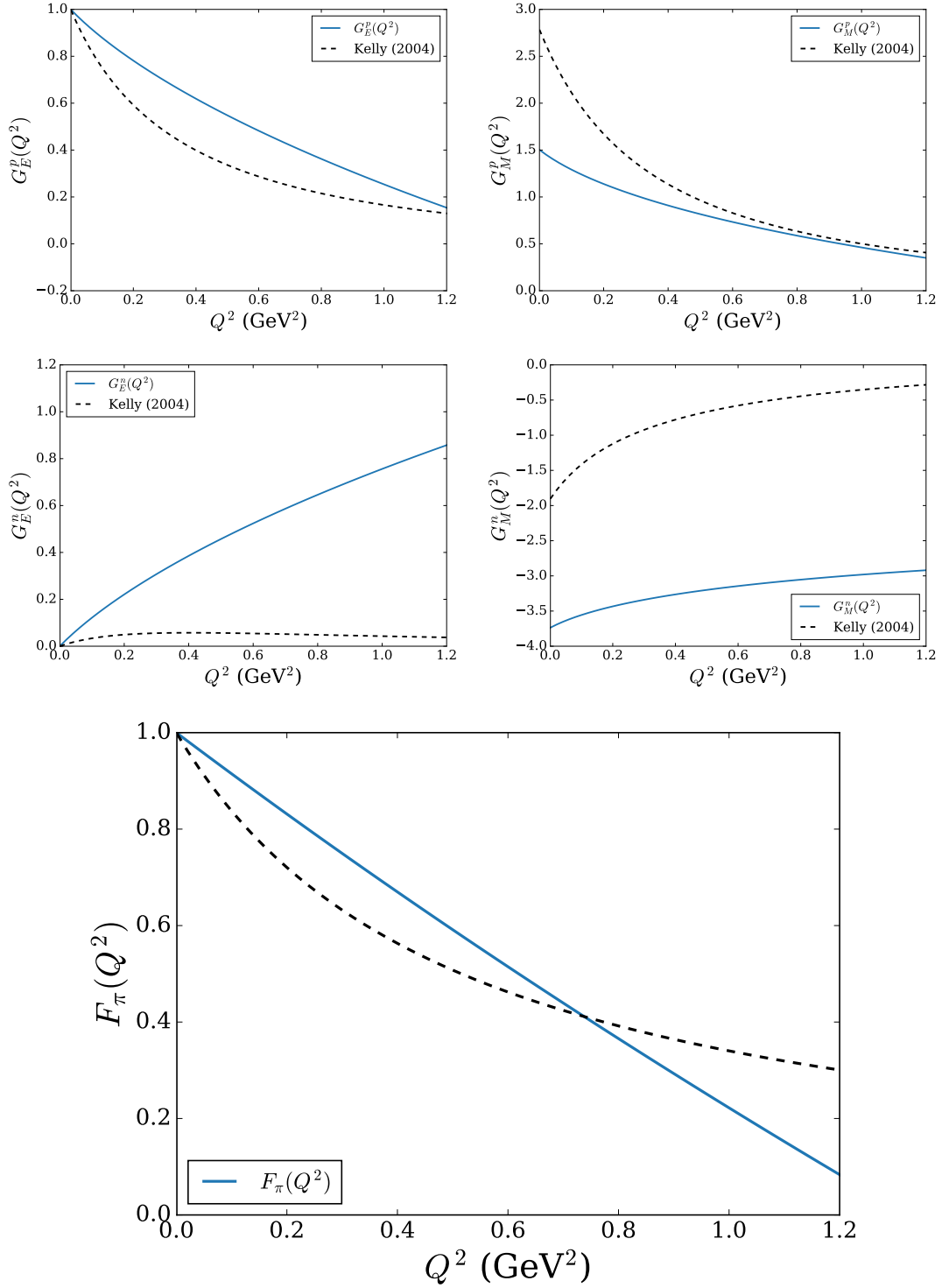


FIGURE 6.3: The predicted nucleon and pion form factors in the simple fermionic model. Note that while the broad behaviour of the form factors is matched, the agreement between the model and the parameterisation of data is poor. In the case of the nucleon, we use the empirical parameterisation from Ref. [93]. For the pion, we use a monopole parameterisation fit to the pion form factor extracted from low energy electron pion elastic scattering data.

Due to our choice of renormalisation point, the strong $g_{\pi N}$ coupling has changed sufficiently to require a refitting of this parameter in the VGL Model. In order to do this, we fit the low Q^2 cross section data, where we expect the contribution from the pion form factor to be close to unity. We find the effective $g_{\pi N}$ coupling to be $g_{\pi N} = 19.3$. With this parameter fit, we proceed to extract the pion form factor from the pseudodata. We choose a monopole form of the pion form factor

$$F_{\pi}(Q^2) = \frac{1}{1 + \frac{Q^2}{\Lambda_{\pi}^2}}. \quad (6.34)$$

We fit Λ_{π}^2 to the pseudodata calculated from our one-loop model and aim to determine whether the effects observed in the scalar field theory study carry over in a model with the correct implementation of the nucleon's spin. In particular, we wish to verify that the form factor may be more accurately extracted for larger W . We also seek to understand whether there are any systematic errors incurred by using the VGL extraction method. Thus instead of recreating the F_{π} data points, we choose to scan over Q^2 for two different values of W . Fits of the VGL Model to the pseudodata for the two values of W are shown in Fig. 6.4 and Fig. 6.5, respectively. Going to higher Q^2 values for both W values examined leads to a poorer overall fit to the pseudodata. In particular, the simple model overestimates the t -dependence. Interestingly, this failure of the VGL model to fully recreate the t -dependence of the cross section is also observed at comparable kinematic points in the 2008 analysis of real electroproduction data (see Fig. 5, Ref. [97]). As we have explained previously, the approach employed by the F_{π} Collaboration was to fit the model to each data point individually and perform an extrapolation of Λ_{π} to the smallest $|t|$ value kinematically allowed. We will return to this point after we have examined the extracted values of the pion form factor.

6.4 Discussion of Results

The resulting extracted pion form factor values and their comparison to the form factor calculated to one-loop are shown in Fig. 6.6. Interestingly, unlike the last chapter, the extracted pion form factor has the wrong slope. We also note that, as with the scalar toy model, we see that the $W = 2.22$ GeV data provides a slightly better extraction of the pion form factor. This again demonstrates the importance of choosing the kinematics wisely. As we have explained previously, larger values allow one to approach closer to the physical pion pole, and thus improve the sensitivity of the cross section to the pion form factor.

In the previous study of the extraction of the pion form factor in a scalar field theory, we observed that all extracted values of the pion form factor were overestimated. When considering the percentage difference between the extracted pion form factor and the analytically calculated form factor in this model, we see that this behaviour carries over. We mentioned then that in order to improve the fits to data in the high virtuality region, the F_{π} collaboration fit each data point individually and that in the context of our data, this would lead to a smaller value of the pion form factor.

By varying the t range fit to the VGL Model, we can determine the dependence of the extracted pion form factor on kinematics chosen. By reducing the fit window by a factor of four, we

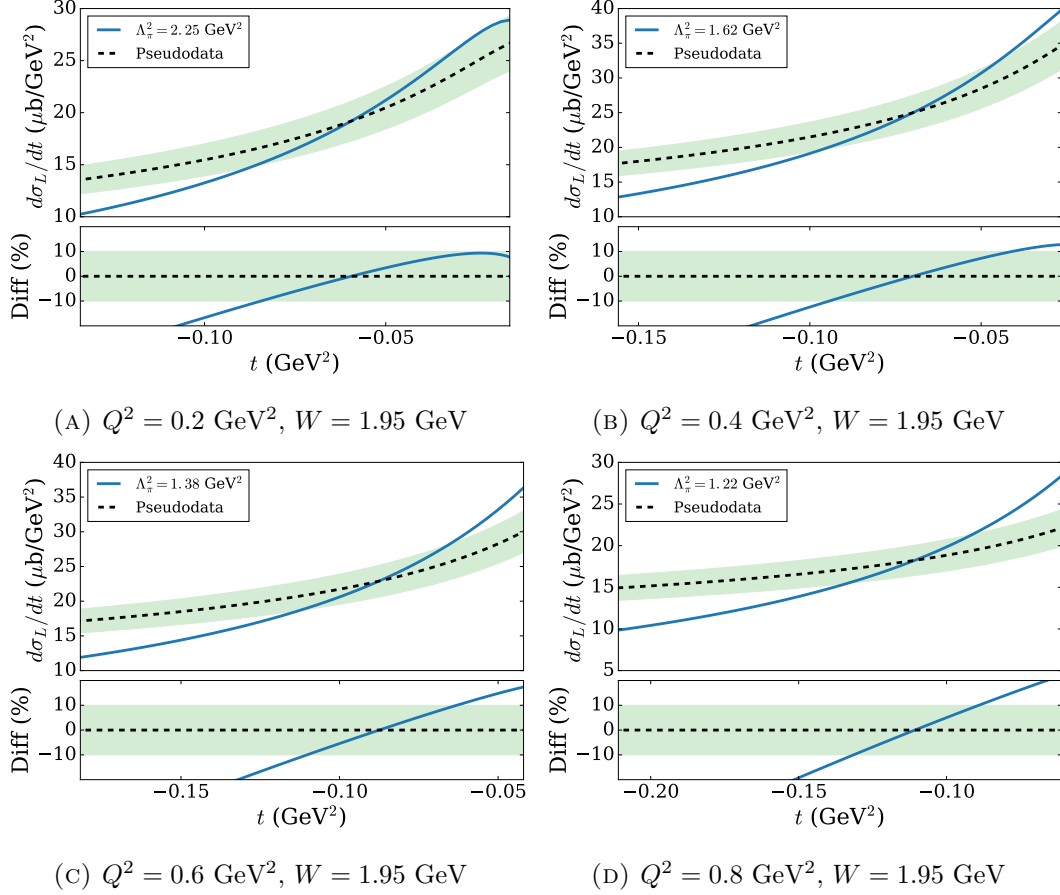


FIGURE 6.4: Fitting the model to pseudodata for a range of Q^2 values at fixed $W = 1.95$ GeV. For higher photon virtuality, the fit becomes worse.

obtain values for the pion form factor which are smaller by about five percent at $Q^2 = 1$ GeV^2 . Thus while it is possible to obtain a slightly smaller pion form factor, the approach used in the F_π Collaboration's analysis of the pion form factor is insufficient to remove the disagreement between the extracted pion form factor, and the true form factor, which are of the order 80-100 percent at these photon virtualities (see Fig. 6.7).

It is also interesting to note that in this model, the pion's electromagnetic form factor and the proton's Dirac form factor are approximately equal. In fact, they agree to within four percent for a photon virtuality less than 0.6 GeV^2 . Thus while we argued that the physical pion and proton Dirac form factors should not be approximated as equal, in this model the approximation is much better. Thus to a good approximation

$$F_1^p(Q^2) \approx F_\pi(Q^2). \quad (6.35)$$

Since this approximation is more applicable than the physical theory, we would expect the results to be a best case scenario. Note that even with this approximation, we still obtain a measurement which is dependent on the invariant mass W , and generally leads to an extracted value which is larger than the physical value. Thus it would appear that the approximation

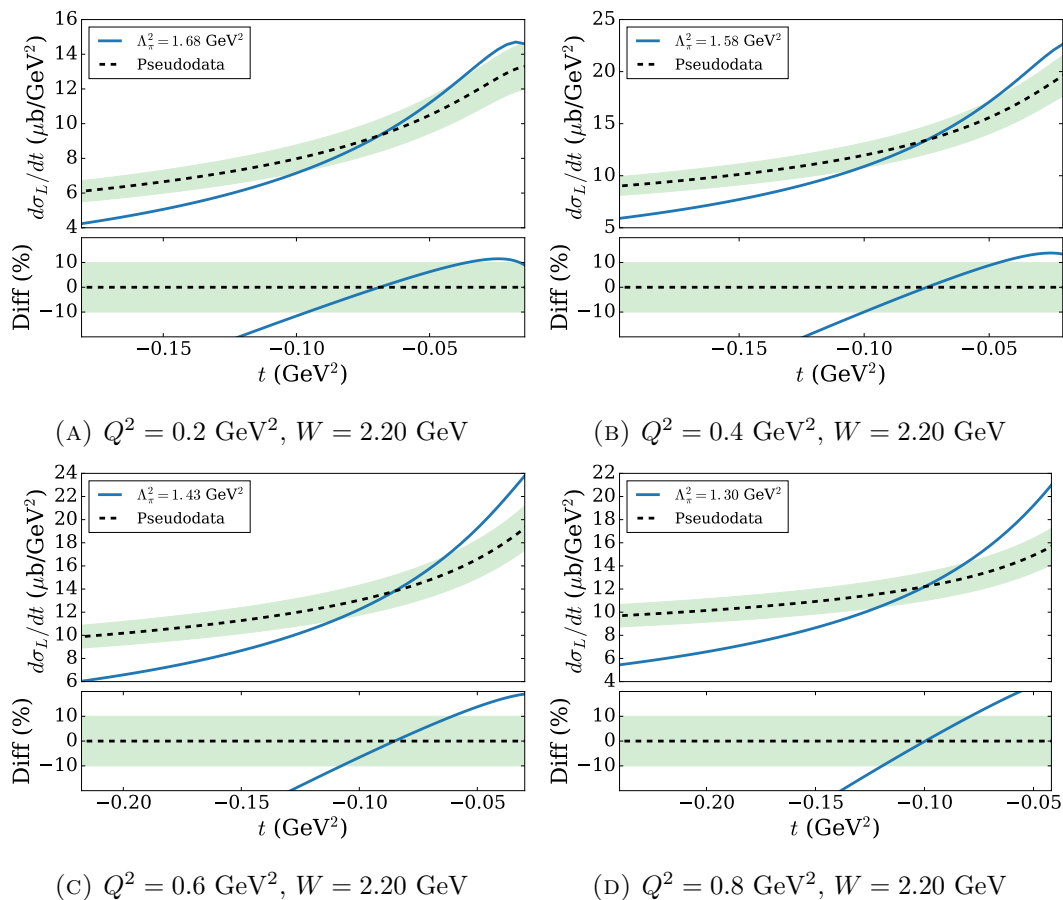


FIGURE 6.5: Fitting the model to pseudodata for a range of Q^2 values at fixed $W = 2.2 \text{ GeV}$. For higher photon virtuality, the fit becomes worse.

where one replaces the s -channel electromagnetic interaction with on-shell elastic form factors is too simplistic, and will lead to systematically incorrect results.

6.5 Conclusion

In this work, we have attempted to understand within a simple fermionic model of pion electroproduction whether the currently extracted pion form factor constitutes a reliable measurement of the physical form factor. Previously we studied this in the context of a simple scalar model, and found that over a range of Q^2 values, the extracted value of the pion form factor was consistent with true form factor, but that higher W data allowed one to approach closer to the physical pion pole and thus obtain a better extraction. In our more complicated model, we observed that performing the measurement at larger pion-photon invariant mass led to a slighter better extraction of the pion form factor. Unlike the previous study, there was no region of Q^2 where the pion form factor was accurately extracted. Instead, the slope of the pion form factor was underestimated, leading to extracted values of the pion form factor disagreeing by 100 percent at $Q^2 = 1 \text{ GeV}^2$. Importantly, this over extraction of the pion form factor could not be ‘repaired’ using the method employed by the F_π Collaboration,

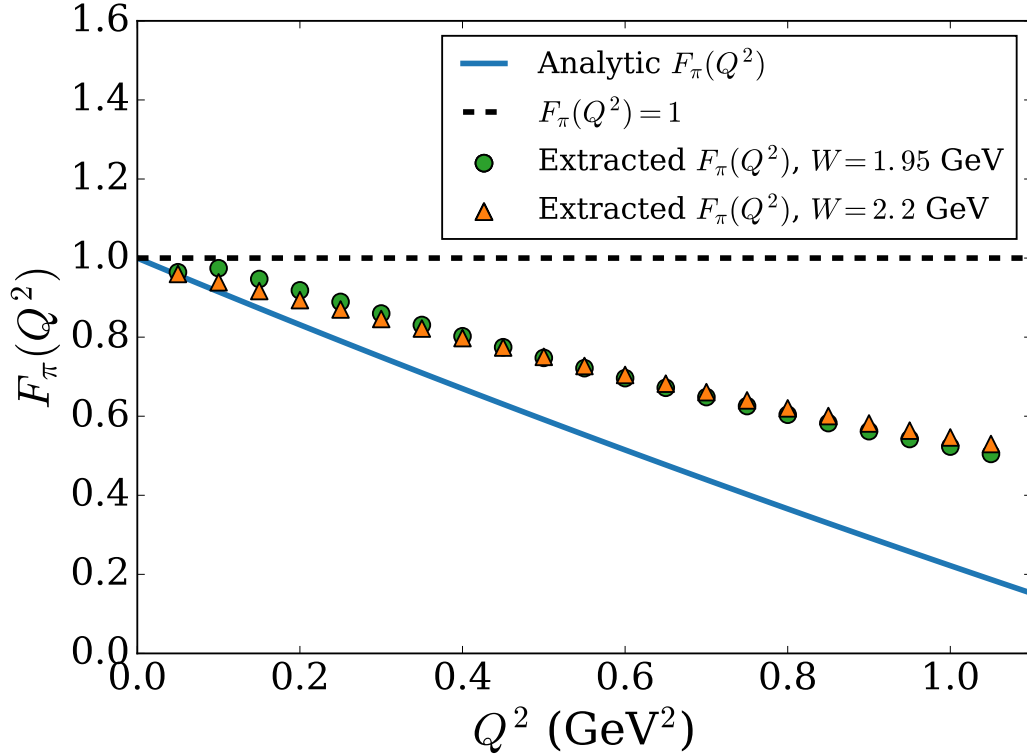


FIGURE 6.6: Comparison of extracted values of F_π using the VGL Model approach with the true form factor. Note that the pion form factor is systematically overextracted.

where the fit window was modified to extrapolate the extracted values of F_π to the minimum kinematically allowed value of $|t|$.

Together, the two studies of the measurement of the pion's electromagnetic form factor raise questions about the validity of the current quoted values. In particular, we are led to conclude that the current measurements of the pion form factor are overestimated.

Unfortunately, the electromagnetic form factors predicted in this model are clearly too coarse to attempt to use the model to extract the physical pion form factor. Nevertheless, this model has clearly shown how the VGL model is likely failing. By being able to explicitly calculate the electromagnetic form factors, our fermionic model is the perfect test for more sophisticated models. By successfully extracting the pion's electromagnetic form factor in this model, one would be able to gain confidence that when applied to real data, the resulting measured form factor is a good representation of the underlying form factor.

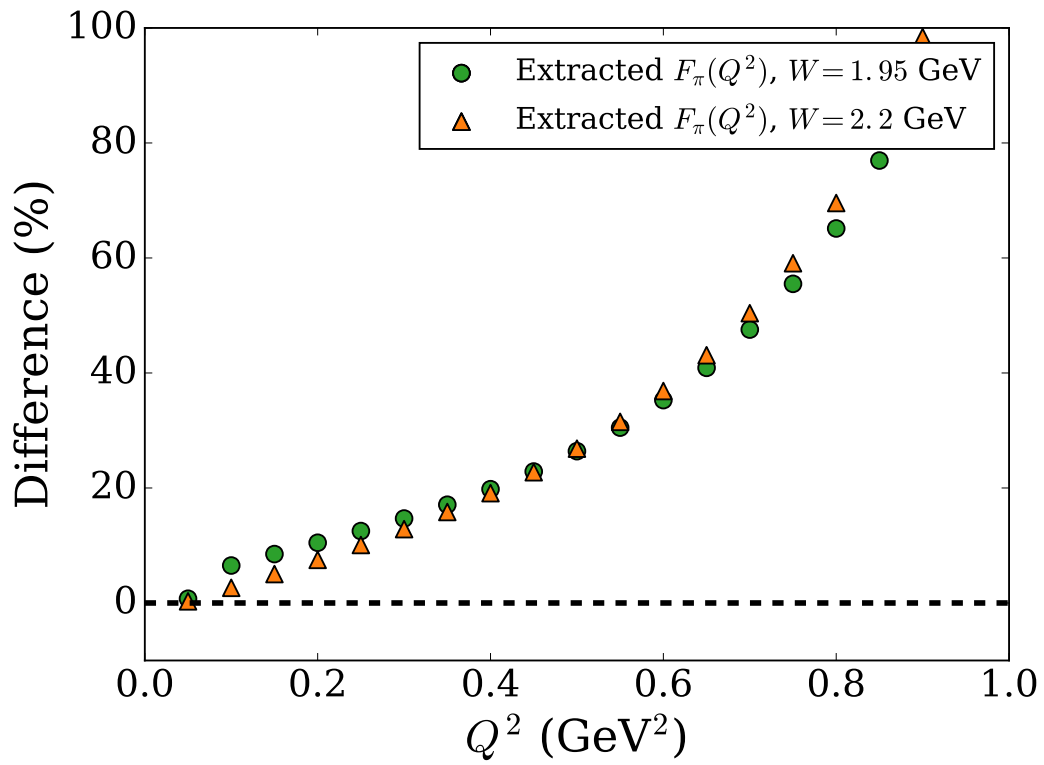


FIGURE 6.7: Percentage difference between the extracted pion form factor and the true form factor.

Summary and Outlook

Over ninety years after the first observations of the anomalous magnetic moment of the proton by Otto Stern in 1933, the understanding of hadronic structure is still incomplete. One window into the structure of hadrons are their electromagnetic form factors, which may be related to the electric and magnetic charge densities. This thesis has been primarily concerned with the prediction and extraction of these quantities.

We began this thesis with a discussion of the characteristic features of the strong force: asymptotic freedom, and confinement. These features - unique to QCD - lead to a rich and complex phenomenology which result in the baryons and mesons observed in nature. The empirical absence of free quarks and gluons at low energy motivated a description of QCD in terms of the baryon and meson degrees of freedom. This concept was made concrete with the formalism of chiral effective field theory which we developed by noting the approximate chiral symmetry of the light quarks of QCD. This approach formed the primary technique of analysis in this thesis.

We introduced the electromagnetic interaction as a way of probing the electric charge distribution of the quarks inside hadrons. Importantly the electromagnetic interaction is a consequence of the gauge symmetry of QED. This places a further constraint on the form of the electromagnetic form factors present in nature. In particular, we showed how the most general form of the electromagnetic vertex reduced to the well-known experimental parameterizations.

With the formalisms established, we introduced the first original research conducted for this thesis, *Chiral Corrections to Electromagnetic Form Factors in the Nambu–Jona-Lasinio Model*. Here we made predictions for the nucleon and Sigma hyperon electromagnetic form factors, where we paid particular attention to the implementation of chiral symmetry. In particular, we showed that while nucleon was insensitive to the method by which chiral corrections were implemented, the correct implementation of chiral symmetry was essential to reproduce the magnetic moment of the Σ^- . This finding is in agreement with earlier work which suggested that the magnetic moment was particularly sensitive to the implementation due to the large non-analytic term.

As we have established, the pion is central to our understanding of low energy QCD. Importantly though there exist predictions of the pion form factor at high photon virtuality derived in

the context of perturbative QCD. This theoretical result has motivated the measurement of the pion form factor at increasingly high Q^2 values in search for this posited behaviour. To date, this behaviour has not been observed. This motivated the second work, *Investigating the Model Dependence of the Pion Electromagnetic Form Factor in a Scalar Field Theory*. In this work, we examined the model used in the extraction of the pion form factor from pion electroproduction, and showed that the implementation of gauge invariance was unnatural. Based on this result, we examined the possibility that the pion form factor was incorrectly extracted from experimental data with the aid of a simple scalar model. In the context of this model, we found that the extracted values of the pion form factor were systematically large when compared with the true form factor calculated at one loop within the scalar field theory. Importantly, we showed that the disagreement worsened with increasing Q^2 , and also with decreasing W . We concluded that the primary origin of this result was due to the kinematics. By measuring at higher W one would be able to approach closer to the pion pole, and thus achieve a better estimation of the pion form factor.

Motivated by this finding we considered the question of model dependence in a more complicated fermionic model. In this third original work, *Investigating the Model Dependence of the Pion Electromagnetic Form Factor Using Chiral Effective Field Theory*, we again observed the systematic over extraction of the pion form factor as well as the importance in making the measurement at the largest available W , in ensuring an accurate extraction.

Combined, the results of these two studies suggest that while the current measurements of the pion form factor are likely to be accurate, at least at low photon virtuality, it is clear that the measurements obtained from VGL Model are likely overestimates of the pion form factor. Given the original motivation for the measurement of the pion form factor at large photon virtuality stems from the desire to observe the transition to perturbative QCD, a model which fails at higher momentum is clearly not desirable. It is thus of importance to develop alternative models of the pion electroproduction cross section, which also allow the extraction of the pion form factor, and which do not suffer from this problem. The approach developed here has the advantage of allowing one to rigorously maintain gauge invariance while having different form factors at every vertex in the problem. It will certainly be possible to generalize the simple models constructed here to build both an accurate description of the nucleon form factors, while having sufficient flexibility in the pion form factor to fit the experimental electroproduction data. Importantly, while the models presented here are not sophisticated enough for a direct extraction of the physical form factor, we propose that they should serve as an important cross check for any new proposed model: before attempting to extract the form factor from real data, any proposed model should first be tested on our simplified model. In this way, one would be able to confidently conclude that the extracted pion form factor is a true representation of the underlying form factor.

A

Conventions and Useful Identities

Unless explicitly stated otherwise, the following conventions are followed in the thesis. Expressions in this thesis are given in ‘natural units’, where

$$\hbar = 1 = c. \tag{A.1}$$

The Minkowski metric for flat space-time is taken to be the ‘mostly negative’

$$g^{\mu\nu} = \text{diag}(1, -1, -1, -1). \tag{A.2}$$

The gamma matrices form a Clifford algebra, and are defined by their commutator relation

$$\{\gamma^\mu, \gamma^\nu\} = 2g^{\mu\nu}. \tag{A.3}$$

We emphasize that this definition is consistent with our sign convention for the metric.

A.1 The Group Structure of Isospin

The Pauli Matrices are defined as

$$\sigma_1 = \begin{pmatrix} 0 & 1 \\ 1 & 0 \end{pmatrix}, \quad \sigma_2 = \begin{pmatrix} 0 & -i \\ i & 0 \end{pmatrix}, \quad \sigma_3 = \begin{pmatrix} 1 & 0 \\ 0 & -1 \end{pmatrix}. \tag{A.4}$$

These three matrices may be related to the Lie algebra $\mathfrak{su}(2)$, and thus the Lie Group $SU(2)$. In particular, one may show that the Lie Algebra $\mathfrak{su}(2)$ is given as

$$\mathfrak{su}(2) = \text{span} \left\{ \frac{i\sigma_1}{2}, \frac{i\sigma_2}{2}, \frac{i\sigma_3}{2} \right\}, \tag{A.5}$$

In other words, $i\sigma_j$ are the generators for the group $SU(2)$. Elements of $SU(2)$ may be obtained via exponentiation. Thus the most general form of an element of the group $SU(2)$ may be written

$$U = \exp\left(i \sum_{j=1}^3 \theta_j \frac{\sigma_j}{2}\right), \quad (\text{A.6})$$

where θ_j are real constants.

A.2 The Group Structure of Colour

The eight Gell-Mann matrices are given as

$$\begin{aligned} \lambda_1 &= \begin{pmatrix} 0 & 1 & 0 \\ 1 & 0 & 0 \\ 0 & 0 & 0 \end{pmatrix}, & \lambda_2 &= \begin{pmatrix} 0 & -i & 0 \\ i & 0 & 0 \\ 0 & 0 & 0 \end{pmatrix}, & \lambda_3 &= \begin{pmatrix} 1 & 0 & 0 \\ 0 & -1 & 0 \\ 0 & 0 & 0 \end{pmatrix}, \\ \lambda_4 &= \begin{pmatrix} 0 & 0 & 1 \\ 0 & 0 & 0 \\ 1 & 0 & 0 \end{pmatrix}, & \lambda_5 &= \begin{pmatrix} 0 & 0 & -i \\ 0 & 0 & 0 \\ i & 0 & 0 \end{pmatrix}, & \lambda_6 &= \begin{pmatrix} 0 & 0 & 0 \\ 0 & 0 & 1 \\ 0 & 1 & 0 \end{pmatrix}, \\ \lambda_7 &= \begin{pmatrix} 0 & 0 & 0 \\ 0 & 0 & -i \\ 0 & i & 0 \end{pmatrix}, & \lambda_8 &= \frac{1}{\sqrt{3}} \begin{pmatrix} 1 & 0 & 0 \\ 0 & 1 & 0 \\ 0 & 0 & -2 \end{pmatrix}. \end{aligned} \quad (\text{A.7})$$

As with the Pauli matrices, the Gell-Mann matrices are a representation of the Lie Algebra $\mathfrak{su}(3)$. The Lie Algebra $\mathfrak{su}(3)$ is given as

$$\mathfrak{su}(3) = \text{span}\left\{\frac{i\lambda_1}{2}, \frac{i\lambda_2}{2}, \dots, \frac{i\lambda_8}{2}\right\}, \quad (\text{A.8})$$

where $i\lambda_j$ are the generators for the group $SU(3)$. Elements of $SU(3)$ may be obtained from exponentiation. Thus the most general form of an element of the group $SU(3)$ may be written

$$U = \exp\left(i \sum_{j=1}^8 \alpha_j \frac{\lambda_j}{2}\right), \quad (\text{A.9})$$

where α_j are real constants.

B

Pion Nucleon Feynman Rules

B.1 Pseudo-Scalar Pion Nucleon Effective Theory

The unrenormalised pseudoscalar pion nucleon theory is given as

$$\mathcal{L}_{\pi N}^{\text{PS}} = \bar{\Psi}_N(i\not{\partial} + m_{N0})\Psi_N + \frac{1}{2}(\partial_\mu\boldsymbol{\pi})^2 - \frac{1}{2}m_{\pi 0}^2\boldsymbol{\pi}^2 - g_{\pi N 0}\bar{\Psi}_N i\gamma_5\boldsymbol{\tau}\cdot\boldsymbol{\pi}\Psi_N, \quad (\text{B.1})$$

where Ψ_N is the nucleon doublet

$$\Psi_N = \begin{bmatrix} \psi_p \\ \psi_n \end{bmatrix}, \quad (\text{B.2})$$

where ψ_p and ψ_n are the proton and neutron field operators, respectively. $\boldsymbol{\pi}$ is a triplet of real scalar fields given by

$$\boldsymbol{\pi} = (\pi_1, \pi_2, \pi_3), \quad (\text{B.3})$$

and $\boldsymbol{\tau}$ is the isospin operator in nucleon isospin space, which is related to the Pauli matrices defined in Appendix A via

$$\boldsymbol{\tau} = \frac{1}{2}\boldsymbol{\sigma}. \quad (\text{B.4})$$

It is useful to perform a field redefinition of the pion fields to make contact with the physical charged pions. We write

$$\boldsymbol{\pi} = (\pi_+, \pi_-, \pi_0), \quad (\text{B.5})$$

where these fields are related to the three scalar fields via $\pi_\pm = (\pi_1 \mp i\pi_2)/\sqrt{2}$ and $\pi_0 = \pi_3$. Note that $\pi_+^* = \pi_-$ and $\pi_-^* = \pi_+$. In this basis, the isospin operator takes the form

$$\boldsymbol{\tau} = (\tau_+, \tau_-, \tau_0), \quad (\text{B.6})$$

where $\tau_{\pm} = (\tau_1 \pm i\tau_2)/\sqrt{2}$. We use the gauge principle to incorporate electromagnetic interactions. This amounts to the replacement $\partial_{\mu} \rightarrow D_{\mu} = \partial_{\mu} + ie_0 A_{\mu}$

$$\begin{aligned} \mathcal{L}_{\pi N}^{\text{PS}} = & \bar{\Psi}_N (i\not{\partial} + m_{N0}) \Psi_N + \frac{1}{2} (\partial_{\mu} \boldsymbol{\pi})^2 - \frac{1}{2} m_{\pi 0}^2 \boldsymbol{\pi}^2 - g_{\pi N 0} \bar{\Psi}_N i\gamma_5 \boldsymbol{\tau} \cdot \boldsymbol{\pi} \Psi_N \\ & - e_0 \bar{\Psi}_N \gamma^{\mu} \hat{Q}_N \Psi_N A_{\mu} + ie_0 (\partial^{\mu} \boldsymbol{\pi}) \cdot (\hat{Q} \boldsymbol{\pi}) A_{\mu}. \end{aligned} \quad (\text{B.7})$$

The corresponding Feynman Rules are

$$\text{Nucleon:} \quad \begin{array}{c} \text{---} \blacktriangleright \text{---} \\ p \end{array} \quad S_F(p) = \frac{i}{\not{p} - m_N} \quad (\text{B.8})$$

$$\text{Pion:} \quad \begin{array}{c} \text{---} \text{---} \\ k \end{array} \quad S_{\pi}(k) = \frac{i}{k^2 - m_{\pi}^2} \quad (\text{B.9})$$

$$\gamma p \rightarrow p \quad \begin{array}{c} \text{wavy} \\ \text{---} \blacktriangleright \bullet \blacktriangleright \text{---} \end{array} \quad -iQ_N e \gamma^{\mu} \quad (\text{B.10})$$

$$\gamma \pi \rightarrow \pi \quad \begin{array}{c} \text{wavy} \\ \text{---} \bullet \text{---} \\ k \quad k' \end{array} \quad -iQ_{\pi} e (k + k')^{\mu} \quad (\text{B.11})$$

$$\begin{aligned} p(n) \rightarrow \pi^0 p(n) & \quad \begin{array}{c} \text{---} \blacktriangleright \text{---} \\ | \\ k \end{array} \quad +1(-1)g_{\pi N} \gamma_5 \\ p(n) \rightarrow \pi^+ (\pi^-) p(n) & \quad \begin{array}{c} \text{---} \blacktriangleright \bullet \blacktriangleright \text{---} \\ | \\ k \end{array} \quad \sqrt{2}g_{\pi N} \gamma_5 \not{k} \end{aligned} \quad (\text{B.12})$$

B.2 Pseudo-Vector Pion Nucleon Effective Theory

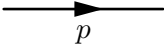
The pseudo-vector realization of pion-nucleon effective field theory to lowest order in derivatives of the pion field is

$$\begin{aligned} \mathcal{L}_{\pi N}^{\text{PV}} = & \bar{\Psi}_N(i\cancel{\partial} + m_N)\Psi_N + \frac{1}{2}(\partial_\mu\boldsymbol{\pi})^2 - \frac{1}{2}m_\pi^2\boldsymbol{\pi}^2 \\ & + \frac{g_A}{2f_\pi}\bar{\Psi}_N\gamma^\mu\gamma_5\boldsymbol{\pi}\cdot\partial_\mu\boldsymbol{\pi}\Psi_N - \frac{1}{(2f_\pi)^2}\bar{\Psi}_N\gamma^\mu\boldsymbol{\tau}\cdot(\boldsymbol{\pi}\times\partial_\mu\boldsymbol{\pi})\Psi_N. \end{aligned} \quad (\text{B.13})$$

We introduce the electromagnetic interaction via the principle of minimal substitution. This leads to electromagnetic interactions of the form

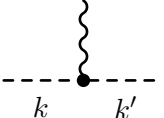
$$\begin{aligned} \mathcal{L}_{\gamma\pi N}^{\text{PV}} = & -\bar{\Psi}_N\gamma^\mu\hat{Q}_N\Psi_N A_\mu + i(\partial^\mu\boldsymbol{\pi})\cdot(\hat{Q}\boldsymbol{\pi})A_\mu + \frac{ig_A}{2f_\pi}\bar{\Psi}_N\gamma^\mu\gamma_5\boldsymbol{\tau}\cdot\hat{Q}_\pi\Psi_N A_\mu \\ & - \frac{i}{(2f_\pi)^2}\bar{\Psi}_N\gamma^\mu\boldsymbol{\tau}\cdot(\boldsymbol{\pi}\times\hat{Q}_\pi\boldsymbol{\pi})\Psi_N A_\mu, \end{aligned} \quad (\text{B.14})$$

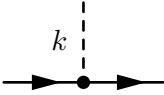
where g_A is the nucleon axial vector charge ($g_A \approx 1.26$), and f_π is the pion decay constant. There exist in the literature a number of different conventions for f_π . In our case, $f_\pi = 0.093$ GeV. \hat{Q}_N and \hat{Q}_π are the charge operators for the nucleon and pion, respectively. The Feynman Rules are [155]:

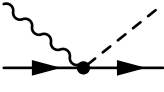
Nucleon:  $S_F(p) = \frac{i}{\not{p} - m_N}$ (B.15)

Pion:  $S_\pi(k) = \frac{i}{k^2 - m_\pi^2}$ (B.16)

$\gamma p \rightarrow p$  $-iQ_N e \gamma^\mu$ (B.17)

$\gamma \pi \rightarrow \pi$  $-iQ_\pi e(k + k')^\mu$ (B.18)

$p(n) \rightarrow \pi^0 p(n)$
 $p(n) \rightarrow \pi^+(\pi^-) p(n)$  $+1(-1) \frac{g_A}{2f_\pi} \gamma_5 \not{k}$
 $\frac{g_A}{\sqrt{2}f_\pi} \gamma_5 \not{k}$ (B.19)

$\gamma p(n) \rightarrow \pi^+(\pi^-) n(p)$  $-1(+1) e \frac{g_A}{\sqrt{2}f_\pi} \gamma_5 \gamma^\mu$ (B.20)

C

Hadronic Charge Radii and Magnetic Moments

In Chapter 3, we calculated chiral corrections to baryon electromagnetic form factors. In order to better display the charge radii and magnetic moments, we plotted the predicted observables against their experimental values. For completeness, we include the numerical values in tabular form.

TABLE C.1: Comparison of the predicted electric charge radii to experimental results for the proton, neutron, Σ^- and Σ^+ baryons. Experimental results are taken from [93, 95, 154], except for the Σ^+ charge radius, for which there is currently no experimental value. In this case, a recent lattice QCD result [131, 132] is given instead. This value is denoted with an asterisk. Charge radii are quoted in femtometres.

	p	$\langle r^2 \rangle^{\frac{1}{2}}$ n	Σ^-	Σ^+
Prev. NJL	0.87	0.38	0.86	0.97
Calc.				
This Work	0.89	0.41	0.78	0.88
Exp.	0.84	0.335	0.780	0.61(8)*

TABLE C.2: Comparison of the predicted magnetic moments to experimental results for the proton, neutron, Σ^- and Σ^+ baryons. Experimental results are taken from [93, 95]. Magnetic moments are in units of nuclear magnetons ($\mu_N = e/2m_N$).

	p	μ n	Σ^-	Σ^+
Prev. NJL	2.78	-1.81	-1.58	2.60
Calc.				
This Work	2.78	-1.71	-1.17	2.33
Exp.	2.793	-1.913	-1.160(25)	2.458(10)

D

Derivation of the Pion Electroproduction Cross Section

This appendix contains the definitions of kinematic variables and a derivation of the relation between the hadronic matrix elements and the structure functions which are of interest in studies of the pion's electromagnetic form factor. We begin this appendix with a discussion of kinematic variables and reference frames of particular interest.

D.1 Kinematic Variables and Reference Frames

In introducing the pion electroproduction cross section, we must choose labels to represent the initial and final four-momenta of the particles involved in the interaction. Momenta are chosen as shown in Fig. D.1.

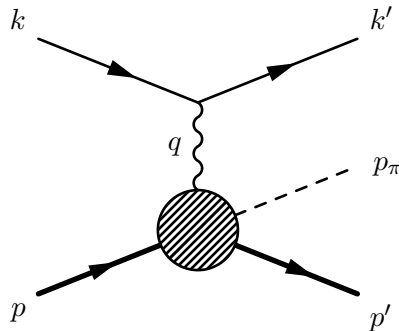


FIGURE D.1: External four-momenta labels used in the description of pion electroproduction. The virtual photon is defined as flowing into the hadronic matrix element.

Initial particles are defined to have ingoing momentum and final particles are defined to have outgoing momentum. We define the direction of the exchanged virtual photon via $q = k - k'$. Thus overall conservation of momentum $k + p = k' + p' + p_\pi$ leads to $p + q = p' + p_\pi$.

D.1.1 Kinematic Variables

In the following work, Mandelstam variables are used extensively. While the Mandelstam variables themselves are scalars it is also useful to define the four-vectors which produce these invariants. We define the ‘Mandelstam four-vectors’ as

$$p_s^\mu = (p + q)^\mu = (p' + p_\pi)^\mu, \quad (\text{D.1})$$

$$p_t^\mu = (p_\pi - q)^\mu = (p - p')^\mu, \quad (\text{D.2})$$

$$p_u^\mu = (p' - q)^\mu = (p - p_\pi)^\mu. \quad (\text{D.3})$$

The squares of these four-vectors give the conventional Mandelstam variables. They are defined as

$$s = p_s^2 = W^2 = (p + q)^2, \quad (\text{D.4})$$

$$t = p_t^2 = (p_\pi - q)^2, \quad (\text{D.5})$$

$$u = p_u^2 = (p' - q)^2. \quad (\text{D.6})$$

We note that we have introduced the invariant mass of the proton-photon system W . We shall use W rather than s . This decision follows the convention for the discussion of this cross section in Chapter 5. It is possible to show that the sum of the Mandelstam Variables leads to

$$\begin{aligned} s + t + u &= p^2 + q^2 + p'^2 + p_\pi^2 \\ &= 2m_N^2 + m_\pi^2 - Q^2, \end{aligned} \quad (\text{D.7})$$

and thus we may exchange the u dependence for the photon’s virtuality Q^2 . In what follows, we shall describe the cross section with the variables (Q^2, W, t) . Amaldi Fubini and Furlan in Ref. [149] show that the evaluation of the cross section, is most easily completed in the $p\gamma^*$ centre of momentum frame. As a result, it is of interest to determine the four-vectors of external particles in this frame.

D.1.2 $p\gamma^*$ Centre of Momentum Frame

We denote energies and three-momenta evaluated in the $p\gamma^*$ centre of momentum frame with the tilde (\sim) symbol. This frame is defined by the relations

$$\tilde{\mathbf{p}} = -\tilde{\mathbf{q}}, \quad (\text{D.8})$$

$$\tilde{\mathbf{p}}' = -\tilde{\mathbf{p}}_\pi. \quad (\text{D.9})$$

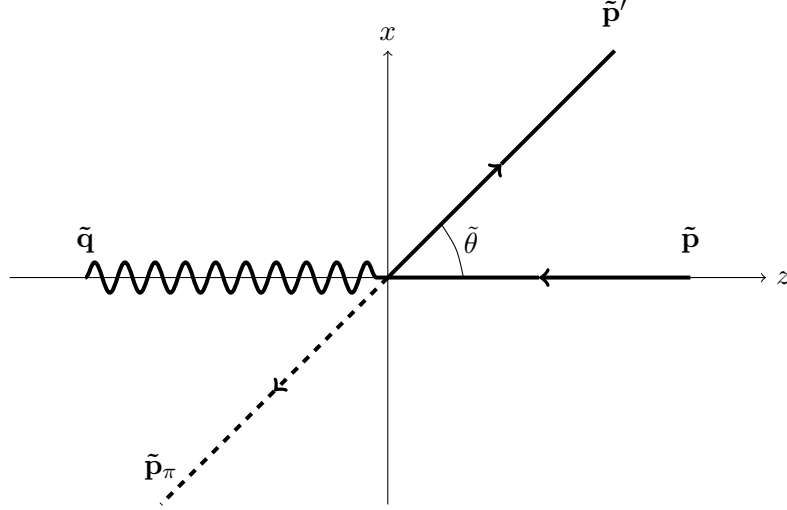


FIGURE D.2: Kinematics in the $p\gamma^*$ centre of momentum frame. We choose the x - z plane as the interaction plane, and further define the z axis to be the direction of the initial photon. The angle between the initial and final nucleons is $\tilde{\theta}$.

In this frame, the Mandelstam four-vector takes the simple form

$$\begin{aligned} p_s^\mu &= (p + q)^\mu = (p' + p_\pi)^\mu \\ &= (E_{\tilde{p}} + E_{\tilde{q}}, 0, 0, 0) = (E_{\tilde{p}'} + E_{\tilde{p}_\pi}, 0, 0, 0). \end{aligned} \quad (\text{D.10})$$

The corresponding invariant mass W takes the particularly simple form $W = E_{\tilde{p}} + E_{\tilde{q}}$. Using this relation allows other relations to be derived. Momentum conservation gives us

$$\begin{aligned} q^2 &= (p' + p_\pi - p)^2 \\ &= W^2 + m_N^2 - 2p_s \cdot p \\ &= W^2 + m_N^2 - 2WE_{\tilde{p}}, \end{aligned} \quad (\text{D.11})$$

and thus

$$E_{\tilde{p}} = \frac{W^2 + m_N^2 + Q^2}{2W}. \quad (\text{D.12})$$

By isolating different four-vectors, we can determine the energies for each of the four particles in terms of Lorentz invariant quantities. We can show

$$E_{\tilde{\mathbf{p}}} = \frac{W^2 + m_N^2 + Q^2}{2W}, \quad (\text{D.13})$$

$$E_{\tilde{\mathbf{q}}} = \frac{W^2 - m_N^2 - Q^2}{2W}, \quad (\text{D.14})$$

$$E_{\tilde{\mathbf{p}}'} = \frac{W^2 - m_\pi^2 + m_N^2}{2W}, \quad (\text{D.15})$$

$$E_{\tilde{\mathbf{p}}_\pi} = \frac{W^2 + m_\pi^2 - m_N^2}{2W}. \quad (\text{D.16})$$

Note that it is easy to see that $W = E_{\tilde{\mathbf{p}}} + E_{\tilde{\mathbf{q}}} = E_{\tilde{\mathbf{p}}_\pi} + E_{\tilde{\mathbf{p}}'}$. The magnitudes of the three-momenta may be determined by noting that $p^2 = E_{\tilde{\mathbf{p}}}^2 - \mathbf{p}^2$. Thus

$$\tilde{\mathbf{p}}^2 = \left(\frac{W^2 + m_N^2 + Q^2}{2W} \right)^2 - m_N^2, \quad (\text{D.17})$$

$$\tilde{\mathbf{q}}^2 = \left(\frac{W^2 - m_N^2 - Q^2}{2W} \right)^2 + Q^2, \quad (\text{D.18})$$

$$\tilde{\mathbf{p}}'^2 = \left(\frac{W^2 - m_\pi^2 + m_N^2}{2W} \right)^2 - m_N^2, \quad (\text{D.19})$$

$$\tilde{\mathbf{p}}_\pi^2 = \left(\frac{W^2 + m_\pi^2 - m_N^2}{2W} \right)^2 - m_\pi^2. \quad (\text{D.20})$$

We may relate the angle $\tilde{\theta}$ to Lorentz invariants via

$$\begin{aligned} t &= (p - p')^2 \\ &= 2m_N^2 - 2p \cdot p' \\ &= 2m_N^2 - 2E_{\tilde{\mathbf{p}}}E_{\tilde{\mathbf{p}}'} + 2|\tilde{\mathbf{p}}||\tilde{\mathbf{p}}'| \cos \tilde{\theta}, \end{aligned} \quad (\text{D.21})$$

and thus

$$\cos \tilde{\theta} = \frac{t - 2m_N^2 + 2E_{\tilde{\mathbf{p}}}E_{\tilde{\mathbf{p}}'}}{2|\tilde{\mathbf{p}}||\tilde{\mathbf{p}}'|}. \quad (\text{D.22})$$

As a result, we may write down the full four-vectors as

$$p^\mu = (E_{\tilde{\mathbf{p}}}, 0, 0, -|\tilde{\mathbf{q}}|), \quad (\text{D.23})$$

$$q^\mu = (E_{\tilde{\mathbf{q}}}, 0, 0, |\tilde{\mathbf{q}}|), \quad (\text{D.24})$$

$$p'^\mu = (E_{\tilde{\mathbf{p}}'}, -|\tilde{\mathbf{p}}_\pi| \sin \tilde{\theta}, 0, -|\tilde{\mathbf{p}}_\pi| \cos \tilde{\theta}), \quad (\text{D.25})$$

$$p_\pi^\mu = (E_{\tilde{\mathbf{p}}_\pi}, |\tilde{\mathbf{p}}_\pi| \sin \tilde{\theta}, 0, |\tilde{\mathbf{p}}_\pi| \cos \tilde{\theta}), \quad (\text{D.26})$$

where we again emphasize that these expressions have been written in terms of Lorentz invariants only.

D.1.3 Cross Section Reduction

Much of what is discussed in the following may be found in Ref. [149]. It is well known that the expression for the differential cross section $d\sigma$ for a general $2 \rightarrow 3$ process is given by

$$d^9\sigma = \frac{1}{4\sqrt{(p \cdot k)^2 - m_e^2 m_N^2}} \frac{d^3k'}{(2\pi)^3} \frac{d^3p'}{(2\pi)^3} \frac{d^3p_\pi}{(2\pi)^3} \frac{1}{2E_{\mathbf{k}'}} \frac{1}{2E_{\mathbf{p}'}} \frac{1}{2E_{\mathbf{p}_\pi}} \sum |\mathcal{M}|^2 (2\pi)^4 \delta(p+k-p'-k'-p_\pi), \quad (\text{D.27})$$

where as always $q = k - k'$ is the four-momentum transferred from the electron to the hadronic system and \sum is a general sum over all the spin states in the final and initial states. The electron mass is given by m_e , and in the following, we approximate the electron as massless, so $m_e \approx 0$. In the one-photon-exchange approximation, the matrix element for this process is

$$\begin{aligned} i\mathcal{M} &= \frac{e^2}{q^2} \bar{u}_e(k', r') \gamma_\mu u_e(k, r) \times \langle p', p_\pi | V^\mu | p \rangle \\ &= -\frac{e^2}{q^2} l_\mu i\mathcal{M}^\mu, \end{aligned} \quad (\text{D.28})$$

where $l_\mu = \bar{u}_e(k', r') \gamma_\mu u_e(k, r)$ contains the leptonic component, and $i\mathcal{M}^\mu = \langle p', p_\pi | V^\mu | p \rangle$ contains the hadronic component. Note that in the above expression for the differential cross section, one requires the modulus squared of the matrix element $i\mathcal{M}$, where for unpolarized beams, the spin states of the ingoing and outgoing particles must be averaged and summed over, respectively. Thus one obtains

$$\sum |\mathcal{M}|^2 = \frac{1}{4} \sum_{s, s', r, r'} \frac{e^4}{q^4} l_\mu^\dagger l_\nu \mathcal{M}^{\mu\dagger} \mathcal{M}^\nu, \quad (\text{D.29})$$

where for simplicity, it is possible to define

$$L_{\mu\nu} = \frac{1}{4} \sum_{r,r'} l_{\mu}^{\dagger} l_{\nu}, \quad (\text{D.30})$$

$$\mathcal{M}^{\mu\nu} = \frac{1}{2} \sum_{s,s'} \mathcal{M}^{\mu\dagger} \mathcal{M}^{\nu}, \quad (\text{D.31})$$

so that the equation is simplified to

$$\sum |\mathcal{M}|^2 = \frac{2e^4}{q^4} L_{\mu\nu} \mathcal{M}^{\mu\nu}. \quad (\text{D.32})$$

Substituting this into the above expression for the differential cross section leads to

$$d^9\sigma = \frac{1}{(2\pi)^5} \frac{1}{4p \cdot k} \frac{2e^4}{q^4} L_{\mu\nu} \mathcal{M}^{\mu\nu} \frac{d^3k'}{2E_{\mathbf{k}'}} \frac{d^3p'}{2E_{\mathbf{p}'}} \frac{d^3p_{\pi}}{2E_{\mathbf{p}_{\pi}}} \delta(p + k - p' - k' - p_{\pi}). \quad (\text{D.33})$$

Now recall that $\alpha = e^2/4\pi$, and $Q^2 = -q^2$. Using these two identities leads to

$$d^9\sigma = \frac{\alpha^2}{4\pi^3} \frac{1}{p \cdot k} \frac{1}{Q^4} L_{\mu\nu} \mathcal{M}^{\mu\nu} \frac{d^3k'}{2E_{\mathbf{k}'}} \frac{d^3p'}{2E_{\mathbf{p}'}} \frac{d^3p_{\pi}}{2E_{\mathbf{p}_{\pi}}} \delta(p + k - p' - k' - p_{\pi}). \quad (\text{D.34})$$

We may reduce this ninefold differential cross section by integrating over the final neutron three-momentum \mathbf{p}' , with the aide of the delta function. This enforces conservation of three-momentum:

$$\mathbf{p} + \mathbf{k} = \mathbf{p}' + \mathbf{k}' + \mathbf{p}_{\pi}, \quad (\text{D.35})$$

and results in the sixfold differential cross section

$$d^6\sigma = \frac{\alpha^2}{4\pi^3} \frac{1}{p \cdot k} \frac{1}{Q^4} L_{\mu\nu} \mathcal{M}^{\mu\nu} \frac{d^3k'}{2E_{\mathbf{k}'}} \frac{d^3p_{\pi}}{2E_{\mathbf{p}_{\pi}}} \frac{1}{2E_{\mathbf{p}'}} \delta(E_{\mathbf{p}} + E_{\mathbf{k}} - E_{\mathbf{p}'} - E_{\mathbf{k}'} - E_{\mathbf{p}_{\pi}}). \quad (\text{D.36})$$

The asymptotic states are on-shell, and so obey relativistic energy-momentum relations:

$$E_{\mathbf{p}} = \sqrt{\mathbf{p}^2 + m_N^2}, \quad (\text{D.37})$$

$$E_{\mathbf{k}} = |\mathbf{k}|, \quad (\text{D.38})$$

$$E_{\mathbf{p}'} = \sqrt{\mathbf{p}'^2 + m_N^2}, \quad (\text{D.39})$$

$$E_{\mathbf{k}'} = |\mathbf{k}'|, \quad (\text{D.40})$$

$$E_{\mathbf{p}_{\pi}} = \sqrt{\mathbf{p}_{\pi}^2 + m_{\pi}^2}. \quad (\text{D.41})$$

To further reduce the differential cross section, we choose to work in the $p\gamma^*$ centre of momentum frame. In this frame, the above energy-momentum relations for the final states may be simplified to

$$E_{\tilde{\mathbf{p}}'} = \sqrt{\tilde{\mathbf{p}}_\pi^2 + m_N^2}, \quad (\text{D.42})$$

$$E_{\tilde{\mathbf{k}}'} = |\tilde{\mathbf{k}}'|, \quad (\text{D.43})$$

$$E_{\tilde{\mathbf{p}}_\pi} = \sqrt{\tilde{\mathbf{p}}_\pi^2 + m_\pi^2}. \quad (\text{D.44})$$

Where we use the tilde again to denote that these relations are true in the $p\gamma^*$ centre of momentum. Note that overall momentum conservation (obtained from the three-momentum delta function) reduces to the constraint in the $p\gamma^*$ centre of momentum frame

$$\tilde{\mathbf{k}}' = \tilde{\mathbf{p}} + \tilde{\mathbf{k}}, \quad (\text{D.45})$$

and so we may write $E_{\tilde{\mathbf{k}}'} = |\tilde{\mathbf{p}} + \tilde{\mathbf{k}}|$. Thus the remaining one-dimensional delta function is dependent only on $|\tilde{\mathbf{p}}_\pi|$. After transforming to spherical coordinates, the differential cross section becomes

$$d^6\sigma = \frac{\alpha^2}{4\pi^3} \frac{1}{p \cdot k} \frac{1}{Q^4} L_{\mu\nu} \mathcal{M}^{\mu\nu} \frac{d^3k'}{2E_{\mathbf{k}'}} \frac{\tilde{p}_\pi^2 d\tilde{p}_\pi d\tilde{\Omega}_\pi}{2E_{\tilde{\mathbf{p}}_\pi}} \frac{1}{2E_{\tilde{\mathbf{p}}'}} \delta(E_{\tilde{\mathbf{p}}} + E_{\tilde{\mathbf{k}}} - E_{\tilde{\mathbf{p}}'} - E_{\tilde{\mathbf{k}}'} - E_{\tilde{\mathbf{p}}_\pi}). \quad (\text{D.46})$$

We have the identity

$$\delta(f(p)) = \frac{\delta(p - p')}{|f'(p')|}, \quad (\text{D.47})$$

where $f(p') = 0$. After making the identification $f(\tilde{p}_\pi) = E_{\tilde{\mathbf{p}}} + E_{\tilde{\mathbf{k}}} - E_{\tilde{\mathbf{p}}'} - E_{\tilde{\mathbf{k}}'} - E_{\tilde{\mathbf{p}}_\pi}$, one may show that

$$\delta(f(\tilde{p}_\pi)) = \frac{\delta(\tilde{p}_\pi - |\tilde{\mathbf{p}}_\pi|)}{\left| -|\tilde{\mathbf{p}}_\pi| \left(\frac{1}{E_{\tilde{\mathbf{p}}_\pi}} + \frac{1}{E_{\tilde{\mathbf{p}}'}} \right) \right|}, \quad (\text{D.48})$$

and so evaluation of the delta function gives

$$d^5\sigma = \frac{\alpha^2}{4^2\pi^3} \frac{1}{p \cdot k} \frac{1}{Q^4} L_{\mu\nu} \mathcal{M}^{\mu\nu} \frac{|\tilde{\mathbf{p}}_\pi|}{E_{\tilde{\mathbf{p}}_\pi} + E_{\tilde{\mathbf{p}}'}} \frac{d^3k'}{2E_{\mathbf{k}'}} d\Omega_\pi \quad (\text{D.49})$$

Now recall from the above energy relations, that $E_{\mathbf{k}'} = |\mathbf{k}'|$. Changing variables is thus trivial, and one obtains

$$\frac{d^5\sigma}{dE_{\tilde{\mathbf{k}}'}d\Omega'd\Omega_\pi} = \frac{\alpha^2}{2.4^2\pi^3} \frac{1}{p \cdot k} \frac{1}{Q^4} \frac{|\tilde{\mathbf{p}}_\pi| E_{\mathbf{k}'}}{E_{\tilde{\mathbf{p}}_\pi} + E_{\tilde{\mathbf{p}}'}} L_{\mu\nu} \mathcal{M}^{\mu\nu}. \quad (\text{D.50})$$

Finally, note that $p \cdot k$, being a Lorentz invariant, may be evaluated in any frame. Choosing the hadron rest frame gives $p \cdot k = m_N E_{\mathbf{k}}$, which leads to

$$\frac{d^5\sigma}{dE_{\tilde{\mathbf{k}}'}d\Omega'd\Omega_\pi} = \frac{\alpha^2}{32\pi^3} \frac{1}{m_N W} \frac{1}{Q^4} |\tilde{\mathbf{p}}_\pi| \frac{E_{\mathbf{k}'}}{E_{\mathbf{k}}} L_{\mu\nu} \mathcal{M}^{\mu\nu}. \quad (\text{D.51})$$

A further factorization exists in the literature, where the differential cross section is written as

$$\frac{d^5\sigma}{dE_{\tilde{\mathbf{k}}'}d\Omega'd\Omega_\pi} = \frac{\alpha}{2\pi^2} \frac{E_{\mathbf{k}'}}{E_{\mathbf{k}}} \frac{1}{Q^2} \frac{k_L}{1 - \epsilon} \frac{d\sigma}{d\Omega_\pi}, \quad (\text{D.52})$$

where

$$\frac{d\sigma}{d\Omega_\pi} = \frac{\alpha}{16\pi} \frac{|\tilde{\mathbf{p}}_\pi|}{k_L} \frac{1}{m_N W} \frac{1 - \epsilon}{Q^2} L_{\mu\nu} \mathcal{M}^{\mu\nu}. \quad (\text{D.53})$$

In the above, k_L is termed the photon equivalent energy

$$k_L = \frac{W^2 - m_N^2}{2m_N}, \quad (\text{D.54})$$

and ϵ is the photon polarization parameter. Commonly, experiment differential cross sections are given in terms of the Lorentz invariant t mandelstam variable instead of θ . The above differential cross section is easily transformed by noting that in the center of mass frame, the differentials may be related by $dt = 2|\tilde{\mathbf{p}}||\tilde{\mathbf{p}}'|d\cos\theta$, which leads to

$$\frac{d\sigma}{dt d\phi} = \frac{\alpha}{32\pi} \frac{1}{|\tilde{\mathbf{q}}|} \frac{1}{k_L m_N W} \frac{1 - \epsilon}{Q^2} L_{\mu\nu} \mathcal{M}^{\mu\nu}. \quad (\text{D.55})$$

Finally, it is conventional to normalize the differential cross section by a factor of 2π , to cancel the factor obtained from doing the angular integral:

$$(2\pi) \frac{d\sigma}{dt d\phi} = \frac{\alpha}{16} \frac{1}{|\tilde{\mathbf{q}}|} \frac{1}{k_L m_N W} \frac{1 - \epsilon}{Q^2} L_{\mu\nu} \mathcal{M}^{\mu\nu}. \quad (\text{D.56})$$

These kinematical factors are of course model independent; all the model dependent physics may be found in the term $L_{\mu\nu} \mathcal{M}^{\mu\nu}$.

D.1.4 Evaluating $L_{\mu\nu}\mathcal{M}^{\mu\nu}$

One may show (see Ref. [149]) for details) that

$$L_{\mu\nu}\mathcal{M}^{\mu\nu} = \frac{Q^2}{1-\epsilon} \left[\frac{1}{2} \left(\tilde{\mathcal{M}}^{11} + \tilde{\mathcal{M}}^{22} \right) + \epsilon_L \tilde{\mathcal{M}}^{33} + \frac{1}{2} \left(\tilde{\mathcal{M}}^{11} - \tilde{\mathcal{M}}^{22} \right) \epsilon \cos(2\phi) \right. \\ \left. + \frac{1}{2} \left(\tilde{\mathcal{M}}^{13} + \tilde{\mathcal{M}}^{31} \right) \sqrt{2\epsilon_L(\epsilon+1)} \cos(\phi) \right], \quad (\text{D.57})$$

where

$$\epsilon_L = \left(\frac{Q^2}{E_{\mathbf{q}}^2} \right) \epsilon. \quad (\text{D.58})$$

D.1.5 Decomposing the Experimental Cross Section

It is well known that the unpolarized π^+ electroproduction cross section may be decomposed into four response functions¹:

$$(2\pi) \frac{d^2\sigma}{dt d\phi} = \frac{d\sigma_T}{dt} + \epsilon \frac{d\sigma_L}{dt} + \sqrt{2\epsilon(\epsilon+1)} \frac{d\sigma_{LT}}{dt} \cos\phi + \epsilon \frac{d\sigma_{TT}}{dt} \cos 2\phi. \quad (\text{D.59})$$

Using the identity derived in the previous section for the squared matrix element $L_{\mu\nu}\mathcal{M}^{\mu\nu}$, one may write the derived cross section as

$$(2\pi) \frac{d\sigma}{dt d\phi} = \frac{\alpha}{16} \frac{1}{|\tilde{\mathbf{q}}|} \frac{1}{k_L m_N W} \left[\frac{1}{2} (\mathcal{M}^{11} + \mathcal{M}^{22}) + \epsilon \mathcal{M}_{33} \left(\frac{Q^2}{E_{\mathbf{q}}^2} \right) \right. \\ \left. + \sqrt{2\epsilon(\epsilon+1)} \frac{1}{2} (\mathcal{M}^{31} + \tilde{\mathcal{M}}^{13}) \sqrt{\frac{Q^2}{E_{\mathbf{q}}^2}} \cos\phi + \frac{1}{2} (\mathcal{M}^{11} - \mathcal{M}^{22}) \epsilon \cos 2\phi \right], \quad (\text{D.60})$$

which allows an immediate identification of the individual response functions as

¹Note the sign of the fourth response function, as some authors choose a negative sign, ie $d\sigma_{TT}/dt \rightarrow -d\sigma_{TT}/dt$. This work follows the ‘all positive’ convention of Ref. [134].

$$\frac{d\sigma_T}{dt} = A \times \left[\frac{1}{2}(\tilde{\mathcal{M}}^{11} + \tilde{\mathcal{M}}^{22}) \right], \quad (\text{D.61})$$

$$\frac{d\sigma_L}{dt} = A \times \left(\frac{Q^2}{E_{\tilde{\mathbf{q}}}^2} \right) \left[\tilde{\mathcal{M}}_{33} \right], \quad (\text{D.62})$$

$$\frac{d\sigma_{LT}}{dt} = A \times \sqrt{\frac{Q^2}{E_{\tilde{\mathbf{q}}}^2}} \left[\frac{1}{2}(\tilde{\mathcal{M}}^{31} + \mathcal{M}^{13}) \right], \quad (\text{D.63})$$

$$\frac{d\sigma_{TT}}{dt} = A \times \left[\frac{1}{2}(\tilde{\mathcal{M}}_{11} - \tilde{\mathcal{M}}_{22}) \right], \quad (\text{D.64})$$

where

$$A = \frac{\alpha}{16} \frac{1}{|\tilde{\mathbf{q}}|} \frac{1}{k_L m_N W}. \quad (\text{D.65})$$

E

Regularisation Prescriptions

This thesis has been primarily concerned with calculating perturbative corrections to tree level results. These loop diagrams often contain ultraviolet divergences which must be systematically regularized before they are absorbed in the process of renormalization. In this appendix, we discuss the regularisation prescriptions used in this thesis.

E.1 Some Loop Integrals Diverge

It is possible to show that a general one-loop Feynman diagram may be reduced to an integral of the form

$$I_0(\Delta, n) = \int \frac{d^4l}{(2\pi)^4} \frac{1}{[l^2 - \Delta + i\epsilon]^n}. \quad (\text{E.1})$$

Note that for $n \geq 3$, this integral converges. We can see this by simple dimensional analysis. In order for the integral to converge, we require that as $l \rightarrow \infty$, the integrand is suitably suppressed. In this limit, the factor of Δ becomes irrelevant, and our integrand becomes

$$\frac{d^4l}{(2\pi)^4} \frac{1}{l^{2n}}. \quad (\text{E.2})$$

Note that our four dimensional volume element $d^4l = dl^0 dl^1 dl^2 dl^3$ contributes four units of momentum. Thus for $n = 3$, this combination goes like

$$\frac{d^4l}{(2\pi)^4} \frac{1}{l^6} \underset{\text{large } l}{\sim} \frac{1}{l^2} \rightarrow 0, \quad (\text{E.3})$$

so this integral will converge. Note however that for $n = 2$, the integrand is no longer suitably suppressed:

$$\frac{d^4 l}{(2\pi)^4} \frac{1}{l^4} \underset{\text{large } l}{\sim} 1. \quad (\text{E.4})$$

Thus for the case of $n = 2$, $I_0(\Delta, n)$ is divergent. Obviously for $n = 1$, there is less momentum suppression, and the integral will also be divergent.

Stated simply, a regularization prescription amounts to a modification of the above integral $I_0(\Delta, n)$ which allows us to control the divergences. There are many ways one may modify the integrand to soften the ultraviolet behaviour of the integral, and in principle, any such prescription is suitable. However, many of these modifications break symmetries of the theory, and are thus undesirable. In this appendix, we shall discuss two different regularization prescriptions used in this thesis.

E.2 The Wick Rotation

Prior to the regularization of integrals of the above form, it is highly convenient to perform a so-called Wick rotation. While not part of the regularization procedure per se, it is a step we will perform identically in each of the regularization prescriptions we discuss. Consider again the basic integral obtained in one-loop calculations

$$\begin{aligned} I_0(\Delta, n) &= \int \frac{d^4 l}{(2\pi)^4} \frac{1}{[l^2 - \Delta + i\epsilon]^n} \\ &= \int \frac{d^3 l}{(2\pi)^3} \int_{-\infty}^{\infty} \frac{dl_0}{(2\pi)} \frac{1}{[l_0^2 - \mathbf{l}^2 - \Delta + i\epsilon]^n} \\ &= \int \frac{d^3 l}{(2\pi)^3} \int_{-\infty}^{\infty} \frac{dl_0}{(2\pi)} \frac{1}{[(l_0 - \sqrt{\mathbf{l}^2 + \Delta - i\epsilon})(l_0 + \sqrt{\mathbf{l}^2 + \Delta - i\epsilon})]^n}. \end{aligned} \quad (\text{E.5})$$

Written this way, it is possible to see that if we analytically continue the loop energy, we will encounter poles at $\pm\sqrt{\mathbf{l}^2 + \Delta - i\epsilon}$. We define a contour as shown in Fig. E.1. Since there are no poles inside this contour, from the residue theorem we immediately have that

$$\oint \frac{dl_0}{(2\pi)} \frac{1}{[l_0^2 - \mathbf{l}^2 - \Delta + i\epsilon]^n} = 0. \quad (\text{E.6})$$

It is possible to show that the contributions from the arc lengths vanish. Thus the integral along the real axis is related to the integral along the complex axis via

$$\int_{-\infty}^{\infty} \frac{dl_0}{(2\pi)} \frac{1}{[l_0^2 - \mathbf{l}^2 - \Delta + i\epsilon]^n} = - \int_{\infty}^{-\infty} \frac{idl_{0,E}}{(2\pi)} \frac{1}{[-l_{0,E}^2 - \mathbf{l}^2 - \Delta + i\epsilon]^n}. \quad (\text{E.7})$$

Where in the second integral we have made the transformation $l_0 = il_{0,E}$ so that $l_{0,E}$ is purely real. For consistency of notation, we also perform the transformation $\mathbf{l} = \mathbf{l}_E$. This transformation is known as the Wick Rotation. To summarize, we have

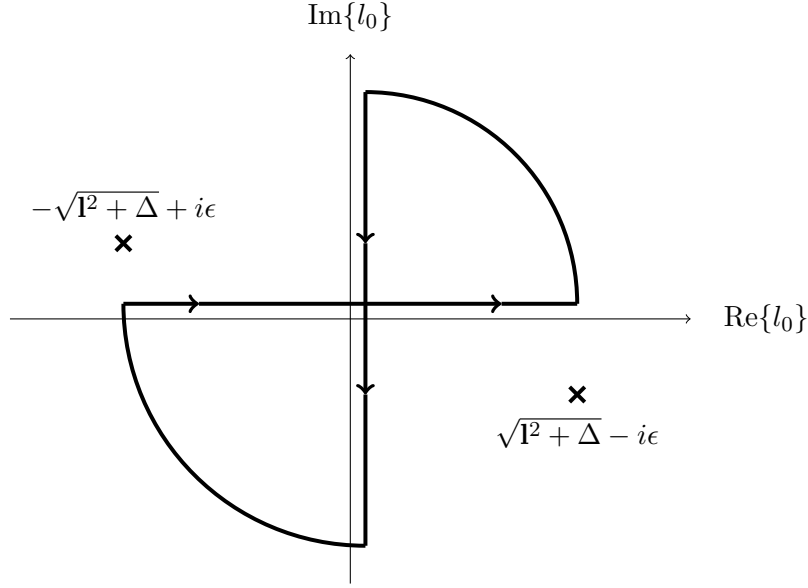


FIGURE E.1: Performing the Wick Rotation of the one-loop integral. We analytically continue l_0 to the complex plane, and relate the integral over the real axis to the integral over the complex axis.

$$l_0 = i l_{0,E}, \quad (\text{E.8})$$

$$\mathbf{l} = \mathbf{l}_E. \quad (\text{E.9})$$

The result of the Wick Rotation is thus

$$I_0(\Delta, n) = i(-1)^n \int \frac{d^4 l_E}{(2\pi)^4} \frac{1}{[l_E^2 + \Delta - i\epsilon]^n}, \quad (\text{E.10})$$

where we emphasize the factor of i in the numerator comes from the Jacobian, and $l_E^2 = l_{0,E}^2 + \mathbf{l}_E^2$.

E.3 Proper Time Regularisation

We begin our discussion of regularization prescriptions with the Proper Time Regularization prescription. This is based on the identity

$$\frac{1}{X^n} = \frac{1}{\Gamma(n)} \int_0^\infty d\tau \tau^{n-1} e^{-\tau X}, \quad (\text{E.11})$$

and thus

$$I_0(\Delta, n) = \frac{i(-1)^n}{\Gamma(n)} \int \frac{d^4 l_E}{(2\pi)^4} \int_0^\infty d\tau \tau^{n-1} e^{-\tau(l_E^2 + \Delta - i\epsilon)}. \quad (\text{E.12})$$

Interchanging the order of integration gives

$$I_0(\Delta, n) = \frac{i(-1)^n}{\Gamma(n)} \int_0^\infty d\tau \tau^{n-1} e^{-\tau(\Delta-i\epsilon)} \int \frac{d^4 l_E}{(2\pi)^4} e^{-\tau l_E^2}. \quad (\text{E.13})$$

Now note that $l_E^2 = l_{0,E}^2 + \mathbf{l}_E^2$, so these integrals are now factorisable. Using the identity

$$\begin{aligned} \int \frac{dx}{(2\pi)} e^{-\tau x^2} &= \frac{1}{2\pi} \sqrt{\frac{\pi}{\tau}} \\ &= \frac{1}{\sqrt{4\pi\tau}}. \end{aligned} \quad (\text{E.14})$$

We may perform the momentum integral to obtain

$$\begin{aligned} I_0(\Delta, n) &= \frac{i(-1)^n}{\Gamma(n)} \int_0^\infty d\tau \tau^{n-1} e^{-\tau(\Delta-i\epsilon)} \left(\frac{1}{\sqrt{4\pi\tau}} \right)^4 \\ &= \frac{i(-1)^n}{(4\pi)^2} \frac{1}{\Gamma(n)} \int_0^\infty d\tau \tau^{n-3} e^{-\tau(\Delta-i\epsilon)}. \end{aligned} \quad (\text{E.15})$$

Note that for $n \geq 3$, the integral will be well behaved at $\tau = 0$. We can see this explicitly by performing the change of variables $t = \tau(\Delta - i\epsilon)$. This gives

$$I_0(\Delta, n) = \frac{i(-1)^n}{(4\pi)^2} \frac{1}{\Gamma(n)} \frac{1}{[\Delta - i\epsilon]^{n-3}} \int_0^\infty dt t^{n-3} e^{-t}. \quad (\text{E.16})$$

Note the definition of the gamma function

$$\Gamma(n) = \int_0^\infty dt t^{n-1} e^{-t}. \quad (\text{E.17})$$

Thus we have

$$I_0(\Delta, n) = \frac{i(-1)^n}{(4\pi)^2} \frac{\Gamma(n-2)}{\Gamma(n)} \frac{1}{[\Delta - i\epsilon]^{n-3}}. \quad (\text{E.18})$$

Using the identity $\Gamma(n) = (n-1)\Gamma(n-1)$, we obtain

$$I_0(\Delta, n) = \frac{i(-1)^n}{(4\pi)^2} \frac{1}{(n-2)(n-1)} \frac{1}{[\Delta - i\epsilon]^{n-3}}. \quad (\text{E.19})$$

In this way, we see the divergences appearing as poles in n for $n = 1$ and $n = 2$. Note that at this stage, the divergences have not been controlled. In proper time regularization, we replace the lower bound of the integral with a ‘short time’ cutoff. We can write this as

$$\tau_{\text{short}} = \frac{1}{\Lambda_{\text{UV}}^2}, \quad (\text{E.20})$$

where through dimensional analysis, Λ_{UV} has units of (energy)². Using this prescription, we have

$$I_0(\Delta, n) = \frac{i(-1)^n}{(4\pi)^2} \frac{1}{\Gamma(n)} \int_{\tau_{\text{short}}}^{\infty} d\tau \tau^{n-3} e^{-\tau(\Delta - i\epsilon)}, \quad (\text{E.21})$$

where we emphasize that the effect of this short time cutoff has been to remove the divergence associated with this integral. This particular regularization prescription is used in Chap. 4 to regularize the loop integrals due to the NJL Model. As described in the main text, this regularization prescription has the advantage that in the context of the NJL Model, confinement may be simulated by imposing an infrared cutoff τ_{long} of the scale $1/\Lambda_{\text{QCD}}$. That is

$$\tau_{\text{long}} = \frac{1}{\Lambda_{\text{IR}}} \sim \frac{1}{\Lambda_{\text{QCD}}}. \quad (\text{E.22})$$

This further modification leads to

$$I_0(\Delta, n) = \frac{i(-1)^n}{(4\pi)^2} \frac{1}{\Gamma(n)} \int_{\tau_{\text{short}}}^{\tau_{\text{long}}} d\tau \tau^{n-3} e^{-\tau(\Delta - i\epsilon)}. \quad (\text{E.23})$$

E.4 Dimensional Regularization

One may also regularize loop integrals by Dimensional Regularization [156]. Let us return to our basic integral $I_0(\Delta, n)$:

$$I_0(\Delta, n) = \int \frac{d^d l}{(2\pi)^d} \frac{1}{[l^2 - \Delta + i\epsilon]^n}. \quad (\text{E.24})$$

The important step in dimensional regularization is to realize that it is the interplay between the number of units of momentum in the numerator due to the volume element and the number of units of momentum in the denominator due to the number of propagators which determines whether the integral will converge or not. To be clear, let us define

$$I_0(\Delta, n, d) = \int \frac{d^d l}{(2\pi)^d} \frac{1}{[l^2 - \Delta + i\epsilon]^n}, \quad (\text{E.25})$$

where now d denotes the number of space-time dimensions over which we are integrating. Following our dimensional analysis arguments discussed previously, the combination of terms we must consider is

$$\frac{d^d l}{(2\pi)^d} \frac{1}{l^{2n}}. \quad (\text{E.26})$$

If we had formulated our theory in three space-time dimensions, we would have $d = 3$. Let us consider the $n = 2$ integral again. Then,

$$\frac{d^3 l}{(2\pi)^3} \frac{1}{l^4} \underset{\text{large } l}{\sim} \frac{1}{l} \rightarrow 0, \quad (\text{E.27})$$

and so the integral converges. The effect of manipulating the dimension d on the convergence properties of our basic integral $I_0(\Delta, n)$ are depicted below in Table E.1.

TABLE E.1: Numerical results of calculating basic integral in d dimensions, were we have set $\Delta = 1$ for simplicity. Note that as we expected, the cases corresponding to $n = 1$ and $n = 2$ are divergent in four space-time dimensions.

		d		
		3	4	5
n	1	0.080	∞	-0.004
	2	0.040	∞	-0.006
	3	-0.010	-0.003	-0.001

Put simply, in order to utilize dimensional regularization, we calculate this integral for arbitrary d , and then set $d \rightarrow 4$ at the end of the calculation. Note that, as with any regularisation prescription, we must be careful with this last step; simply setting $d = 4$ will yield these divergences, as it must. We will discuss the exact way this step is to be performed after we have derived the formal result. Let us now explicitly perform the integration.

E.4.1 Dimensional Analysis

Formally, dimensional regularisation is constructed at the level of the action. Recall that the usual action is given by

$$S = \int d^4x \mathcal{L}. \quad (\text{E.28})$$

We note that while the Lagrangian and the metric are dimensionful:

$$[d^4x] = M^{-4}, \quad (\text{E.29})$$

and

$$[\mathcal{L}] = M^4, \quad (\text{E.30})$$

their product is dimensionless. Consider the case of ϕ^4 theory. The Lagrangian is given by

$$\mathcal{L} = \frac{1}{2}(\partial_\mu\phi)(\partial^\mu\phi) - \frac{1}{2}m_\phi^2\phi^2 - \lambda_4\phi^4, \quad (\text{E.31})$$

where, for reasons which will become obvious, we define λ_4 to be the value of the coupling in four space-time dimensions. Clearly,

$$[\phi] = M, \quad (\text{E.32})$$

and

$$[\lambda_4] = 1. \quad (\text{E.33})$$

In other words, scalar fields have mass dimension 1 (M^1), and the interaction parameter λ has mass dimension 0 (M^0). As we modify the dimensionality of the space we are integrating, we must compensate by varying the mass dimension of the fields and constants to ensure that the action remains dimensionless. To be clear, we define the dimensionally regularized action by

$$S_d = \int d^d x \mathcal{L}_d. \quad (\text{E.34})$$

Note that now we have

$$[d^d x] = M^{-d}. \quad (\text{E.35})$$

It is desirable to keep masses in the same mass dimension. Thus we require that

$$[m_\pi^2] = M^2. \quad (\text{E.36})$$

Thus by looking at the mass term, we can show that the scalar field's mass dimension must transform as

$$[\phi] = M^{d/2-1}. \quad (\text{E.37})$$

We may use these results to determine how the dimensionality of the coupling varies as we change the dimensionality of the integral. We have

$$[\lambda_d \phi^4] = M^d = [\lambda_d] \cdot M^{2d-4}. \quad (\text{E.38})$$

Rearranging this expression, we find that we must have

$$[\lambda_d] = M^{4-d}. \quad (\text{E.39})$$

It is convenient to separate the extra mass dimensions of the coupling by defining

$$\lambda_d = \mu^{4-d} \lambda_4, \quad (\text{E.40})$$

where μ is an arbitrary parameter of mass dimension 1. Note that this parameter is not physical, and will vanish in all physical quantities. With this definition, we may write the d -dimensional Lagrangian as

$$\mathcal{L}_d = \frac{1}{2}(\partial_\mu \phi)(\partial^\mu \phi) - \frac{1}{2}m_\phi^2 \phi^2 - \mu^{4-d} \lambda_4 \phi^4. \quad (\text{E.41})$$

Note that a general loop integral with n interactions will also have n propagators, and thus lead to an integral of the form

$$I_0(\Delta, n, d) = (\mu^n)^{4-d} \int \frac{d^d l}{(2\pi)^d} \frac{1}{[l^2 - \Delta + i\epsilon]^n}. \quad (\text{E.42})$$

This is the starting point for evaluation of dimensionally regulated integrals.

E.4.2 Performing the Integration

As previously discussed, we perform a Wick Rotation, which leads to

$$I_0(\Delta, n, d) = i(-1)^n (\mu^n)^{4-d} \int \frac{d^d l_E}{(2\pi)^d} \frac{1}{[l_E^2 + \tilde{\Delta} - i\epsilon]^n}. \quad (\text{E.43})$$

We may convert this to d dimensional spherical coordinates:

$$I_0(\Delta, n, d) i(-1)^n (\mu^n)^{4-d} \int \frac{d\Omega_d}{(2\pi)^d} \int_0^\infty dl \frac{l^{d-1}}{[l^2 + \Delta - i\epsilon]^n}, \quad (\text{E.44})$$

Where $d\Omega_d$ is the d dimensional solid angle. We may determine an expression for this by noting that

$$\sqrt{\pi} = \int dx e^{-x^2}. \quad (\text{E.45})$$

Raising both sides to the d th power gives

$$\begin{aligned}
(\sqrt{\pi})^d &= \left(\int dx e^{-x^2} \right)^d \\
&= \int dx_1 dx_2 \dots dx_d \exp\left(-\sum_{i=1}^d x_i^2\right) \\
&= \int d\Omega_d \int_0^\infty dx x^{d-1} e^{-x^2} \\
&= \frac{1}{2} \int d\Omega_d \Gamma(d/2).
\end{aligned} \tag{E.46}$$

Rearranging this expression, and dividing by $(2\pi)^d$ gives

$$\int \frac{d\Omega_d}{(2\pi)^d} = \frac{2}{(4\pi)^{\frac{d}{2}}} \frac{1}{\Gamma(d/2)}. \tag{E.47}$$

Let us now consider the radial part of the integral. We may perform a variable transformation $dl^2 = 2l dl$ and thus write

$$\int_0^\infty dl \frac{l^{d-1}}{[l^2 + \Delta - i\epsilon]^n} = \frac{1}{2} \int_0^\infty dl^2 \frac{(l^2)^{\frac{d}{2}-1}}{[l^2 + \Delta - i\epsilon]^n}. \tag{E.48}$$

We perform a second transformation $x = (\Delta - i\epsilon)/(l^2 + \Delta - i\epsilon)$ to obtain

$$\int_0^\infty dl \frac{l^{d-1}}{[l^2 + \Delta - i\epsilon]^n} = \frac{1}{2} \left(\frac{1}{\Delta - i\epsilon} \right)^{n-\frac{d}{2}} \int_0^1 dx x^{n-1-\frac{d}{2}} (1-x)^{\frac{d}{2}-1}. \tag{E.49}$$

This integral is now of the form of a beta function:

$$B(\alpha, \beta) = \frac{\Gamma(\alpha)\Gamma(\beta)}{\Gamma(\alpha + \beta)} = \int_0^1 dx x^{\alpha-1} (1-x)^{\beta-1}, \tag{E.50}$$

and so we find

$$\int_0^\infty dl \frac{l^{d-1}}{[l^2 + \Delta - i\epsilon]^n} = \frac{1}{2} \left(\frac{1}{\Delta - i\epsilon} \right)^{n-\frac{d}{2}} \frac{\Gamma(n - d/2)\Gamma(d/2)}{\Gamma(n)}. \tag{E.51}$$

Putting the two parts of our equation together, we find

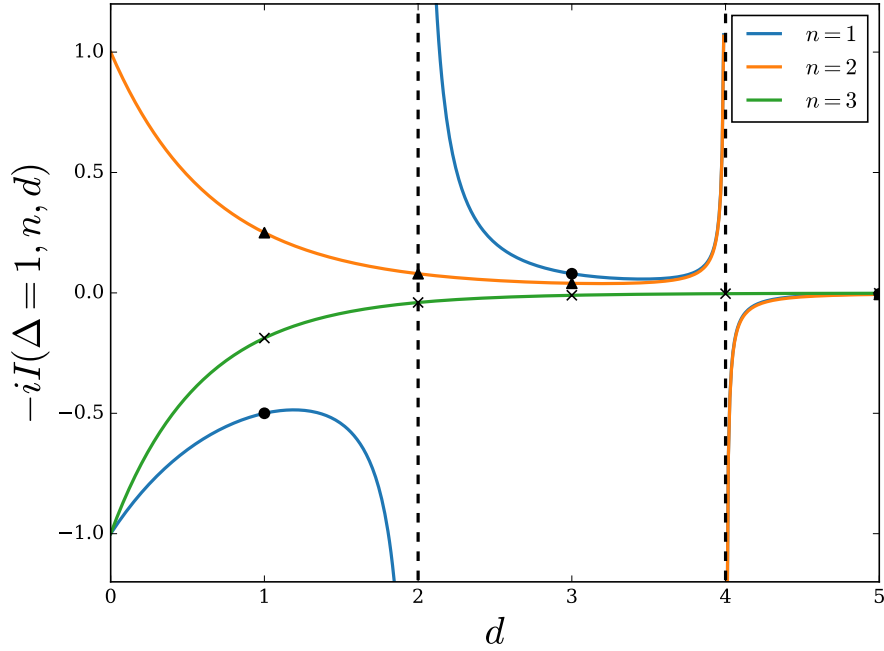


FIGURE E.2: Analytic continuation of the basic integral $I_0(\Delta, n, d)$ to non integer space-time dimensions allows one to plot the values of the integral along the real d axis. Note that in four dimensions, $I_0(\Delta, n = 1, 4)$ and $I_0(\Delta, n = 2, 4)$ diverge, while $I_0(\Delta, n \geq 3, 4)$ converge. The energy scale μ has been set to 1. It is interesting to note that in odd space-time dimension, these integrals are all finite.

$$I_0(\Delta, n, d) = \frac{i(-1)^n (\mu^n)^{4-d} \Gamma(n - d/2)}{(4\pi)^{\frac{d}{2}} \Gamma(n)} \left(\frac{1}{\Delta - i\epsilon} \right)^{n - \frac{d}{2}}. \quad (\text{E.52})$$

E.4.3 Analytic Continuation

The formally calculated basic integral is still divergent for $n = 1$, and $n = 2$. We can see this by setting $d = 4$. We would like to instead consider the limit as $d \rightarrow 4$. But d is the dimensionality of the integral, so it clearly only makes sense as an integer. Note however that our expression for I_0 is in fact well defined for non integer values of d . It turns out that our definition $I_0(\Delta, n, d)$ is valid for non-integer d . In order to completely rigorously define the dimensionally regularized integral, we must analytically continue d into the complex plane. Technical details about this process may be found in Ref. [157]. This concept is demonstrated in Fig. E.2. Note that our expression is correct for integer d , but now allows us to perform an expansion around $d = 4$. We write

$$d = 4 - 2\epsilon, \quad (\text{E.53})$$

and Taylor Expand functions for small ε . Note that the factor of 2 is simply a choice, but must be made consistently everywhere in the calculation. It should be noted that this ε differs from the ϵ used to ensure the time-ordering of the propagator.

E.4.4 d -Dimensional Dirac Algebra

In d -dimensions, we must modify our identities for Dirac Algebra. The Dirac gamma matrices are defined by the equation

$$\{\gamma^\mu, \gamma^\nu\} = 2g^{\mu\nu}. \quad (\text{E.54})$$

We require this defining relation to be true in d dimensions. Written explicitly, γ^μ is

$$\gamma^\mu = (\gamma^0, \gamma^1, \dots, \gamma^d). \quad (\text{E.55})$$

Tracing over the metric tensor $g^{\mu\nu}$ gives the dimensionality. Thus

$$g^{\mu\nu} g_{\mu\nu} = d. \quad (\text{E.56})$$

With these two points, we can derive results for our d -dimensional Dirac Algebra. For example,

$$\begin{aligned} \gamma^\mu \gamma_\mu &= \frac{1}{2} \left(\gamma^\mu \gamma_\mu + \gamma_\mu \gamma^\mu \right) \\ &= \frac{1}{2} \left(\gamma^\mu \gamma^\nu + \gamma^\nu \gamma^\mu \right) g_{\mu\nu} \\ &= g^{\mu\nu} g_{\mu\nu} \\ &= d, \end{aligned} \quad (\text{E.57})$$

and

$$\begin{aligned} \gamma^\mu \gamma^\nu \gamma_\mu &= (2g^{\mu\nu} - \gamma^\nu \gamma^\mu) \gamma_\mu \\ &= (2 - d) \gamma^\nu. \end{aligned} \quad (\text{E.58})$$

Other relations may be derived as required.

E.4.5 Trace Identities for d -Dimensional Dirac Algebra

Note that as the dimensionality increases, one must choose a new explicit representation of the gamma matrices, to ensure that the defining relation (eq. E.54) remains true. The standard

representation of these matrixs has dimension $2^{\frac{d}{2}}$ [157]. In four dimensions, $\text{tr}[\mathbb{I}_4] = 4$. Thus in general, as we vary the dimensionality of the integral, this trace should change. Mathematically, we have

$$\text{tr}[\mathbb{I}_d] = f(d). \quad (\text{E.59})$$

Following our above argument then,

$$f(d) = 2^{\frac{d}{2}}. \quad (\text{E.60})$$

It turns out that this argument, while correct, is needlessly complicated. Since we are only interested in dimensional regularization from the point of view of regularizing loop integrals, we are free to set

$$\text{tr}[\mathbb{I}_d] = f(d_0), \quad (\text{E.61})$$

where d_0 is the dimension in which the integrals diverge. Thus it is most convinient to work with the definition that

$$\text{tr}[\mathbb{I}_d] = f(d_0 = 4) = 4. \quad (\text{E.62})$$

Whenever fermion loops appear in Feynman Diagrams, we must take a trace. The trace of a matrix $M = aA + bB$, where A and B are matrices, and a and b are numbers is linear:

$$\text{tr}(aA + bB) = a \text{tr}(A) + b \text{tr}(B), \quad (\text{E.63})$$

and is cyclic:

$$\text{tr}(ABC) = \text{tr}(CAB). \quad (\text{E.64})$$

For $d = 4$, we have the result

$$\text{tr}(\gamma^\mu \gamma^\nu) = 4g^{\mu\nu}. \quad (\text{E.65})$$

We can show that that natural generalization exists in d -dimensions. Consider

$$\begin{aligned} \text{tr}(\gamma^\mu \gamma^\nu) &= \text{tr}(\gamma^\nu \gamma^\mu) \\ &= \text{tr}(2g^{\mu\nu} - \gamma^\mu \gamma^\nu) \\ 2 \text{tr}(\gamma^\mu \gamma^\nu) &= 2g^{\mu\nu} \text{tr}(\mathbb{I}_d), \end{aligned} \quad (\text{E.66})$$

and so we find

$$\text{tr}(\gamma^\mu \gamma^\nu) = 4g^{\mu\nu}. \quad (\text{E.67})$$

Consistent with our usual four dimensional definition. We can show that in d -dimensions, $\text{tr}(\gamma^\mu) = 0$. Note that

$$\begin{aligned} \text{tr}(\gamma^\mu) &= \frac{1}{2-d} \text{tr}(\gamma^\alpha \gamma^\mu \gamma_\alpha) \\ &= \frac{1}{2-d} \text{tr}(\gamma^\mu \gamma_\alpha \gamma^\alpha) \\ &= \frac{d}{2-d} \text{tr}(\gamma^\mu). \end{aligned} \quad (\text{E.68})$$

Thus we find

$$2(1-d) \text{tr}(\gamma^\mu) = 0. \quad (\text{E.69})$$

Thus for $d \neq 1$, we have $\text{tr}(\gamma^\mu) = 0$.

E.4.6 Chiral Theories in Dimensional Regularization

While dimensional regularization has a number of attractive properties, difficulties are encountered in chiral theories, and in particular, in the definition of γ_5 in d -dimensions. To see how problems arise, recall the definition of γ_5

$$\gamma_5 = i\gamma_0\gamma_1\gamma_2\gamma_3. \quad (\text{E.70})$$

How shall we interpret this in d -dimensions? There are a number of different ways of generalizing γ_5 to d -dimensions existing in the literature. For example, in Ref. [156], the authors suggest a scheme where the d -dimensional version of γ_5 anticommutes with $\mu = 0, 1, 2, 3$, and commutes with other values of μ . To make this explicit, we write

$$l^\mu = l_{\parallel}^\mu + l_{\perp}^\mu, \quad (\text{E.71})$$

where

$$l_{\parallel}^\mu = (l_0, l_1, l_2, l_3, 0, \dots, 0) \quad (\text{E.72})$$

$$l_{\perp}^\mu = (0, 0, 0, 0, l_4, l_5, \dots, l_d). \quad (\text{E.73})$$

Then we may commute $\not{L}\gamma_5$ as

$$\begin{aligned}\not{L}\gamma_5 &= \not{L}_\parallel\gamma_5 + \not{L}_\perp\gamma_5 \\ &= -\gamma_5\not{L}_\parallel + \gamma_5\not{L}_\perp \\ &= \gamma_5(-\not{L}_\parallel + \not{L}_\perp).\end{aligned}\tag{E.74}$$

F

Loop Diagrams for Scalar Pion Electroproduction

Here we collect the contributions from the individual diagrams shown in Fig. 5.10. We note that the propagators for the scalar nucleon and pion are given as

$$D_F^N(p) = \frac{i}{p^2 - m_N^2 + i\epsilon}, \quad (\text{F.1})$$

$$D_F^\pi(p) = \frac{i}{p^2 - m_\pi^2 + i\epsilon}, \quad (\text{F.2})$$

respectively.

F.1 One Loop Diagrams

Two diagrams correct the nucleon's electromagnetic vertex. The first may be written

$$\begin{aligned} i\mathcal{M}^{(1a)\mu} &= (-i\sqrt{2}g_{\pi N})D_F^N(p_s) \\ &\times \left[\int \frac{d^4k}{(2\pi)^4} (-ig_{\pi N})D_F^N(p_s - k)(-ie)(p + p_s - 2k)^\mu D_F^N(p - k)(-ig_{\pi N})D_F^\pi(k) \right], \end{aligned} \quad (\text{F.3})$$

the second electromagnetic vertex correction may be written

$$\begin{aligned}
i\mathcal{M}^{(1b)\mu} &= (-i\sqrt{2}g_{\pi N})D_F^N(p_s) \\
&\times \left[\int \frac{d^4k}{(2\pi)^4} (-i\sqrt{2}g_{\pi N})D_F^\pi(p_s - k)(-ie)(p + p_s - 2k)^\mu \right. \\
&\left. \times D_F^\pi(p - k)(-i\sqrt{2}g_{\pi N})D_F^N(k) \right].
\end{aligned} \tag{F.4}$$

The first self energy correction corresponding to the exchange of a charged pion is

$$\begin{aligned}
i\mathcal{M}^{(1c)\mu} &= (-i\sqrt{2}g_{\pi N})D_F^N(p_s) \left[\int \frac{d^4k}{(2\pi)^4} (-i\sqrt{2}g_{\pi N})D_F^N(k)D_F^\pi(p_s - k)(-i\sqrt{2}g_{\pi N}) \right] D_F^N(p_s) \\
&\times (-ie)(p + p_s)^\mu.
\end{aligned} \tag{F.5}$$

The second self energy diagram due the exchange of a neutral pion is

$$\begin{aligned}
i\mathcal{M}^{(1d)\mu} &= (-i\sqrt{2}g_{\pi N})D_F^N(p_s) \left[\int \frac{d^4k}{(2\pi)^4} (-ig_{\pi N})D_F^N(k)D_F^\pi(p_s - k)(-ig_{\pi N}) \right] D_F^N(p_s) \\
&\times (-ie)(p + p_s)^\mu.
\end{aligned} \tag{F.6}$$

The strong vertex loop correction is

$$\begin{aligned}
i\mathcal{M}^{(1e)\mu} &= \left[\int \frac{d^4k}{(2\pi)^4} (-ig_{\pi N})D_F^N(p_s - k)S_N^N(p' - k)(-ig_{\pi N})D_F^\pi(k) \right] (-i\sqrt{2}g_{\pi N})D_F^N(p_s) \\
&\times (-ie)(p + p_s)^\mu.
\end{aligned} \tag{F.7}$$

The pion electromagnetic vertex correction is

$$\begin{aligned}
i\mathcal{M}^{(1f)\mu} &= (-i\sqrt{2}g_{\pi N})D_F^\pi(p_t) \\
&\times \left[\int \frac{d^4k}{(2\pi)^2} (-i\sqrt{2}g_{\pi N})D_F^N(p_t - k)(-ie)(p_t + p_\pi - 2k)^\mu \right. \\
&\left. \times D_F^N(p_\pi - k)(-i\sqrt{2}g_{\pi N})D_F^N(k) \right].
\end{aligned} \tag{F.8}$$

The pion self energy diagram is

$$i\mathcal{M}^{(1g)\mu} = (-i\sqrt{2}g_{\pi N})D_F^\pi(p_t) \left[\int \frac{d^4k}{(2\pi)^4} (-i\sqrt{2}g_{\pi N})D_F^N(k)(-i\sqrt{2}g_{\pi N})D_F^N(p_t - k) \right] D_F^\pi(p_t) (-ie)(p_t + p_\pi)^\mu. \quad (\text{F.9})$$

The strong vertex loop correction is

$$i\mathcal{M}^{(1h)\mu} = \left[\int \frac{d^4k}{(2\pi)^4} (-ig_{\pi N})D_F^N(p' - k)D_F^N(p - k)(-ig_{\pi N})D_F^\pi(k) \right]. \quad (\text{F.10})$$

At tree-level, there are no u -channel diagrams, since the neutron is neutral. However, quantum corrections modify the tree-level result. There are two corrections to the electromagnetic vertex:

$$i\mathcal{M}^{(i)\mu} = (-ie) \left[\int \frac{d^4k}{(2\pi)^4} (-i\sqrt{2}g_{\pi N})D_F^N(p - k)(p_u + p' - 2k)^\mu D_F^N(p_u - k)(-i\sqrt{2}g_{\pi N})D_F^\pi(k) \right] \times D_F^N(p_u)(-i\sqrt{2}g_{\pi N}), \quad (\text{F.11})$$

and

$$i\mathcal{M}^{(j)\mu} = -(-ie) \left[\int \frac{d^4k}{(2\pi)^4} (-i\sqrt{2}g_{\pi N})D_F^\pi(p - k)(p_u + p' - 2k)^\mu D_F^\pi(p_u - k)(-i\sqrt{2}g_{\pi N})D_F^N(k) \right] \times D_F^N(p_u)(-i\sqrt{2}g_{\pi N}). \quad (\text{F.12})$$

Note that these come in with the opposite sign. Since we choose $m'_\pi = 0.7$ GeV and $m'_N = 0.71$ GeV, these two terms have approximately the same magnitude, but opposite sign. Thus the neutron's effect on the cross section is negligible. The box diagram is

$$i\mathcal{M}^{(1k)\mu} = \int \frac{d^4k}{(2\pi)^2} (-ig_{\pi N})D_F^N(p + q - p_\pi - k)(-i\sqrt{2}g_{\pi N})D_F^N(p + q - k)(-ie)(2p + q - 2k)^\mu \times D_F^N(p - k)(-ig_{\pi N})D_F^\pi(k). \quad (\text{F.13})$$

G

Loop Diagrams for Fermionic Pion Electroproduction

We use the Feynman Rules outlined in Appendix B for the pseudoscalar (PS) interaction. We note that

G.1 s -Channel Electromagnetic Vertex

We define the proton's electromagnetic vertex as

$$\Gamma_p^\mu(p, q, p_s) = \gamma^\mu + \delta\Gamma_p^\mu(p, q, p_s), \quad (\text{G.1})$$

where γ^μ is the contribution from the tree level diagram, and δ_e is the proton charge counter term. There are two diagrams which contribute to the vertex function. We write

$$\delta\Gamma_p^\mu(p, q, p_s) = \delta\Gamma_{p,a}^\mu(p, q, p_s) + \delta\Gamma_{p,b}^\mu(p, q, p_s), \quad (\text{G.2})$$

where the individual contributions are

$$\delta\Gamma_{p,a}^\mu(p, q, p_s) = \int \frac{d^4k}{(2\pi)^4} g_{\pi N} \gamma_5 S_F(k + p_s) \gamma^\mu S_F(k + p) g_{\pi N} \gamma_5 D_F(k), \quad (\text{G.3})$$

$$\delta\Gamma_{p,b}^\mu(p, q, p_s) = \int \frac{d^4k}{(2\pi)^4} \sqrt{2} g_{\pi N} \gamma_5 S_F(k + p_s) \gamma^\mu S_F(k + p) \sqrt{2} g_{\pi N} \gamma_5 D_F(k). \quad (\text{G.4})$$

G.2 s -Channel Self Energy

We obtain two self energy corrections; the first from the emission of a neutron pion and the second from the emission of a positive pion. These two terms only differ by a simple isospin factor. Thus we may sum these two terms to obtain

$$\begin{aligned}
-i\Sigma_N(p_s) &= \int \frac{d^4k}{(2\pi)^4} \sqrt{2}g_{\pi N}\gamma_5 S_F(k+p_s)\sqrt{2}g_{\pi N}\gamma_5 D_F(k) \\
&\quad + \int \frac{d^4k}{(2\pi)^4} g_{\pi N}\gamma_5 S_F(k+p_s)g_{\pi N}\gamma_5 D_F(k).
\end{aligned} \tag{G.5}$$

We emphasize that by explicitly factorizing a factor of $-i$ in the definition of the self energy, a positive value of $\Sigma(p_s)$ corresponds to a positive mass correction.

G.3 s -Channel Strong Vertex

We define the s -channel strong vertex as

$$\Gamma_5(p_s, p_\pi, p') = \gamma_5 + \delta\Gamma_5(p_s, p_\pi, p'), \tag{G.6}$$

where we define

$$\delta\Gamma_{\pi N}(p_s, p_\pi, p') = \int \frac{d^4k}{(2\pi)^4} g_{\pi N} S_F(k+p_s-p_\pi)\sqrt{2}g_{\pi N}\gamma_5 S_F(k+p_s)g_{\pi N}\gamma_5 D_F(k). \tag{G.7}$$

G.4 t -Channel Electromagnetic Vertex

We define the t -channel electromagnetic vertex as

$$\Gamma_\pi^\mu(p_t, q, p_\pi) = (p_t + p_\pi)^\mu + \delta\Gamma_\pi^\mu(p_t, q, p_\pi), \tag{G.8}$$

where we define

$$\delta\Gamma_\pi^\mu(p_t, q, p_\pi) = \int \frac{d^4k}{(2\pi)^4} (-1) \text{Tr} \left[\sqrt{2}g_{\pi N}\gamma_5 S_F(k+p_t+q)\gamma^\mu S_F(k+p_t)\sqrt{2}g_{\pi N}\gamma_5 S_F(k) \right]. \tag{G.9}$$

G.5 t -Channel Self Energy

The pion self energy is given by a single diagram:

$$-i\Sigma(p_t) = \int \frac{d^4k}{(2\pi)^4} (-1) \text{Tr} \left[\sqrt{2}g_{\pi N}\gamma_5 S_F(k+p_t)\sqrt{2}g_{\pi N}\gamma_5 S_F(k) \right]. \tag{G.10}$$

G.6 t -Channel Strong Vertex

We define the t -channel Strong Vertex as

$$\Gamma_5(p, p_t, p') = \gamma_5 + \delta\Gamma_5(p, p_t, p'), \quad (\text{G.11})$$

where $\delta\Gamma_5(p, p_t, p')$ is given by

$$\delta\Gamma_5(p, p_t, p') = \int \frac{d^4k}{(2\pi)^4} g_{\pi N} \gamma_5 S_F(k + p - p_t) \sqrt{2} g_{\pi N} \gamma_5 S_F(k + p) g_{\pi N} \gamma_5 D_F(k). \quad (\text{G.12})$$

G.7 u -Channel Electromagnetic Vertex

We define the u -channel electroamgnetic vertex as

$$\Gamma_n^\mu(p, q, p_s) = 0 + \delta\Gamma_n^\mu(p, q, p_s), \quad (\text{G.13})$$

where the factor of 0 arises because the neutron is neutral at tree level; the non-trivial form factor arises purely from the one-loop contributions. There are two contributions at one-loop order:

$$\delta\Gamma_n^\mu(p, q, p_s) = \delta\Gamma_{n,a}^\mu(p, q, p_s) + \delta\Gamma_{n,b}^\mu(p, q, p_s), \quad (\text{G.14})$$

which are given by

$$\delta\Gamma_{n,a}^\mu(p, q, p_s) = \int \frac{d^4k}{(2\pi)^4} \sqrt{2} g_{\pi N} \gamma_5 S_F(k + p_s) \gamma^\mu S_F(k + p) \sqrt{2} g_{\pi N} \gamma_5 D_F(k), \quad (\text{G.15})$$

$$\delta\Gamma_{n,b}^\mu(p, q, p_s) = \int \frac{d^4k}{(2\pi)^4} \sqrt{2} g_{\pi N} \gamma_5 S_F(k + p_s) \gamma^\mu S_F(k + p) \sqrt{2} g_{\pi N} \gamma_5 D_F(k). \quad (\text{G.16})$$

G.8 Box Diagram

We have a single box diagram contribution, given by

$$D(p) = \int \frac{d^4k}{(2\pi)^4} g_{\pi N} \gamma_5 S_F(k + p + q - p_\pi) \sqrt{2} g_{\pi N} \gamma_5 S_F(k + p + q) \gamma^\mu S_F(k + p) g_{\pi N} \gamma_5 D_F(k). \quad (\text{G.17})$$

Bibliography

- [1] H. Yukawa, *On the interaction of elementary particles. I*, Proceedings of the Physico-Mathematical Society of Japan. 3rd Series **17**, 48 (1935).
- [2] *The Nobel Prize in Physics 1949*, nobelprize.org. Nobel Media AB 2014., URL http://www.nobelprize.org/nobel_prizes/physics/laureates/1949/.
- [3] A. W. Thomas, in *Advances in Nuclear Physics* (Springer Science + Business Media, 1984), pp. 1–137.
- [4] S. Scherer and M. R. Schindler, *A Chiral Perturbation Theory Primer* (2005), [hep-ph/0505265](https://arxiv.org/abs/hep-ph/0505265).
- [5] B. Kubis, in *Workshop on Physics and Astrophysics of Hadrons and Hadronic Matter Shantiniketan, India, November 6-10, 2006* (2007), [hep-ph/0703274](https://arxiv.org/abs/hep-ph/0703274).
- [6] P. A. M. Dirac, *The Quantum theory of Emission and Absorption of Radiation*, Proc. Roy. Soc. Lond. **A114**, 243 (1927).
- [7] H. A. Bethe, *The Electromagnetic Shift of Energy Levels*, Phys. Rev. **72**, 339 (1947).
- [8] J. S. Schwinger, *Quantum Electrodynamics. I. A Covariant Formulation*, Phys. Rev. **74**, 1439 (1948).
- [9] J. S. Schwinger, *Quantum electrodynamics. II. Vacuum Polarization and Self-Energy*, Phys. Rev. **75**, 651 (1948).
- [10] J. S. Schwinger, *Quantum electrodynamics. III: The Electromagnetic Properties of the Electron – Radiative Corrections to Scattering*, Phys. Rev. **76**, 790 (1949).
- [11] R. P. Feynman, *Relativistic Cut-Off for Quantum Electrodynamics*, Phys. Rev. **74**, 1430 (1948).
- [12] R. P. Feynman, *Space-Time Approach to Non-Relativistic Quantum Mechanics*, Rev. Mod. Phys. **20**, 367 (1948).
- [13] S. Tomonaga, *On a Relativistically Invariant Formulation of the Quantum Theory of Wave Fields*, Prog. Theor. Phys. **1**, 27 (1946).
- [14] Z. Koba, T. Tati, and S. I. Tomonaga, *On a Relativistically Invariant Formulation of the Quantum Theory of Wave Fields. II: Case of Interacting Electromagnetic and Electron Fields*, Prog. Theor. Phys. **2**, 101 (1947).

-
- [15] S. I. Tomonaga, *On the Effect of the Field Reactions on the Interaction of Mesotrons and Nuclear Particles. III*, Prog. Theor. Phys. **2**, 6 (1949).
- [16] S. I. Tomonaga, *On the Effect of the Field Reactions on the Interaction of Mesotrons and Nuclear Particles. IV*, Prog. Theor. Phys. **2**, 63 (1949).
- [17] S. I. Tomonaga and J. R. Oppenheimer, *On Infinite Field Reactions in Quantum Field Theory*, Phys. Rev. **74**, 224 (1948).
- [18] F. J. Dyson, *The Radiation theories of Tomonaga, Schwinger, and Feynman*, Phys. Rev. **75**, 486 (1949).
- [19] F. J. Dyson, *The S Matrix in Quantum Electrodynamics*, Phys. Rev. **75**, 1736 (1949).
- [20] C. N. Yang and R. L. Mills, *Conservation of Isotopic Spin and Isotopic Gauge Invariance*, Phys. Rev. **96**, 191 (1954).
- [21] T. Nakano and K. Nishijima, *Charge Independence for V-particles*, Prog. Theor. Phys. **10**, 581 (1953).
- [22] M. Gell-Mann, *The Interpretation of the New Particles as Displaced Charge Multiplets*, Nuovo Cim. **4**, 848 (1956).
- [23] S. Sakata, *On a Composite Model for the New Particles*, Prog. Theor. Phys. **16**, 686 (1956).
- [24] Y. Ne'eman, *Derivation of Strong Interactions from a Gauge Invariance*, Nucl. Phys. **26**, 222 (1961).
- [25] M. Gell-Mann, *Symmetries of Baryons and Mesons*, Phys. Rev. **125**, 1067 (1962).
- [26] M. Gell-Mann, in *Proceedings of the International Conference on High-Energy Physics*, edited by J. Prentki (CERN, Geneva, 1962).
- [27] V. E. Barnes et al., *Observation of a Hyperon with Strangeness -3*, Phys. Rev. Lett. **12**, 204 (1964).
- [28] G. Zweig, in *Developments in the Quark Theory of Hadrons. Vol. 1. 1964 - 1978*, edited by D. Lichtenberg and S. P. Rosen (1964), pp. 22–101.
- [29] M. Gell-Mann, *A Schematic Model of Baryons and Mesons*, Phys. Lett. **8**, 214 (1964).
- [30] J. D. Bjorken, *Asymptotic Sum Rules at Infinite Momentum*, Phys. Rev. **179**, 1547 (1969).
- [31] G. Miller et al., *Inelastic Electron-Proton Scattering at Large Momentum Transfers and the Inelastic Structure Functions of the Proton*, Phys. Rev. **D5**, 528 (1972).
- [32] R. P. Feynman, *Very High-Energy Collisions of Hadrons*, Phys. Rev. Lett. **23**, 1415 (1969).
- [33] J. D. Bjorken and E. A. Paschos, *Inelastic Electron-Proton and γ -Proton Scattering, and the Structure of the Nucleon*, Phys. Rev. **185**, 1975 (1969).

- [34] H. Fritzsch and M. Gell-Mann, *Current Algebra: Quarks and What Else?*, eConf **C720906V2**, 135 (1972), [hep-ph/0208010](https://arxiv.org/abs/hep-ph/0208010).
- [35] A. W. Thomas and W. Weise, *The Structure of the Nucleon* (Wiley-Blackwell, 2001).
- [36] D. J. Gross and F. Wilczek, *Ultraviolet Behavior of Nonabelian Gauge Theories*, Phys. Rev. Lett. **30**, 1343 (1973).
- [37] H. D. Politzer, *Reliable Perturbative Results for Strong Interactions?*, Phys. Rev. Lett. **30**, 1346 (1973).
- [38] *The Nobel Prize in Physics 2004*, nobelPrize.org. Nobel Media AB 2019., URL <https://www.nobelprize.org/prizes/physics/2004/summary/>.
- [39] S. Weinberg, *Implications of Dynamical Symmetry Breaking*, Phys. Rev. **D13**, 974 (1976), [Addendum: Phys. Rev. **D19**, 1277 (1979)].
- [40] E. Farhi and L. Susskind, *A Technicolored G.U.T.*, Phys. Rev. **D20**, 3404 (1979).
- [41] M. E. Peskin and D. V. Schroeder, *An Introduction to quantum field theory* (Addison-Wesley, Reading, USA, 1995), ISBN 9780201503975, 0201503972.
- [42] L. D. Landau, A. A. Abrikosov, and I. M. Khalatnikov, *The Electron Mass In Quantum Electrodynamics* (1954).
- [43] M. Tanabashi et al. (Particle Data Group), *Review of Particle Physics*, Phys. Rev. **D98**, 030001 (2018).
- [44] D. Binosi, C. Mezrag, J. Papavassiliou, C. D. Roberts, and J. Rodriguez-Quintero, *Process-independent strong running coupling*, Phys. Rev. **D96**, 054026 (2017), [1612.04835](https://arxiv.org/abs/1612.04835).
- [45] S. J. Brodsky, G. F. de Teramond, and A. Deur, *Nonperturbative QCD Coupling and its β -function from Light-Front Holography*, Phys. Rev. **D81**, 096010 (2010), [1002.3948](https://arxiv.org/abs/1002.3948).
- [46] S. Necco and R. Sommer, *The $N(f) = 0$ heavy quark potential from short to intermediate distances*, Nucl. Phys. **B622**, 328 (2002), [hep-lat/0108008](https://arxiv.org/abs/hep-lat/0108008).
- [47] D. Trewartha, W. Kamleh, and D. Leinweber, *Evidence that centre vortices underpin dynamical chiral symmetry breaking in $SU(3)$ gauge theory*, Phys. Lett. **B747**, 373 (2015), [1502.06753](https://arxiv.org/abs/1502.06753).
- [48] J. C. Biddle, W. Kamleh, and D. B. Leinweber, *Gluon propagator on a center-vortex background*, Phys. Rev. **D98**, 094504 (2018), [1806.04305](https://arxiv.org/abs/1806.04305).
- [49] T. Blum, P. A. Boyle, V. Gülpers, T. Izubuchi, L. Jin, C. Jung, A. Jüttner, C. Lehner, A. Portelli, and J. T. Tsang (RBC, UKQCD), *Calculation of the Hadronic Vacuum Polarization Contribution to the Muon Anomalous Magnetic Moment*, Phys. Rev. Lett. **121**, 022003 (2018), [1801.07224](https://arxiv.org/abs/1801.07224).
- [50] A. Westin et al. (CSSM/QCDSF/UKQCD), in *36th International Symposium on Lattice Field Theory (Lattice 2018) East Lansing, MI, United States, July 22-28, 2018* (2019), [1902.01518](https://arxiv.org/abs/1902.01518).

- [51] S. Hollitt et al., in *36th International Symposium on Lattice Field Theory (Lattice 2018) East Lansing, MI, United States, July 22-28, 2018* (2018), [1811.06677](#).
- [52] T. Appelquist et al. (Lattice Strong Dynamics), *Nonperturbative investigations of $SU(3)$ gauge theory with eight dynamical flavors*, Phys. Rev. **D99**, 014509 (2019), [1807.08411](#).
- [53] K. K. Cushman and G. T. Fleming, in *36th International Symposium on Lattice Field Theory (Lattice 2018) East Lansing, MI, United States, July 22-28, 2018* (2019), [1902.10695](#).
- [54] S.-X. Qin, C. D. Roberts, and S. M. Schmidt, *Spectrum of Light- and Heavy-Baryons*, Few Body Syst. **60**, 26 (2019), [1902.00026](#).
- [55] P. Maris and P. C. Tandy, *The π , K^+ , and K^0 electromagnetic form-factors*, Phys. Rev. **C62**, 055204 (2000), [nucl-th/0005015](#).
- [56] S.-X. Qin, C. Chen, C. Mezrag, and C. D. Roberts, *Off-shell persistence of composite pions and kaons*, Phys. Rev. **C97**, 015203 (2018), [1702.06100](#).
- [57] C. D. Roberts, *Strong QCD and Dyson-Schwinger Equations*, IRMA Lect. Math. Theor. Phys. **21**, 355 (2015), [1203.5341](#).
- [58] C. Patrignani et al. (Particle Data Group), *Review of Particle Physics*, Chin. Phys. **C40**, 100001 (2016).
- [59] H. Pagels, *Departures from Chiral Symmetry: A Review*, Phys. Rept. **16**, 219 (1975).
- [60] P. C. Hohenberg, *Existence of Long-Range Order in One and Two Dimensions*, Phys. Rev. **158**, 383 (1967).
- [61] N. D. Mermin and H. Wagner, *Absence of Ferromagnetism or Antiferromagnetism in One- or Two-Dimensional Isotropic Heisenberg Models*, Phys. Rev. Lett. **17**, 1133 (1966).
- [62] S. R. Coleman, *There are no Goldstone Bosons in Two Dimensions*, Commun. Math. Phys. **31**, 259 (1973).
- [63] G. S. Guralnik, C. R. Hagen, and T. W. B. Kibble, *Broken Symmetries and the Goldstone Theorem*, Adv. Part. Phys. **2**, 567 (1968).
- [64] R. F. Streater, *Spontaneous Breakdown of Symmetry in Axiomatic Theory*, Proc. Roy. Soc. Lond. **A287**, 510 (1965).
- [65] D. Kastler, D. W. Robinson, and A. Swieca, *Conserved Currents and Associated Symmetries; Goldstone's Theorem*, Commun. Math. Phys. **2**, 108 (1966).
- [66] M. Gell-Mann and M. Levy, *The Axial Vector Current in Beta Decay*, Nuovo Cim. **16**, 705 (1960).
- [67] S. Weinberg, *Phenomenological Lagrangians*, Physica **A96**, 327 (1979).
- [68] R. Haag, *Quantum Field Theories with Composite Particles and Asymptotic Conditions*, Phys. Rev. **112**, 669 (1958).
- [69] S. Weinberg, *Dynamical Approach to Current Algebra*, Phys. Rev. Lett. **18**, 188 (1967).

- [70] R. Frisch and O. Stern, *Über die magnetische Ablenkung von Wasserstoffmolekülen und das magnetische Moment des Protons. I*, Zeitschrift für Physik **85**, 4 (1933), ISSN 0044-3328.
- [71] I. Estermann and O. Stern, *Über die magnetische Ablenkung von Wasserstoffmolekülen und das magnetische Moment des Protons. II*, Zeitschrift für Physik **85**, 17 (1933), ISSN 0044-3328.
- [72] R. Hofstadter, H. R. Fechter, and J. A. McIntyre, *High-Energy Electron Scattering and Nuclear Structure Determinations*, Phys. Rev. **92**, 978 (1953).
- [73] R. Hofstadter, *Electron Scattering and Nuclear Structure*, Rev. Mod. Phys. **28**, 214 (1956).
- [74] R. Hofstadter, F. Bumiller, and M. R. Yearian, *Electromagnetic Structure of the Proton and Neutron*, Rev. Mod. Phys. **30**, 482 (1958).
- [75] A. W. Thomas and W. Weise, *The Structure of the Nucleon* (Wiley, Germany, 2001), ISBN 9783527402977, 9783527603145.
- [76] J. Arrington, W. Melnitchouk, and J. A. Tjon, *Global analysis of proton elastic form factor data with two-photon exchange corrections*, Phys. Rev. **C76**, 035205 (2007), [0707.1861](#).
- [77] R. Schiavilla and I. Sick, *Neutron charge form-factor at large q^2* , Phys. Rev. **C64**, 041002 (2001), [nucl-ex/0107004](#).
- [78] H. Zhu et al. (E93026), *Measurement of the Electric Form-Factor of the Neutron through $\vec{d}(\vec{e}, e'n)p$ at $Q^2 = 0.5$ (GeV/c)²*, Phys. Rev. Lett. **87**, 081801 (2001), [nucl-ex/0105001](#).
- [79] J. Bermuth et al., *The Neutron charge form-factor and target analyzing powers from ${}^3\vec{H}e(\vec{e}, e'n)$ scattering*, Phys. Lett. **B564**, 199 (2003), [nucl-ex/0303015](#).
- [80] R. Madey et al. (E93-038), *Measurements of G_E^n/G_M^n from the ${}^2H(\vec{e}, e'\vec{n}){}^1H$ Reaction to $Q^2 = 1.45$ (GeV/c)²*, Phys. Rev. Lett. **91**, 122002 (2003), [nucl-ex/0308007](#).
- [81] G. Warren et al. (Jefferson Lab E93-026), *Measurement of the Electric Form Factor of the Neutron at $Q^2 = 0.5$ and 1.0 GeV^2/c^2* , Phys. Rev. Lett. **92**, 042301 (2004), [nucl-ex/0308021](#).
- [82] D. I. Glazier et al., *Measurement of the electric form factor of the neutron at $Q^2 = 0.3 - 0.8$ (GeV/c)²*, Eur. Phys. J. **A24**, 101 (2005), [nucl-ex/0410026](#).
- [83] E. Geis et al. (BLAST), *The Charge Form Factor of the Neutron at Low Momentum Transfer from the ${}^2\vec{H}(\vec{e}, e'n){}^1H$ Reaction*, Phys. Rev. Lett. **101**, 042501 (2008), [0803.3827](#).
- [84] S. Riordan et al., *Measurements of the Electric Form Factor of the Neutron up to $Q^2 = 3.4$ GeV^2 using the Reaction ${}^3\vec{H}e(\vec{e}, e'n)pp$* , Phys. Rev. Lett. **105**, 262302 (2010), [1008.1738](#).

- [85] B. S. Schlimme et al., *Measurement of the Neutron Electric to Magnetic Form Factor Ratio at $Q^2 = 1.58 \text{ GeV}^2$ Using the Reaction ${}^3\vec{H}e(\vec{e}, e'n)pp$* , Phys. Rev. Lett. **111**, 132504 (2013), [1307.7361](#).
- [86] S. Rock, R. G. Arnold, P. E. Bosted, B. T. Chertok, B. A. Mecking, I. A. Schmidt, Z. M. Szalata, R. York, and R. Zdarko, *Measurement of Elastic Electron-Neutron Cross Sections up to $Q^2 = 10 \text{ (GeV/c)}^2$* , Phys. Rev. Lett. **49**, 1139 (1982).
- [87] A. Lung et al., *Measurements of the Electric and Magnetic Form Factors of the Neutron from $Q^2 = 1.75$ to 4.00 (GeV/c)^2* , Phys. Rev. Lett. **70**, 718 (1993).
- [88] H. Gao et al., *Measurement of the neutron magnetic form-factor from inclusive quasielastic scattering of polarized electrons from polarized ${}^3\text{He}$* , Phys. Rev. **C50**, R546 (1994).
- [89] H. Anklin et al., *Precise measurements of the neutron magnetic form factor*, Phys. Lett. **B428**, 248 (1998).
- [90] G. Kubon et al., *Precise neutron magnetic form factors*, Phys. Lett. **B524**, 26 (2002), [nucl-ex/0107016](#).
- [91] B. Anderson et al. (Jefferson Lab E95-001), *Extraction of the neutron magnetic form-factor from quasi-elastic ${}^3\vec{H}e(\vec{e}, e')$ at $Q^2 = 0.1 - 0.6 \text{ (GeV/c)}^2$* , Phys. Rev. **C75**, 034003 (2007), [nucl-ex/0605006](#).
- [92] J. Lachniet et al. (CLAS), *Precise Measurement of the Neutron Magnetic Form Factor G_M^n in the Few- GeV^2 Region*, Phys. Rev. Lett. **102**, 192001 (2009), [0811.1716](#).
- [93] J. J. Kelly, *Simple parametrization of nucleon form factors*, Phys. Rev. **C70**, 068202 (2004).
- [94] S. Malov et al., *Polarization transfer in the ${}^{16}\text{O}(\vec{e}, e'\vec{p}){}^{15}\text{N}$ reaction*, Phys. Rev. **C62**, 057302 (2000).
- [95] K. A. Olive et al. (Particle Data Group), *Review of Particle Physics*, Chin. Phys. **C38**, 090001 (2014).
- [96] S. R. Amendolia et al. (NA7), *A Measurement of the Space-Like Pion Electromagnetic Form Factor*, Nucl. Phys. **B277**, 168 (1986).
- [97] G. M. Huber et al. (Jefferson Lab), *Charged pion form-factor between $Q^2 = 0.60$ and 2.45 GeV^2 . II. Determination of, and results for, the pion form factor*, Phys. Rev. **C78**, 045203 (2008), [0809.3052](#).
- [98] K. Nishijima, *Time-Ordered Green's Functions and Electromagnetic Interactions*, Phys. Rev. **122**, 298 (1961).
- [99] R. J. Perry, A. W. Thomas, and M. E. Carrillo-Serrano, *Chiral Corrections to Nucleon Electromagnetic Form Factors Calculated in the NJL Model*, PoS **INPC2016**, 257 (2017).
- [100] R. J. Perry, M. E. Carrillo-Serrano, and A. W. Thomas, *Chiral Corrections to Baryon Electromagnetic Form Factors*, Few Body Syst. **59**, 127 (2018), [1703.01032](#).

- [101] Y. Nambu and G. Jona-Lasinio, *Dynamical Model of Elementary Particles Based on an Analogy with Superconductivity. I*, Phys. Rev. **122**, 345 (1961).
- [102] Y. Nambu and G. Jona-Lasinio, *Dynamical Model of Elementary Particles Based on an Analogy with Superconductivity. II*, Phys. Rev. **124**, 246 (1961).
- [103] N. Isgur, G. Karl, and J. Soffer, *Zeros in the Nucleon Form-factors and the Quark Model*, Phys. Rev. **D35**, 1665 (1987).
- [104] T. Melde, K. Berger, L. Canton, W. Plessas, and R. F. Wagenbrunn, *Electromagnetic nucleon form factors in instant and point form*, Phys. Rev. **D76**, 074020 (2007).
- [105] A. Chodos, R. L. Jaffe, K. Johnson, and C. B. Thorn, *Baryon Structure in the Bag Theory*, Phys. Rev. **D10**, 2599 (1974).
- [106] I. C. Cloët, C. D. Roberts, and A. W. Thomas, *Revealing dressed-quarks via the proton's charge distribution*, Phys. Rev. Lett. **111**, 101803 (2013), [1304.0855](#).
- [107] N. Ishii, W. Bentz, and K. Yazaki, *Faddeev approach to the nucleon in the Nambu-Jona-Lasinio (NJL) model*, Phys. Lett. **B301**, 165 (1993).
- [108] O. Schroeder, H. Reinhardt, and H. Weigel, *Nucleon structure functions in the three flavor NJL soliton model*, Nucl. Phys. **A651**, 174 (1999), [hep-ph/9902322](#).
- [109] I. C. Cloët, W. Bentz, and A. W. Thomas, *Role of diquark correlations and the pion cloud in nucleon elastic form factors*, Phys. Rev. **C90**, 045202 (2014), [1405.5542](#).
- [110] M. E. Carrillo-Serrano, W. Bentz, I. C. Cloët, and A. W. Thomas, *Baryon Octet Electromagnetic Form Factors in a confining NJL model*, Phys. Lett. **B759**, 178 (2016), [1603.02741](#).
- [111] D. Ebert, T. Feldmann, and H. Reinhardt, *Extended NJL model for light and heavy mesons without q - anti- q thresholds*, Phys. Lett. **B388**, 154 (1996), [hep-ph/9608223](#).
- [112] S. P. Klevansky, *The Nambu-Jona-Lasinio model of quantum chromodynamics*, Rev. Mod. Phys. **64**, 649 (1992).
- [113] A. L. Fetter, J. D. Walecka, and L. P. Kadanoff, *Quantum Theory of Many Particle Systems*, Physics Today **25**, 54 (1972).
- [114] V. Pascalutsa and M. Vanderhaeghen, *The Nucleon and delta-resonance masses in relativistic chiral effective-field theory*, Phys. Lett. **B636**, 31 (2006), [hep-ph/0511261](#).
- [115] A. W. Thomas and G. Krein, *Chiral aspects of hadron structure*, Phys. Lett. **B481**, 21 (2000), [nucl-th/0004008](#).
- [116] S. Weinberg, *Pion Scattering Lengths*, Phys. Rev. Lett. **17**, 616 (1966).
- [117] A. Manohar and H. Georgi, *Chiral Quarks and the Nonrelativistic Quark Model*, Nucl. Phys. **B234**, 189 (1984).
- [118] N. Iwamoto, *Pseudoscalar Versus Pseudovector Pion - Nucleon Couplings in the Nucleonic Axion Bremsstrahlung Rate of Neutron Star Matter*, Phys. Rev. **D39**, 2120 (1989).

- [119] P. E. Shanahan, Ph.D. thesis, U. Adelaide, Dept. Phys. Math. Phys. (2015).
- [120] G. A. Miller, *Light front cloudy bag model: Nucleon electromagnetic form-factors*, Phys. Rev. **C66**, 032201 (2002), [nucl-th/0207007](#).
- [121] H. H. Matevosyan, G. A. Miller, and A. W. Thomas, *Comparison of nucleon form factors from lattice QCD against the light front cloudy bag model and extrapolation to the physical mass regime*, Phys. Rev. **C71**, 055204 (2005), [nucl-th/0501044](#).
- [122] C.-R. Ji, W. Melnitchouk, and A. W. Thomas, *Equivalence of pion loops in equal-time and light-front dynamics*, Phys. Rev. **D80**, 054018 (2009), [0906.3497](#).
- [123] M. Alberg and G. A. Miller, *Taming the Pion Cloud of the Nucleon*, Phys. Rev. Lett. **108**, 172001 (2012), [1201.4184](#).
- [124] J. R. McKenney, N. Sato, W. Melnitchouk, and C.-R. Ji, *Pion structure function from leading neutron electroproduction and SU(2) flavor asymmetry*, Phys. Rev. **D93**, 054011 (2016), [1512.04459](#).
- [125] A. W. Thomas, *A Limit on the Pion Component of the Nucleon Through SU(3) Flavor Breaking in the Sea*, Phys. Lett. **B126**, 97 (1983).
- [126] W. Melnitchouk, J. Speth, and A. W. Thomas, *Dynamics of light anti-quarks in the proton*, Phys. Rev. **D59**, 014033 (1998), [hep-ph/9806255](#).
- [127] R. D. Young, D. B. Leinweber, and A. W. Thomas, *Convergence of chiral effective field theory*, Prog. Part. Nucl. Phys. **50**, 399 (2003), [hep-lat/0212031](#).
- [128] A. W. Thomas, S. Theberge, and G. A. Miller, *The Cloudy Bag Model of the Nucleon*, Phys. Rev. **D24**, 216 (1981).
- [129] M. B. Hecht, M. Oettel, C. D. Roberts, S. M. Schmidt, P. C. Tandy, and A. W. Thomas, *Nucleon mass and pion loops*, Phys. Rev. **C65**, 055204 (2002), [nucl-th/0201084](#).
- [130] R. D. Young, D. B. Leinweber, A. W. Thomas, and S. V. Wright, *Chiral analysis of quenched baryon masses*, Phys. Rev. **D66**, 094507 (2002), [hep-lat/0205017](#).
- [131] P. E. Shanahan, A. W. Thomas, R. D. Young, J. M. Zanotti, R. Horsley, Y. Nakamura, D. Pleiter, P. E. L. Rakow, G. Schierholz, and H. Stüben, *Electric form factors of the octet baryons from lattice QCD and chiral extrapolation*, Phys. Rev. **D90**, 034502 (2014), [1403.1965](#).
- [132] P. E. Shanahan, A. W. Thomas, R. D. Young, J. M. Zanotti, R. Horsley, Y. Nakamura, D. Pleiter, P. E. L. Rakow, G. Schierholz, and H. Stüben (QCDSF/UKQCD, CSSM), *Magnetic form factors of the octet baryons from lattice QCD and chiral extrapolation*, Phys. Rev. **D89**, 074511 (2014), [1401.5862](#).
- [133] J. J. de Swart, *The Octet model and its Clebsch-Gordan coefficients*, Rev. Mod. Phys. **35**, 916 (1963), [Erratum: Rev. Mod. Phys. **37**, 326 (1965)].
- [134] H. P. Blok et al. (Jefferson Lab), *Charged pion form factor between $Q^2=0.60$ and 2.45 GeV². I. Measurements of the cross section for the $^1H(e, e'\pi^+)n$ reaction*, Phys. Rev. **C78**, 045202 (2008), [0809.3161](#).

- [135] R. J. Perry, A. Kızılersü, and A. W. Thomas, *Model Dependence of the Pion Form Factor Extracted from Pion Electro-production* (2018), [1811.09356](#).
- [136] G. R. Farrar and D. R. Jackson, *The Pion Form-Factor*, Phys. Rev. Lett. **43**, 246 (1979).
- [137] G. P. Lepage and S. J. Brodsky, *Exclusive Processes in Quantum Chromodynamics: Evolution Equations for Hadronic Wave Functions and the Form-Factors of Mesons*, Phys. Lett. **87B**, 359 (1979).
- [138] G. P. Lepage and S. J. Brodsky, *Exclusive Processes in Perturbative Quantum Chromodynamics*, Phys. Rev. **D22**, 2157 (1980).
- [139] L. Chang, I. C. Cloët, C. D. Roberts, S. M. Schmidt, and P. C. Tandy, *Pion electromagnetic form factor at spacelike momenta*, Phys. Rev. Lett. **111**, 141802 (2013), [1307.0026](#).
- [140] E. B. Dally et al., *Measurement of the π^- Form factor*, Phys. Rev. **D24**, 1718 (1981).
- [141] E. B. Dally et al., *Elastic Scattering Measurement of the Negative Pion Radius*, Phys. Rev. Lett. **48**, 375 (1982).
- [142] S. R. Amendolia et al., *Measurement of the Pion Form Factor in the Time-Like Region for q^2 Values Between 0.1 $(\text{GeV}/c)^2$ and 0.18 $(\text{GeV}/c)^2$* , Phys. Lett. **138B**, 454 (1984).
- [143] T. Horn and C. D. Roberts, *The pion: an enigma within the Standard Model*, J. Phys. **G43**, 073001 (2016), [1602.04016](#).
- [144] W. R. Frazer, *Proposal for Determining the Electromagnetic Form Factor of the Pion*, Phys. Rev. **115**, 1763 (1959).
- [145] M. M. Kaskulov, K. Gallmeister, and U. Mosel, *Deeply inelastic pions in the exclusive reaction $p(e, e'\pi^+)n$ above the resonance region*, Phys. Rev. **D78**, 114022 (2008), [0804.1834](#).
- [146] M. Guidal, J. M. Laget, and M. Vanderhaeghen, *Pseudoscalar meson photoproduction at high-energies: From the Regge regime to the hard scattering regime*, Phys. Lett. **B400**, 6 (1997).
- [147] M. Vanderhaeghen, M. Guidal, and J. M. Laget, *Regge description of charged pseudoscalar meson electroproduction above the resonance region*, Phys. Rev. **C57**, 1454 (1998).
- [148] G. A. Miller, *Electromagnetic Form Factors and Charge Densities From Hadrons to Nuclei*, Phys. Rev. **C80**, 045210 (2009), [0908.1535](#).
- [149] E. Amaldi, S. Fubini, and G. Furlan, *Pion-Electroproduction. Electroproduction at Low Energy and Hadron Form Factors*, Springer Tracts Mod. Phys. **83**, 1 (1979).
- [150] R. Mertig, M. Bohm, and A. Denner, *Feyn Calc - Computer algebraic calculation of Feynman amplitudes*, Comput. Phys. Commun. **64**, 345 (1991).
- [151] V. Shtabovenko, R. Mertig, and F. Orellana, *New Developments in Feyn Calc 9.0*, Comput. Phys. Commun. **207**, 432 (2016), [1601.01167](#).

-
- [152] R. K. Ellis and G. Zanderighi, *Scalar one-loop integrals for QCD*, JHEP **02**, 002 (2008), [0712.1851](#).
- [153] G. Passarino and M. J. G. Veltman, *One Loop Corrections for e^+e^- Annihilation Into $\mu^+\mu^-$ in the Weinberg Model*, Nucl. Phys. **B160**, 151 (1979).
- [154] R. Pohl et al., *The size of the proton*, Nature **466**, 213 (2010).
- [155] C.-R. Ji, W. Melnitchouk, and A. W. Thomas, *Anatomy of relativistic pion loop corrections to the electromagnetic nucleon coupling*, Phys. Rev. **D88**, 076005 (2013), [1306.6073](#).
- [156] G. 't Hooft and M. J. G. Veltman, *Scalar One Loop Integrals*, Nucl. Phys. **B153**, 365 (1979).
- [157] J. C. Collins, *Renormalization*, vol. 26 of *Cambridge Monographs on Mathematical Physics* (Cambridge University Press, Cambridge, 1986), ISBN 9780521311779, 9780511867392.